UNIVERSITÉ DE SHERBROOKE
Faculté de génie
Département de génie civil

ASSESSMENT OF LIQUEFACTION POTENTIAL USING THE COMBINED TRIAXIAL SIMPLE SHEAR APPARATUS (T_xSS)

by

Marwan Khashila

A dissertation submitted in partial fulfillment
of the requirements for the degree of
Doctor of Philosophy

In

Civil Engineering
(Geotechnical Engineering)

Sherbrooke (Québec), Canada
Dec. 2019

UNIVERSITÉ DE SHERBROOKE
Faculté de génie
Département de génie civil

Évaluation DU POTENTIEL DE LIQUÉFACTION À L'AIDE DU NOUVEL ESSAI TRIAXIAL EN CISAILLEMENT SIMPLE (T_xSS)

Thèse de doctorat
Spécialité : génie civil

Marwan Khashila

A dissertation submitted in partial fulfillment
of the requirements for the degree of
Doctor of Philosophy
(Civil Engineering)

MEMBRES DU JURY: Mourad Karray (directeur)
Michael James (membre externe)
Alper Sezer (membre externe)
Mathieu Nuth (membre interne)
Mahmoud Ahmed (membre externe)

Sherbrooke (Québec) Canada Dec. 2019

À ma mère, à mon père
À ma femme et mes enfants

ABSTRACT

In recent decades, several total and effective stress constitutive models have been developed in geotechnical engineering practice to perform one-dimensional site response analysis. These constitutive models have been incorporated in either finite difference or finite element dynamic analysis programs. Also, numerous research work has been done to predict more accurately earthquake-induced pore water pressure more accurately. Hitherto, the developed pore pressure models can be classified into stress, strain, and energy-based models. In the current study, strain-based and energy-based pore pressure models were proposed based on a series of strain-controlled cyclic T_xSS tests performed on reconstituted specimens of Baie Saint Paul, Carignan, Ottawa C-109, Ottawa F-65, and Quebec CF6B sands.

The proposed strain-based model was used to investigate the equivalent number of cycles concept and to assess the pore pressure as a damage metric. The energy-based model was combined with the Sigmoidal-model in FLAC 2D to introduce a simplified coupled energy-based pore pressure model. The proposed model was calibrated and verified, in terms of shear stress-strain response and excess pore pressure development, based on a series of strain-controlled cyclic T_xSS test results.

On an elemental-level, the model results were validated under cyclic strain-controlled and stress-controlled tests and a fair agreement was observed between the energy-based model and DSS results in terms of liquefaction resistance. In addition, the proposed model was validated by incorporating the energy-model in FLAC^{3D} platform to study the cyclic behavior under triaxial and simple shear conditions. The numerical simulation clarifies the difference between cyclic triaxial and simple shear conditions as well as the load conditions (i.e. stress or strain-controlled conditions).

Further validation was performed by numerical simulation of a centrifuge model conducted by Ramirez et al. (2017) at the University of Colorado Boulder by using the well-established Finn model and by the proposed energy-based model. The comparison shows the capability of the proposed energy-based model in conjunction with the Sigmoidal-model to very well simulate the seismic response in liquefaction analysis.

The proposed simplified coupled energy-based pore pressure model was implemented to assess the compatibility of the liquefaction charts in the eastern and western North America as

a part of this study. Different hypothetical sand deposits having different fundamental periods were subjected to two scaled-up earthquakes to perform 1-D site response analysis. One is compatible with the National Building Code of Canada 2005 (synthetic earthquake) and another incompatible real earthquake from the western region (Northridge earthquake). The comparison in terms of the generated pore pressure, the equivalent number of cycles and incorporated liquefaction charts (CRR-$(N_1)_{60CS}$) highlights the inaccuracy of using current liquefaction charts in Eastern regions.

RÉSUMÉ

Au cours des dernières décennies, plusieurs modèles constitutifs des contraintes totales et effectives ont été devellope dans la pratique de geotechnique pour effectuer une analyse unidimensionnelle de la réponse du site. Ces modèles constitutifs ont en fait été incorporés dans l'analyse dynamique par différence finie ou par éléments finis. De nombreux travaux de recherche ont été effectués pour prédire avec plus de précision la pression d'eau interstitielle induite par le séisme. Jusqu'à présent, les modèles de pression interstitielle développés peuvent être classés en modèles basés sur la contrainte, la déformation et l'énergie-dissipe. Dans le cadre de la présente étude, un modèle de pression interstitielle basé sur la déformation et un autre modèle de pression interstitielle basé sur l'énergie sont proposés à partir d'une série d'essais TxSS cycliques contrôlés par déformation effectués sur des échantillons de sol reconstitué à Baie Saint-Paul, Ottawa C-109, Ottawa F-65 et dans les sables de Québéc.

Le modèle basé sur la déformation proposé a été utilisé pour étudier le concept du nombre équivalent de cycles et pour évaluer la pression interstitielle comme mesure des dommages. Cependant, le modèle basé sur l'énergie est combiné avec le modèle Sigmoidal dans le logiciel FLAC pour introduire un modèle couplé simplifié de pression interstitielle basé sur l'énergie. Le modèle proposé est calibré et vérifié, en termes de réponse contrainte-déformation et de pression interstitielles, sur la base d'une série de résultats d'essais TxSS cycliques à contrainte contrôlée.

Au niveau des éléments, les résultats du modèle ont été validés dans le cadre d'essais cycliques à contrainte contrôlée et d'essais alternatifs à contrainte contrôlée et une concordance a été observé entre les résultats du modèle énergétique et ceux du DSS en termes de potentielle de liquéfaction. De plus, le modèle proposé a été utilisé en incorporant le modèle d'énergie dans la plate-forme FLAC3D pour étudier le comportement cyclique dans des conditions de cisaillement simple et triaxial. La simulation numérique clarifie la différence entre les conditions de cisaillement cycliques triaxiales et les conditions de cisaillement simples ainsi que les conditions de charge (c'est-à-dire les conditions de contrainte ou de déformation contrôlées).

D'autres validations ont été effectuées par simulation numérique d'un modèle expérimental de centrifugeuse mené par Ramirez et al (2017) à l'Université du Colorado Boulder par le modèle Finn bien établi et par le modèle énergétique proposé. La comparaison obtenue montre la

capacité du modèle énergétique proposé conjointement avec le modèle Sigmoidal à capturer la réponse sismique dans l'analyse de liquéfaction.

Dans le cadre de cette étude, le modèle simplifié de pression interstitielle couplée basée sur l'énergie a été mis en œuvre pour évaluer la capacité des chartes de liquéfaction dans l'Est et l'Ouest de l'Amérique du Nord. Différents dépôts de sable de niveau hypothétique ayant des périodes fondamentales différentes ont été soumis à deux séismes de grande échelle pour effectuer une analyse 1-D de la réponse du site. L'un est compatible avec le Code Nationale du Batiment 2005 (tremblement de terre synthétique) et un autre tremblement de terre réel incompatible de la région ouest (séisme de Northridge). La comparaison en termes de pression interstitielle générée, de nombre équivalent de cycles et de charte de liquéfaction incorporés (CRR-(N1)60CS) souligne une certaines imprecision de l'utilisation des chartes de liquéfaction actuels dans les régions de l'Est.

REMERCIEMENTS

First of all, I am deeply grateful to my supervisor, Prof. Mourad Karray, for his patience, motivation, insight, unbounded support and valuable guidance throughout my PhD. This thesis could not have been accomplished without his scientific support. Prof. Karray gave me much more scientific discussion and his profound practical expertise in soil dynamics and earthquake engineering. It has been a great honor and pleasure for me to study under his supervision.

I am, really, indebted to my post-doctoral, Dr. Mahmoud Nasser for his continuous assistance, enthusiasm, faithful encouragement and extraordinary support since starting my PhD program. In fact, it has not been since starting my PhD program. It has been since my undergraduate study and during my Master program. No word could express my gratitude to you.

Further appreciation is extended to jury members, Prof. Michael James, Prof. Alper Sezer and Prof. Mathieu Nuth for accepting to give me the honor of being the reviewers of my thesis and giving me their constructive, insightful and scientific comments on my thesis.

I wish to thank all my colleagues in our research group for their help and support. The complete list of this wonderful group would be too long to acknowledge here. I would like to acknowledge the laboratory technicians Valérie Dumoulin and Alexandre Sevigny for their appreciated support to do my experimental work in geotechnical and geo-environmental engineering laboratory. I also would like to acknowledge the financial support of Engineering Research Council of Canada (NSERC) and Hydro-Québec research institute.

Special sincere appreciation is expressed to my parents, and my brothers for their extreme patience, support and encourage through my study and for being by my side. My dad and mom, thanks for being my light in this life. Thanks for supporting me since my childhood. Thanks to my beautiful children, Kareem and Carmen for being the light of my world.

TABLE DES MATIÈRES

LISTE DES FIGURES

LISTE DES TABLEAUX

LISTE DES SYMBOLES

Symbole	Définition
τ	Average horizontal shear stress
σ_d	Deviator stress
σ_c	Confining pressure
σ'_{mean}	initial effective mean confining pressure
σ'_{v0}	initial effective vertical confining pressure
C_u	uniformity coefficient
C_c	curvature coefficient
e_{ini}	initial void ratio before consolidation.
e_{cons}	final void ratio after consolidation
e_{max}	maximum void ratio
e_{min}	minimum void ratio
I_D	Relative density of the soil.
σ'_{co}	initial effective confining pressure (kPa).
B	Skempton's pore pressure parameter.
r_d	stress reduction factor that accounts for the non-rigid response of the soil profile.
ϕ	Internal angle of friction
D_{50}	mean grain size
ρ	volumetric mass of soil (t/m^3)
V_s	shear wave velocity
γ	Shear strain
γ_{th}	threshold shear strain
G_s	specific gravity
G_{max}, G^e	Secant shear modulus at very low strain ($\gamma_c \leq 10^{-4}\%$)
K^e	Bulk modulus
K^e_G	elastic shear modulus number
$\{\ddot{u}\}, \{\dot{u}\}$ and $\{u\}$	vector of relative nodal acceleration, velocities and displacements, respectively
$\{\ddot{u}_g\}$	acceleration at the base of the soil column
$\{I\}$	unit vector
N	Number of uniform loading cycles
N_L	Number of liquefaction cycles
$N_{eq\gamma}$	Number of equivalent uniform strain cycles
$N_{eq\tau}$	Number of equivalent uniform stress cycles
R_u	Generated pore water pressure
$D_{(P\text{-}M)}$	Cumulative damage using P-M hypothesis

$D_{(R\text{-}N)}$	Cumulative damage using R-N hypothesis
R_n	Cyclic ratio , $R_n = N/N_L$
W_s	Dissipated energy per unit weight of soil
$Ws_{,ru=0.65}$	Cumulated dissipated energy at $R_u = 0.65$
r	Material parameter
E_r	rebound modulus of static drained unloading test
K_0	Coefficient of earth pressure at rest
α	Pore pressure calibration parameter
β	Empirical Pore pressure parameter
ν	Pore pressure exponent
C1, C2, C3, C4	Calibration parameters of Martin model
μ	Poisson's ratio
$\Delta\eta$	change of shear stress ratio
$\Delta\gamma^p$	plastic shear strain increment
T_0	fundament period of soil deposit
a_{max}	maximum induced acceleration at deposit surface
$(N_1)_{60CS}$	Normalized number of standard penetration blows
qc_1	Normalized cone penetration resistance

LISTE DES ACRONYMES

Acronyme	**Définition**
TxSS	Combined Triaxial Simple Shear
CTX	Cyclic Triaxial
DSS	Direct Simple Shear
CSR	Cyclic Stress Ratio
CSR_t	Threshold shear stress ratio
CRR	Cyclic resistance ratio
$CSR_{M=7.5}$	normalized CSR_{max} to M7.5, $CSR_{7.5} = CSR_{max}/MSF.K_\sigma$
PGA	Peak ground acceleration
PEC	pseudo energy capacity
ENA	Eastern North America
WNA	Western North America
MSF	Magnitude scaling factor

CHAPTER 1

INTRODUCTION

1.1 General

In response to earthquake shaking, loose saturated soil tends to contract and decrease in volume. However, as the period of earthquake shaking is too small, drainage is not allowed. The tendency to decrease in volume results in an increase in pore pressure coincident with a decrease in effective stresses. Ultimately, the soil may lose its stiffness and behaves like a viscous fluid which is known as liquefaction (Seed and Lee 1966).

Liquefaction is one of the most important and damaging phenomena in soil dynamics (Castro and Poulos 1977). Following the destructive failure that occurred during the 1964 Alaska and Niigata earthquakes, special attention has been given to liquefaction potential assessment. Numerous experimental investigations have been done under both monotonic and cyclic loading conditions in attempts to better understanding this phenomenon and of soil behavior under seismic loading (e.g. Peacock and Seed 1968; Castro 1975; Vaid and Chern 1985; Vaid and Sivathayalan 1996). Experimental study of liquefaction potential must replicate the site conditions in terms of loading (initial stress state and stress path) and soil depositional (fabric, density) characteristics.

One of the main challenges in geotechnical earthquake engineering is determining the liquefaction potential of a soil deposit. Several procedures have been developed, over the years, to assess the liquefaction potential of a soil deposit subject to a given earthquake. The most widely used procedure is the simplified method which was developed by Professor H. B. Seed and his colleagues of Berkeley (Seed and Idriss 1971). Applying this semi-empirical procedure and its variants allow prediction of the induced cyclic stress ratio based on the maximum acceleration at the ground surface (a_{max}) and the depth reduction factor (r_d). This procedure has been evolved over the years to consider the type of soil and characteristics of seismic events (Filali and Sbartai 2017; Norambuena et al. 2019). It is originally based on compiled earthquake

data from active tectonic seismic zones (e.g. western United States, Japan, and China). However, it is well recognized that there is a difference between the seismicity and geological crust between eastern and western North America (Jacob 1991; Youd et al. 2001; Humar 2015). Therefore, it has been questioned the validity of this method in eastern regions of North America which will be demonstrated in the present work.

1.2 Objectives of the research

The primary goal of this thesis is to establish and validate a coupled energy-based pore pressure model to be integrated into assessing the compatibility of the simplified method and the available liquefaction design charts for the eastern regions of Canada using the Combined Triaxial Simple Shear apparatus (TxSS). Basically, the objectives of this thesis can be listed as follow:

- A new combined triaxial simple shear test is used in this study to develop a simple strain-controlled pore pressure damage metric formula and an energy-based pore pressure model. The former is employed in computing the equivalent number of uniform strain cycles for a random earthquake history whereas the latter is implemented in defining a coupled energy-based pore pressure model using FLAC^{2D} and FLAC^{3D} (Fast Lagrangian Analysis of Continua).
- Another goal of this study is to apply the proposed energy-based model at the element-level to simulate the new combined triaxial simple shear (T_xSS) test under stress and strain-controlled conditions. Additionally, to simulate cyclic behavior under CTX tests for comparing with the T_xSS numerical and experimental results.
- Compare the liquefaction potential obtained from different experimental configurations (cyclic triaxial (CTX), T_xSS, and direct simple shear (DSS)). Moreover, it emphasizes the effect of shear loading pattern (i.e., strain-or stress-control).
- After confirming the predictive capability in element-level tests performed on different cohesionless soils, another challenge is to validate the proposed model by simulating a dynamic centrifuge-model experiment performed by Ramirez et al. (2017; 2018) numerically using the proposed energy-based model and Finn model (Martin et al. 1975; Byrne 1991). This comparison aims to validate the proposed model to perform one-dimension analysis and estimate the liquefaction initiation in a free–field sand deposit subjected to a seismic event.

- In the end, the proposed model is employed in one-dimensional analysis to investigate the difference between eastern and western North America seismic responses. A synthetic earthquake (Atkinson 2009) compatible with 2005 NBCC and another real earthquake from Western North America (Northridge earthquake) scaled-up to design spectrum class-A are excited at the base of hypothetical deposits of Ottawa sand F65 with different depths and densities.

1.3 Statement of originality

To capture these objectives, an experimental program was performed on selected cohesionless soils collected from different sites in Quebec (Baie-Saint-Paul, Carignan, and CF6B Quebec sands) in addition to two commercial clean sands (Ottawa sand C-109 and Ottawa sand F-65). The new combined triaxial simple shear apparatus (TxSS) is incorporated in this research as well as the conventional triaxial and direct simple shear test.

Cyclic strain-controlled T_xSS test results are employed to develop an energy-based pore pressure model. This proposed model is incorporated in a numerical coupled energy-based model to simulate cyclic stress and strain-controlled tests under T_xSS and CTX conditions. The capability of the proposed model to predict the liquefaction potential curve (CSR-N_{liq}) has been accomplished by comparing the liquefaction potential curves experimentally obtained from CTX, T_xSS, and DSS alongside those from earlier studies with the equivalent numerical results. The numerical simulation reveals the cyclic difference under both test modes. Further, the proposed model and Finn-model are implemented in one-dimensional analysis to predict the pore pressure generation in response to a seismic event and compared to an experimental centrifuge model performed by (Ramirez et al. 2017).

The quantitative validation of the proposed numeric model defined in this study either in element-level (by comparing the T_xSS and CTX tests to equivalent numerical simulations) or in one dimension liquefaction analysis (by comparing to an experimental centrifuge model) confirms its predictive capability to capture cyclic behavior and liquefaction analysis.

The earthquake-induced cyclic stress ratio values of various hypothetical sand deposits are compared to the inherent cyclic resistance ratio obtained from experimental investigation and available liquefaction charts in terms of standard penetration test blow count $(N_1)_{60Cs}$.

Comparison between eastern and western earthquake responses in terms of pore pressure buildup and the equivalent number of uniform stress cycles reveals that the application of the available liquefaction charts in eastern regions of North America is questionable, as these charts were obtained from data compiled from highly seismic zones.

This thesis includes four papers; the first one was published in the Canadian Geotechnical Journal, the second and fourth papers have been submitted to the Canadian Geotechnical Journal, and the third paper has been submitted to the Journal of Computers and Geotechnics. Additionally, three conference papers resulted from this study.

1.4 Thesis outline

This thesis consists of eight chapters as illustrated in Figure 1.1. The contents of each chapter can be summarized as follows:

Chapter 1: Introduction: This chapter presents a brief review of the liquefaction phenomenon, the objective and the originality of this research.

Chapter 2: A literature review on the seismic difference between eastern and western North America, liquefaction evaluation approaches, the equivalent number of uniform cycles concept, and the most used pore pressure models are presented in chapter 2. The difference between liquefaction potential under different experimental configuration is also illustrated in this chapter.

Chapter 3: Experimental work. This chapter shows the apparatus used in the current study (T_xSS, DSS, and CTX). The advantages and limitations of each apparatus are discussed. The physical properties of the sands used and the preparation methods are described.

Chapter 4: First scientific journal article published: An extensive review of the fatigue-damage hypothesis and equivalent number concept in the metal realm and their adaption to liquefaction assessment is discussed in this chapter. A simple pore pressure formula as a function of the number of liquefaction cycles was proposed, as alternative to the R-N damage hypothesis (Richart and Newmark 1948). The results indicate the validity of using pore pressure buildup as a damage metric to compute the equivalent number of uniform strain cycles of random earthquake motion.

Chapter 5: Second scientific journal article submitted:

A comprehensive discussion on the variation of the cyclic behavior under triaxial and direct simple shear is illustrated. Based on T_xSS cyclic strain-controlled tests, a coupled energy-based pore pressure model was developed and successfully validated by relating to physical element-level tests. The influence of the diameter to height (D/H) ratio is discussed based on the T_xSS results. A comparison between liquefaction potential curves obtained in the literature and obtained from this study using DSS, T_xSS and numerical simulation is performed under stress-controlled conditions. Also, the liquefaction potential under strain-controlled condition is examined in this chapter.

Chapter 6: Third scientific journal article submitted:

This chapter aims to validate the calibrated coupled energy-based pore pressure model to simulate the cyclic behavior in element-level test configurations (i.e. cyclic triaxial (CTX) and new combined triaxial simple shear (T_xSS) tests) in FLAC^{3D}. Therefore, a comparative experimental program and numerical simulation of cyclic behavior under CTX and T_xSS tests were performed. The non-uniformity of shear strain distribution in CTX and T_xSS and its effect on the dissipated energy and triggering of liquefaction were closely examined. An empirical correlation between cyclic axial and shear strain was developed and verified successfully based on CTX stress-controlled results.

Chapter 7: Fourth scientific journal article submitted:

This chapter presents the application of the proposed model in a one-dimensional analysis and liquefaction assessment. At first, the proposed model and Finn model were used to simulate an experimental centrifuge model. Good consistency was observed between the numerical simulation and experimental model which confirm the applicability of the proposed energy-based model to perform one-dimensional analysis with an acceptable degree of confidence. Further, a synthetic earthquake (Atkinson 2009) compatible with eastern Canada seismicity and another real earthquake registered after the 1994 Northridge earthquake (M=6.7) were applied to hypothetical soil deposits having different fundamental periods to investigate the difference of seismic response between eastern and western regions and assess the applicability of the liquefaction charts for the eastern North America regions. The obtained results infer the inaccuracy of using the current liquefaction charts in the eastern regions of Canada.

Chapter 8: Conclusion and Recommendations.

This chapter enumerates the conclusion of the numerical and experimental results discussed throughout the dissertation in addition to recommendations for future work.

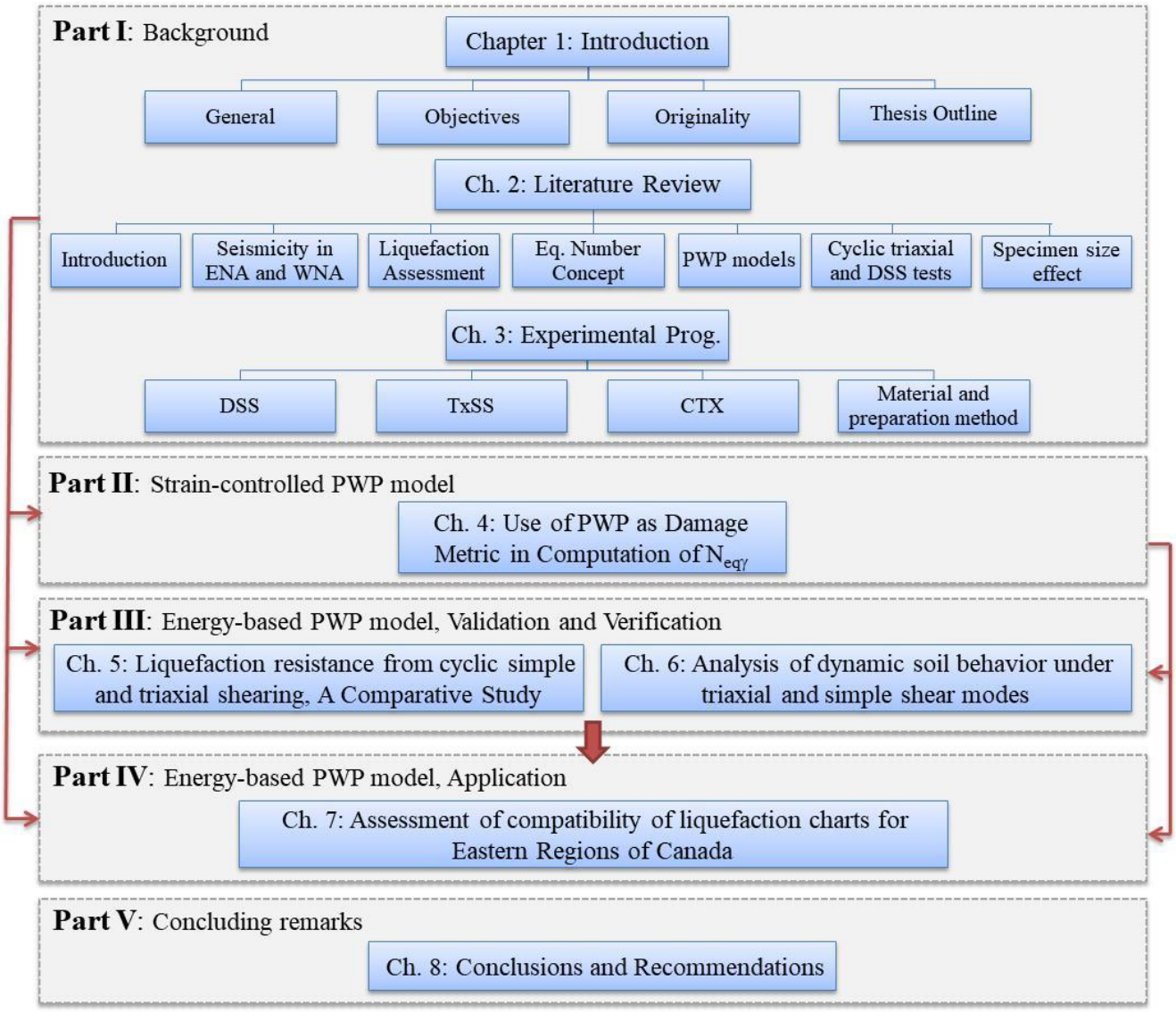

Figure 1.1: organization of the thesis

CHAPTER 2

LITERATURE REVIEW

2.1 Introduction

As the soil liquefaction has induced incredible damage to engineering structures and loss of lives, one of the geotechnical engineers' challenges is determining the liquefaction vulnerability of a soil deposit to earthquake ground motions. It could be obtained by comparing the induced cyclic stress ratio, CSR, during seismic loading (demand) with the cyclic resistance ratio, CRR, representing the soil (capacity). In practice, the most widely used procedure in liquefaction assessment was initially developed by H.B. Seed and his colleagues in California termed “the simplified method” based on a compilation of tectonic earthquake data from highly seismic regions such as western North America, Japan, and China (Seed and Idriss 1971). Afterward, extensive work was done to determine CRR experimentally (e.g. cyclic triaxial, direct simple shear and torsional shear tests) or in-situ quantitative assessment by standard penetration test, SPT, (Seed et al. 1971), cone penetration test, CPT, (Seed et al. 1971; Boulanger and Idriss 2014), or shear wave velocity, V_s, (Andrus and Stokoe 2000).

2.2 The difference in seismic response between Eastern and Western North America

The simplified procedure was incorporated in conjunction with in-situ data to introduce liquefaction charts (e.g. Seed et al. 1971; Cetin et al. 2004; and Idriss and Boulanger 2008). However, these charts are based on screening of actual events data compiled from high seismic regions (e.g., western region of United States) where the ground motions are distinguished by low-frequency content (rich in long-period motions) and lower peak ground acceleration, PGA, comparing to their counterparts in eastern North America at similar magnitude and source to site distance. Figure 2.1 demonstrates the spectral acceleration of two real earthquakes; Southern California (1952) and Saguenay (Quebec) (1988). The difference is evident in the predominated

frequencies of the two earthquakes. Moreover, it is well known that the geological crust between eastern (ENA) and western (WNA) North America are different. The attenuation of earthquake energy in ENA crust is lower with the distance from source compared with those in WNA (Jacob 1991; Adams and Halchuck 2004; Atkinson 1989; Campbell 2013; Humar 2015). Kramer (1996) reported that a higher amplification could occur in the east; due to the harder bedrock in ENA than WNA, i.e. peak ground acceleration is higher in ENA than in WNA, and the applicability of western design criteria in eastern regions is questionable depending on how far equivalent number of cycles is calculated.

In contrary, Youd et al. (2001) indicated that the difference between ENA and WNA is relatively small postulating that to the quick attenuation of earthquake motion throughout soil strata which results in filtering of high-frequency energy during the vertical propagation of shear waves. Moreover, Youd et al. (2001) reported that the difference between the peak horizontal acceleration at the ground surface, a_{max}, in ENA and WNA could be alleviated by computing PGA using the procedure recommended in the 1996 National Center for Earthquake Engineering Research (NCEER) workshop which considered the type of faulting, site condition, and location. Jacob (1992) summarized the difference between ENA and WNA seismic as (i) unknown of the potential failure surface of future events in ENA (lack of documented data), (ii) maintain the high-frequency content for large distance (lack of attenuation) and (iii) higher amplification in eastern regions. Therefore, a question arises here "are the liquefaction assessment procedures adopted in the western applicable to eastern North America?"

In the same contest, Bashir et al. (2017) and Basu et al. (2017), based on nonlinear liquefaction analysis using DEEPSOIL software v6.0, observed that the adopting of simplified method and incorporated liquefaction charts, in terms of SPT and V_s, in one-dimensional (1-D) liquefaction assessment is not compatible in the Indian (Asia) seismicity zone. Similarly, Filali and Sbartai (2017) observed uncertainty of the simplified method compared with nonlinear response analysis for four different sites (three in the USA and one in Algeria). It was observed that, at a_{max}=0.3, the simplified method gives adequate results like the dynamic analysis, however, beyond this value, the simplified method results should be correlated as a function of the maximum ground acceleration as proposed by (Filali and Sbartai 2017).

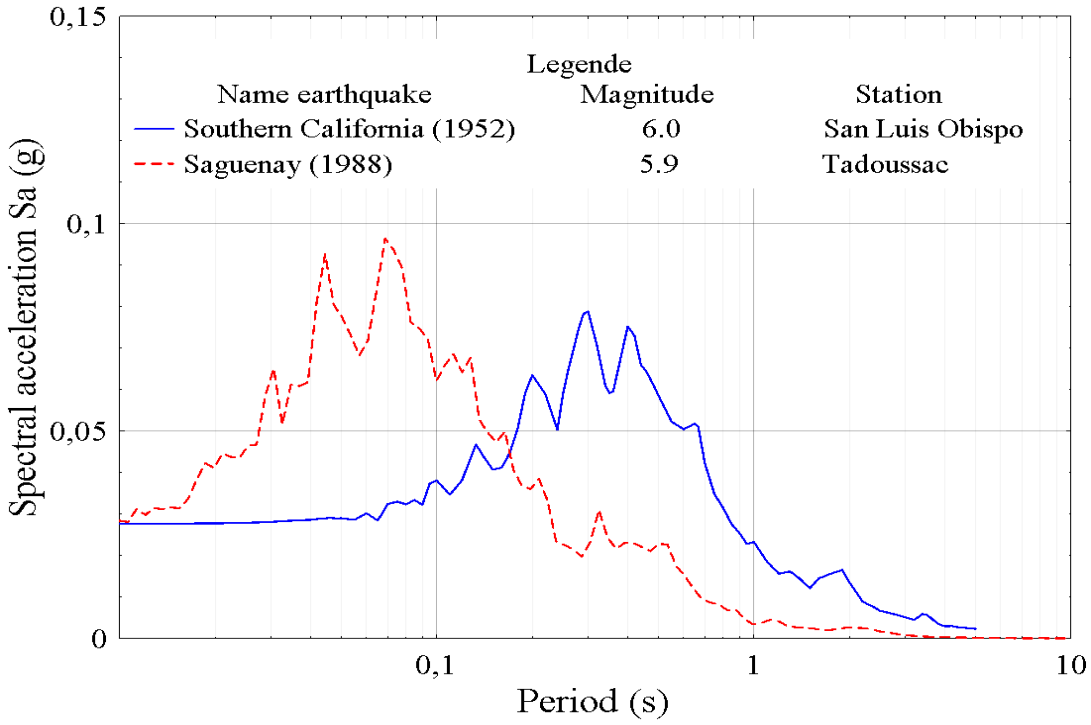

Figure 2.1. Spectral accelerations of Western and Eastern earthquakes

2.3 Liquefaction Assessment

Over past years, liquefaction causes hundreds billion dollars in damage which devoted research centers around the world to assess soil liquefaction and pore pressure generation. Soil liquefaction results in damage to engineering structures and ground subsidence (NRC 1985). The safety factor against liquefaction is the ratio between the “capacity” of soil to sustain the applied load to the “demand load” imparted to the soil by earthquake ground motion, various recognized methodologies have been used in practice in liquefaction potential assessment to determine the safety factor such as:

1. Stress-based approach (e.g. Seed and Idriss 1971).
2. Strain-based approach (e.g. Dobry 1982)
3. Energy-based approach (Davis and Berrill 2001).
4. Numerical modeling analysis (e.g. Seed and Idriss 1969; Finn et al. 1977)
5. Arias intensity approach (e.g. Kayen and Mitchell 1997).

2.3.1 Stress-based liquefaction evaluation approach

In a stress-controlled test, a uniform stress wave at a significant frequency is applied on representative soil specimens whereas the response in terms of pore pressure buildup and induced shear strain is monitored. The liquefaction potential is obtained as the variation of CSR with the liquefaction cycles number, N_{liq}. In this approach, the initial liquefaction is defined as the generated pore pressure ratio reaches unity or the induced shear strain reaches a significant value, single shear strain amplitude of 3.75%, (Seed and Lee 1966). It is common to determine CRR for a magnitude earthquake M=7.5 using the liquefaction potential curve corresponding to 15 cycles which represent the number of equivalent uniform cycles (Seed and Idriss 1982).

It is noteworthy that the reconstituted specimen is more affected by many factors such as strain history, fabric, aging, and cementation. Therefore, correlating CRR with in-situ tests parameters such as V_s (Andrus and Stokoe 2000), the number of standard penetration blows, $(N_1)_{60cs,}$ (Seed et al. 1983), and the normalized cone penetration resistance, q_{c1n} (Robertson and Wride 1998) are advocated to acquire CRR in liquefaction assessment. In this thesis, $(N_1)_{60cs}$ is incorporated in the liquefaction assessment. This may be justified as $(N_1)_{60cs}$ correlates much better to relative density, I_D, wherein I_D reflects the inherent contractive tendencies of soil under shearing load. [Note: $(N_1)_{60cs}$ is the number of standard penetration blows counted in standard penetration test (SPT) based on a hammer impact efficiency of 60% correlated to clean sand and an overburden pressure of 1 atm].

Stress-controlled liquefaction evaluation approach was recommended over years particularly after the development of the “simplified stress-controlled method” in the 1960s by H.B Seed and his colleagues and its application in the equivalent number concept. Seed et al. proposed a direct relation between the induced shear stress and maximum acceleration induced at the ground surface as discussed in detail in the next subsection.

2.3.1.1 The simplified stress-based method

Predicting earthquake-induced shear stresses is the challenge of researchers over the years. It may be predicted by numerical 1-D, 2-D or 3-D response analysis or empirically using the simplified stress-based method. The simplified method was established based on a compilation of earthquake data from active tectonic seismic zones such as California, Japan, and New Zealand (Seed and Idriss 1971). This method has undergone updates periodically based on the

evolution in understanding of liquefaction phenomenon and seismic behavior of soil depended on the previous earthquakes records besides experimentally and/or field data (e.g., SPT, CPT, and Vs) (e.g. Seed and Idriss 1983; Youd et al. 2001; Cetin et al. 2004; and Idriss and Boulanger 2008).

The simplified method aimed at computing the safety factor by comparing the induced CSR during seismic loading (demand) with the CRR (capacity) of soil.

$$FS = \left(\frac{CRR_{M=7.5}}{CSR} \right).MSF \tag{2.1}$$

where $CRR_{M=7.5}$ is the cyclic resistance ratio corresponding to magnitude earthquake M=7.5, CSR is the cyclic stress ratio in the response of earthquake shaking, and MSF is the magnitude scaling factor. Generally, susceptibility to liquefaction decreases with increasing the factor of safety.

Based on Newton's Second Law, Seed and Idriss (1971) proposed the following formulation to compute the CSR at a given depth in the soil deposit:

$$CSR = \left(\tau_{av} / \sigma'_{v0} \right) = 0.65 \left(a_{\max} / g \right) \left(\sigma_{v0} / \sigma'_{v0} \right) r_d \tag{2.2}$$

where τ_{av} is the average cyclic shear stress; a_{max} is the peak horizontal acceleration at the ground surface; g is the acceleration of gravity; σ_{v0} and σ'_{v0} is the initial total and effective vertical stress; r_d is the stress reduction factor that accounts for the non-rigid response of the soil profile.

Figure 2.2 demonstrates the application of the simplified method as a comparison between the estimated CSR and CRR to ascertain where liquefaction may occur. As demonstrated, if the induced CSR is higher than CRR, i.e. safety factor < 1, liquefaction triggering is expected. The two questionable parameters in Eq. (1) are the value of r_d and defining of a_{max} for ground motion.

2.3.1.1.a Stress reduction factor r_d

The stress reduction factor is a quantitative value account for the flexibility of the soil deposit during the earthquake shaking. It has the maximum value of unity at the ground surface and decreases by the profile depth, Figure 2.2(c), as a function of ground motion characteristics (magnitude and the frequency content) and dynamic characteristics of the soil profile (Seed and Idriss 1971; Idriss 1999). Cetin et al. (2004) reported that the proposed r_d curves of Seed and Idriss (1971), Figure 2.2(c), tend to overestimate CSR. Many formulations were proposed to

estimate r_d values (e.g. Liao and Whitman 1986; Robertson and Wride 1998; Idriss 1999; Youd et al. 2001; Cetin et al. 2004; Idriss and Boulanger 2008).

In the routine practice of geotechnical engineering, the recommended formula, Eq. (2.3), by the NCEER experts, has been used to estimate the average value of r_d (Liao and Whitman 1986b; Youd et al. 2001).

$$r_d = 1.0 - 0.00765z \quad \text{for } z \leq 9.15 \text{ m} \tag{2.3a}$$

$$r_d = 1.174 - 0.00267z \quad \text{for } 9.15 \text{ m} < z \leq 23 \text{ m} \tag{2.3b}$$

where z is the depth in meters

Cetin (2004) performed an extensive numerical analysis on a compilation of 50 actual stratigraphy soil sites subjected to a wide range of actual ground motions (which cover the range from low to high magnitude and represented near-, mid- and far-field events). Most recently, extending to Cetin's work, Lasley et al. (2016) performed a large number of equivalent linear site response analyses subjected to different ground motions. Using robustness statistical and regression analysis of response results, Lasley et al. (2016) introduced a modified r_d relationship (Eq. 2.4) having the least bias comparing to the previous preceding models.

$$r_d = (1-\alpha)\exp\left(-z/\beta\right) + \alpha \tag{2.4a}$$

$$\alpha = \exp\left(-4.373 + 0.4491.Mw\right) \tag{2.4b}$$

$$\beta = -20.11 + 6.247.Mw \tag{2.4c}$$

where α is limiting value of r_d and can be range from 0 to 1; β is a curvature coefficient at shallow depths; z is the depth in meters.

2.3.1.1.b Maximum ground acceleration

Another parameter related to the application of the simplified method is defining a_{max} value. In general, a_{max} has been used to determine from field measurements or numerical analysis. SHAKE program is one of the most widely used programs to study the nonlinear behavior during the shear wave propagation (Schnabel et al. 1972). Afterward, approximate relations between maximum acceleration on rock and soil surface have been developed (Idriss 1990).

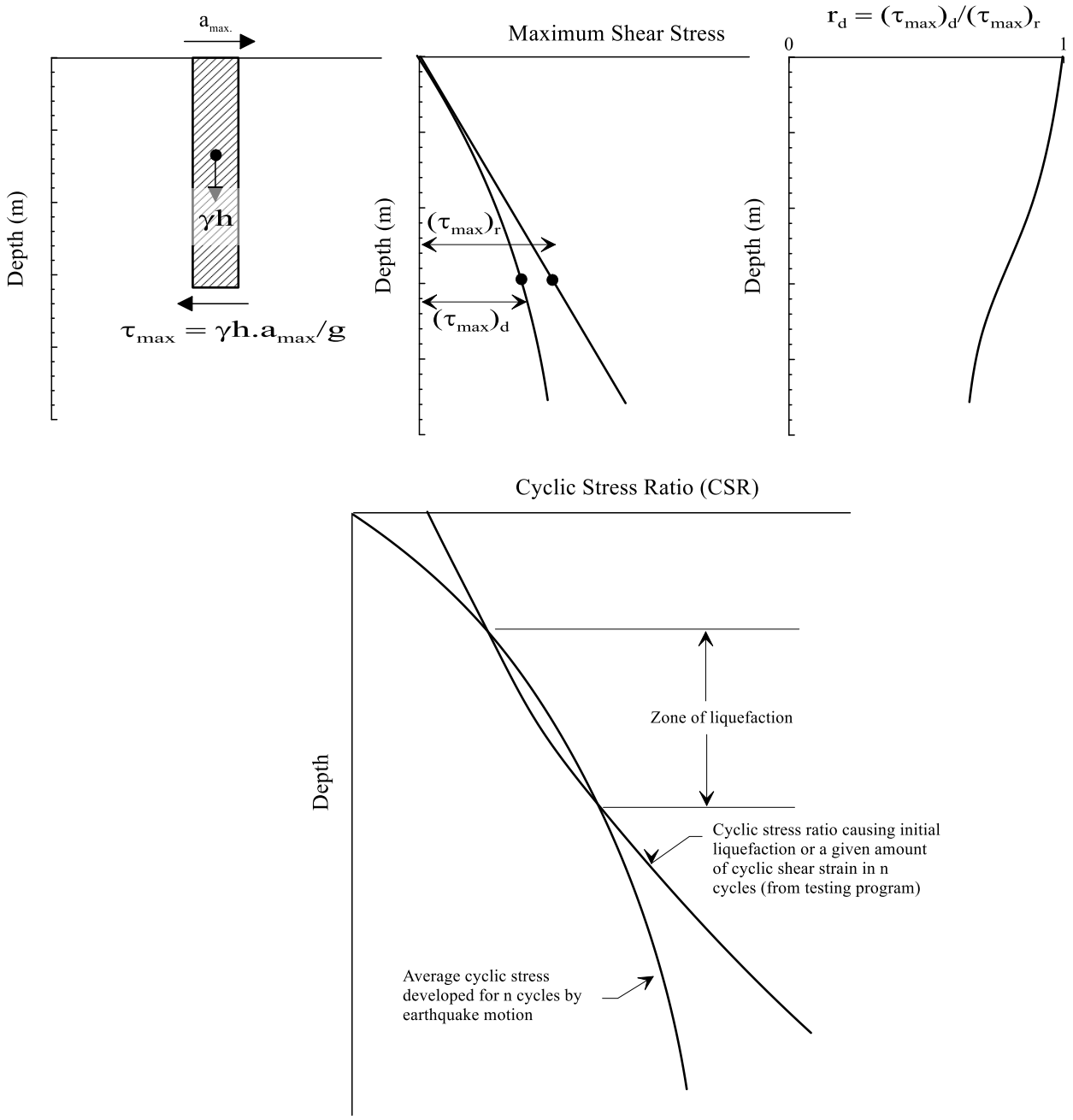

Figure 2.2. Schematic illustration of the simplified stress-based method (after Seed and Idriss 1971)

Youd et al. (2001) recommended using the geometric mean of the two maximum horizontal accelerations (when there is available data). Boulanger and Idriss (2014) reported the difference between geometric mean and a_{max} of horizontal motions is often about 10% for a level ground surface that may have a relatively small effect on liquefaction analysis. Also, using the geometric mean alleviates the uncertainty of estimating a_{max} particularly for geotechnical structures that have weak/strong directions. It is noteworthy that, in the liquefaction studies, the a_{max} of the vertical component is usually neglected because of its very small value relative to the two orthogonal horizontal components. However, other researchers preferred to consider the vertical component in liquefaction analysis (e.g. Atkinson 1989; Law et al. 1990).

2.3.1.1.c Cyclic resistance ratio (CRR)

Applying the simplified method enables expecting the induced cyclic shear stress profile after earthquake shaking, as shown in Figure 2.2. The variation of inherent CRR with depth can be obtained from the laboratory tests and/or from the correlation with in-situ tests such as SPT (Seed et al. 1985; Boulanger and Idriss 2008), CPT (Boulanger and Idriss 2014), and V_s (Andrus and Stokoe 2000). In this study, SPT was adopted throughout to investigate the difference between ENA and WNA seismic response (Chapter 7).

The $(N_1)_{60CS}$ values were computed within this work using its correlation to relative density, I_D, coefficient of uniformity, C_u, mean grain size, D_{50}, and particles two-dimensional angularity, A_{2D}, (Ghali et al. 2019) as follows:

$$\frac{N_1}{I_D^2} = 140 \times D_{50}^{0.22} \times \exp^{-0.002 A_{2D}} \times C_u^{0.5} \tag{2.5}$$

Based on the screening of extensive review of actual earthquakes from tectonic active seismic zones (e.g., WNA, Japan and Chine), a correlation between CRR and $(N_1)_{60cs}$ was driven (e.g. Youd et al. 2001). The most widely used CRR-$(N_1)_{60cs}$ correlation for the clean sand in practical liquefaction assessment was obtained by Boulanger and Idriss (2008), Figure 2.3, Eq. 2.6.

$$CRR_{M=7.5,\sigma'_v=1atm} = \exp\left(\frac{(N_1)_{60cs}}{14.1} + \left(\frac{(N_1)_{60cs}}{126}\right)^2 - \left(\frac{(N_1)_{60cs}}{23.6}\right)^3 + \left(\frac{(N_1)_{60cs}}{25.4}\right)^4 - 2.8\right) \tag{2.6}$$

2.3.1.1.d Magnitude scaling factors

The available liquefaction resistance curves in terms of $(N_1)_{60}$, q_{c1N}, or V_{s1} apply to clean-sand at earthquake magnitude M7.5. Therefore, proposing a correlation to other magnitudes is needed in the liquefaction assessment framework. Seed and Idriss (1982), based on the limited earthquake data available in the 1970s, proposed a correction factor to correlate the produced CSR by different magnitude earthquakes to its equivalent at M7.5 termed "Magnitude scaling factor, MSF". This correlation was revised by I. M. Idriss in the form:

$$MSF = 10^{2.24} / M_w^{2.56} \tag{2.7}$$

In the 1980s, from compiled data of different earthquake magnitude, Ambraseys (1988) proposed a correlation between CRR, $(N_1)_{60}$ and MSF. This correlation reveals the conserve of MSF developed by Seed and Idriss. Arango (1994 and 1996) proposed a magnitude scaling factor based the largest compiled field data by applying the energy concept and Neq-Magnitude relationships developed by Seed and Idriss (1982). It was observed that the magnitude scaling factor values derived by Ambraseys (1988) and Arango (1996) induce larger MSF values for earthquake magnitude values less than 7. Andrus and Stokoe (1997) adopted the shear wave velocity technique to develop a correlation between V_s and CRR. After applying CRR-V_s to different magnitude earthquakes another MSF formula was obtained.

Liu et al. (2001) applied a regression analysis on the two horizontal components of a huge earthquake data to introduce MSF relationships for clean sands. It was observed that the MSF is not simple as previously proposed, however, it varies systematically with earthquake characteristics (magnitude and duration), site to source distance, and soil characteristics.

Recently, cyclic behavior and soil characteristics have been considered in MSF relations. Cetin and Bilge (2012) developed MSF relationships that accounted for the dilational behavior as a relative function of relative density and overburden pressure.

Considering the characteristics of liquefaction potential curve, Idriss and Boulanger (2008), and Kishida and Tsai (2014) proposed a MSF relationship as function of soil parameter (b) and correlations of the earthquake magnitude with number of equivalent cycles, wherein soil parameter (b) is the slope of CSR-N_{liq} curves in log-log scale.

Idriss and Boulanger (2008) relation was revisited by Boulanger and Idriss (2008), as shown in Figure 2.4 for different $(N_1)_{60cs}$ and q_{caNcs}, in general form as:

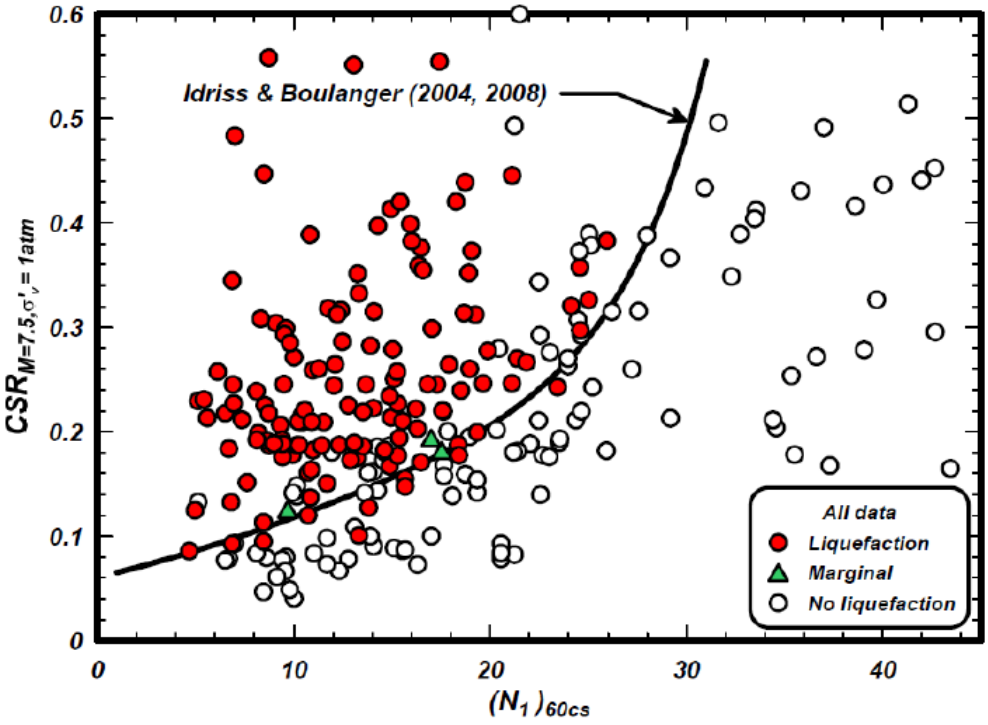

Figure 2.3. Cyclic resistance ratio (CRR) correlation from $(N_1)_{60cs}$ (from Idriss and Boulanger 2008)

$$MSF = 1 + (MSF_{\max} - 1)\left(8.64 \exp\left(\frac{-M}{4}\right) - 1.325\right) \tag{2.8}$$

where MSF_{max} is the maximum computed value corresponding to M=5.25 wherein its typical values are 1.8 for sand and 1.09 for clay and plastic silt. It can be obtained by

$$MSF_{\max} = 1.09 + \left(\frac{q_{C1Ncs}}{180}\right)^3 \leq 2.2 \tag{2.9a}$$

$$MSF_{\max} = 1.09 + \left(\frac{(N_1)_{60cs}}{31.5}\right)^2 \leq 2.2 \tag{2.9b}$$

Although the simple application of the stress-based simplified method and the abundance of empirical correlations between CRR and in-situ tests, the cyclic behavior and cyclic volume change of soils is affected more fundamentally by the cyclic strain amplitude than the cyclic stress amplitude (Wer and Dobry 1982; Dobry and Vucetic 1988; Vucetic 1994) as discussed in details in the following points:

- Undrained cyclic strain-controlled tests produce a quite consistent pore pressure data, regardless of differences in specimen fabric. Such consistent results obtained in strain-

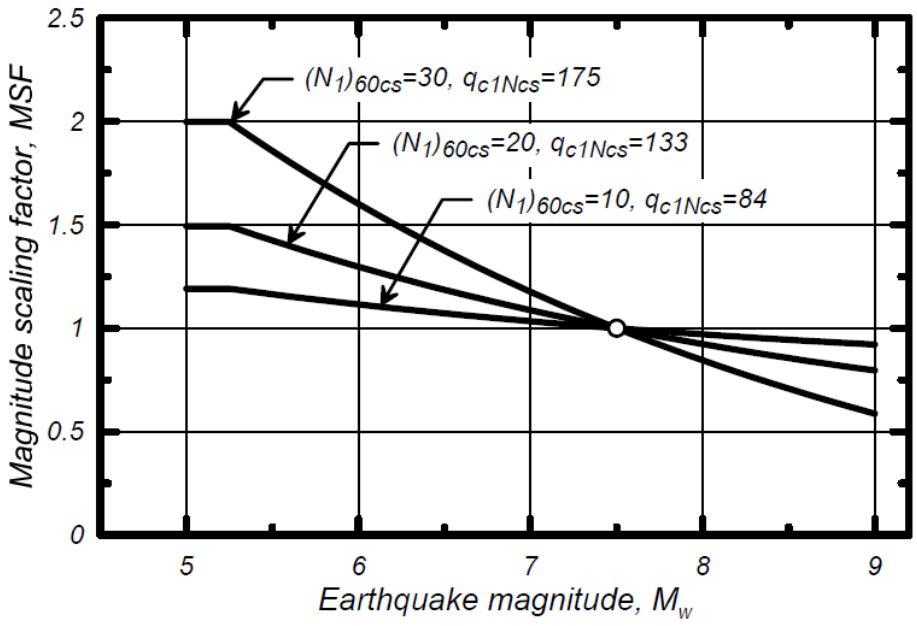

Figure 2.4. Magnitude scaling factor based on qc1Ncs for cohesionless soil (from Boulanger and Idriss 2014)

controlled testing of sands strongly reveals that the shear strain is dominant parameter governing the densification of dry sand and the cyclic behavior of saturated sand in terms of pore pressure generation in saturated soils is the cyclic shear strain amplitude rather than cyclic shear stress amplitude (Silver and Seed 1971; Dobry and Vucetic 1988).

- Silver and Seed (1971) observed that the strain-controlled tests cause less water content redistribution in soil specimens before initial liquefaction occurs and provides more realistic predictions of in-situ pore pressures than those obtained from stress-controlled tests.
- Strain-controlled loading system enables proper characterization of strain-softening materials, although the stress-controlled loading system is generally simpler and permits prescribed stress paths to be followed with ease, (Vipulanantham 2011).
- Strain-controlled tests account for the post-cyclic volume change values to the cyclic shear strain amplitude. Neglecting these values in the stress-controlled test makes it less reliable in determination of shear modulus and damping ratio values, which are the main factors governing the cyclic behavior of soils (Sitharam et al. 2012; Almani et al. 2013).
- In general, cyclic strain-controlled loading directly relates pore pressure generation with the amplitude of shear strains (Martin et al. 1975; Byrne 1991).

2.3.2 Strain-controlled liquefaction evaluation approach

The cyclic strain approach is an alternative to the stress-based approach and considers shear strain rather than shear stress in liquefaction potential assessment (Silver and Park 1976; Dobry et al. 1982; Dobry and Abdoun 2015). Based on cyclic strain-controlled tests, Dobry et al. (1982) discerned a firm relation between cyclic shear strain amplitude and generated pore pressure ratio regardless of specimen fabric, density, deposition method or overconsolidation ratio as opposed to the stress-controlled tests as shown in Figure 2.5. This may be justified as the pore pressure generation is a shear strain phenomenon. In stress-controlled tests, the induced shear strains differ according to the reconstitution methods, wherein reconstitution methods inherently have a significant effect on soil stiffness. As noted by Vaid et al. (1987), the stress-controlled cyclic loading is preferred to simulate earthquake loading whereas similar cyclic strain-controlled loading is recommended in the volumetric strain and pore pressure generation studies.

Moreover, it was observed that no pore pressure can be generated if the shear strain amplitude is lower than the volumetric shear strain threshold value (γ_{tv} = 0.01%) regardless of the number of loading cycles, as shown in Figure 2.5. The compiled results of different sand revealed that the γ_{tv} is independent of specimen fabric and initial effective confining pressure (Dobry et al. 1982; NRC 1985). Hazirbaba and Rathje (2009) investigated the influence of fines content on the γ_{tv} and observed the increase of γ_{tv} with increasing the fines content. In general, for most clean sand γ_{tv} ranged from 0.01% to 0.03%.

Liquefaction assessment using this approach was based on the premise of a volumetric shear strain threshold; if the earthquake-induced shear strain is higher than γ_{tv} level, pore pressure will be generated. The cyclic shear strain can be calculated alternatively to the stress-based simplified equation by (Dobry et al. 1982):

$$\gamma_c = \frac{\tau_c}{G} \tag{2.10a}$$

$$\gamma_c = 0.65\left(\frac{a_{\max}}{g}\right)\left(\frac{\sigma_v\, r_d}{G_{\max}\left(G/G_{\max}\right)_{\gamma_c}}\right) \tag{2.10b}$$

where G_{max} is the secant shear modulus corresponding to very low strain ($\gamma_c \leq 10^{-4}$%); $(G/G_{max})_{\gamma c}$ is the normalized secant shear modulus reduction ratio of soil corresponding to γ_c. This formula

must be used along with a modulus reduction curve (e.g., Darendeli 2001) to predict the G/G_{max} corresponding to γ_c.

A schematic illustration of the iterative solution of Eq. (2.10b) is shown in Figure 2.6. At first, an assumed value of G/G_{max} is used to compute γ_c (iteration 1). The value of γ_c is used to calculate the G/G_{max} at the second iteration. This procedure is repeated many times until the difference between the assumed and computed G/G_{max} is within a tolerable error.

The generated pore pressure ratio may be estimated as a function of calculated γ_c, Eq. (2.11), and the number of equivalent uniform strain cycles, $N_{eq\gamma}$, in conjunction with R_u-γ_c experimental obtained curves (Vucetic and Dobry 1988). [Note, Number of equivalent uniform strain cycles $N_{eq\gamma}$ is calculated corresponding to the assumption of $N_{eq\gamma} = N_{eq\tau}$ which is a function of earthquake characterization (Tokimatsu and Seed 1987; Green and lee 2006)].

$$R_u = \frac{\rho . f . N_{eq\gamma} . F . (\gamma_c - \gamma_{th})^s}{1 + f . N_{eq\gamma} . F . (\gamma_c - \gamma_{th})^s} \tag{2.11}$$

where R_u is the excess pore pressure ratio generated after $N_{eq\gamma}$ cycles of applied loading; f =1 or 2 for one- or two-dimensional loading, respectively; and p, F, and s are curve-fitting constants.

Although there is a consensus on the importance of the strain-based approach in pore pressure buildup and liquefaction assessment, it has not been employed in practice. In an attempt to adopt this approach practically in liquefaction evaluation, Rodriguez-Arriaga and Green (2018) proposed a substitute procedure based on a strain-based pore pressure model. They assessed the efficacy of their approach based on a compiled shear wave velocity (Kayen et al. 2013) and standard penetration (Boulanger et al. 2012) database. Their statistical analysis reveals the accuracy of the stress-based approach rather than the strain-based approach in liquefaction assessment. They postulated the deficiency of their alternative approach to ignoring the inherent softening effect, i.e. decrease of soil stiffness, occurred due to pore pressure buildup during the iteration simulation of the earthquake loading. In contrast, as will be discussed later, the softening effect is re-evaluated through the current study.

It is recognized that the main deficiency of strain-based method is determining the cyclic shear strain compared with cyclic shear stress during earthquake excitation (Seed 1980; Zhang et al. 2015). Castro (1987) proposed that the maximum shear strain experienced by the soil during cyclic loading is equal to the maximum induced displacement divided by the layer thickness.

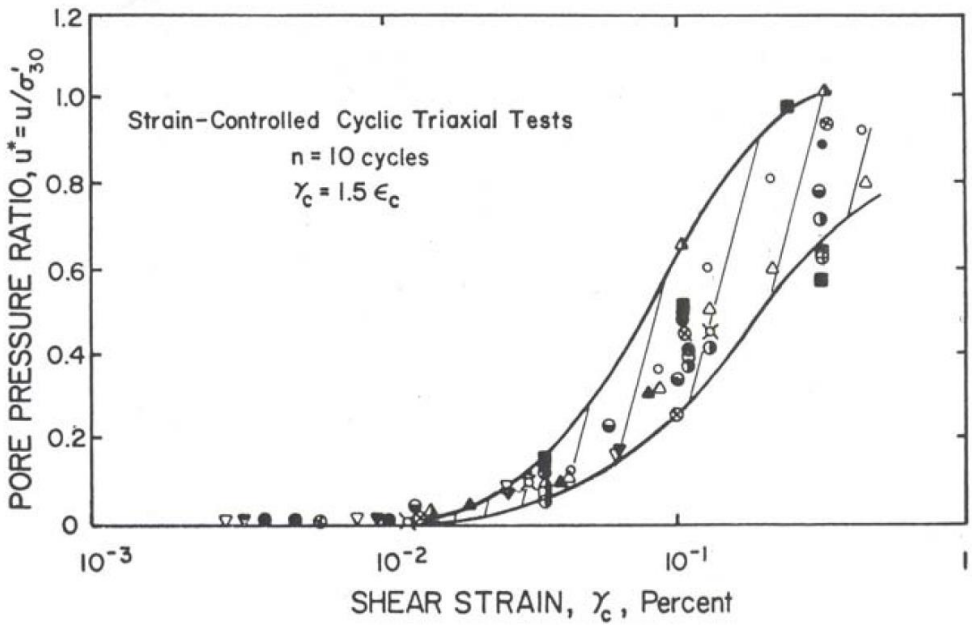

Symbol	Sand	σ'_{30} (psf)	D_r (%)	Samples/ Fabric	Measured u Peak (P) or Residual (R)
○	Crystal Silica	2,000	60	Dry Vibration	P
△	" "	2,000	60	Wet Rodding	P
▲	" "	2,000	60	Dry Vibration	P
▼	Sand No. 1	2,800	60	Moist Tamping	P
▽	" "	1,400	60	" "	P
○	Monterey No. 0	2,000	60	" "	P
●	" "	2,000	80	" "	P
□	" "	2,000	45	" "	P
⊠	" "	2,000	45	" "	R
■	" "	533	60	" "	P
⊕	" "	4,000	60	" "	P
⊖	" "	2,000	20	" "	R
•	Banding	2,000	60	" "	R
▲	"	2,000	40	" "	R
●	"	2,000	20	" "	R
●	Heber Road Point Bar	2,000	Dense	Tube Sample	R
◑	Heber Road Channel Fill	2,000	Loose	" "	R
⋈	Owi Island	2,000	40	Moist Tamping	R
⬡	" "	1,500	40	" "	R
⊕	" "	2,000	Medium Dense	Tube Sample	R
⊖	Mt. St. Helen Debris	2,000-4,000	50	Moist Tamping	R

Figure 2.5. Boundaries of generated pore water pressure ratio versus shear strain at N = 10 cycles for various sands and densities (from Dobry 1985)

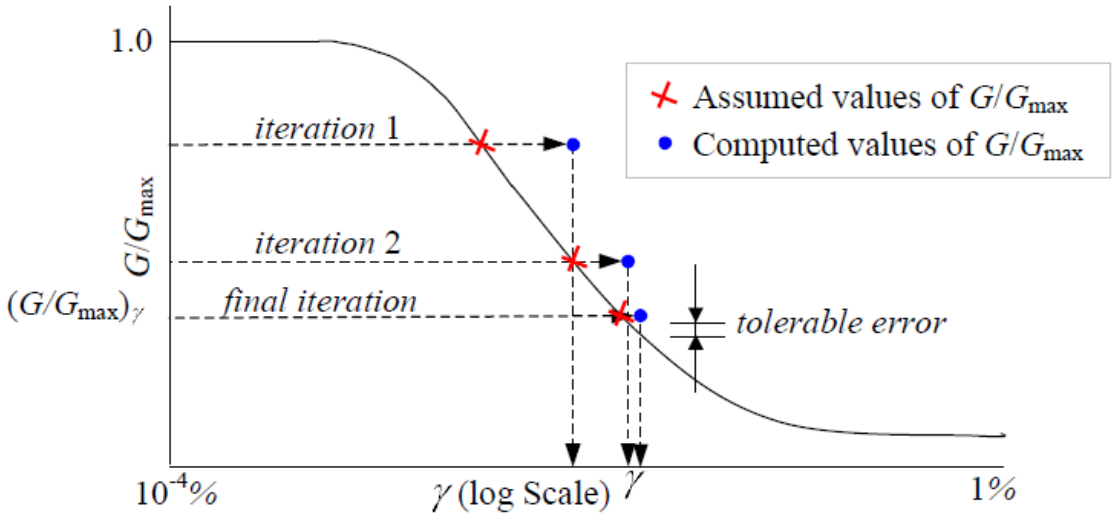

Figure 2.6. Determination of G/G_{max} corresponding to γ_c iteratively (from Green 2000)

2.3.3 Energy-based evaluation approach

In the 1970s, numerous energy-based liquefaction evaluation procedures have been developed after the pioneer work introduced by Nemat-Nasser and Shokooh (1979). Nemat-Nasser and Shokooh (1979) mathematically linked between the densification of soil in a drained test (infer to the excess pore pressure under undrained condition) to the needed dissipated energy for rearranging sand particles during cyclic loading. In the field realm, Davis and Berrill (1982) and Berrill and Davis (1985) adopted this approach in liquefaction potential evaluation by relating the pore pressure during earthquake loading to its magnitude, epicentral distance, initial effective overburden pressure, and SPT values. As much more, the energy concept was implemented in computing equivalent uniform stress cycles of irregular ground motion (Green and and Terri 2005) as well as in computing magnitude scaling factor (e.g. Arango 1996; Green 2001).

The normalized dissipated energy, W_s, is estimated by integrating the area bounded by hysteresis loops (CSR-shear strain relation). Under cyclic direct simple shear test, W_s can be indicated by the trapezoidal rule as schematically shown in Figure 2.7 and formulated as:

$$W_s = \frac{1}{2}\sum_{i=1}^{n-1}(CSR_{i+1} + CSR_i)(\gamma_{i+1} - \gamma_i) \qquad (2.12a)$$

for cyclic triaxial, CTX, formulated as:

$$W_s = \frac{1}{2\sigma_{co}^{'}} \sum_{i=1}^{n-1} (\sigma_{d,i+1} + \sigma_{d,i})(\varepsilon_{a,i+1} - \varepsilon_{a,i}) \quad (2.12b)$$

where $\sigma_{d,i}$ and $\varepsilon_{a,i}$ are the applied deviator stress and axial strain, respectively, at load increment i; τ_i and γ_i are the applied shear stress and strain, respectively, at load increment i.

Even though the energy-based procedure was proposed over 20 years ago, it is considered an important new direction in the liquefaction analysis (NCEER 1997) because it has several advantages comparing to other liquefaction procedures. For example,

(i) It is a typical scalar quantity that correlated to earthquake characteristics (e.g. the source to site distance, R, and earthquake magnitude, M) (Baziar and Sharafi 2011).

(ii) There is a unique correlation between the dissipated energy per unit volume of soil (W_s) and the generated pore pressure. The corollary of this finding is that variant energy-based pore pressure models have been integrated into the dynamic analysis (e.g. Yamazaki et al. 1985; Figueroa 1994; Green et al. 2000; Polito et al. 2008; Karray et al. 2015).

(iii) Recent liquefaction studies reveal that the required dissipated energy per unit volume of soil to triggering of liquefaction in laboratory is unique value and independent of the loading pattern (uniform, nonuniform or irregular) (e.g., Kokusho and Kaneko 2013; Polito et al. 2013) nor the frequency ranges (Law et al. 1990). Therefore, in liquefaction assessment, the dissipated energy imparted by an earthquake to soil layer "demand energy" is compared with that required to induce liquefaction "capacity energy" (e.g. Berrill and Davis, 1985; Law et al. 1990). Various relations have been obtained to determine the required dissipated energy to triggering of liquefaction as follows:

$$\log(W) = 2.02 + 0.00477\ \sigma_{\text{mean}}^{'} + 0.0116\ I_D \quad \text{(Figueroa et al. 1994)} \quad (2.13a)$$

$$\log(W) = 2.062 + 0.0039\ \sigma_{\text{mean}}^{'} + 0.0124\ I_D \quad \text{(Liang 1995)} \quad (2.13b)$$

$$\log(W) = 1.164 + 0.0124\ \sigma_{\text{mean}}^{'} + 0.0209\ I_D \quad \text{(Dief and Figueroa 2007)} \quad (2.13c)$$

$$\log(W) = 2.1028 + 0.004566\ \sigma_{\text{mean}}^{'} + 0.005685\ I_D + 0.001821\ FC - 0.02868\ C_u + 2.0214\ D_{50}$$

(Baziar and Jafarian 2007) (2.13d)

$$W = 0.1363\ \sigma_{\text{mean}}^{'}.I_D^{\,4.925} + 5.375\ (10^{-3}\sigma_{\text{mean}}^{'}) \quad \text{(Jafarian et al. 2012)} \quad (2.13f)$$

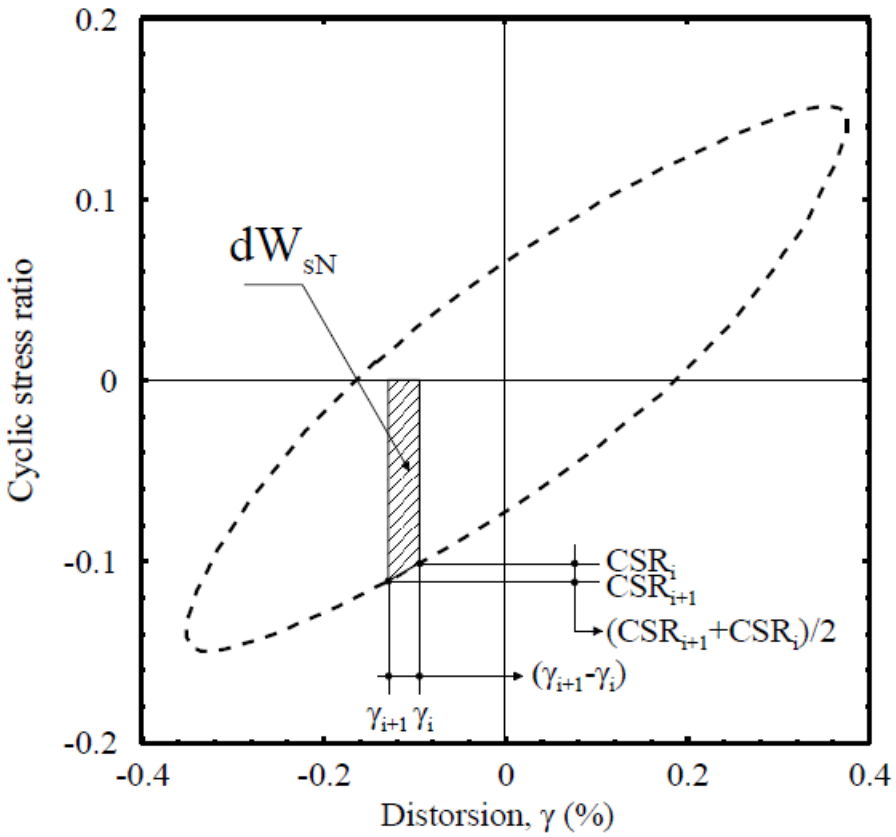

Figure 2.7. Schematic illustration of calculation the dissipated energy from the hysteresis loop (from Karray et al. 2015)

where W is the required strain energy for triggering of liquefaction (capacity), σ'_{mean} is the initial effective mean confining pressure (kPa) and I_D is the initial relative density in percent. FC is the percentage of fines content, C_u is the uniformity coefficient, and D_{50} is the mean grain size (mm).

(iv) In contrast to of stress- or strain-based method, adopting the energy concept in the liquefaction assessment circumvents the need for converting an arbitrary earthquake wave to equivalent uniform stress or strain cycles having the same damage effect. This may be the main limitation of stress- and strain-based models, as discussed in section 2.4.

In an actual liquefaction case study of in Tanno-Cho during the 2003 Tokachi-Oki earthquake, Kokusho and Mimori (2015) observed the superiority of the energy-based procedure in liquefaction assessment over the stress-based in case of a far-field earthquake. In spite of the low PGA (PGA = 0.056g), the 2003 far-field Tokachi-Oki ground motion is characterized by a long

duration and long-dominant period. Thus, the imparted energy is enough to trigger the liquefaction despite the low PGA. It may be attributed to the difference between the acceleration and the imparted energy during earthquake excitation. Moreover, the stress-based method does not consider the plasticity and the aging of liquefaction deposits which are implicitly counted in the cyclic response and dissipated energy during cyclic loading.

2.3.4 Numerical modeling analysis

Numerous research works have been done to simulate the dynamic response of soil deposits. As the induced shear strain exceeds the linear threshold values (i.e. 10^{-5}) the soil response becomes nonlinear which means that the tangential shear modulus deviates from its maximum values as a function of the induced shear strain. At low shear strain, soil stiffness is high with low damping, the effect of non-linearity at larger strains is magnified as reducing stiffness and increasing damping. Many elasto-plastic models have been developed over the last decades to simulate the nonlinearity of soils under cyclic loading. Practically, the most widely used models in geotechnical engineering are nonlinear and equivalent linear type models. A concise review of the equivalent linear and nonlinear analysis is presented in the following sections.

2.3.4.1 Equivalent linear method

The equivalent linear method was originally developed by Seed and Idriss (1969) which has been used in practice engineering to predict the seismic response. This method models the soil as linearly visco-elastic material by iterative updating the strain-dependent shear modulus (G) and damping ratio (D) during dynamic analysis in the frequency domain. This step is repeated iteratively until the convergence of estimated G/G_{max} and D between two successive iterations is within a tolerable error. Then, these values are incorporated in the dynamic analysis to determine the shear strain to be used in the subsequent step.

In the earlier attempts to code this procedure, Schnabel et al. (1972) introduced the SHAKE computer program to perform this iterative linear algorithm. Other updated versions of SHAKE software have been developed such as PROSHAKE, SHAKE91 (Idriss and Sun 1992) and SHAKE2000 (Ordóñez 2010).

To apply the equivalent linear method in dynamic analysis:

a. At first, estimate the maximum shear modulus G_{max} through the common relation:

$$G_{\max} = \rho V_s^2 \tag{2.14}$$

where ρ is the volumetric mass of soil

b. Define the reduction curves G/G_{max} and the damping curves versus the maximum cyclic strain γ_c. where G is the secant shear modulus which describes the slope of the hysteresis loop (Eq. 2.15, Figure 2.8). The damping ratio represents the hysteresis damping released during cyclic loading and proportional to the area bounded by the hysteresis loop normalized by elastic strain energy as formed by Eq. 2.16 and shown in Figure 2.8. The G/G_{max} degradation and damping ratio curves are usually obtained from laboratory tests or using the family of curves obtained by Darendeli (2001), as shown in Figure 2.9.

$$G_{\sec} = \frac{\tau_c}{\gamma_c} \tag{2.15}$$

$$D = \frac{1}{4\pi}\frac{A_l}{A_t} = \frac{1}{2\pi}\frac{A_{cycle}}{G_{\sec}\,\gamma_c^2} \tag{2.16}$$

It should be noted, although this method usually gives a good result, the obtained results from the nonlinear analysis are able to provide more accurate soil behavior. Moreover, the effective stress analysis cannot be formulated using the equivalent linear method. Practically, however, the equivalent linear analysis method is widely used among geotechnical engineers. The reason for that is the complexity of stress-strain constitutive models incorporated in the nonlinear method to simulate the subtle dynamic behavior as discussed in the following section.

2.3.4.2 Non-linear procedure

The nonlinear procedure is an alternative method to the equivalent linear method used, particularly, at higher intensity earthquakes which induce higher shear strain response (Beaty and Byrne 2000). In these cases, the equivalent linear method cannot capture accurately the dynamic response (in terms of shear modulus and damping ratio). The fully nonlinear produces a more accurate prediction of liquefaction-induced damage of geotechnical structures using a prescribed nonlinear shear-strain relation. There are many programs have been used to perform 1-D non-linear site analysis such as SUMDES (Li et al. 1992), OpenSees (Yang et al. 2008), and DEEPSOIL (Hashash et al. 2005). In contrast to the equivalent linear procedure, one run is

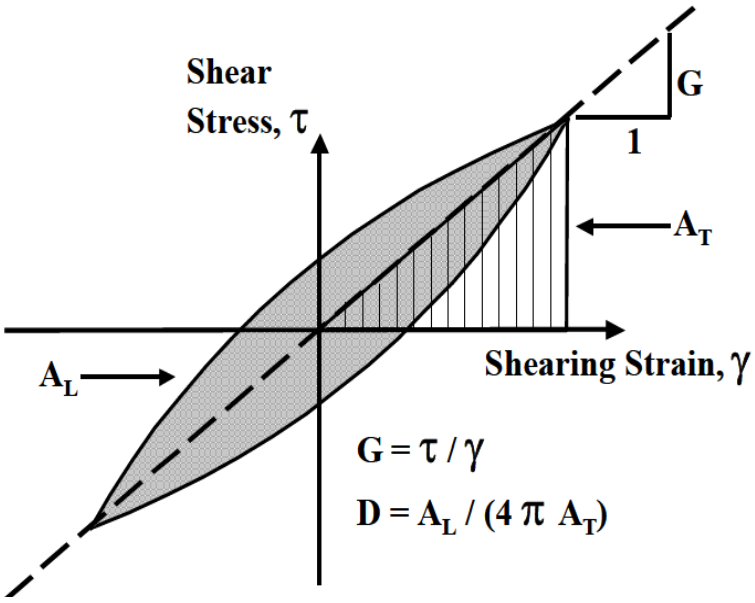

Figure 2.8. Definition of shear modulus and damping ratio in a shear test

performed to determine the dynamic response by solving the dynamic equilibrium equation of motion, Eq. (2.17), in the time-domain using the Newmark β method (1959).

$$[M]\{\ddot{u}\}+[C]\{\dot{u}\}+[K]\{u\}=-[M]\{I\}\ddot{u}_g \quad (2.17)$$

where [M], [C] and [K] are the mass, the viscous damping, and the stiffness matrices, respectively, {ü}, {u̇}and {u} are the vector of relative nodal acceleration, velocities and displacements, respectively.{$ü_g$} is the acceleration at the base of the soil column and{I} is a unit vector

Masing (1926) developed the earliest rules to simulate the nonlinear and hysteresis behavior of soil under cyclic loading. This model developed a hyperbolic rule to simulate the initial skeleton curve (the initial loading stress-strain curve). Masing rule assumed the formula of unloading/reloading is the same, however, scaled-up by a factor of two. However, Pyke (1979) reported that the factor of two is not rigorous while the unloading/reloading hysteresis loop is a function of the reversal stress level.

Figure 2.10 demonstrates loading, unloading and reloading curves according to Masing's Rule. The initial loading function can be expressed in the hyperbolic model as (Kondner and Zelasko 1963):

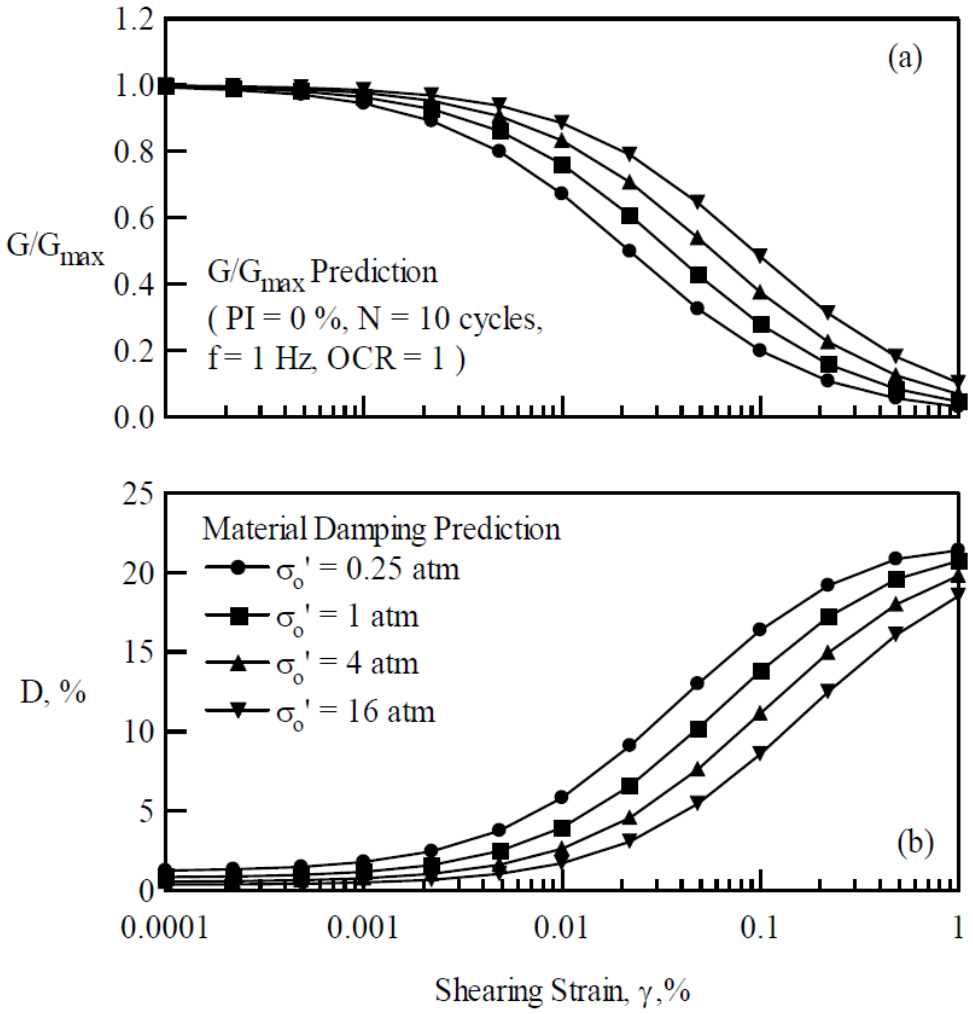

Figure 2.9. (a) G/G_{max} degradation curves (b) damping ratio as a function of shear strain (from Darendeli 2001)

$$\tau = f(\gamma) = \frac{G_{max}.\gamma}{1+(G_{max}/\tau_{max})|\gamma|} \tag{2.18}$$

where G_{max} is the maximum shear modulus at very low strain, τ_{max} is the shear strength of the soil.

The hysteresis loop during unloading and reloading can be described as:

$$\frac{\tau \pm \tau_a}{2} = f\left(\frac{\gamma \pm \gamma_a}{2}\right) \tag{2.19}$$

where γ_a and τ_a are the shear strain and shear stress at reversed point A, respectively. The negative sign is for unloading and the positive one for reloading.

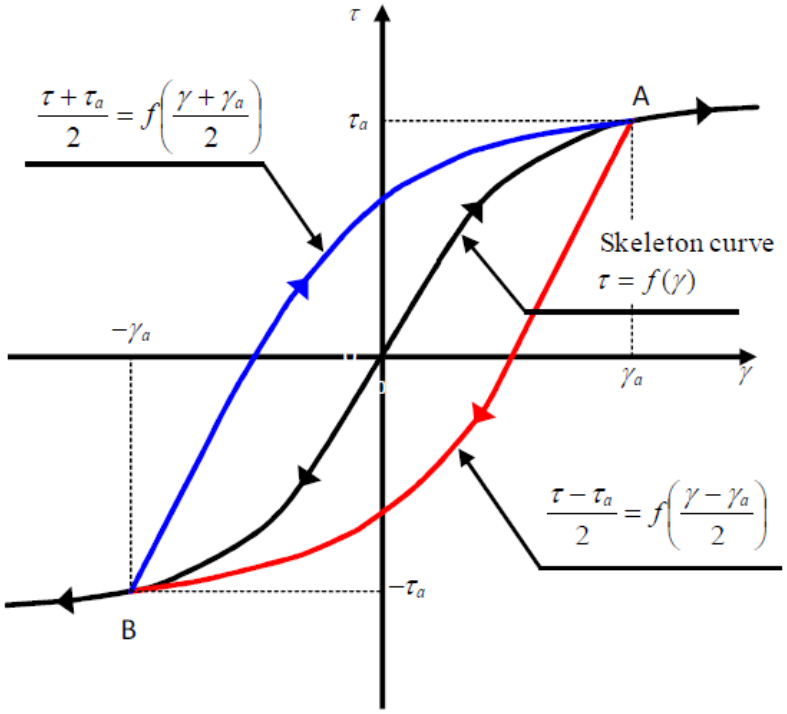

Figure 2.10. Loading, unloading and reloading curves based on Masing's Rule (from Ishihara 1996)

Other subsequent forms were developed to modify Kondner and Zelasko model (e.g. Hardin and Drnevich 1972; Matasović and Vucetic 1993; Ni et al. 1997; Hashash and Park 2001). Based on undrained cyclic tests on liquefiable sands, Matasovic and Vucetic (1993) modified Kondner and Zelasko (referred as MKZ) model by considering the vertical effective consolidation stress (σ'_{v0}) as the following form:

$$\tau^* = f^*(\gamma) = \frac{G^*_{max}.\gamma}{1+\beta\left(\frac{G^*_{max}}{\tau^*_{max}}\gamma\right)^s} \tag{2.20}$$

where $\tau^* = \tau/\sigma'_{v0}$, $\tau^*_{max} = \tau_{max}/\sigma'_{v0}$, $G^*_{max} = G_{max}/\sigma'_{v0}$, β and s are curve fitting parameters.

The soil softening in successive cycles due to pore pressure generation compiled by the degradation of soil stiffness is considered by updating the shear modulus (G) each time step as a function of the generated pore pressure ratio, R_u, as:

$$G = G_{max.}\left(1-R_u\right)^{0.5} \tag{2.21}$$

Phillips and Hashash (2009) developed a simplified non-linear constitutive model (Quadratic/Hyperbolic (GQ/H)) to accommodate Masing and non-Masing loading and unloading/reloading stress-strain curves, Eq. 2.22 and Eq. 2.23 respectively, which adopted in DEEPSOIL software.

$$\tau = \frac{G_{\max}.\gamma}{1+\left|\frac{\gamma}{\gamma_{ref}}\right|^{s}} \tag{2.22}$$

$$\tau = \frac{2\,G_{\max}((\gamma-\gamma_{rev})/2)}{1+\beta\left(\frac{\gamma-\gamma_{A}}{2.\gamma_{ref}}\right)^{s}} + \tau_{A} \tag{2.23}$$

$$\gamma_{ref} = a\left(\sigma_{v0}{}'/\sigma_{ref}\right)^{c} \tag{2.24}$$

where a and c are constants depend on the soil type and σ_{ref} is reference stress. Further, Groholski et al. (2016) incorporated the GQ/H model with a PWP model, termed (GQ/H+u) to compute the PWP and accounted for the soil softening and degradation of soil stiffness during shaking. This model featured by establishing a backbone curve formulation captures both small- and large-strain soil behavior.

In this study, the nonlinear behavior is implemented into FLAC software (Itasca) via the sigmoidal equation (referred SIG4 model) with four parameters (a, b, x_0 and y_0) which incorporate the shear modulus and damping ratio functions to simulate the non-linear stress-strain relationships. The secant shear modulus, G_s, is obtained from SIG4 model parameters as formed in Eq. (2.25). The SIG4 model parameters are calibrated from the degradation and damping ratio curves obtained from a set of cyclic strain-controlled tests conducted in the new combined triaxial simple shear apparatus (referred as T_xSS) as discussed in chapter 7.

$$G_s = y_0 + \frac{a}{1+\exp\left(-(L-x_0)/b\right)} \tag{2.25}$$

2.4 Equivalent number concept

The concept of equivalent number of uniform cycles is based on the premise that an irregular earthquake load can be represented by uniform cycles that have the same damage effect. It was first applied to metal fatigue analysis to convert nonuniform loading resulting from machines and traffic loads to equivalent-damage uniform loads using various cumulative damage hypotheses (Green and Terri 2005). The equivalent number concept was adopted in the realm of liquefaction evaluation by H.B. Seed and his colleague in Niigata liquefaction analysis by adopting the Palmgren–Miner (*P–M*) cumulative damage hypothesis (e.g., Seed and Idriss 1971; Seed et al. 1975; Annaki and Lee 1977). The equivalent uniform cycles may be either stress or strain histories with an average amplitude equals to a percent (R) of the maximum amplitude in irregular earthquake pattern, $S_{ref} = R*S_{max}$ (Seed et al. 1975). The recommended value of R is 0.65 based on historical events. Other researchers observed that the computed equivalent number, $N_{eq\tau}$, is independent of the selected R value and can be ranged from 0.55 to 0.85 (Lee and Chan 1972; and Annaki and Lee 1977). Through cyclic triaxial tests conducted by Pan and Yang (2017), it was found that the converting factor is not unique and depends on the cyclic amplitude and sequence of loading cycles. An empirical formal was proposed by Tokimatsu and Yoshimi (1983) to determine this reduction value (R) as a function of earthquake magnitude (M) as:

$$R = 0.1(M-1) = 0.65/MSF \tag{2.26}$$

The main advantage of the conversion process is one set of laboratory test data can be used to evaluate many earthquake motions in addition to facilitate the liquefaction assessment (Seed et al. 1975).

2.4.1 Palmgren-Miner cumulative damage hypothesis (P-M)

The converting concept was applied first in standard fatigue evaluation of metal components using several applicable approaches. The widely used approach is the Palmgren–Miner (P–M) cumulative damage hypothesis. It was introduced by Palmgren (1924) and further developed by Miner (1945). The P–M method was considered less than ideal, nevertheless it is logical, simple procedure, and relatively in good agreement with experimental data for various metals at different test conditions. The *P-M* hypothesis was intended for high cycle fatigue conditions

(large number of cycles – low amplitude). So it was applied for the strains constrained to the elastic range of material.

The basic assumption of the *P-M* hypothesis is that the damage accumulates linearly during cyclic loading. Thus, the cumulative damage under uniform or nonuniform load cyclic loading can be obtained from Eq. (2.27) irrespective of the load characteristics (e.g. frequency and amplitude). However, Martin et al. (1975) founded that the absolute amplitude and sequence of peaks in shear strain time history influence the resulting volumetric strain.

$$D = \sum_i \frac{n_i}{N_{fi}} \tag{2.27}$$

where i defines each stress level; n_i is the number of cycles having peak stress amplitude S_i; N_{fi} is the number of cycles required to cause failure (D = 1) at the same stress intensity.

Miner (1945) founded that the applied work (energy) during any stress cycle has accumulative damage, D, effect on the material which was assumed to be directly proportional to the energy level at failure regardless of the loading pattern and load sequence (Annaki and Lee 1977). Thus, Eq. (2.27) can be written as:

$$D = \sum_{i=1}^{m} \frac{w_i}{W} = \sum_{i=1}^{m} \frac{n_i}{N_{fi}} \tag{2.28}$$

where w_i is the absorbed work after n_i cycles; m is the number of peaks in loading time history, and W is the absorbed work at failure.

The equivalent number of uniform stress cycles, $N_{eq\tau}$, having reference stress amplitude S_{ref}, which has the same damage effect of an arbitrary pattern and induces failure in N_{ref} cycles, can be obtained following the P-M hypothesis (Annaki and Lee 1977):

$$D = \frac{N_{eq\tau}}{N_{ref}} = \sum_i \frac{n_i}{N_i} \tag{2.29}$$

or

$$N_{eq\tau} = N_{ref} \sum_i \frac{n_i}{N_i} \tag{2.30}$$

Eq. (2.29) is valid only when the material response is constrained to the elastic range (high cycle fatigue conditions). N_{ref}/N_i is commonly referred as weighting factor (WF) (e.g. Liu et al. 2001; Green and Terri 2005; Green and Lee 2006).

2.4.1.1 Weighting factor

In the late 1960s to the early 1970s, H.B. Seed and his colleagues adopted the P-M hypothesis to compute N_{eq}, for site response analysis and for evaluating soil liquefaction potential. A weighting procedure was developed in which the effect of each cycle of an irregular pattern was given a weighting factor based on the liquefaction potential (CSR–N_{liq}) curve (Seed et al. 1975). The CSR–N_{liq} curve for soil can be determined by performing uniform cyclic tests with different stress amplitude and obtain the number of liquefaction cycles, where CSR = $\tau_{cyc.}/\sigma'_{vo}$ and N_{liq} is the number of applied cycles required to trigger the liquefaction, as shown in Figure 2.11. By using the CSR-N_{liq} curve, any given stress cycle can be simulated with a number of equivalent damage stress cycles having a reference stress amplitude. CSR-N_{liq} curve is analogous to well-known S-N curve introduced by Palmgren (1924) and Miner (1945) for metal fatigue studies, where S is uniform cyclic shear stress amplitude applied on a metal component, N is a number of cycles to cause a specific degree of strength deterioration (Annaki and Lee 1977).

As shown in Figure 2.11, the fatigue limit in the CSR-N_{liq} curve is the CSR corresponding to the threshold strain ($CSR_{threshold\ strain}$). Lefebvre and Serge (1987) defined the threshold cyclic stress from cyclic triaxial tests performed on sensitive clay as the maximum cyclic stress amplitude at which no failure can be observed regardless of the number of applied cycles. In the same contest, the threshold strain is defined as a cyclic shear strain below which there is no pore water pressure buildup of saturated sands (Dobry 1982; Vucetic 1994). If the threshold strain is not exceeded, no pore pressure generation will happen, irrespective of the number of loading cycles. As previously discussed, the cyclic threshold is approximately constant ($\gamma_c=10^{-2}$ %) for a given type of sand irrespective of reconstitution characteristics (e.g. relative density, fabric, over-consolidation ratio) (Dobry 1982).

It is well recognized that the shape and position of the CSR-N_{liq} curve vary from site to other based on the earthquake and soil characteristics (e.g. soil fabric, soil density), Seed et al. 1975 normalized the CSR–N_{liq} curve such that the resulting shape was fairly representative of most sands regardless of soil state, Figure 2.12, wherein CSR_1 is the needed cyclic stress ratio to cause liquefaction in one cycle, FS is a “safety factor” and α is the normalized peak amplitude of the resulting uniform cyclic load. The value of α was selected as 0.65 (Seed and Idriss 1971;

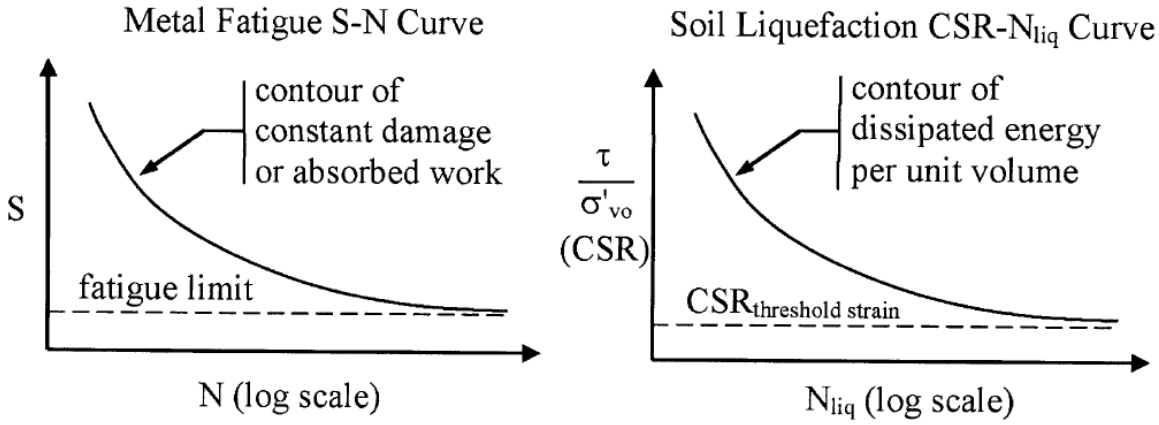

Figure 2.11. Metal fatigue (*S–N* curve) and liquefaction potential (CSR-N_{liq}) curves (from Green and Terri 2005)

Seed et al. 1975). However, Lee and Chan (1972) used another value (0.65 and 0.85). The weighting factor curve proposed by Seed et al. (1975), with FS=1.5 and α=0.65, is shown in Figure 2.12. This curve is implemented in computing the N_{eq} to demonstrate the difference of cyclic response between eastern and western North America (Chapter 7).

Based on the one-dimensional analysis of 15m deposit subjected to different seismic events, using the Imperial College Finite Element Program (ICFEP), Norambuena et al. (2019) demonstrated that the validity of the simplified method is motion dependant (i.e., Shock or vibratory). They observed that the findings of vibratory type motions are very conservative in contrast to Shock type motions, non-conservative. Green et al. (2018) criticized the computing of N_{eq} using Seed et al. procedure as:

- The assumption of the constant N_{eq} along the depth is not usually reliable. This issue was previously discussed by Annaki and Lee (1977) and Green and Terri (2005). Annaki and Lee (1977) reported the variation of N_{eq} with depth may be more related to the relative ratio between the fundamental period of deposit and predominated period of motion. Green and Terri (2005) observed that N_{eq} is different within the depth as a function of earthquake magnitude, M and site to source distance, r. This difference between both conclusions may be attributed to the adopted hypothesis. Lee and Chan (1972) used the P-M hypothesis which constrained to high cycle fatigue and did not consider the non-linear behavior of the soil while Green and Terri (2005) adopted an alternative P-M hypothesis in computing N_{eq}

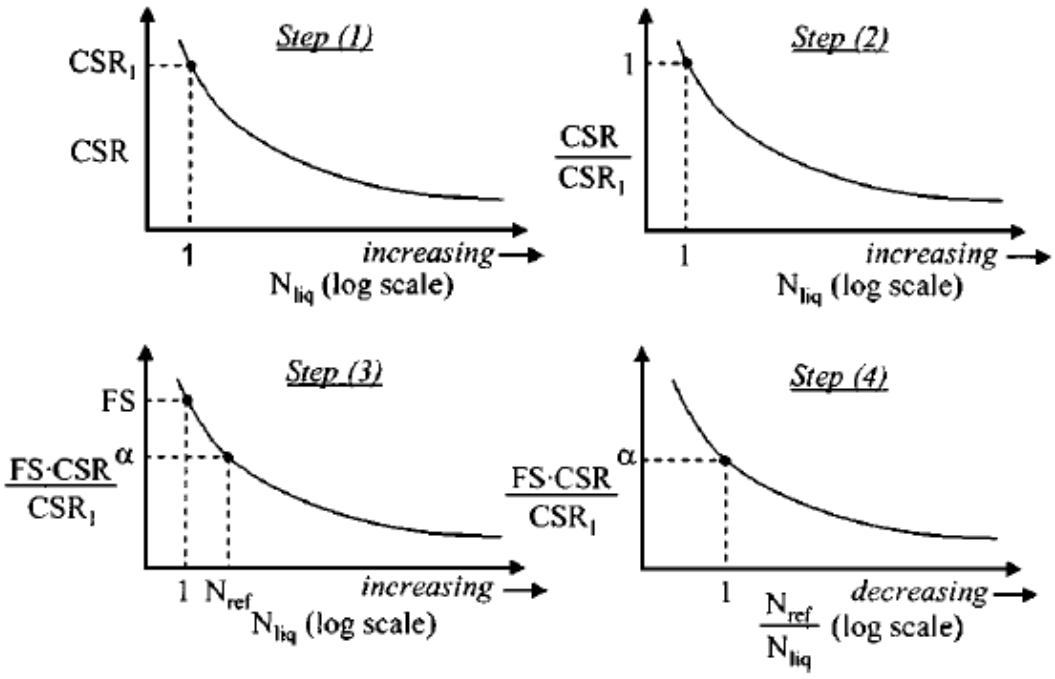

Figure 2.12. The sequence of steps used by Seed et al. (1975) to normalize a CSR-Nliq curve (from Green and Terri 2005)

(section 2.4.3). Gheibi and Bagheripour (2011) performed nonlinear dynamic analysis using the DEEPSOIL program and observed that the N_{eq} decreases by depth. They justified that as the earthquake loads impose more vibrating cycles to upper layers.

- Seed et al. (1975) neglected the weight of stresses having a relative amplitude ratio less than 35% of the maximum shear stress. They postulated that as these stresses do not have a significant contribution to the overall effect of the stress history developed.
- The assumption of the similar characteristics of both two horizontal earthquake motion and treat each component separately is not valid in all cases particularly in the near-fault region (Carter et al. 2014).

2.4.2 Richart-Newmark cumulative damage hypothesis (R-N)

Richart and Newmark (1948) proposed a variant of the P-M hypothesis in which the cumulative damage depends on stress level and load sequence as well as cyclic ratio (R_n), where $R_n=n/N_f$, where n is number of cycle in time history and N_f is number of failure cycles, in contrary to P-M hypothesis. As the material is load dependent, the relation between cumulative

damage and cycle ratio (D-R ratio), is represented by family of curves as shown in Figure 2.13 and can be simulated by;

$$D = \left(\frac{n}{N_f} \right)^r \tag{2. 31}$$

where r is the material parameter that depends on the load amplitudes. For applied cyclic stress or strain time history consisting of sequential cycles n_1, n_2, and n_m have varying peak amplitudes of S_1, S_2, and S_m, the cumulative damage has the functional form:

$$D_m = \left[\left(D_{m-1} \right)^{\frac{1}{r_m}} + \left(\frac{n_m}{N_m} \right) \right]^{r_m} \tag{2.32}$$

where m is the total number of sequence peaks in the load history. The previous arbitrary load which results in cumulative damage, D, can be represented with equivalent number of cycles, $N_{eq,}$ having amplitude S_{ref} and induce failure in N_{ref} cycles as:

$$D = \left(\frac{N_{eq}}{N_{ref}} \right)^{r_{ref}} \tag{2.33}$$

$$N_{eq} = N_{ref} \left[\left(D_{m-1} \right)^{\frac{1}{r_m}} + \left(\frac{n_m}{N_m} \right) \right]^{r_m / r_{ref}} \tag{2.34}$$

where r_{ref} is the material parameter corresponding to the load amplitude S_{ref}. The P-M hypothesis can be considered as a special case of the R-N hypothesis when r = 1 for all load amplitudes. That case occurs when the material is load-independent, i.e. D-R ratio (Figure 2.13) is simulated at different stress ratios with one line as in P-M hypotheses. Another limitation of applying either P-M or R-N hypotheses is the definition of "peak or valleys" in acceleration time histories. There are many counting methods compiled by Dowling (1971) and revisited by ASTM (2011). However, most of researches that concerned by the computation of N_{eq} do not explicitly state which counting method is employed.

However, Green and Terri (2005) believed that the peak-between-mean crossing count, as shown in Table 2.1, has been used in most previous studies, wherein only the largest peak between successive zero-crossing was counted. It is noteworthy that the peak count method is considered, where all peaks above the mean and all valleys below the mean were counted, in computing $N_{eq\gamma}$ using the R-N hypothesis (Green and Terri 2005; Hancock and Bommer 2005; ASTM 2011).

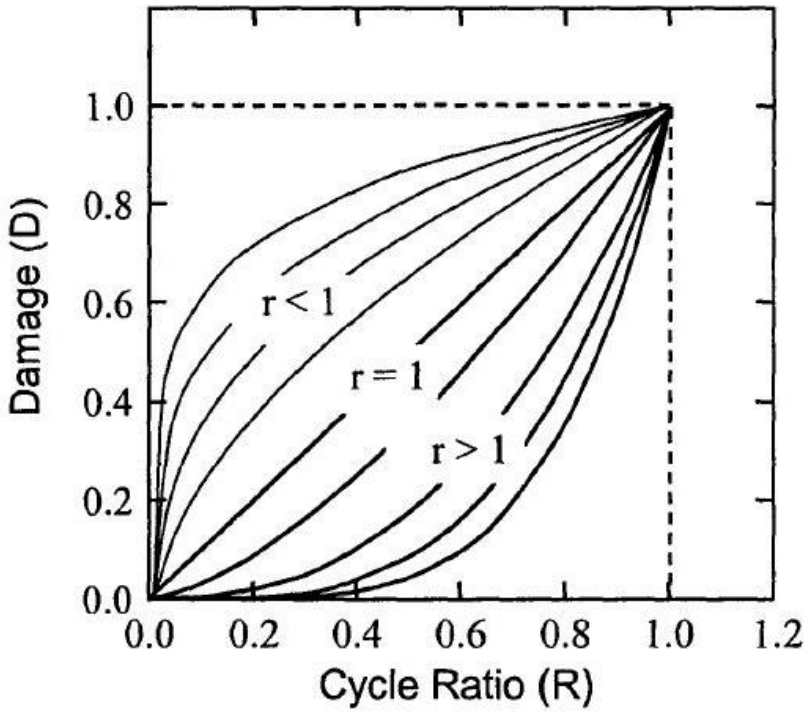

Figure 2.13. Damage-cycle ratio relationship proposed by Richart and Newmark (1948)

Table 2.1. Peak counting methods (adapted from Dowling 1971)

Name	Example	Description
Peak count	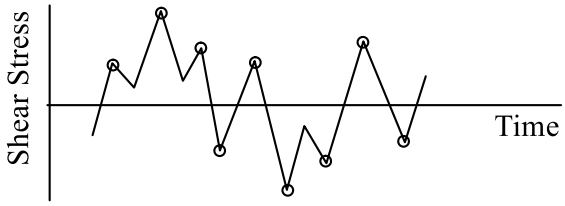	All maximums above the mean and all minimums below the mean are counted
Peak-between-mean crossing count	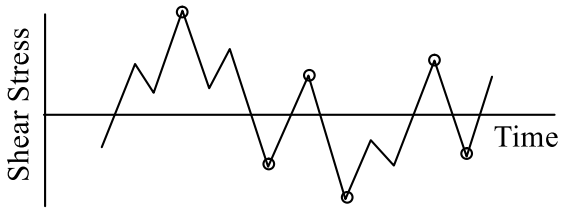	Only the largest peak between successive crossings of the mean is counted

As previously mentioned, adopting the energy concept in liquefaction assessment circumvents the need for converting earthquake motion to equivalent uniform cycles. However, due to the importance of N_{eq} in liquefaction assessment, Green and Terri (2005) adopted the energy concept in N_{eq} computing.

2.4.3 Alternative Implementation of Palmgren–Miner Hypothesis for Liquefaction Evaluations

Dividing Eq. (2.29) by Eq. (2.28) gives:

$$\frac{W}{w_1}\sum_{i=1}^{m}\frac{w_i}{W}=\frac{N}{n_1}\sum_{i=1}^{m}\frac{n_i}{N_{fi}} \tag{2. 35a}$$

$$\sum_{i=1}^{m}\frac{w_i}{w_1}=\frac{1}{n_1}\sum_{i=1}^{m}\frac{N_1}{N_{fi}}n_i \tag{2. 35b}$$

The right hand side of the above expression reduces to Eq. (2.28) when n_1 is equal to 1:

$$\sum_{i=1}^{m}\frac{w_i}{w_{ref\,(1cycle)}}=\sum_{i=1}^{m}\frac{N_{ref}}{N_{fi}}n_i \tag{2.35c}$$

where N_{ref} / N_i is commonly referred as a weighting factor (WF), $\omega_{ref\,(1cycle)}$ is the absorbed work resulting from the application of one cycle of loading having amplitude S_{ref}. Accordingly, N_{eq} can be expressed in terms of absorbed work;

$$N_{eq}=\sum_{i=1}^{m}\frac{w_i}{w_{ref\,(1cycle)}} \tag{2.36}$$

An alternative implementation of the P-M hypothesis Eq. (2.36) is more applicable as it alleviates the inherent constraint of the P-M hypothesis in elastic range. Consequently, Eq. (2.36) can be used to compute N_{eq} for both cases of low cycle fatigue conditions and high cycle fatigue conditions. However, applying this formula in undrained cyclic loading does not consider the softening of the soil due to the pore pressure buildup (Green 2001).

Thus the following expression was referred as "Green–Mitchell energy-based liquefaction evaluation procedure" which derived to consider the soil softening in dissipated energy calculating.

$$w_{(1cycle)0j} \approx w_{(1cycle)\,j}\cdot\left(\frac{\sigma'_{mj}}{\sigma'_{m0}}\right)^{1.65} \tag{2.37}$$

where σ'_{mo} is the initial mean effective confining stress, σ'_{mj} is the mean effective confining stress at the j^{th} cycle of loading ($\sigma'_{mo} \geq \sigma'_{mj}$), $w_{(1\ cycle)j}$ is the amount of the energy per unit volume dissipated in the soil during the j^{th} cycle of loading, and $w_{(1\ cycle)\ 0j}$ is the dissipated energy per unit volume when it had been shear at confined of σ'_{mo}.

Eq (2.28) for the P–M hypothesis can be written as:

$$\sum_{i=1}^{m} \frac{w_{0i}}{w_0} = \sum_{i=1}^{m} \frac{n_i}{N_{fi}} \tag{2.38}$$

where w_{oi} is the adjusted dissipate energy per unit volume of soil after n_i cycles (Eq. 2.17). w_0 is the adjusted energy dissipated in a unit volume of soil at failure (Green and Mitchell 2001).

As reported by Green and Terri (2005), adopting of energy concept and the variant Green–Mitchell in the liquefaction evaluation procedure magnify the using the P–M hypothesis in liquefaction evaluation and computing N_{eq}. Hence, Eq. (2.36) can be rewritten in the following formula:

$$N_{eq} = \sum_{i=1}^{m} \frac{w_{0i}}{w_{ref\,(1cycle)0}} \tag{2.39}$$

It is noteworthy that the previous formula was applied in the present study to demonstrate the difference between eastern and western North America earthquake response (Chapter 7).

Computer Code SHAKE91 was used by Green and Lee (2006) to perform dynamic response analysis of the Landers earthquake (1992 - M7.3) in South California. As shown in Figure 2.14, the number of equivalent strain cycles, $N_{eq\gamma}$, for each layer were computed by using both of R-N and P-M hypotheses as well as computed by the alternative P-M hypothesis outlined in Green and Terri (2005), Eq. (2.39). It was concluded that $N_{eq\gamma}$ values are over predicted using the P-M hypothesis, as previously discussed in the limitations of the P-M hypothesis. In contrast, there is a good agreement between $N_{eq\gamma}$ determined using the R-N approach and $N_{eq\tau}$ determined by equating dissipated energy, Eq. (2.39). In this vein, the Byrne model was adopted to compute N_{eq} for a random load by equating the cumulative volumetric strains induced by the random load to that induced by N_{eq} of a sinusoidal load having amplitude equal to 0.65 times the maximum absolute value in earthquake motion (Carter et al. 2014). In the same contest, Lee (2009) compared the difference in the cyclic response between ENA and WNA in terms of $N_{eq\tau}$, $N_{eq\gamma}$, earthquake magnitude, depth, and site distance. Their finding reveals that the $N_{eq\tau}$ and $N_{eq\gamma}$ either

in ENA or WNA increase with distance and magnitude increase. The predicted $N_{eq\gamma}$ for ENA model is more depth dependent comparing to the WNA model.

In this study, the R-N hypothesis was implemented in conjunction with an experimental program to propose a simple pore pressure buildup formula to be used as damage metric in determining the number of equivalent uniform strain cycles. This concept was used to compare the results obtained in the folds of this thesis.

2.5 Pore pressure build-up and energy concept.

The build-up of earthquake-induced excess pore-water pressure may be viewed as analogous to the cumulative damage of saturated granular materials caused by cyclic loading. Numerous research works have been performed over years to study the pore water pressure generation to reveal the mechanism of generation and develop constitutive numerical model for predicting site response (e.g. Seed et al. 1975; Martin et al. 1975; Dobry 1985; Matasovic and Vucetic 1993; Green et al. 2000; Polito et al. 2008; Chiaradonna et al. 2016; Pan and Yang 2017). These models have been embodied in software codes to perform 1-D dynamic site analysis such as DESRAMOD, DMOD, and DEEPSOIL.

The generated excess pore pressures in a saturated soil during earthquake shakings or cyclic loading can be separated into two components: transient and residual. The transient pore pressure represents the changes in the applied mean normal stresses resulting from the dynamic loading, while the residual excess pore pressures resulting from the progressive rearrangement of soil particles and collapse of soil the skeleton during each successive cycle of loading (i.e., plastic deformations) (Ishibashi et al. 1977; Polito et al. 2008; Lenart 2008; Yang and Pan 2018). Sitharam et al. (2002) explained the pore pressure generation according to microstructure changes during a dynamic loading as the internal force changes simultaneously with the reverse of shear stress direction in dynamic loading to be in equilibrium with the applied loading. However, the anisotropic fabric for loose specimens cannot be immediately changed to the new direction which results in de-structuring of the bond between particle contacts in the minor stress direction represented in “average co-ordination number”. The decrease in the average co-ordination number leads to a decrease in the effective mean stress and an increase in pore pressure under undrained conditions.

Expecting the pore pressure buildup during cyclic loading considered as the main challenging in the numerical simulation and liquefaction investigation. A variety of stress- (Seed et al. 1975) and strain-based (Martin et al. 1975; Dobry et al. 1985) models have been developed to estimate residual pore water pressure generation in saturated soil subjected to earthquake loading. Nemat-Nasser and Shokooh (1979) developed differential equations relating energy dissipation to the densification of dry specimens and to the generation of excess pore-water pressure in saturated specimens. This mathematical model linked the energy dissipated per unit volume in the densification of dry sands and pore pressure generation of fully saturated sands. Subsequently, energy-based pore pressure models have received considerable attention as there is no need to convert earthquake motions to equivalent uniform cycles in contrast to other stress- and strain-based methods (e.g., Berrill and Davis 1985; Green et al. 2000; Green and Mitchell 2001; Kokusho 2013; Karray et al. 2015). Recently, Ivšic´ (2006) implemented the damage concept, which previously proposed by Finn and Bhatia (1982), to develop a damage-based pore water pressure model. Park et al. (2015) incorporated Ivšic´ model to propose an alternative Seed model that can be used in coupled effective stress analysis without the need to convert the earthquake motion to equivalent uniform cycles.

A summary of the most used pore pressure models with brief advantages and limitations is listed in Table 2.2. Throughout the current study, a simple formula was proposed based on the number of loading cycles and another one based on the energy concept. The latter was incorporated in numerical simulation of cyclic behavior under direct simple shear and triaxial conditions (Chapter 5 and 6) as well as in 1-D effective stress analysis (Chapter 7).

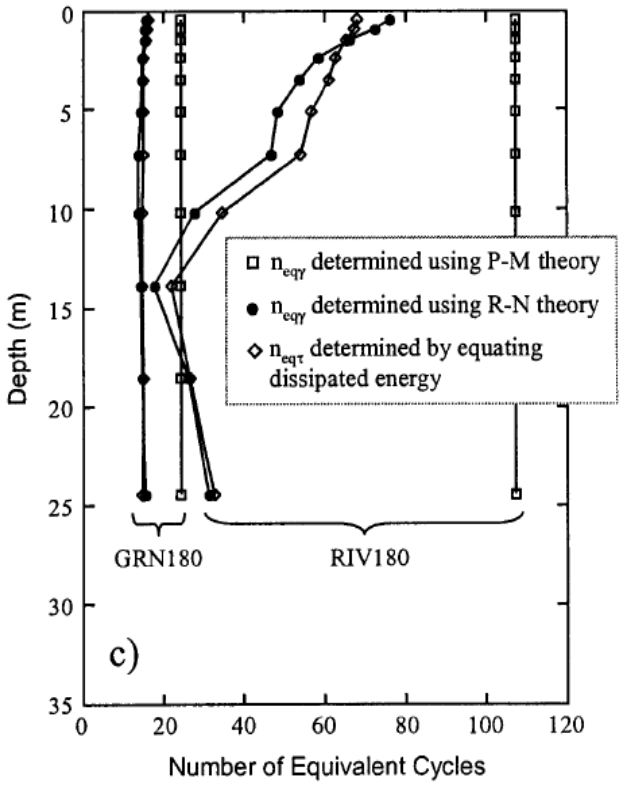

Figure 2.14. Computed $N_{eq\gamma}$ and $N_{eq\tau}$ for two earthquake motions from the 1992 M7.3 Landers earthquake using different methods (from Green and Lee 2006)

Table 2.2. Summary of the commonly used pore pressure models

Model	***Model Formula***	***Description and limitation***
Seed et al. (1975)	$R_u = \frac{1}{2} + \frac{1}{\pi} arc\sin\left[2\left(R_n{}^{1/\alpha}\right) - 1\right]$	- It is considered as the earliest pore pressure model obtained from the experimental results of simple shear tests performed on Monterey No.0 sand by (De Alba et al. 1975). - α is an empirical parameter suggested to be equal to 0.7. Polito et al. (2008) statistically evaluated Seed et al. model and concluded that α=0.7 is too low, except for silty sands subjected to small CSR. Moreover, it depends on FC, I_d, and CSR. - It was incorporated in a finite element model by numerous researchers for effective stress analysis (e.g. Martin and Seed 1979). - It has been applicable for non-plastic silts and for different experimental elements Baziar et al. (2011). - Limitations: - Earthquake motion shall be converted to equivalent uniform cycles. - It is not applicable to plastic soil, i.e. non-liquefiable soil.
Booker et al. (1976) (adjusted Seed et al. 1975 model)	$R_u = \frac{2}{\pi} arc\sin(2R_n{}^{1/2\alpha})$	
Ishibashi- Sherif (1978) and Ishibashi et al. (1982)	$\Delta R_{uN} = (1 - \Delta R_{u\,N-1}) * (\frac{6.13N}{N^{1.77} - 0.46})(\frac{\tau_N}{\sigma'_{N-1}})^{2.4}$	- It is applicable for uniform and nonuniform cyclic loading. - Frequency was not considered because it doesn't have a highly significant effect on the pore pressure rise.
Martin et al. (1975)	$\Delta R_u = E_r . \Delta\varepsilon_{vd}$	- Based on strain-controlled cyclic simple shear tests on cubic dry sand specimens.

	$\Delta\varepsilon_{vd} = C_1(\gamma - C_2.\varepsilon_{vd}) + \frac{C_3.\varepsilon_{vd}^2}{\gamma + C_4.\varepsilon_{vd}}$ $E_r = \frac{(\sigma_v^{'})^{1-m}}{mk_2(\sigma_{v0}^{'})^{n-m}}$	- A semi-empirical model linking the increment of volumetric strain per loading cycle and the rebound modulus, E_r, to excess pore pressure generation in undrained saturated sand. - Converting earthquake loading to equivalent uniform cycles is not necessary. - Finn et al. (1976, 1977) incorporated this model in an effective stress based constitutive model, program DESRA, which has been widely used for ground response and liquefaction assessments. Also, it is written in the library of dynamic coupled stress flow finite difference software Fast Lagrangian Analysis of Continua (FLAC).
Byrne (1991) (modified Martin et al. 1975 model)	$\frac{\Delta\varepsilon_{vd}}{\gamma} = C_1.\exp\left(-C_2.\frac{\varepsilon_{vd}}{\gamma}\right)$ $C_1 = 7600\ (I_d)^{-2.5}$ $C_2 = 0.4/C_1$	- Simplified Martin et al. model developing a new model implemented in the FLAC. - Limitation: soil skeleton during unloading is not the same for drained as for undrained condition, (Ishibashi et al. 1977; Dobry et al. 1985, and recently by Ueng et al. 2000). - Martin et al. (1975) model was underestimated the excess pore water pressure value compared with VELACS laboratory (centrifuge results), (Nabili et al. 2008a,b).
Dobry et al. (1985), *Vucetic and Dobry (1988).*	$R_u = \frac{\rho.N.F.(\gamma_c - \gamma_{th})^s}{1 + N.F.(\gamma_c - \gamma_{th})^s}$	- Based on strain-controlled cyclic test results of Dobry (1982) and the model of Martin et al. (1975). - Finn and Bhatia (1980) model which based on the results of a series of constant-volume, cyclic strain controlled DSS tests. - Limitation: It is not considered the dilatancy effect of medium dense (I_D =

		60%) or dense sand (I_D = 80%) when shearing at $\gamma_c \geq 0.8\%$.
Green et al. (2000) (GMP)	$R_u = \sqrt{\frac{W_s}{PEC}}$ $PEC = \frac{W_{S,R_u=0.65}}{0.4225}$ $PEC = \begin{cases} \exp\ (c_3 I_d) + c_4 \\ c_1\ FC^{c_2} + \exp\ (c_3 I_d) + c_4 \end{cases}$ c_1 = -0.597,c_2 = 0.312, c_3 = 0.0139, and c_4 = -1.021	- GMP model relates pore water pressure ratio, R_u to the energy dissipated per unit volume of soil and Pseudo Energy Capacity, PEC. - Earthquake motions are not required to convert to an equivalent uniform load. - W_s is calculated from the hysteresis loop during cyclic loading. - It was developed for non-plastic silt-sand mixtures from clean sands to pure silts. However, it is not applicable to plastic soil. - It does not consider the dilatancy effect of dense sand ($I_D \geq 85\%$) during dynamic loading.
Park et al. (2015)	$R_u = \frac{2}{\pi}\arcsin\left(\frac{D}{D_{r_u=1}}\right)^{1/2\beta}$	- It was calibrated based on the test data of different sand specimens conducted by Silver and Park (1976); Carraro et al. (2003); and Park and Kim (2013). - It can be incorporated in a coupled effective stress analysis model without the need to convert earthquake motion to equivalent uniform cycles. - It needs further verification based on cyclic direct simple shear besides cyclic triaxial tests.
Chiaradonna et al. (2016)	$r_u = a\left(\frac{\kappa}{\kappa_L}\right)^b + c\left(\frac{\kappa}{\kappa_L}\right)^d$	- It is based on the damage parameter. - It was employed in the non-linear code SCOSSA to perform total and effective stress 1-D analysis.

Chen et al. (2019)	$r_u = m\ln(n\,\varepsilon_{vd}+1)$ $(\varepsilon_{vd})_N/(\varepsilon_{vd})_{15} = B_1\ln(B_2N+B_3)$ $(\varepsilon_{vd})_{15} = C_D(\gamma-\gamma_{th})^{C_3}$ $C_1=7.05(I_D)^{-0.5}$ $C_1=B_1B_2C_D$	- It is an amended formula of Martin et al. 1975 model. - It may be applied for cyclic triaxial, torsional and direct simple shear tests with different loading patterns (strain- or stress-controlled). - It is independent of density. - I_D is in percentage form
Konstadinou and Georgiannou (2014)	$r_u = a.\left[\left(10^{-2(D_r-0.7)}\right)\frac{W}{p_i'}\right]^{\beta}$	- In the general formula of pore pressure and dissipated energy per unit volume of soil relationship. - The optimum value of β, obtained from the torsional shear test and independent of sand origin, is 0.6. - a parameter may be related to the mean grain size as $a=1.68\,(d_{50})^{-1.46}$ - This relationship is independent of the shear stress amplitude, density, and initial effective stress level.
Beaty MH, Byrne PM (2011) (UBCSAND)	$G^e = k_G^e.P_a\left(\frac{\sigma'}{P_a}\right)^{n_e}$ $K^e = \alpha.G^e \approx \frac{2(1+\mu)}{3(1-2\mu)}.G^e$ $\Delta\gamma^p = \frac{1}{G^p/\sigma'}\Delta\eta$ $\Delta\varepsilon_v^p = (\sin\Phi_{cv}-\sin\Phi_{mob}).\Delta\gamma^p$	- It is a fully coupled model based on hyperbolic stress-plastic strain relation. - It could be used in liquefaction and post liquefaction investigations as it could capture the nonlinear behavior under cyclic loading conditions. - n_e is an elastic stess exponent usually assumed to be approximately 0.5; α depends on o Poison's ratio and can be assumed to be 0.67-133; K^e_G is an elastic shear modulus number (ranged between 500-2000).

Boulanger and Ziotopoulou (2015) (PM4SAND)	$G_0 = 167\sqrt{64(D_r/100\%)^2 + 2.5}$ (for all formula please refer to the original reference)	- It is a critical state bounding surface plasticity model. - Account for the change of fabric in calculating the plastic strains (considers the effects of pre-loading history. - hp_0 is contraction rate parameter that accounts for the dilative and contractive behavior.

** There are many pore water pressure models while the energy-based and loosely coupled pore pressure models are focused in tis table.

2.6 Comparison between cyclic triaxial and simple shear tests

In order to study the liquefaction potential and determine dynamic soil properties of soil experimentally, a wide range of devices have been used (e.g. triaxial, simple shear, torsional simple shear (solid and hollow cylinder), and shaking table). A comparison between the advantages and disadvantages of each apparatus was introduced by Woods (1978) and Saada and Townsend (1981).

Cyclic simple shear testing is commonly used in liquefaction assessment as it provides the closest mimic of particle rotation and particle-particle relative slips during the vertical propagation of shear waves (Zhang and Evans 2018). In addition, principal stresses rotate smoothly during cyclic simple shear loading when soil specimen is kept under a plane strain condition (Wood et al. 1979).

Even though the cyclic simple shear is preferred to represent the behavior under earthquake loading, liquefaction resistance in the laboratory is often determined using cyclic triaxial tests because of its simplicity and capability of defining the principle stresses during cyclic loading. However, it has been found that the obtained liquefaction resistance from CTX is overestimated. Therefore, the measured cyclic triaxial resistance must be correlated using an empirical correction factor, C_r, to predict the equivalent simple shear, or in-situ response (Seed et al. 1969; Seed and Idriss 1971; Seed and Peacock 1971; Lee and Chan 1972).

Tatsuoka (1986) attributed the difference between triaxial and simple shear tests to the difference of the shearing mechanism. Peacock and Seed (1968) and Bhatia et al. (1985) attributed the deficiencies of cyclic triaxial to

(i) the abrupt rotation of principal stress directions by 90^o at the instant of stress reversal,
(ii) the difference in soil behavior under axial compression and extension relative to the simple shear stress, and
(iii) the lack of plane strain conditions that occurred during the vertical wave propagation.

As reported by Seed and Peacock (1971), the main difference between triaxial and field condition as well as in simple shear is the shear stress determined in triaxial is the maximum value that could be imposed on soil specimen (i.e., $\tau_{max.}=(\sigma_1- \sigma_3)/2$) whereas the actually induced field shear stress is considerably lower than the maximum stress, τ_{max}. In CTX tests, the tendency of soil grains to settle during cyclic loading results in non-uniformity of density and straining of

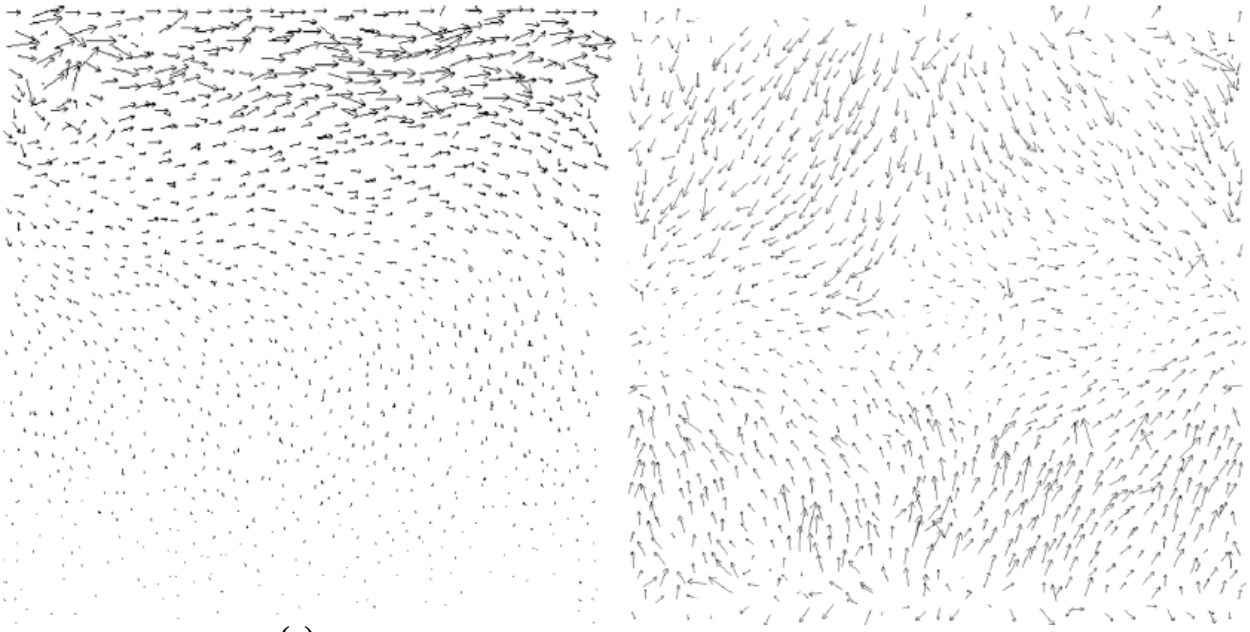

(a) (b)

Figure 2.15. Scaled velocities at 20% of total displacement in the first loading cycle, (a) simple shear specimen, and (b) triaxial specimen (from Zhang and Evans 2018)

the soil specimen in the form of bulging and necking (e.g. Castro 1975; Kramer 1996). The induced axisymmetric lateral deformation that occurs in triaxial tests does not mimic in-situ boundary conditions (Vipulanantham 2011). Budhu (1984) ascribed the difference of monotonic drain behavior in triaxial and DSS tests to the influence of the intermediate principal stress (σ_2). Micromechanically, Zhang and Evans (2018) performed quantitative comparison analysis between cyclic behavior under triaxial and simple shear tests using DEM simulation. They attributed this difference to the rotation of particles which play a determinative role in pore pressure generation. The particle rotation is much larger in DSS, under shear waves, than in its counterparts in CTX, under prevailing compression waves, as shown in Figure 2.15. Therefore, the number of liquefaction cycles, under a significant cyclic stress ratio (CSR) is higher in CTX compared with DSS. Accordingly, it must be correlated by applying a correction factor (C_r) that can be expressed as (Seed and Peacock 1971):

$$\left(\tau_h / \sigma'_{v0}\right)_{DSS} = C_r \left(\sigma_{dc} / 2\sigma'_c\right)_{CTX} \tag{2.40}$$

where τ_h is the applied shear stress on soil specimen confined under vertical pressure σ'_{v0} in DSS and σ_{dc} is the applied deviator stress on soil specimen consolidated isotropically under effective confining pressure σ'_c.

Based on the analysis of laboratory results in conjunction with 35 earthquake sites, it was concluded that the CSR ($\sigma_d/2\sigma'_c$) of triaxial compression test data should be correlated by (C_r = 0.55 to 0.7) as a function of I_D and the duration of the earthquake. This correction factor considers the difference in K_0 condition and initial stress conditions between field and laboratory tests in addition to the effect of test equipment and test procedure (Seed and Peacock 1971). Peacock and Seed (1968) observed that the correction factor depends on the relative density and criterion of liquefaction (i.e. R_u = 1 or significant shear strain value). In the same contest, Silver et al. (1980) performed cyclic tests using triaxial and modified simple shear on Monterey No.0 sand. It was discerned that the preparation method has a great influence on the liquefaction resistance in general and particularly on the correction factor. It was observed that there is no significant difference in the liquefaction resistance when air pluviated preparation method was employed to prepare reconstituted soil specimens at I_D = 60%, wherein liquefaction criterion was 10% double amplitude (DA) axial strain in triaxial and 15% DA in a simple shear test, as shown in Figure 2.16. In contrast, when soil specimens prepared by the wet tamped preparation method, cyclic triaxial obtain higher resistance than simple shear test and C_r, Eq. (2.40), was observed to be 0.55.

By analyzing the laboratory test data obtained by Lefebvre and Serge (1987), the cyclic triaxial resistance ($\sigma_d/2\sigma'_c$) should be correlated by 0.65 for sand (I_D = 50%) and 0.6 for silty sand (I_D = 70%) to be identical to simple shear resistance (τ/σ'_{vo}). A summary of previously suggested correction factors is listed in Table 2.3. However, Vaid and Sivathayalan (1996) observed that the correction factor is not as simple as those presented in Table 2.3. They demonstrated that the correction factor depends on the relative density of the sand and the applied confining pressure, as shown in Figure 2.17. In general, the correction factor depends on the duration of the earthquake (Seed and Peacock 1971), soil behavior (dilative or contractive under static loading) (Berghe et al. 2001), and the geometry of the soil specimen (cubical in Roscoe DSS or cylindrical in NGI DSS). As previously mentioned, the liquefaction resistance has been obtained either from in-situ characteristic tests-CRR correlation or from the stress-controlled laboratory tests. However, up to the present, the comparison between CTX and DSS has not been studied under cyclic strain-controlled tests. Different studies discussed the liquefaction potential under cyclic strain-controlled conditions, however, without comparing the results of DSS and CTX. This challenging, as one of this thesis aims, is discussed throughout the current study in addition

to emphasis the liquefaction resistance under stress-controlled conditions in Chapter 5 and Chapter 6.

Table 2.3: Correction Factor, C_r suggested in previous studies:

Correction factor, C_r	**Reference**	**Apparatus**
0.55 – 0.72	Seed and Peacock (1971)	Roscoe DSS (Cubical specimen, K_0 = 0.4-1)
$\frac{1+K_0}{2}$	Finn et al. (1971) Seed and Peacock (1971)	Roscoe DSS (Cubical specimen, K_0 = 0.39 and 0.47)
$\frac{2(1+2K_0)}{3\sqrt{3}}$	Castro (1975)	Triaxial (K_0= 0.67 and 1) and SPT data
$1-0.71(1-K_0)$	Ishihara and Li (1972)	Triaxial torsional shear. (K_0 = 0.33, 0.5 and 0.75)
$\frac{1+2K_0}{3}$ (wet tamped) 1 (air pluviated)	Silver et al. (1980)	DSS under conf. pressure (cylindrical specimen, K_0 = 0.4)

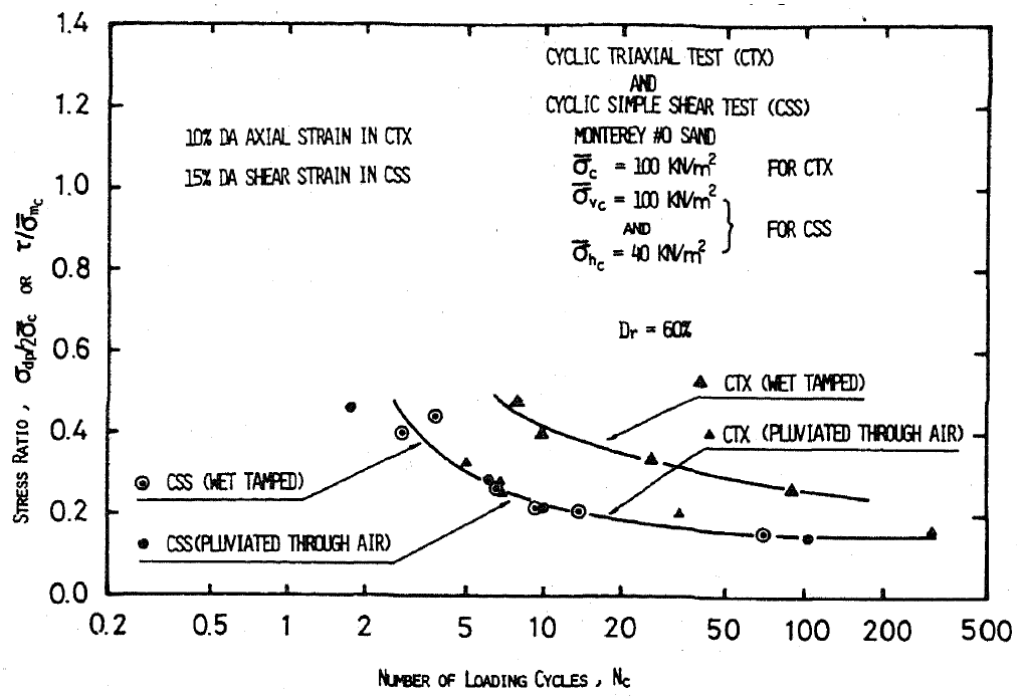

Figure 2.16. Liquefaction potential curves of Monterey No. 0 sand at I_D = 60% obtained from DSS and CTX (from Silver at al. 1980)

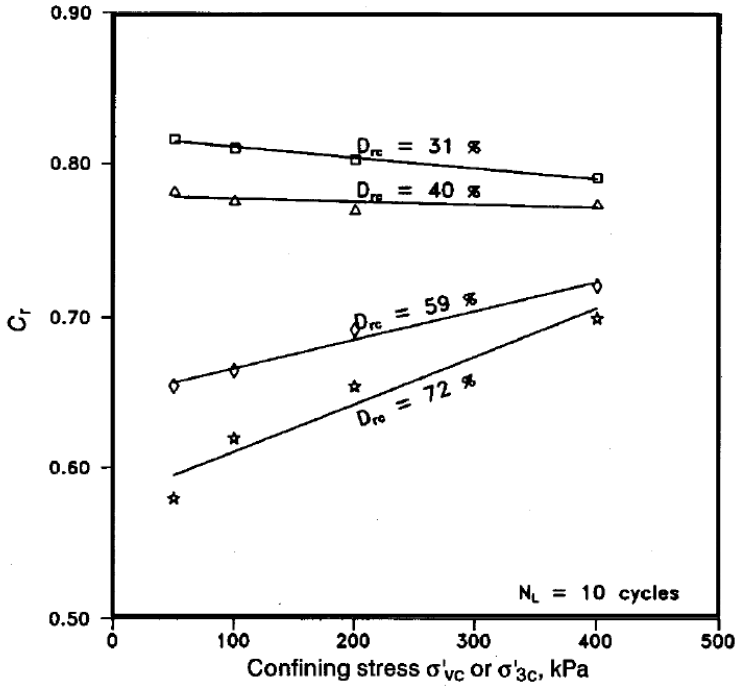

Figure 2.17. The proposed C_r of Fraser Delta sand (from Vaid and Sivathayalan 1996)

2.7 Specimen size effect on simple shear test results

Despite the merits of DSS in simulation plain strain condition under earthquake loading, one of its limitations is the lack of complementary shear stress on vertical boundaries that leads to non-uniform stresses within the DSS specimen (Boylan and Long 2009). The imposed nonuniformities of normal and shear stresses significantly affect on the soil behavior and lead to premature failure (Casagrande 1976). In addition, Prevost and Hoeg (1976) found that the non-uniformity slippage in the upper and lower plates-soil interface increases the non-uniformity of normal and shear stresses. However, the findings of linear stress analysis by Roscoe (1953) and Budhu and Britto (1987) and experimental observations of DeGroot et al. (1994) showed that the non-uniformities of stresses occur at a peripheral layer but the specimen core (the central third) imposes uniform distribution under ideal simple shear condition. The thickness of the affected peripheral layer depends on the Poisson's ratio (Saada and Townsend 1981). Stroud (1971) concluded that the central third, middle third perpendicular to shear direction, of specimen sheared in Cambridge DSS, imposed uniform strain up to maximum shear stress. Chang et al. (2016), using the Particle Flow Code in Two Dimensions (PFC 2D), concluded that

approximately 70% of soil specimen experienced uniform stress. This was previously reported by Ladd and Edgers (1972) and by Lucks et al. (1972) using linear elastic three-dimensional finite element analysis on the NGI-DSS configuration. To tackle the non-uniformity of shear stress, it was suggested to use a high diameter to height ratio (D/H) (Shen et al. 1978, Seed 1979, Amer 1987, Chang et al. 2016). Previous researchers interpreted that as the induced external moment developed at a thinner specimen, at the same horizontal displacement, produces more uniform stress. In other words, the problem is an exacerbation of the induced moment with decreasing D/H ratio.

There is a controversy on the determination of an adequate D/H ratio at which the shear stress distribution is almost uniform irrespective of the specimen size. This question was previously investigated experimentally (e.g. Carroll 1979; D/H ranged between 2 to 8, Franke et al. 1979; D/H = 3.75 and 7.5, Kovacs and Leo 1981; D/H= 3, 6 and 12, Vucetic and Lacasse 1982; D/H= 3, 5 and 7) and numerically (e.g. Finn 1963; Shen et al. 1978; D/H= 2, 4 and 8). Amer et al. (1987) studied the specimen size effect on the dynamic soil characteristics (shear modulus and damping) experimentally and numerically for D/H range of 3 to 12. They observed that the specimen size effect on the shear modulus and shear stress distribution is negligible when D/H ratio reaches 8. This value was previously concluded by Shen et al. (1978) by adopting a linear elastic isotropic model in three dimensional finite element analysis. Based on his elastic numerical simulation of Roscoe-DSS type, Finn (1963) concluded that at D/H = 6 the uniformity of normal and shear stress are greatly improved comparing to D/H = 2. However, the ASTM D6528 specified the minimum D/H ratio as 2.5. Vucetic and Lacasse (1982), following to their experimental work on a medium-stiff clay (Haga clay) specimens with different D/H ratios, concluded that the D/H ratio has no significant influence on the stress non-uniformity under monotonic loading controversy to the previous work. Vucetic and Lacasse attributed this contradiction to the inability of theoretical linear elastic analyses to consider actual nonlinear clay behavior beyond the yield. Moreover, Budhu and Britto (1987) indicated that the stress concentration produced in elastic analysis is higher than that in the modified Cam Clay analysis. Later, Airey (1984) and Airey and Wood (1984), using an elaborately instrumented NGI-DSS developed by Budhu (1979), pointed out that Vucetic and Lacasse's conclusion is applicable only for clay while the sand behavior depends on D/H ratio. Further, Budhu (1984) represented the shear stress ratio (shear stress/normal stress)-strain curves of Leighton Buzzard sand in a

Cambridge NGI apparatus in which the stresses were recorded from stress transducers embedded in three locations in the top and bottom horizontal boundaries. The results showed that the peak stress ratio in the principal third (representative of average measurement) is 6% lower than the stress ratio in the core and by 12% in the Cambridge type. However, stress ratio in the principal third is higher than that in the central third. Using the modified Cam Clay model in finite element analysis of UWA DSS, Doherty and Fahey (2011) pointed out a 10% underestimation of shear strength obtained from shear stress in 3D simulation.

Kovacs and Leo (1981), using large scale direct simple shear apparatus (D=12 in), observed that at D/H=3, Ottawa sand (20-30) specimen is stiffer in comparing to thinner specimens (i.e. D/H = 6, 12) at low strain (< 1 %). However, at higher shear strain, the effect of the D/H ratio is not significant on the shear modulus. In contract, Wood and Budhu (1980) found the nonuniformity occurred beyond to shear strain value of 1 – 2% while Hussien et al. (2015) observed that the deviation of shear stress-strain curves of two sand specimen of D/H = 3 and 1.9 tested in the T_xSS occurs beyond 1% shear strain.

Chang et al. (2016) observed that the effect of D/H on the shear resistance is not significant when H/d_{max} is higher than 7 while ASTM D6528 specifies this value to 10 to diminish the effect of the width of shear band, where, d_{max} is the maximum particle size.

In his cyclic investigation on Drammen clay, Anderson (1975) indicated that the number of cyclic loading to failure is independent of specimen size (D/H). The same conclusion was observed by Franke et al. (1979) using the BAW DSS where saturated sand can be confined hydrostatically in a triaxial cell. It was found that the cyclic undrained resistance of D/H ratio = 7.5 and 3.75 are equal. Presumably, because the horizontal stress remains constant in BAW DSS at the vertical boundary of specimens in the triaxial chamber. A preliminary experimental study was initially performed to investigate the effect of D/H ratio cyclic soil behavior under undrained conditions in T_xSS. This is discussed in Chapter 5.

2.8 Summary

The liquefaction assessment procedures are described with a focus on the widely used stress-based procedure. The difference between seismicity in the eastern and western North America regions in terms of frequency content, attenuation of earthquake energy, and amplification of peak ground acceleration are acknowledged.

The particularities of the equivalent number concept are described and the common used cumulative damage hypotheses in liquefaction assessment are reviewed (i.e. P-M, R-N, and alternative P-M). The evolution of the P-M hypothesis and implementation of the R-N hypothesis to predict the cumulative damage are discussed. These hypotheses are addressed in Chapter 4 to link between the induced cumulative damage and the build-up of earthquake-induced pore-water pressure. Involving the energy concept in Green and Mitchell's hypothesis to consider soil softening in equivalent number calculation are addressed. This hypothesis is used to indicate the variation of $N_{eq\tau}$ between ENA and WNA in Chapter 7.

The characteristics of pore water pressure generation during cyclic loading are presented. A review of the most used pore pressure models is presented in section 2.5 with a focus on the energy-based models. Based on the preliminary results of the combined triaxial simple shear tests (T_xSS), a new energy-based pore water model is established and implemented in the numerical simulation of the cyclic behavior under T_xSS and CTX conditions, as represented in Chapter 5 and 6.

The characteristics of cyclic behavior under triaxial and simple shear tests are also addressed in section 2.6. Laboratory test results show that the cyclic triaxial overestimates the liquefaction resistance. This difference is interpreted and compared to the T_xSS cyclic behavior of different sands in Chapters 5 and 6.

Finally using the energy-based model, proposed and verified in the element-level in Chapters 5 and 6, to perform nonlinear dynamic analysis (section 2.3.4.2). The softening of soil is considered by iterative updating of shear modulus each time-step in numerical analysis. The cyclic responses in terms of liquefaction charts (section 2.3.1.1.c), equivalent number (sections 2.4 and 2.4.3) and generated pore pressure (section 2.5) are discussed.

CHAPTER 3

EXPERIMENTAL PROGRAM

3.1 Introduction

Since the severe damage associated with the M9.2 Great Alaskan earthquake and the M7.5 Niigata earthquake, the dynamic behavior of soil has become the most important research subject in geotechnical engineering. Extensive field investigations and experimental research have been conducted aiming to grasp a more complete understanding of this phenomenon.

This chapter describes the laboratory test methods employed in this work. It is aimed to study the undrained cyclic behavior of different cohesionless soil collected from Quebec (Baie-Saint-Paul, Carignan, and Quebec CF6B sands) and commercially available clean sands (Ottawa C-109 and Ottawa F-65). Moreover, it is intended to introduce an energy-based pore pressure model to be incorporated in one-dimensional (1D) site response analysis. Undrained cyclic stress- and strain-controlled tests were carried out to determine the liquefaction potential of reconstituted specimens of the aforementioned sands. Additional monotonic tests were conducted.

Many advanced laboratory testing devices have been employed in investigating the cyclic behavior at low shear strains (e.g. resonant column, RC), and at medium to large strains (cyclic triaxial, CTX), cyclic torsional (CTT) and cyclic direct simple shear (DSS)). In this study, various configurations of the combined triaxial simple shear (T_xSS), DSS, and CTX were employed.

3.2 Direct Simple Shear device (DSS)

The direct simple shear device (DSS) is the preferred laboratory testing apparatus. It is designed to reasonably well simulate field conditions during shear wave propagation. The first version of DSS was developed in the 1950s to overcome the flaws of the direct shear (Kjellman 1951) wherein the cylindrical soil specimen is encased in a rubber membrane surrounded by a stack of

rings (SGI type). Later, Bjerrum and Landva (1966) used a wire reinforced membrane to confine the soil specimen under K_0 condition (NGI type). Roscoe (1953) used a cubical specimen in lieu of a cylindrical specimens and used rigid steel walls to confine the specimens (Roscoe-type). Figure 3.1 shows the typical lateral confinement methods provided by (a) rigid walls, (b) stacked aluminum rings and (c) wire-reinforced membranes.

Since then, variant configurations, with differant confinement methods, loading mechanisms, and specimen diemnsions have been developed with other features to better replicate the cyclic response under earthquake excitation (e.g. Peacock and Seed 1968; Ishihara and Yamazaki, 1980; Boulanger et al., 1998; Sivathayalan and Ha, 2011, etc.). Franke et al. (1979) noted that in DSS, back pressure cannot be used because of bulging of the reinforced rubber membrane. Casagrande (1976) developed another configuration of simple shear apparatus which was termed a "gyratory apparatus", where a rubber membrane was supported by a number of flat springs in the triaxial cell. Franke et al. (1979) developed the Bundersantal fur Wasserbau (BAW) DSS version, in which radial and vertical strains were restrained by an automatic adjustment of the cell pressure. Similarly, Mao and Fahey (2003) developed an updated DSS version at the University of Western Australia (UWA). Kang et al. (2015) developed a circumferential deformation device to monitor the radial deformation of a modified DSS that accommodate cylindrical specimens in a latex membrane.

Figure 3.2 depicts the typical loading conditions in DSS. It is shown that at first, the soil element is anisotropically confined under K_0 condition ($\sigma'_h = K_0.\sigma'_v$). During a cyclic loading, the soil element is subjected to horizontal shear stress (τ_h) as shown in Figure 3.2. To achieve plane strain conditions, a constant volume test is performed, or constant height as the radial stain is constrained. The decrease in the vertical stress during a constant volume cyclic DSS loading has been assumed to be equal to the increase of pore pressure that would be generated in an undrained DSS test (Dyvik et al. 1987).

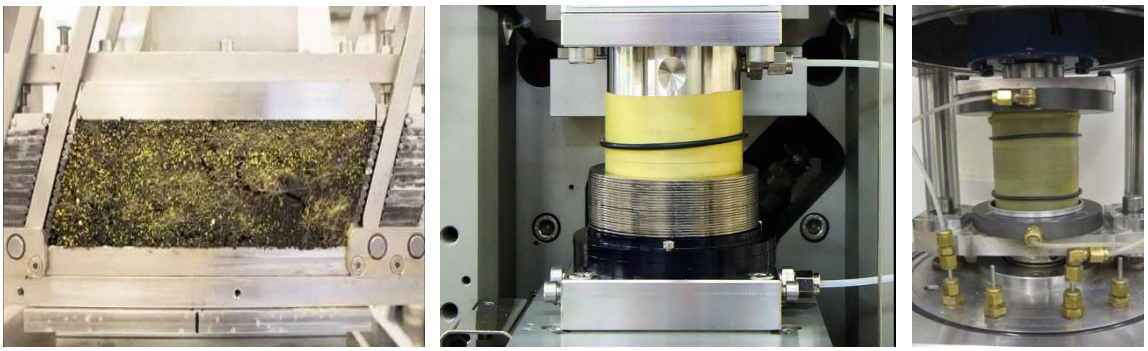

(a) (b) (c)

Figure 3.1. (a) Roscoe-type (Rigid wall) (b) SGI-type (stacks of annular plates/rings) (c) NGI-type (Reinforced membrane)

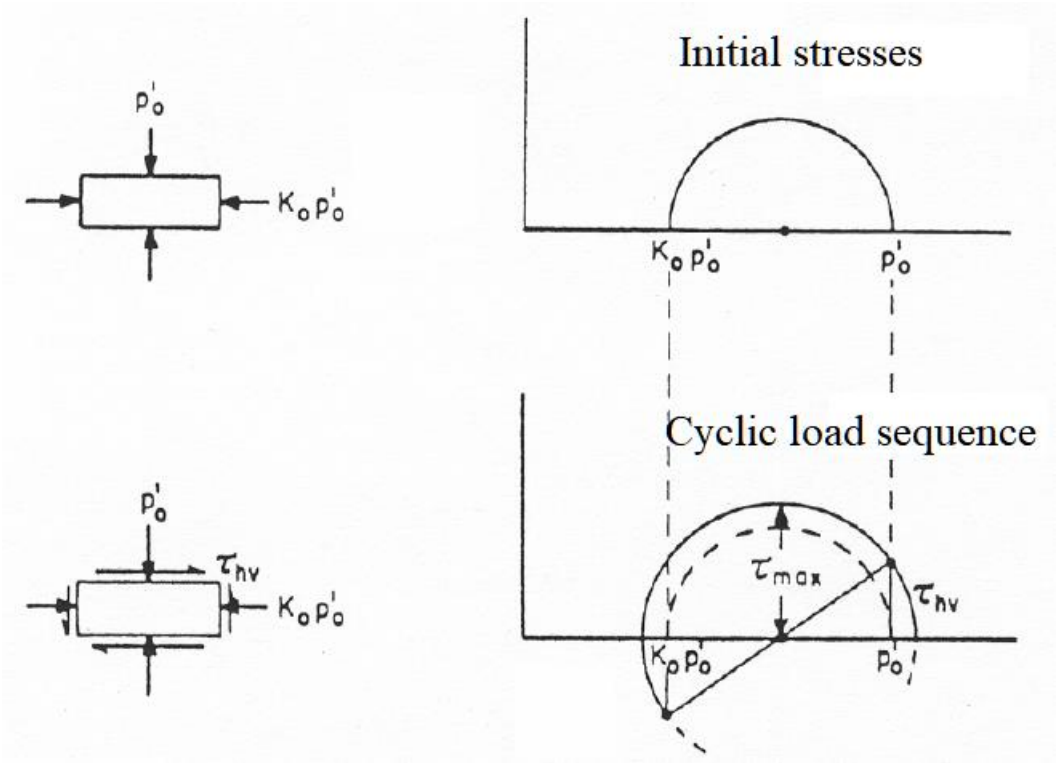

Figure 3.2. loading conditions in DSS before and during cyclic loading (from Seed and Peacock 1971)

In DSS, the applied shear stress and the induced shear strain are measured on the horizontal plane while the lateral confining stress is assumed to be equal $K_0.\sigma'_v$. Thus, considerable studies have been devoted to simulate the DSS numerically to capture the stress conditions during static (e.g. Budhu 1987) or cyclic loading (e.g. Amer et al. 1987).

The DSS device has advantages over the triaxial device because of smooth rotation of principal stresses until failure, which is closer to field conditions during vertical shear wave propagation. It was believed that the main advantage of simple shear tests is that the shear force is applied on a horizontal plane. However, recently, it was found that the horizontal surface does not represent the failure surface and the obtained shear strength from measuring the horizontal surface results in an overestimation of shear strength (Antonio et al. 2016). Like other laboratory element, DSS has its shortcomings. The most acknowledged flaw is the shear stress across the top and bottom is non-uniformity in the specimen because of the lack of complementary shear stresses that implicitly has a significant effect on monotonic and cyclic resistance. Therefore, it is recommended to use a high D/H ratio (at least 2.5 as specified by ASTM D6528-17) to ensure uniform distribution of shear stress, as discussed in section 2.7.

In the current study, the conventional DSS apparatus by GDS Ltd. Company (Electromechanical Dynamic Cyclic Simple Shear, EMDCSS) was used. It is competent in performing monotonic/cyclic tests at a wide range of shear strain (0.005% to 10%). It has the ability to apply cyclic loading at frequency ranges between 0 to 5. It includes a clamping mechanism to maintain the specimen height constant during the shear stage by decreasing the vertical stress. It was recognized that the decrease in vertical stress is equivalent to the pore pressure development that would be generated under fully undrained conditions (Dyvik et al. 1987).

The soil specimen is encased in a latex membrane surrounded by a fiberglass tape or by staked rings to induce K_0 conditions, as shown in Figures 3.3(a) and 3.3(b), respectively. All specimens were prepared with a height of 20 mm and a diameter of 79 mm which infers a D/H ratio of 4 as recommended by ASTM D6528-17.

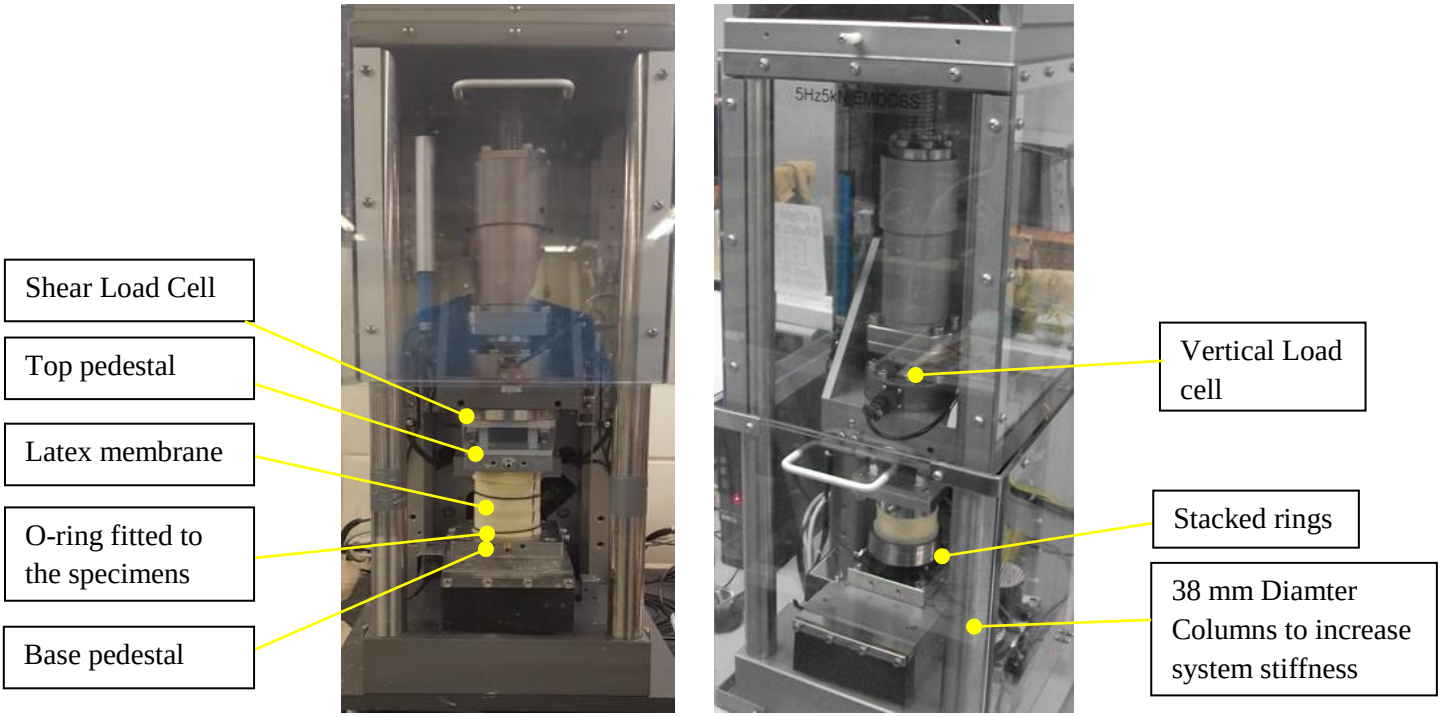

Figure 3.3. The DSS apparatus used in this research

3.2.1 Variation of lateral stress Coefficient during cyclic DSS loading

It has been observed that, the lateral stress coefficient (K_0) in DSS test does not maintain constant during cyclic loading in the case of confinement of radial strain. Dabeet et al. (2012) simulated the cyclic behavior under DSS loading using a discrete element model (DEM) in PFC^{3D} software and observed that the K_0 increases from its initial value to unity at the triggering of liquefaction (Figure 3.4). This confirms the results previously found by Youd and Croven (1975) and Budhu (1985). Youd and Croven (1975) founded that the rate of increase depends on the applied shear strain amplitude and most of the increase is occurred at first cycle (Figure 3.5). Ishihara and Li (1972) performed torsional shear tests on redaial confinement radial strain soil specimens. They observed that there is a reasonable consistency between the evolution of pore water pressure and K_0 until liquefaction triggering. Moreover, they observed that the liquefaction triggering is irrespective of the radial strain confinement. However, confinement of the soil specimen in a triaxial chamber allows maintaining the K_0 value constant during cyclic loading, which will be discussed in the next section.

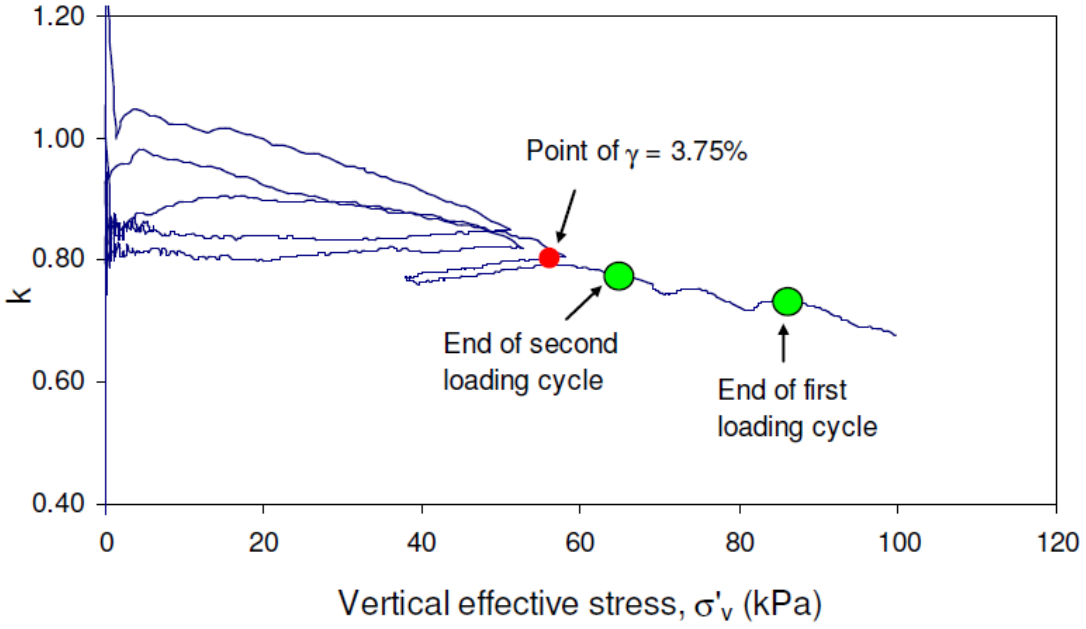

Figure 3.4. Variation of K_0 during numerical simulation of cyclic DSS stress-controlled tests (from Dabeet et al. 2012)

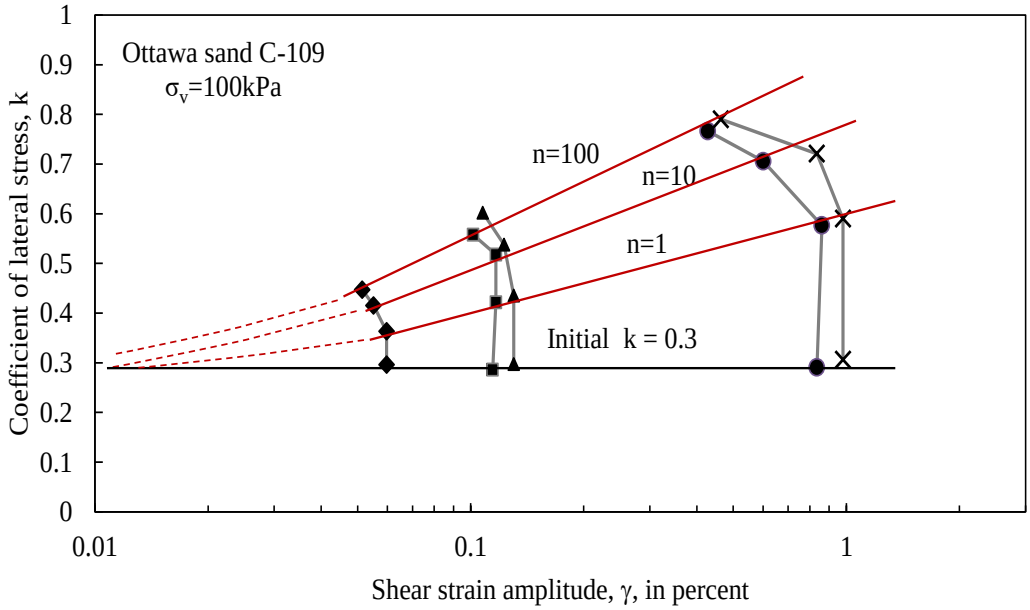

Figure 3.5. evolution of K_0 during cyclic DSS loading (from Youd and Croven 1975)

3.3 Combined triaxial simple shear apparatus (T_xSS)

The combined triaxial simple shear apparatus (T_xSS), shown in Figure 3.6, has been designed and manufactured at the Institut de Recherche d'Hydro-Québec (IREQ) in collaboration with the geotechnical group at the Université de Sherbrooke (Chekired et al. 2015; Karray and Chekired 2019). It can host a cylindrical soil specimens of 80 mm diameter (D) and varying heights (H) (Note: height of 25 mm and 80 mm diameter corresponding D/H= 3.2, which is recommended to meet ASTM D6528-17 specifications; D/H = 3.2).

The soil specimens are placed in a rubber membrane between rigid metal top and bottom platens. Porous stones are embedded in the upper and lower platens to allow application of back-pressure during the saturation phase. The upper cap contains spikes to ensure transfer of the shear stress to the specimens without any slip at the platen-sample interface (ASTM D6528-17). To prevent occurrence of rocking during shearing stage, the top platen has a vertical shaft inserted deeply and tightly fixed in the top cap.

During the shearing stage, the top platten is displaced by a shear ram connected to an electromagnetic shaker mounted on a rigid table. The shaker used has a capacity up to 100000 N with a precision of 0.07 µm. The imposed stress and strain by the top platten are controlled precisely up to frequencies of 10 Hz by a computer-automated feedback-loop-controlled system developed specifically for the T_xSS apparatus.

The T_xSS can be used to apply either regular or irregular cyclic shear strain to isotropic or anisotropic consolidated saturated soil specimens under simple shear condition. The main advantage of an electrically operated T_xSS over the conventional DSS is the capability of performing simple shear tests on saturated specimens when confined in a triaxial chamber (Figure 3.7a) or simply when confined by a reinforced wire membrane or stacked annular plates (Figure 3.7b). Moreover, a fiberglass tape could be adopted to confine the radial strain in the T_xSS tests (Figure 3.7c).

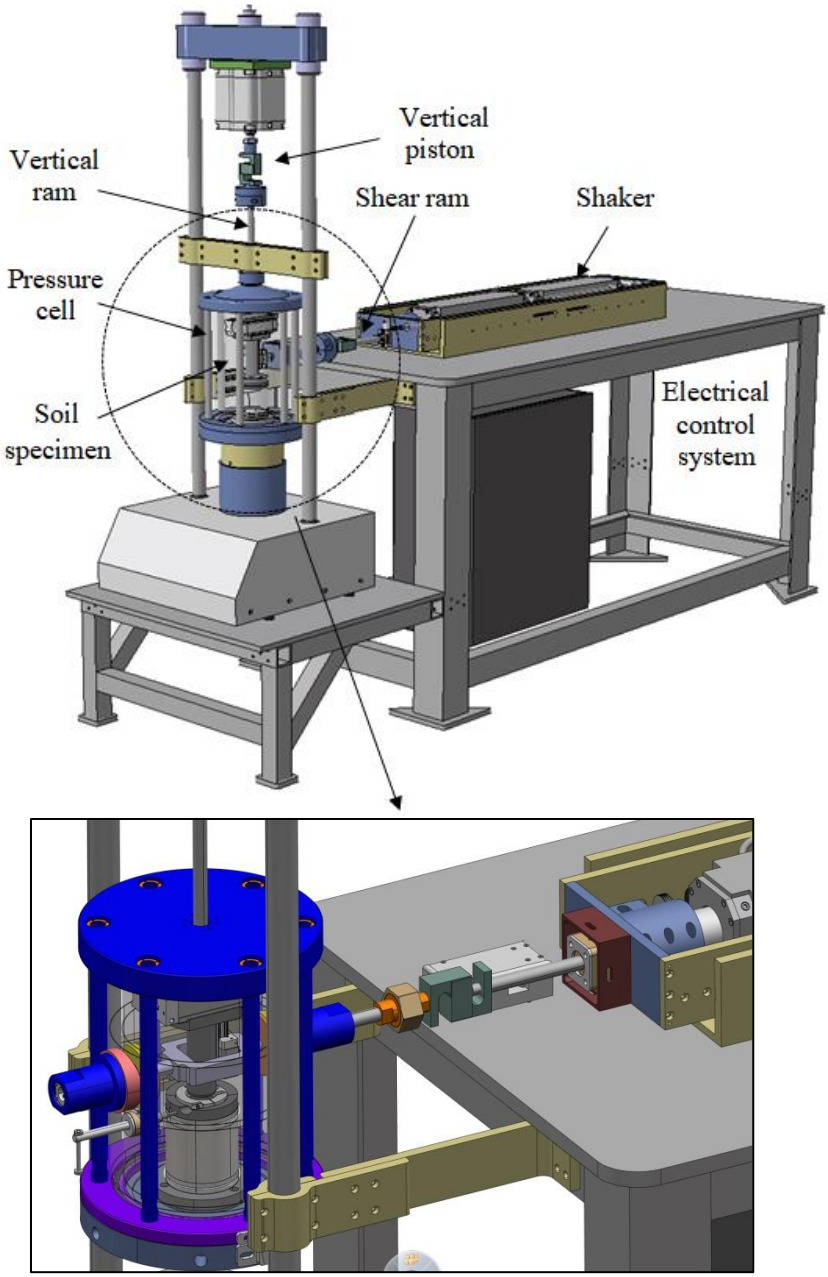

Figure 3.6. Schematic sketch of the triaxial simple shear (T_xSS) apparatus

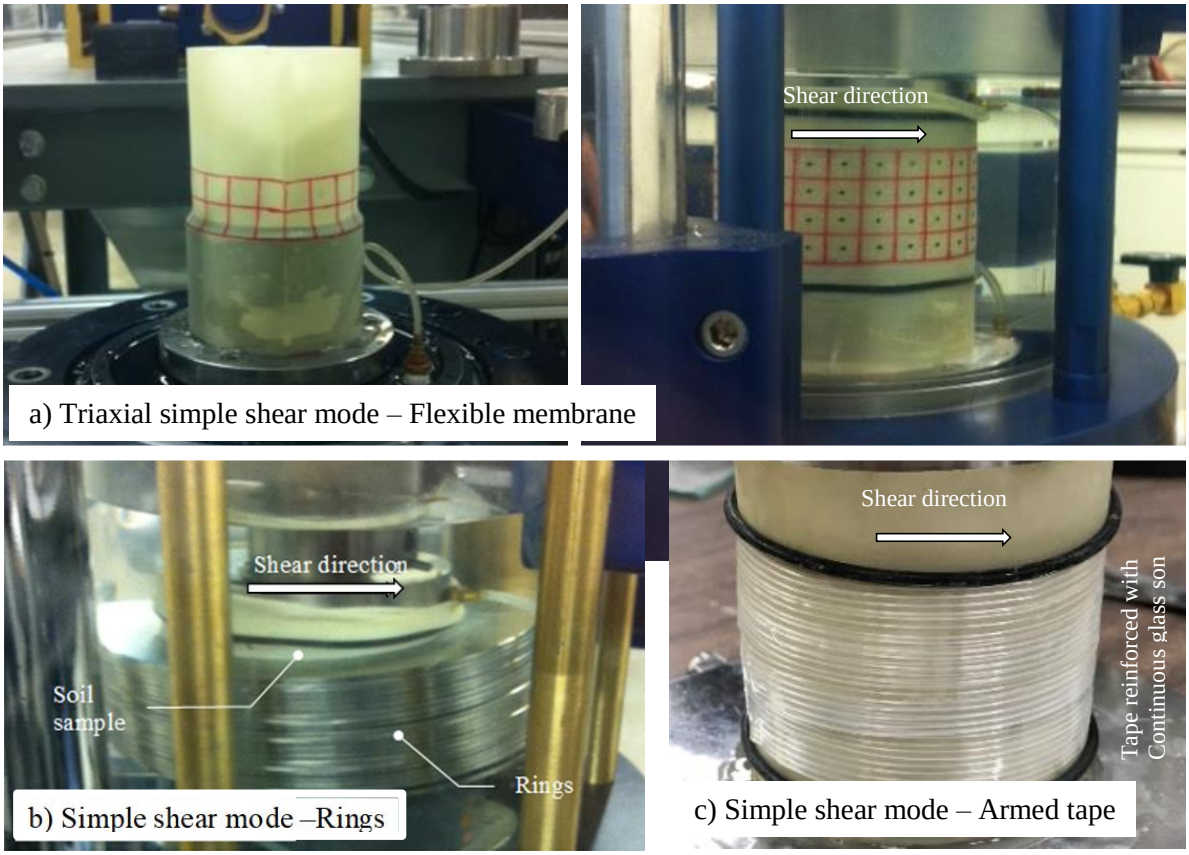

Figure 3.7. soil specimen prepared in (a) latex membrane, (b) latex membrane and annular rings

Vucetic and Dobry (1988) noted that the NGI-DSS device cannot precisely measure the generated pore pressures at very low shear strains (around the threshold value) because of its compliance. In contrast, the T_xSS has the ability to directly measure the generated pore pressure during cyclic or monotonic shear test using highly precise electric piezometer even at very low strains. The vertical and horizontal displacements are recorded by highly sensitive internally and externally mounted LVDTs. Using these LVDTS allows examining both small (0.001%, Chehat et al. 2018) and medium to large (0.5%, Khashila et al. 2018; Karray et al. 2019; Abdellaziz et al. 2019) strain behavior.

3.4 Cyclic Triaxial testing apparatus (CTX)

The cyclic triaxial testing device is the most widely used tool for cyclic behavior characterization and liquefaction investigations (Ishihara 1996), particularly, due to its simplicity, straightforward testing procedures, and capability of defining the principle stresses during cyclic loading. As demonstrated in Figure 3.8, initially the specimen is consolidated isotropically (or anisotropically) under an effective stress σ'_0 (phase a). Then, a cyclic deviator stress σ_d is applied at the top surface under undrained condition (phase b and c). As shown, the maximum shear stress ($\sigma_d/2$) occurs on a plane of 45^o.

After saturation and consolidation, an axial load is applied on the rigid top platen. In monotonic testing, the confining pressure is maintained constant and axial load is increased (compression test, Figure 3.8b) or decreased (extension test, Figure 3.8c). In a compression test the confining pressure represents the intermediate principal and minor principal stresses ($\sigma_2=\sigma_3$) while the axial stress is equal to the major principal stress (σ_1). However, in an isotropically consolidated extension test the major and the intermediate principal stress are equal to confining pressure, while the axial stress is equal to minor principal stress. Thus, the intermediate principal parameter, $b=(\sigma_2-\sigma_3)/(\sigma_1-\sigma_3)$, is zero and one in compression and extension tests, respectively.

The friction between the top and bottom end platens and soil specimen results in stress and strain non-uniformity and void ratio redistribution within the specimen. The end effects were observed to be reduced by using height to diameter ratio (H/D) of 1.5 to 2.5 (Bishop and Henkel 1962; Tatsuoka et al. 1986; ASTM D5311). Other researchers suggested using lubricated end platens to reduce end effects (Rowe and Barden 1964). However, this technique was observed to produce bedding errors. In this study the customary size of 76 mm height and diameter of 38 mm is used.

Another limitation of CTX is the major and minor stresses vary instantaneously (jump rotation) by 90° corresponding to alteration from compression to extension during a cyclic loading, as shown in Figure 3.8. The shear plane is not horizontal in contrast to in-situ conditions (Silver et al. 1980; Kramer 1996). The induced necking phenomenon during axial extension does not replicate field conditions. Thus, CTX exaggerates the cyclic deformations. Moreover, the induced lateral strains do not precisely represent in-situ plane strain conditions.

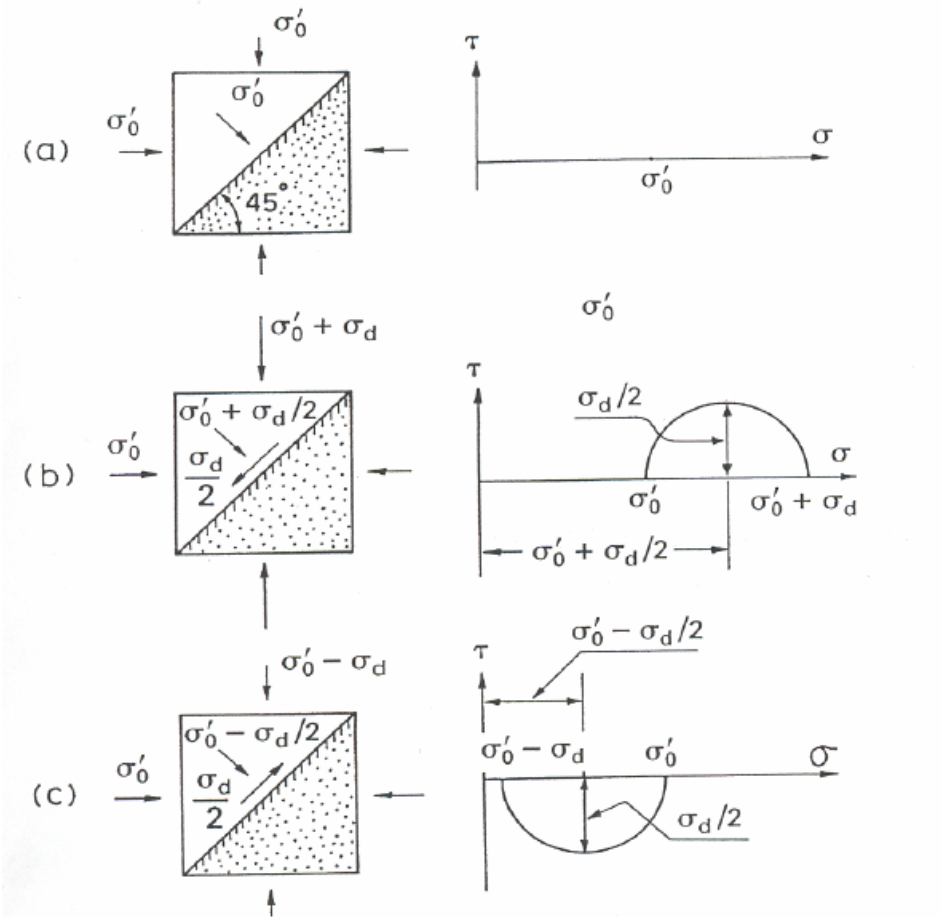

Figure 3.8. Simulation of the induced stresses under cyclic triaxial conditions (from Ishihara 1996)

The triaxial apparatus used in this work is the commercial triaxial manufactured by GDS company, Figure 3.9. The automated system permits performing either strain or stress-controlled monotonic or cyclic loading on undisturbed or reconstituted soil specimens. It is fully controlled by GDSLAB and data acquisition software. The apparatus is also equipped with a submersible load cell, highly sensitive displacement sensors while the back, cell and excess pore water pressure are controlled using a back pressure controller, Figure 3.9.

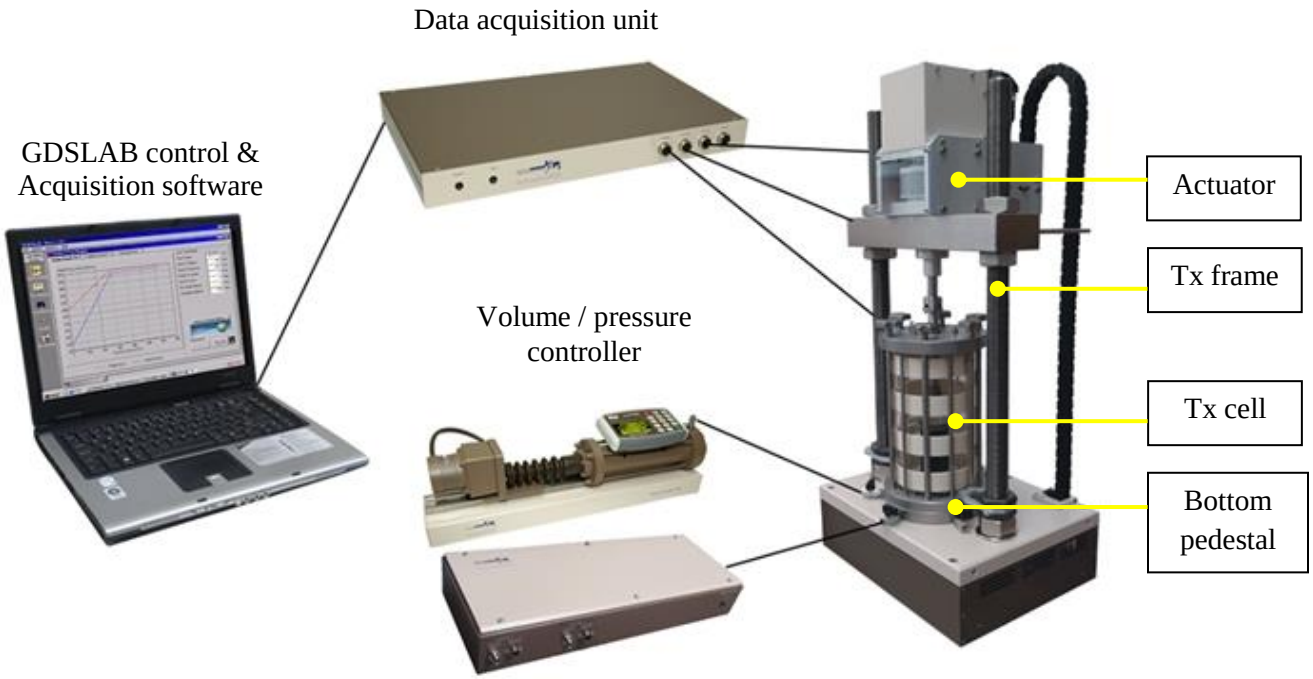

Figure 3.9. An automated triaxial apparatus

3.5 Material and specimen preparation

3.5.1 The sands used in the current study

Different cohesionless soils, with different physical properties, collected from Quebec (Baie-Saint-Paul, Carignan, and Quebec CF6B sands) were used in the current study. Also, commercial clean sands (Ottawa C-109 and Ottawa F-65) were used to introduce and validate an energy-based pore water pressure model. These commercial sands have been used as a reference sand for liquefaction investigations for the last decades. They were selected because of an abundance of cyclic testing results readily available.

Material properties are summarized in Table 3.1. The grain-size distribution curves of theses sands are shown in Figure 3.10. Figure 3.10 shows also the range of grain-size distribution curves for liquefaction susceptible soils as proposed by Xenaki and Athanasopoulos (2003). As shown in Figure 3.10, the used material is considered to be liquefiable.

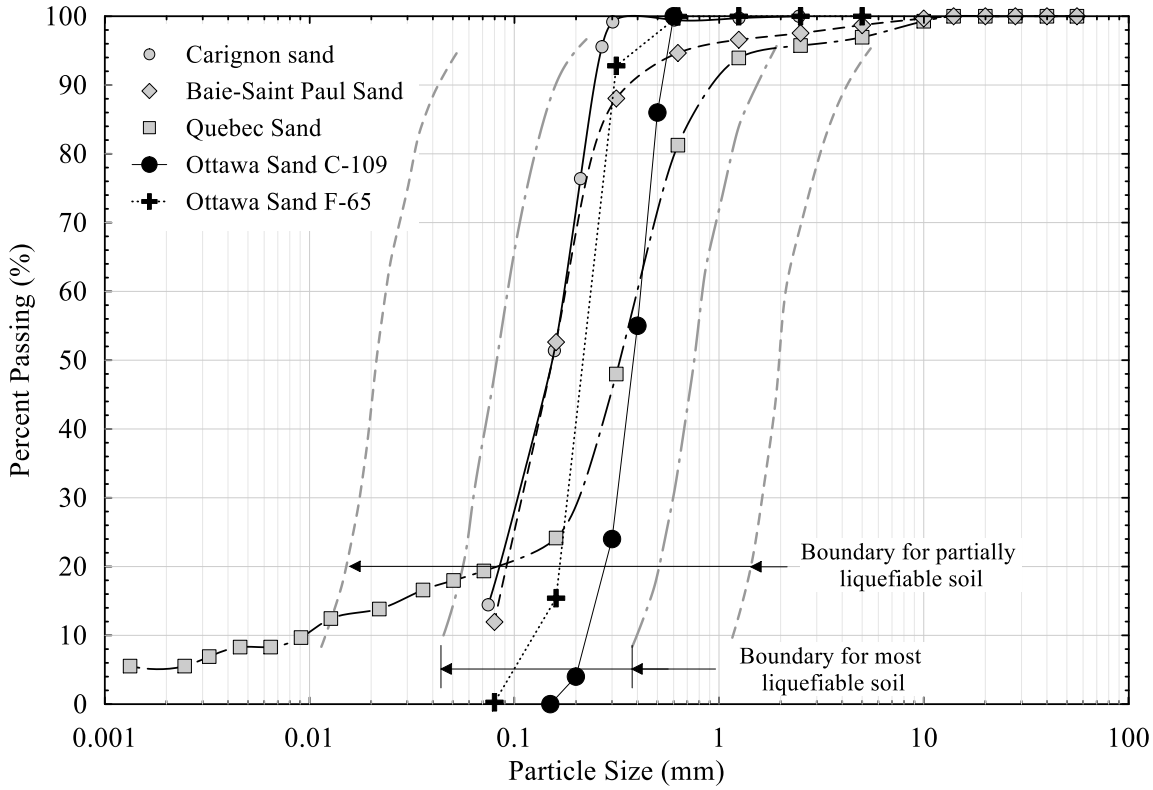

Figure 3.10. Grain-size distribution of the material used and boundaries for liquefiable soils proposed byXenaki and Athanasopoulos (2003)

Table 3.1. Physical properties of sands used.

Soil properties	Baie-Saint-Paul sand	Carignan sand	Quebec sand CF6B	Ottawa C-109	Ottawa F65
G_s	2.78	2.71	2.71	2.67	2.668
e_{max}	0.91	1.12	0.95	0.82	0.82
e_{min}	0.60	0.73	0.55	0.5	0.53
C_u	2.25	2.45	44.44	1.75	1.68
C_c	1.00	1.00	12.25	1.016	1.28
D_{50}	0.15	0.15	0.33	0.4	0.217

Note: G_s, specific gravity; e_{max} and e_{min}, maximum and minimum void ratio, respectively; C_u, coefficient of uniformity; C_c, coefficient of curvature; D_{50}, median grain size.

3.5.2 Preparation of specimens

Many methods are widely used for preparing soil specimens in laboratories. Since the different methods of specimen reconstitution create different fabrics, the responses to the applied load and liquefaction resistance are different (Tatsuoka et al. 1986 ; Ishihara 1996). Intensive research has been done to investigate this different under variant load condition (e.g. Ladd 1974; Mulilis et al. 1977; Vaid and Sivathayalan 2000, Wijewickreme et al. 2005).

Silver et al. (1980) and Wijewickreme et al. (2005) observed that the specimen preparation method does not have a significant influence on simple shear test results. On the other hand, centrifuge test results obtained by Abdoun et al. (2013) show there is a dramatic effect of the deposition method on sand fabric and subsequently on the generated pore pressure under stress-controlled conditions. They observed that the air pluviation method results in the weakest specimen in contrast to vibrating the soil in a moist condition method. However, the specimens prepared by wet tamping always experience higher strength than specimens prepared by the dry vibration method (Ladd 1974).

In this work, the wet tamping preparation method was used to prepare reconstituted soil specimens in CTX, DSS and T_xSS. The wet tamping was chosen among other procedures as it allows preparing specimens with a wide range of void ratios, with an acceptable uniformity (Ishihara 1996). The under-compaction method was applied to produce uniform density through soil specimen, (Ladd 1978). The dry sand is mixed with a small amount of deaired water to produce moist sand. Two dry porous stone (one at top and another at bottom) are used with two discs filter paper to allow the water come in/out during consolidation and saturation stage. This moisture content value produces a small amount of matric suction which helps to stabilize the soil specimens during preparation. The moist sand was placed into the rubber membrane in three sub-layers where the compacted sub-layers have the same height. In triaxial tests, the soil specimen is around 76 mm height and 38 mm diameter (H/D = 2). The sand was compacted in the rubber membrane in six layers. Each layer is gently tapped using a hand tamper until the pre-estimated height was reached. Then, the surface of each layer was inscribed to increase the bonding to the next sub-layer. While placing the soil in rubber membrane, the rubber membrane was confined by an air-tight split mold attached to the bottom cap of the cell, Figure 12(a). The diameter and height of the compacted specimen were measured using a caliper, Figure 12(b). After replacing the final layer, the top cap was placed and two O-rings were used to seal both

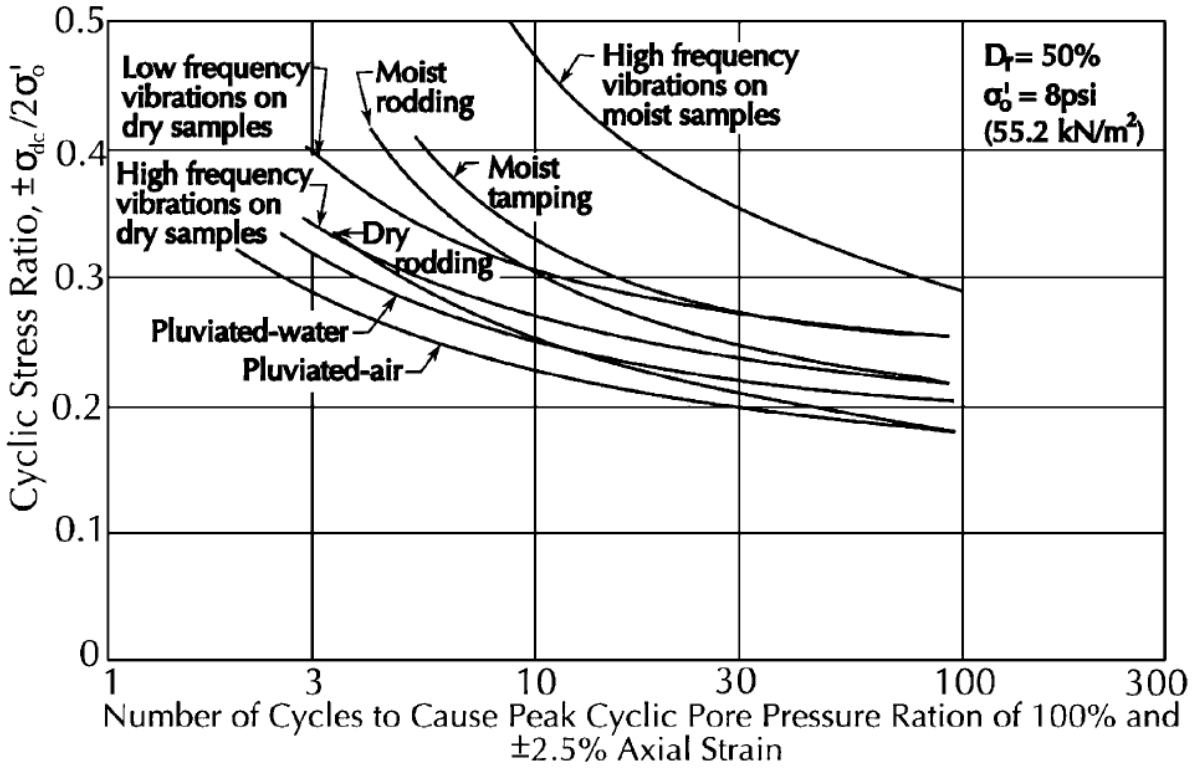

Figure 3.11. Liquefaction resistance obtained from different preparation methods (from Seed 1979)

ends of the membrane on the caps, Figure 3.12(c). Then, the split mold was removed from the specimen, Figure 3.12(d). The specimen diameter was measured at three locations (top, bottom, and middle) and the average value was used to verify the final density.

- Saturation process

After encasing the soil in a rubber membrane saturation was initiated. To hasten the saturation process in CTX and T_xSS, carbon dioxide gas (CO_2) was flushed for 15 minutes under a low cell pressure to displace air bubbles. Then de-aired water under a slight back-pressure of 50 kPa was applied to the specimen simultaneously with cell-pressure of 40 kPa for 2 hours. Next, a back-pressure of 200 kPa was applied with a cell pressure of 190 kPa at least for 15 hours. To ensure the full saturation of the soil, the Skempton's pore pressure parameter B ($\Delta u/\Delta\sigma_3$) was estimated for each test by measuring the increase in pore-water pressure, Δu, induced by increasing cell pressure by $\Delta\sigma_3$, where σ_3 is the minor principal stress. Full saturation was defined when $B \geq 0.96$ was achieved.

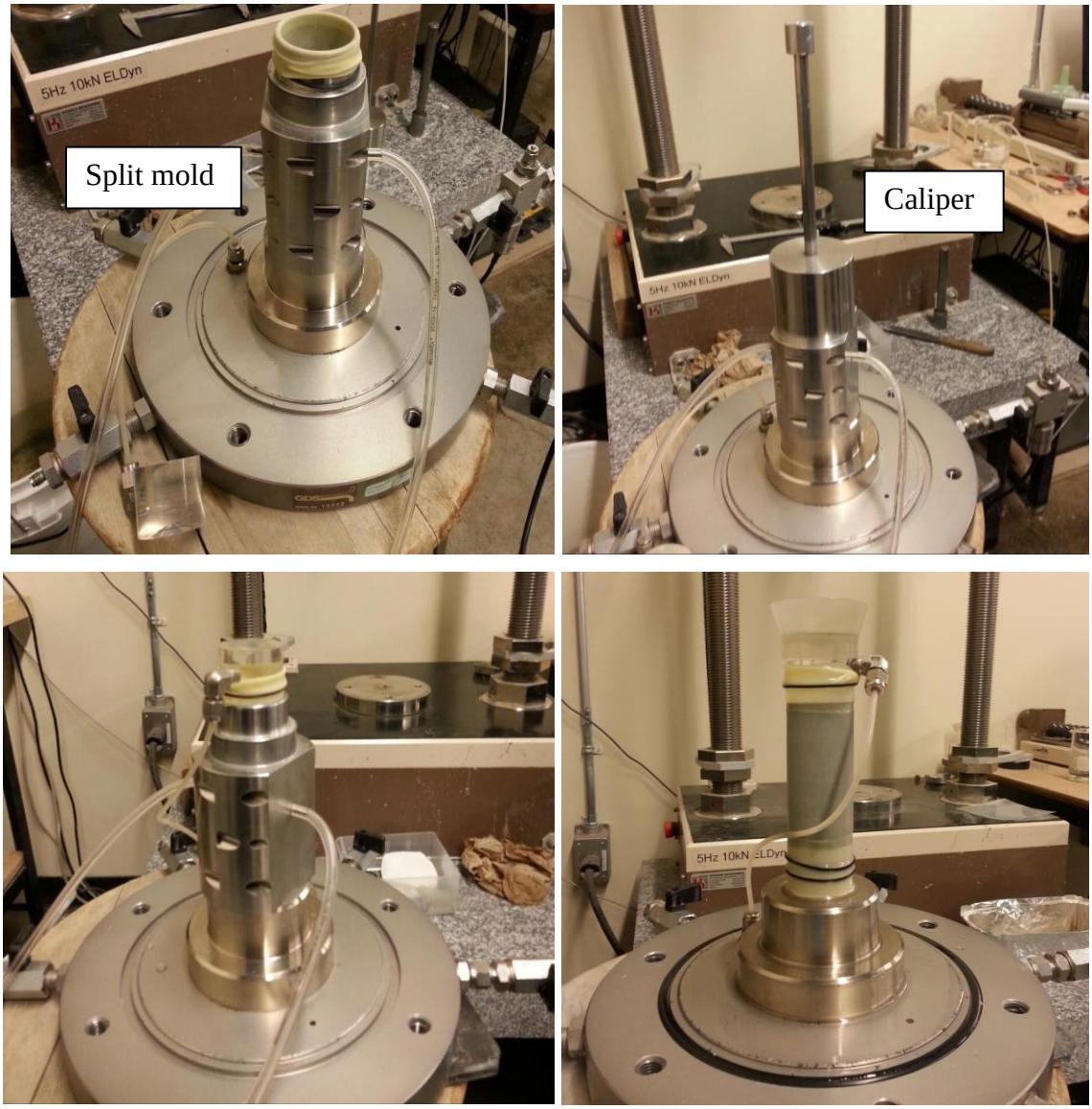

Figure 3.12. Triaxial specimen preparation

- Consolidation stage

Once an acceptable B value had been obtained, the soil specimen was either isotropically (in CTX and T_xSS) or anisotropically (in DSS) consolidated under an effective confining pressure of 75, 60, and 78 kPa for BSP, Carignan and Quebec CF6B sands, respectively. However, for Ottawa sand the reference confining pressure of 100 kPa was selected. The process of consolidation was assumed to be completed if the volume change is less than 5 mm^3/hr. The volume change was used to calculate the density after consolidation and prior to shearing.

- Shearing phase

After the consolidation stage, a monotonic /or sinusoidal cyclic stress/strain wave was applied in CTX and DSS while only strain-controlled tests were performed in the T_xSS under undrained conditions. All sand specimens were cyclically sheared under cyclic loading within a certain range of stress/strain at a frequency of 1 Hz except Carignan sand was sheared under frequency of 1.8 Hz until initial liquefaction occurs. It is noteworthy that the frequency does not have a significant effect on liquefaction potential (Boulanger et al. 1991; Polito 1999; Hazirbaba and Rathje 2009; ASTM-D5311-17).

During the loading phase sequence, pore pressure is generated accompanied by a progressive increment deformation under stress-controlled conditions. Moreover, the effective stress path of loose specimens, in the modified Mohr plane (p′-q), immigrates from its initial effective mean stress value until reaches the phase transformation line (PTL) imparting a contractive behavior. Upon reaching the PTL, the cyclic behavior alternates between contractive and dilative behavior following a butterfly-shaped loop and approaches the failure envelope rapidly, as shown in Figure 3.13. Thus, the soil specimen loss its stiffness and cannot sustain any loading.

Under strain-controlled testing, pore water pressure ratio, R_u curves are flattened out and plateau at a value close to 0.96 as previously observed by (Hazirbaba 2005). Therefore the initial liquefaction has been assumed to occur throughout the current study when the excess pore water pressure ratio, R_u reached 0.9 for stress- and strain-controlled tests. Because of the thickness of the used membrane in the current study is 0.2 mm, the correction of membrane penetration was neglected as suggested by Frydman et al. (1973). The induced shear load/strain, pore/equivalent pore water pressure, and vertical displacement were recorded using a high accuracy pressure transducers and displacement transducers as previously discussed.

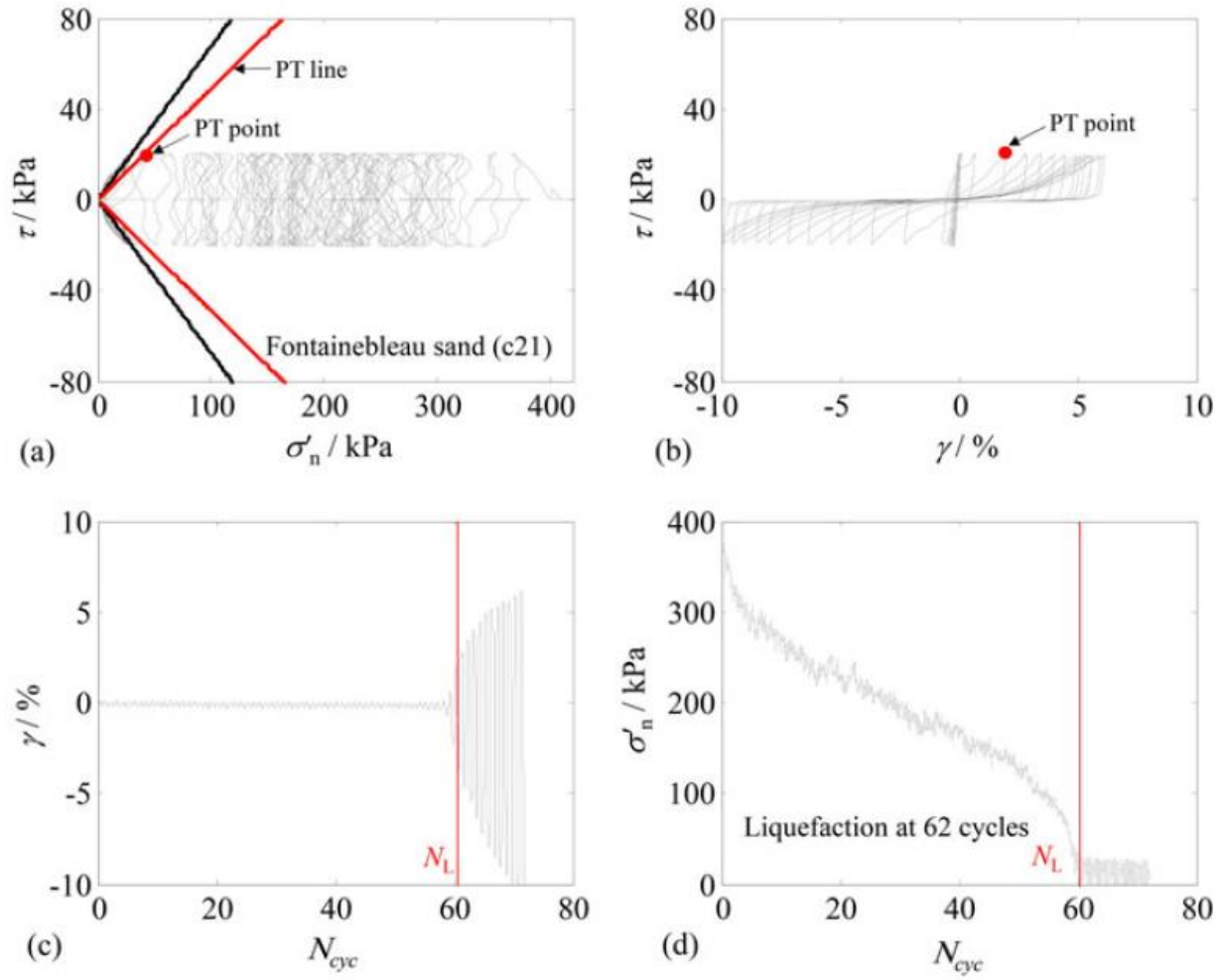

Figure 3.13. Typical cyclic records under DSS: (a) effective stress path; (b) hysteresis loops; (c) cyclic shear strain; (d) degradation of effective vertical stress (from Wu et al. 2018)

CHAPTER 4

USE OF PORE PRESSURE BUILD-UP AS DAMAGE METRIC IN COMPUTATION OF EQUIVALENT NUMBER OF UNIFORM STRAIN CYCLES

Authors and Affiliation:

Marwan Khashila: PhD Candidate, Sherbrooke University, Faculty of Engineering, Sherbrooke, QC.

Mahmoud N. Hussien: Associate Professor, Assiut University, Faculty of Engineering, Assiut, Egypt
Researcher, Sherbrooke University, Faculty of Engineering, Sherbrooke, QC

Mourad Karray: Professor, Sherbrooke University, Faculty of Engineering, Sherbrooke, QC.

Mohamed Chekired: Researcher, Institut de Recherche d'Hydro-Québec, Varennes, Quebec, Canada.

Date of submission: April 2017

State of submission: Published

Journal: Canadian Geotechnical Journal

Reference: Khashila, M. M. Hussien, M., N., Karray, M., Chekired, M., 2018. Use of pore pressure build-up as damage metric in computation of equivalent number of uniform strain cycles. Can Geotech J., 55(4): 538-550. https://doi.org/10.1139/cgj-2017-0231.

French title: Utilisation de la pression interstitielle en tant que mesure du dommage dans le calcul de nombre équivalent de cycles de déformation uniformes.

Contribution in the thesis:

This chapter introduces a strain-based pore water pressure model based on a series of cyclic strain-controlled tests performed on the combined triaxial simple shear (T_xSS) apparatus. The applicability of this model in converting an irregular earthquake loading to an equivalent number of uniform strain cycles, N_{eq} is discussed. The validity of using the earthquake-induced pore-water pressure as damage metric is presented. This model will be adopted in the following chapters to predict the generated pore-water pressure in comparison to another proposed energy-based pore-water pressure model. Additionally, the preliminary cyclic behavior under strain-controlled loading is discussed.

Abstract: The build-up of earthquake-induced excess pore-water pressure may be viewed as analogous to the cumulative damage of saturated granular materials caused by cyclic loading, and consequently as a damage metric when converting an irregular earthquake loading to an equivalent number of uniform cycles, N_{eq}. In this paper, a comprehensive series of strain-

controlled tests have been conducted using the new combined triaxial simple shear (T_xSS) apparatus developed at Institute de Recherche d'Hydro-Quebec (IREQ) in collaboration with the geotechnical group at the Université de Sherbrooke to verify the hypothesis of adopting the pore-water pressure ratio, R_u, as a damage metric when converting earthquakes to an equivalently damaging number of uniform strain cycles. Different reconstituted saturated samples of Baie-Saint-Paul, Carignan, and Quebec CF6B sands have been tested under undrained conditions up to liquefaction. The experimental results from this study have been utilized to develop an empirical expression to compute N_{eq} from both the number of cycles required to trigger liquefaction, N_{liq}, and the material parameter, r. The parameter r had been experimentally calibrated a priori from a separate set of tests using uniform strain cycles following the theoretical framework outlined by Green and Lee (2006). The present results reveal that the measured pore-water pressure ratio, R_u, is in agreement with predicted cumulative damage using the Richart and Newmark (R–N) hypothesis. However, the Palmgren–Miner (P–M) hypothesis underestimates the cumulative damage (i.e., the generated pore-water pressure) during cyclic loading.

Keywords**:** Liquefaction; pore water pressure ratio; number of equivalent cycles; triaxial simple shear apparatus; cumulative damage.

Résumé : L'accumulation de la pression de l'eau des pores excédentaire provoquée par un tremblement de terre peut être considérée comme analogue au dommage cumulatif des matériaux granulaires saturés causés par le chargement cyclique et par conséquent comme mesure des dégâts lors de la conversion d'un chargement de tremblement de terre irrégulier en un nombre équivalent de cycles uniformes, N_{eq}. Dans cet article, une série complète de tests contrôlés par la contrainte a été menée a` l'aide du nouvel appareil de cisaillement simple triaxial combiné (TxSS) développé chez l'Institute de Recherche d'Hydro-Quebec (IREQ) en collaboration avec le groupe géotechnique de l'Université de Sherbrooke pour vérifier l'hypothèse d'adopter le rapport de la pression de l'eau interstitielle, R_u, en tant que mesure de dommage lors de la conversion des tremblements de terre en un nombre équivalent de cycles de contrainte uniformes. Différents échantillons saturés reconstitués de sables Baie-Saint-Paul, Carignan et Québec ont été testés dans des conditions non drainées jusqu'a` la liquéfaction. Les résultats expérimentaux de cette étude ont été utilisés pour développer une expression empirique pour calculer $N_{eq}$, a` partir du nombre de cycles requis pour déclencher la liquéfaction, N_{liq}, et le paramètre matériel r. Le paramètre r, a été étalonné expérimentalement a priori a` partir d'un ensemble distinct de tests utilisant des cycles de

contraintes uniformes suite au cadre théorique décrit par Green et Lee en 2006. Les résultats actuels révèlent que le rapport de pression d'eau des pores mesurée, Ru, est en accord avec les dommages cumulatifs prévus en utilisant l'hypothèse Richart and Newmark (R–N). Cependant, l'hypothèse Palmgren–Miner (P–M) sous-estime le dommage cumulatif (c'est-a` -dire la pression de l'eau des pores générée) pendant la charge cyclique. [Traduit par la Rédaction]

Mots-clés : liquéfaction, taux de pression de l'eau des pores, nombre de cycles équivalents, appareil de cisaillement simple triaxial, dégâts cumulatifs.

4.1 Introduction

Liquefaction of saturated sand deposits under seismic loading is one of the most important damaging phenomena in soil dynamics that can be regarded as a special case of soil fatigue failure resulting from the gradual build-up of excess pore water pressure accompanied by the accumulative loss of strength and stiffness. Over the last several decades, numerous experimental (e.g., Silver and park 1976; Rahman et al. 2014) and field (e.g., Seed et al. 1983; Juang et al. 2003) investigations have been carried out aiming to achieve a closer understanding of the liquefaction phenomenon and to develop reliable procedures to evaluate its potential occurrence in the field. Among these procedures, the simplified procedure developed from empirical evaluations of field and laboratory test data by H. B. Seed and his colleagues at the University of California at Berkeley (hereafter referred to as the Seed et al. procedure) stands as the most widely used procedure. In this procedure, laboratory testing on soil samples subjected to uniform shear stress (i.e., stress-controlled cyclic test) with continuous monitoring of pore-water pressure build-up (undrained tests) or volume change (drained tests) is utilized to construct the soil cyclic loading strength ($CSR–N_{liq}$) curves, where the CSR represents the cyclic stress ratio required to generate liquefaction and N_{liq} represents the corresponding number of cycles (Seed and Idriss 1971). However, applying this procedure intuitively required the conversion of the irregular earthquake motion measured in the field to an equivalent number of uniform stress cycles ($N_{eq\tau}$). In fact, Seed et al. (1975a) applied minor modifications to the well-known Palmgren–Miner (P–M) hypothesis (Palmgren 1924; Miner 1945), originally proposed for metal fatigue analyses, to compute $N_{eq\tau}$ for evaluating the soil liquefaction potentials. Based on the Seed et al. procedure, an intensive research has been done to correlate $N_{eq\tau}$ of earthquake ground motion to facilitate the assessment of liquefaction potential (e.g., Annaki and lee 1977; Liu et al.

2001; Lasley et al. 2017). Although the Seed et al. procedure is simple, empirical, and is based on both laboratory and field observations, several authors (e.g., Silver and Park 1976; Wer and Dobry 1982; NRC 1985; Kazama et al. 2000) pointed out some limitations of the stress-controlled testing adopted in the simplified procedure; for example, the difficulty in defining the exact state at which the liquefaction initiates and the abrupt increase of the pore-water pressure at a higher number of cycles. The limitations of the stress-controlled test were discussed in detail in Kramer (1996) and Liu and Xu (2015).

Moreover, it is well known that the cyclic behavior and cyclic volume change of soils are fundamentally affected more by the cyclic strain amplitude than the cyclic stress amplitude (Dobry and Vucetic 1987; Vucetic 1994). In fact, cyclic strain-controlled tests produce quite consistent and more realistic pore water pressure data because they alleviate the effect of soil fabric and sample disturbance (Silver and Seed 1971; Dobry et al. 1982; Dobry and Vucetic 1987; Vucetic 1994; Chang et al. 2007). For this particular reason, some researchers suggested using cyclic strain-controlled tests as a basis for the computation of the excess pore water pressures (Dobry et al. 1982; Dobry et al, 1985; Vucetic and Dobry 1988), and consequently to construct the (γ_{cyc}–N_{liq}) curves, where γ_{cyc} is the shear strain amplitude required to trigger liquefaction (Talaganov 1996; Sitharam et al. 2012). The (γ_{cyc}-N_{liq}) curve is analogous to the well-known (CSR-N_{liq}) curve obtained from stress-controlled liquefaction tests. The latter curve was previously adopted by Seed et al. (1975a) following the (S-N) metal fatigue curve introduced by Palmgren (1924) and Miner (1945) for metal fatigue studies, where N is the number of uniform stress cycles having amplitude S required to cause a specific degree of strength deterioration of the metal component (Annaki and Lee 1977). To assess soil liquefaction potential, using strain-controlled tests, it is also required to convert an irregular earthquake motion to the number of uniform strain cycles ($N_{eq\gamma}$). Tokimatsu and Seed (1987) assumed that $N_{eq\gamma}$ is equal to $N_{eq\tau}$ for an earthquake motion and presented a correlation relating earthquake magnitude and $N_{eq\tau}$ or $N_{eq\gamma}$ adopting a variant of the P–M hypothesis (Green and Lee 2006). Green and Lee (2006) outlined a theoretical framework supported by some practical examples for computing $N_{eq\gamma}$ adopting the incremental volumetric strain ($\Delta\varepsilon_v$) model proposed by Martin et al. (1975) and its further development by Byrne (1991). In their calculations, Green and Lee (2006) used both P-M (Palmgren 1924; Miner 1945) and R-N (Richart and Newmark 1948) hypotheses of material damage. They pointed out that the P–M hypothesis over-predicts $N_{eq\gamma}$ as compared to the R–N hypothesis. Moreover, the values of the $N_{eq\gamma}$ computed by the R-N hypothesis are significantly equal to

$N_{eq\tau}$ computed by equating the dissipating energy approach outlined earlier by Green and Terri (2005). However, their theoretical work lacks a direct experimental verification for a definite conclusion with respect to the computation of $N_{eq\gamma}$ from the P-M or R–N hypotheses, which is the main objective of the current study.

In this paper, an experimental program was adopted to pursue the theoretical framework of Green and Lee (2006) by adopting the recorded pore water pressure ratio, R_u, ($=\Delta u/\sigma'_{co}$), in strain-controlled tests as a damage metric; where, Δu is the measured excess pore-water pressure, and σ'_{co} is the initial effective stress. The main purposes of this study can be summarized as follows: (i) to investigate the liquefaction potential under strain-controlled condition, (ii) to study the use of pore-water pressure as a damage metric, and (iii) to develop an empirical expression to compute $N_{eq\gamma}$ from both the number of cycles required to trigger liquefaction, N_{liq}, and the material parameter r, experimentally calibrated a priori from a separate set of tests using uniform intensity cycles. To this end, cyclic uniform, non-uniform, and irregular tests were performed in the new combined triaxial simple shear (T_xSS) apparatus (Chekired et al. 2015) developed at the Institut de Recherche d'Hydro-Québec (IREQ) in collaboration with the geotechnical group at the Université de Sherbrooke.

Before describing the experimental program and the experimental results, a brief review of both the P–M and R–N cumulative damage theories and their application in computing equivalent number is presented, followed by an overview of some of the existing pore pressure build-up models relevant to the study described herein.

4.1.1 Equivalent number concept and cumulative damage: a review

The concept of equivalent number of cycles involves converting an irregular earthquake motion to uniform strain or stress cycles having the same damage effect. It was first applied on metal fatigue analysis to convert nonuniform loading resulting from machines and traffic loads to equivalent-damage uniform loads using various cumulative damage hypotheses (Green and Terri 2005). The two main advantages of the conversion process are: (i) one set of laboratory test data can be used to evaluate many earthquake motions (Seed et al. 1975a); (ii) the comparison between the induced earthquake stresses in the field and the resistance obtained from cyclic uniform experimental tests is facilitated.

The P–M approach is the most widely used procedure and it is considered the basis for most engineering problems dealing with irregular loading. It was first introduced by Palmgren (1924) and further developed by Miner (1945) to predict fatigue damage D, of metal under a cyclic non-uniform load. However, the main limitation of the P-M hypothesis

is that it is intended for high cycle fatigue conditions (i.e., large number of cycles with low amplitude). In addition, it does not consider the sequencing of peaks in earthquake time history, which has a significant influence on pore-water pressure build-up in saturated soil (e.g., Martin et al., 1975; Ishihara and Nagase 1988). The main assumption of the P-M hypothesis is that the damage accumulates linearly during cyclic loading. Therefore, the relation between the cumulative damage D, after n cycles with constant load amplitude, versus cyclic ratio R_n, ($R_n=n/N_f$, where, N_f is number of failure cycles) can be obtained by a unique linear relation irrespective of the load amplitude value (i.e., load-independent relationship) (Green and Lee 2006). For a given time history of uniform or nonuniform load amplitude, the total fatigue damage D, according to the P-M hypothesis can be estimated from Eq. (4.1), regardless of load peak sequence (Annaki and Lee 1977).

$$D = \sum_i \frac{n_i}{N_{fi}} \tag{4.1}$$

where i defines each stress level; n_i is the number of cycles having peak stress amplitude S_i; N_{fi} is the number of cycles required to cause failure (D=1) at the same stress intensity. The equivalent number of uniform stress cycles, $N_{eq\tau}$, having reference stress amplitude S_{ref}, which has the same damage effect of an arbitrary pattern and induces failure in N_{ref} cycles, can be obtained following the P-M hypothesis (Annaki and Lee 1977):

$$D = \frac{N_{eq\tau}}{N_{ref}} = \sum_i \frac{n_i}{N_i} \tag{4.2}$$

or

$$N_{eq\tau} = N_{ref} \sum_i \frac{n_i}{N_i} \tag{4.3}$$

In the late 1960s to the early 1970s, H.B. Seed and his colleagues, in their intensive work at Berkeley, adopted the P–M hypothesis to compute $N_{eq\,\tau}$ for evaluation of liquefaction potential (e.g., Lee and Chan 1972; Seed et al. 1975a; Annaki and Lee 1977). Green (2001) introduced adjustments to the P-M method to overcome the aforementioned shortcomings of the P-M hypothesis and to alleviate the influence of soil-softening on the computed dissipated energy (Green and Terri 2005).

Based on the P-M hypothesis, Richart and Newmark (1948) developed a different cumulative damage hypothesis denoted as R-N. The R-N hypothesis accounts for both the amplitudes of the peaks and their sequencing in the ground motion time history. Unlike the P-M hypothesis, the R-N hypothesis is applicable to both high and low cycle fatigue analyses. The R-N hypothesis is also considered as an alternative form to the widely used model

introduced by Martin et al. (1975) and the Byrne (1991) procedure (Green and Lee 2006). In contrast to the P-M hypothesis, R-N is a load-dependent hypothesis, i.e., the relation between cumulative damage D, after n uniform stress or strain cycles, versus cyclic ratio R_n depends on load amplitude and can be obtained according to Green and Lee (2006) by:

$$D = (R_n)^r \tag{4.4}$$

where r is a material parameter that depends on the load amplitudes and R_n is the cyclic ratio. For an applied cyclic stress or strain time history consisting of sequential cycles n_1, n_2, and n_m having varying peak amplitudes of S_1, S_2,and S_m, the cumulative damage D can be estimated after each sequential cycles by:

$$D_1 = \left(\frac{n_1}{N_1}\right)^{r_1} \tag{4.5a}$$

$$D_2 = \left[(D_1)^{\frac{1}{r_2}} + \left(\frac{n_2}{N_2}\right)\right]^{r_2} \tag{4.5b}$$

$$D_m = \left[(D_{m-1})^{\frac{1}{r_m}} + \left(\frac{n_m}{N_m}\right)\right]^{r_m} \tag{4.5c}$$

where D_1, D_2, and D_m are the cumulative damages induced after n_1, n_2, and n_m cycles, respectively; N_1, N_2, and N_m are the number of cycles required to cause liquefaction corresponding to uniform cycles having amplitudes S_1, S_2, and S_m, respectively; r_1, r_2, r_m are the material parameters corresponding to amplitude S_1, S_2, and S_m, respectively, where m is the total number of cycles in the time history. By equating the cumulative damage of earthquake time history, obtained from Eq. (4.5), with that obtained from equivalent uniform cycles (Eq. (4.6)), the equivalent number of uniform cycles, Neq, can be computed from Eq. (4.7).

$$D = \left(\frac{N_{eq}}{N_{ref}}\right)^{r_{ref}} \tag{4.6}$$

$$N_{eq} = N_{ref}\left[(D_{m-1})^{\frac{1}{r_m}} + \left(\frac{n_m}{N_m}\right)\right]^{r_m/r_{ref}} \tag{4.7}$$

where r_{ref} is the material parameter corresponding to the load amplitude S_{ref}. The P-M hypothesis can be considered as a special case of the R-N hypothesis when $r = 1$ for all load amplitudes. That case occurs when the material is load-independent.

4.1.2 Pore pressure build-up models

During earthquake loading on saturated soil, pore water pressure dissipation is not allowed as load is applied in a very short time. Therefore, some of the intergranular effective stresses are transferred to pore-water, which leads to progressive pore water pressure build-up and a decrease of the effective stress (Seed and Lee 1966; Rahman et al. 2014). A variety of models have been developed over the years to predict pore-water pressure ratio R_u, in saturated soil subjected to uniform and earthquake loading as a function of cyclic ratio R_n (Polito et al. 2008). These early models were based on two main approaches: cyclic stress (Seed et al. 1975b) and cyclic strain (Martin et al.1975), which was followed by a strain energy-based model (Nemat-Nasser and Shokooh 1979).

Seed et al. (1975b) introduced the first empirical relation between pore-water pressure ratio, R_u, and cyclic ratio, R_n (Eq. (4.8)), based on the experimental work done by DeAlba et al. (1975).

$$R_u = \frac{1}{2} + \left[\frac{1}{\pi} . \arcsin(2.(R_n)^{\frac{1}{\alpha}} - 1) \right] \tag{4.8}$$

where α is an empirical constant that depends on the soil properties and test conditions (Polito et al. 2008). R_u from Eq.(4.8) was adopted by Wer and Dobry (1982) as a damage metric to compute $N_{eq\tau}$. The advantage of this procedure is that it considers the consequence effect of each half cycle in the time history on pore water pressure build-up. However, its limitations are that it depends on the numerical pore pressure model in addition to the difficulty of defining the exact value for α. According to Polito et al. (2008), the value of α is a function of fine content (FC), relative density (I_D), and CSR and does not equal to 0.7 for all cases. In the current study, the pore water pressure measured in the T_xSS apparatus during application of earthquake time history is used directly as damage metric to compute $N_{eq\gamma}$ by equating the generated pore-water pressure ratio to the one generated by $N_{eq\gamma}$ for uniform strain cycles. In contrast, the use of pore-water pressure build-up in saturated soil as damage metric to compute N_{eq} is generally not recommended by several research studies, particularly with strong ground motions (Haldar and Hochaimi 1984). Haldar and Hochaimi attributed their recommendation to the fact that the R_u may exceed unity prior to the end of shaking in major earthquakes; therefore, the subsequent motions do not contribute to the computation of N_{eq} (Carter et al. 2013). However, cases where R_u exceeds unity are beyond the scope of the current study. The current study, in fact, focuses chiefly on pore-water pressure build-up up to liquefaction (i.e., $R_u = 0.9$).

4.2 Experimental work

4.2.1 Testing apparatus

The combined triaxial simple shear (T_xSS) apparatus developed at IREQ in collaboration with the geotechnical group at the Université de Sherbrooke was used in the current study. The T_xSS was designed to perform simple shear stress testing on a soil specimen in a triaxial condition under strain-controlled drained or undrained conditions. The apparatus allows saturating and consolidating the soil specimen under hydrostatic confining pressure in a triaxial chamber. In addition, it allows testing on reconstituted and intact soil samples under an isotropic or anisotropic conditions. It has the ability to host a cylindrical soil specimen placed in a rubber membrane with a diameter of 80 mm and varying heights. The soil specimen confined in the triaxial chamber can be subjected to both monotonic as well as cyclic uniform and irregular shear stresses. Cyclic tests can be performed on saturated soil specimens and pore-water pressure can be measured during the undrained test. More details about T_xSS can be found in Chekired et al. (2015).

Table 4.1. Physical properties of sands used.

Soil properties	Baie-Saint-Paul sand	Carignan sand	Quebec sand CF6B
G_s	2.78	2.71	2.71
e_{max}	0.91	1.12	0.95
e_{min}	0.60	0.73	0.55
C_u	2.25	2.45	44.44
C_c	1.00	1.00	12.25
D_{50}	0.15	0.15	0.33

4.2.2 Testing Program

Three types of sands with different physical properties were collected from different areas in the province of Quebec: Baie-Saint-Paul (BSP), I_D= 55%; Carignan sand, I_D = 47 and 80%; and Quebec sand CF6B, I_D = 64%. Physical properties of the sands used are summarized in Table 4.1. The grain-size distribution curves of these sands are shown in Figure 4.1. Figure 4.1 also shows the range of grain-size distribution curves for liquefaction-susceptible soils as proposed by Xenaki and Athanasopoulos (2003). As shown in Figure 4.1, the sands used fall in the grain-size distribution ranges of liquefiable soils. A total of 24 tests were conducted on isotropically consolidated soil samples using the T_xSS apparatus. Table 4.2 summarizes the conditions of all tests performed in this study.

Preparation method has a significant effect on the pore pressure build-up and deformation pattern during cyclic loading (Sze and Yang 2014). The wet tamping preparation

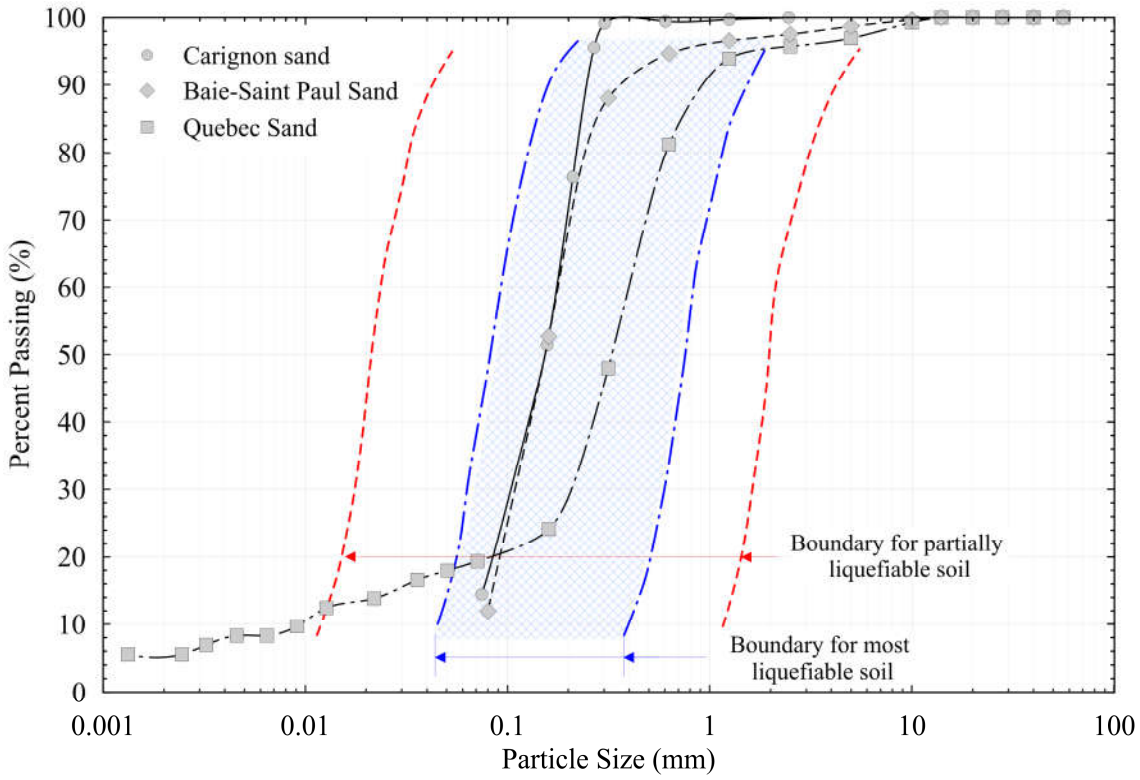

Figure 4.1. Grain-size distribution curves of sands used

method was adopted to prepare reconstituted soil specimens in a rubber membrane in the T_xSS cell. This method was selected in the current study as it enables preparation of reconstituted soil samples at a wide range of initial densities with a high degree of precision (Sze and Yang 2014). In addition, it provides more isotropic fabric samples (Yang et al. 2008). Moist soil specimens of 80-mm diameters (d) and 25 mm height (h) (d/h = 3.2 (ASTM 2017)) were prepared in three layers from the aforementioned sands. Park (1999) and Frost and Park (2003) concluded that the compaction stress must not be higher than the confining pressure used, to avoid pre-stressing soil sample. Thus, each layer was compacted gently using a 340 g hand tamper until the desired density was achieved. To saturate the soil specimen, carbon dioxide (CO_2) gas was flushed through each soil sample for 15 minutes. Subsequently, de-aired water was percolated through the soil sample under a slight back-pressure of 50 kPa with a cell pressure of 40 kPa for 2 hours. Next, a back-pressure of 200 kPa was applied with a cell pressure of 190 kPa for 15 hours. To ensure the full saturation of the soil, the Skempton's pore pressure parameter B ($\Delta u/\Delta\sigma_3$) was estimated for each test by measuring the increase in pore-water pressure, Δu, induced by increasing cell pressure by $\Delta\sigma_3$, where σ_3 is the minor principal stress. Full saturation was defined when $B \geq 0.96$ was achieved. Once an acceptable B value had been obtained, the soil specimen was isotropically

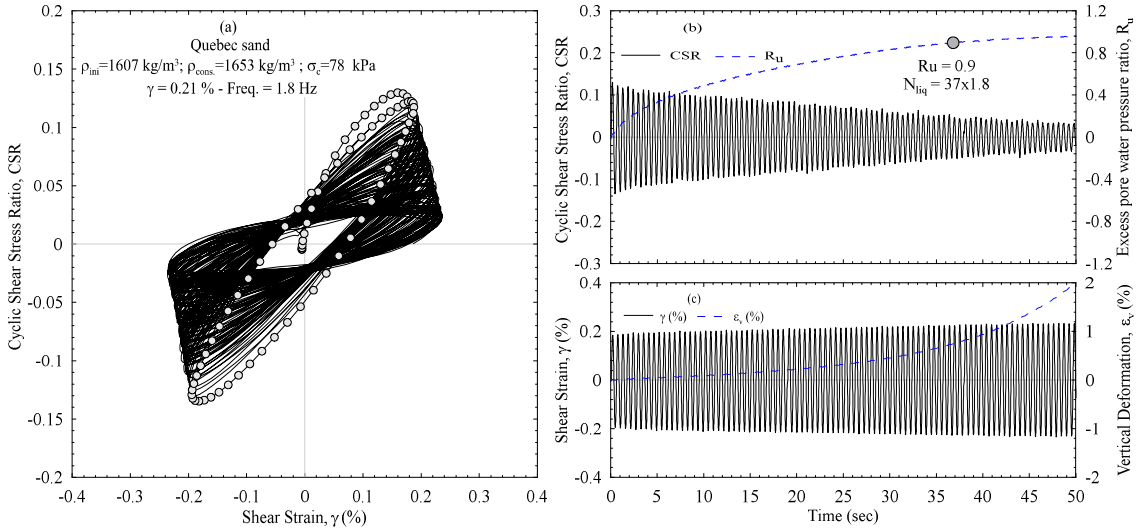

Figure 4.2. Typical records of T_xSS test (Q4) on Quebec sand (a) hysteresis loop (CSR-γ_{cyc}), (b) CSR and R_u versus time, (c) shear strain and vertical deformation versus time

consolidated under an effective confining pressure of 75, 60, and 78 kPa for BSP, Carignan, and Quebec CF6B sands, respectively. After the consolidation stage, all soil specimens under undrained condition were subjected to cyclic uniform or irregular shear strain time histories (strain-controlled) until initial liquefaction had occurred. Initial liquefaction is defined throughout this study as R_u = 0.9. The uniform shear strains were applied on BSP and Carignan sands at a loading frequency of 1.0 Hz, while Quebec sand CF6B was tested at 1.8 Hz. It is noteworthy that frequency does not have significant effect on liquefaction potential (Boulanger et al. 1991; Polito 1999; Hazirbaba and Rathje 2009).

4.2.3 Experimental results

Typical records of the T_xSS test (Q4) on Quebec CF6B sand under uniform shear strain are presented in Figure 4.2. Figure 4.2(a) portrays the variation of the cyclic stress ratio, *CSR,* with the applied shear strain, γ_{cyc}. Figure 4.2(b) shows the build-up of the pore-water pressure ratio, R_u, with the time, while Figure 4.2(c) presents the variation of the vertical deformation, ε_v, with time. Figure 4.2(a) shows that the hysteresis (*CSR*-γ_{cyc}) loops become flatter with the increase of number of cycles and ultimately become horizontal at initial liquefaction. Generation of the pore-water pressure is accompanied by a gradual decrease in the *CSR* as shown in Figure 4.2(b). The increase in R_u is associated with an increase in the vertical deformation ε_v, of soils as shown in Figure 4.2(c). The decrease of the *CSR* value results from degradation of the shear modulus of the soil that can be related to the pore water pressure ratio R_u (Eq. 4.9) (Matasovic and Vucetic 1993; Chang et al. 2007; Moreno-Torres et al. 2010):

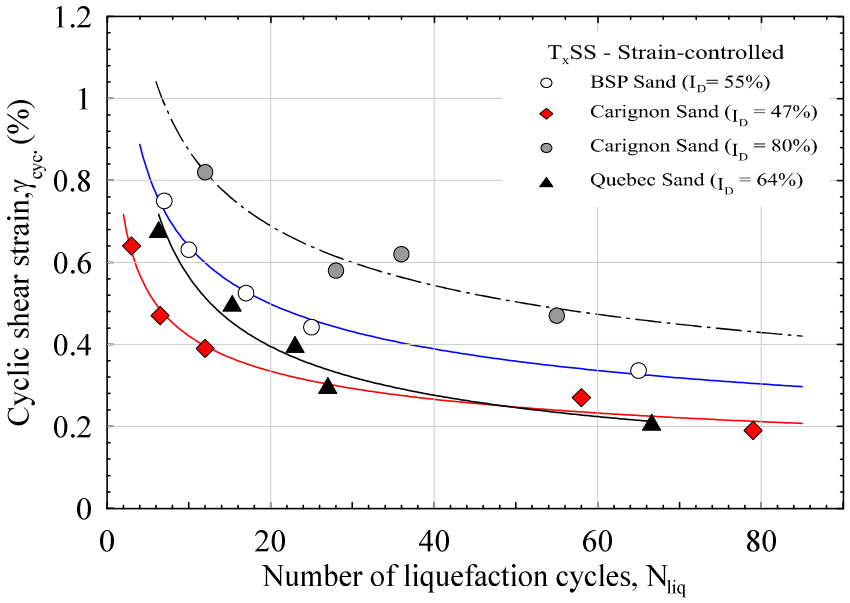

Figure 4.3 Variation of cyclic shear strain, γ_{cyc} with N_{liq}

$$G = G_{max}\left[1 - R_u\right]^{0.5} \tag{4.9}$$

in which G_{max} is the maximum shear modulus and G is the shear modulus at any cycle.

Figure 4.3 presents liquefaction potential curves (γ_{cyc}-N_{liq}) of BSP, Carignan sand, and Quebec CF6B sand, where γ_{cyc} is the uniform shear strain and N_{liq} is the number of cycles required to cause liquefaction (R_u = 0.9). Table 4.2 summarizes the N_{liq} values obtained from all the tests conducted in the current study. All resistance (γ_{cyc}-N_{liq}) curves have the same trend, like the *CSR*- N_{liq} curve, wherein N_{liq} is inversely proportional to the shear strain amplitude. Figure 4.3 shows the effect of the relative density of soils on the liquefaction potential wherein denser Carignan sand (I_D= 80%) has higher liquefaction resistances than the looser one (I_D = 47%) at different strain levels. This is in agreement with earlier observations by several researchers (e.g., Peacock and Seed 1968; Tatsuoka et al. 1982; Liu and Xu 2015). Although BSP (I_D = 55%, σ'_{co} = 75 kPa) and Carignan (I_D = 47%, σ'_{co} = 60 kPa) sands have close D_{50}, C_u, and C_c values (Table 4.1), where D_{50}, C_u, and C_c are the median grain size, coefficient of uniformity, and coefficient of curvature, respectively, and are prepared at similar relative density, $I_{D\ (consolidated)} \cong 60\%$, their liquefaction potential curves are very different. This difference can be attributed to: (1) the difference in the particle shape characteristics (e.g., Kramer 1996; Cabalar et al. 2013) wherein the liquefaction potential of sand that has angular-shaped particles (BSP sand) is higher than sand that has round-shaped particles (Quebec sand CF6B) and (2) the state of stress wherein liquefaction potential increases with increasing effective confining pressure (e.g., Youd et al. 2001; Liu and Xu 2015).

Table 4.2. Summary of test conditions and results

Sand	Test No.	γ_{cyc}	e_{ini}	e_{cons}	ρ_{dry}	$I_D(\%)$	σ'_{co}	B	N_{liq}	r
Baie-Saint-	B1	0.75	0.771	0.738	1.6	55	75	0.95	7.0	0.40
Paul[a]	B2	0.44	0.768	0.735	1.6	55	75	0.97	25.0	0.45
	B3	0.63	0.767	0.732	1.6	55	75	0.97	10.0	0.50
	B4	0.53	0.773	0.732	1.6	55	75	0.97	17.0	0.55
	B5	0.33	0.771	0.743	1.6	55	75	0.97	65.0	0.60
	B6	Nonuniform (Fig. 4.6a)	0.766	0.739	1.6	55	75	0.97	--	Variable
	B7	Nonuniform (Fig. 4.6b)	0.765	0.751	1.6	55	75	0.97	--	Variable
	B8	Earthquake (Synthetic 1)	0.775	0.738	1.6	55	75	0.97	--	Variable
	B9	Earthquake (Synthetic 2)	0.772	0.740	1.6	55	75	0.97	--	Variable
Carignan sand[a]	C1-1	0.47	0.932	0.881	1.4	47	60	0.97	6.5	0.48
	C1-2	0.64	0.936	0.884	1.4	47	60	0.97	3.0	0.40
	C1-3	0.39	0.938	0.889	1.4	47	60	0.97	12.0	0.50
	C1-4	0.19	0.938	0.871	1.4	47	60	0.97	79.0	0.63
	C1-5	0.27	0.932	0.859	1.4	47	60	0.97	58.0	0.55
	C1-6	Earthquake (Synthetic 3)	0.934	0.880	1.4	47	60	0.97	--	Variable
	C2-1	0.62	0.824	0.795	1.5	80	60	0.97	36.0	0.50
	C2-2	0.47	0.819	0.790	1.5	80	60	0.97	55.0	0.55
	C2-3	0.58	0.812	0.785	1.5	80	60	0.97	28.0	0.49
	C2-4	0.82	0.807	0.774	1.5	80	60	0.97	12.0	0.45
Quebec sand	Q1	0.50	0.690	0.610	1.6	64	78	0.97	15.3	0.32
CF6B[b]	Q2	0.40	0.689	0.616	1.6	64	78	1.00	23.0	0.35
	Q3	0.30	0.689	0.618	1.6	64	78	1.00	27.0	0.40
	Q4	0.21	0.686	0.639	1.6	64	78	0.97	66.6	0.47
	Q5	0.68	0.687	0.626	1.6	64	78	0.97	6.3	0.40

Note:
[a]Frequency = 1.0 Hz.
[b]Frequency = 1.8 Hz.

Based on the uniform strain-controlled test results and following the R-N cumulative damage hypothesis (Eq. (4.5)), an empirical expression (Eq. (4.10)) was developed to calibrate the material parameter *r*, using the pore water pressure build-up as a damage metric

$$R_u = 0.9\left[R_n\right]^r \tag{4.10}$$

where R_n is cyclic ratio ($R_n = n/N_{liq}$)

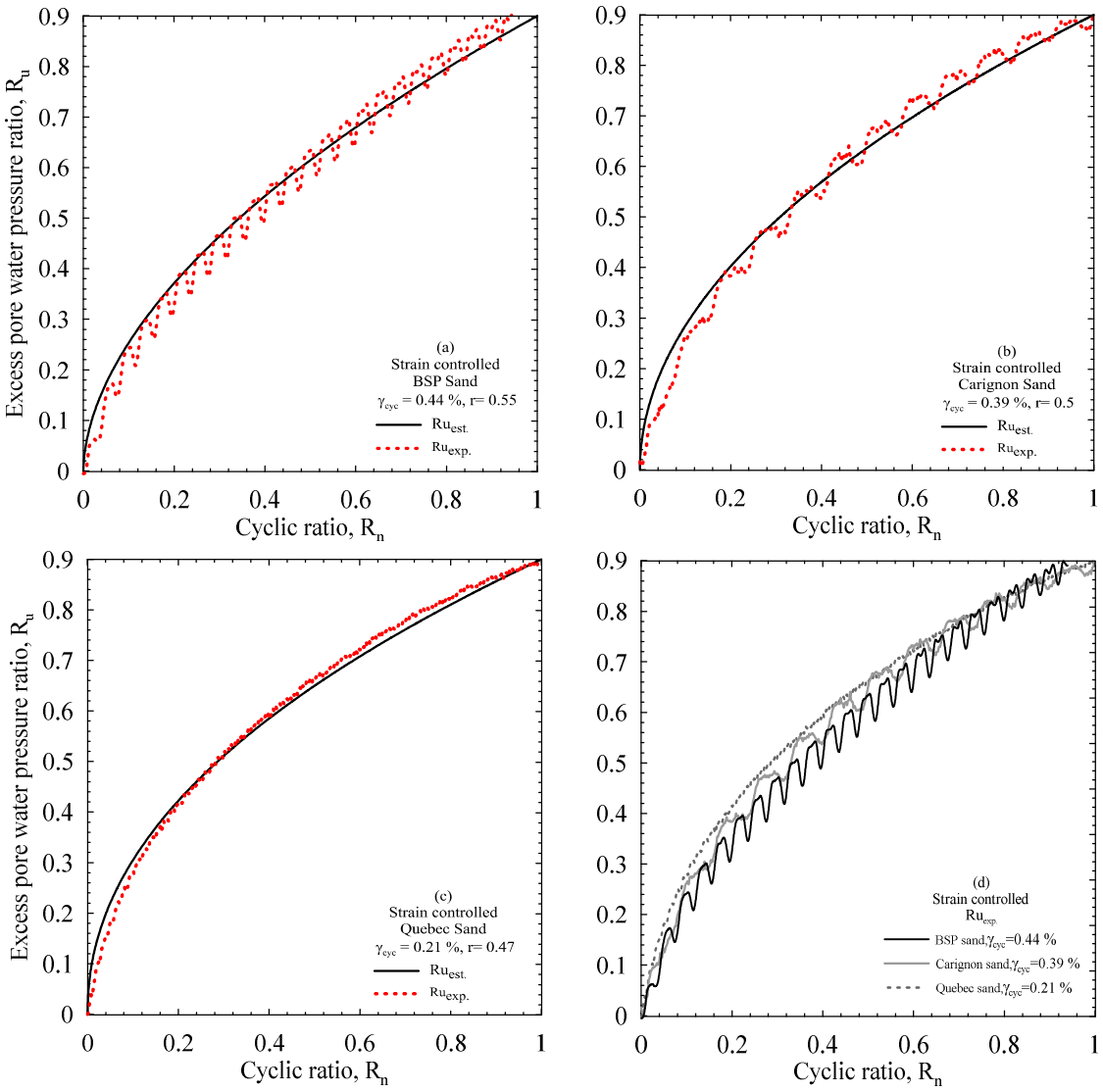

Figure 4.4. Validation of proposed relation: (a) BSP sand, (b) Carignan sand, (c) Quebec sand, and (d) R_u-R_n relations for all the aforementioned sands.

Figure 4.4 presents a comparison between the measured pore-water pressure ratio, $R_{u.exp.}$, and that estimated from Eq. (4.10), $R_{u.est.}$, using the calibrated material parameter r. It can be observed that there is a good correspondence between measured and estimated pore-water pressure ratio R_u. Therefore, the use of Eq. (4.10) in conjunction with measured pore-water pressure can be considered as an alternative approach to calibrate r. In contrast, Green and Lee (2006) adopted the volumetric change procedure to calibrate the parameter r based on the Martin et al. (1975) model and its subsequent development by Byrne (1991).

The calibrated values of material parameter r, from Eq. (4.10) for BSP sand (I_D = 55%), Carignan sand (I_D = 47 and 80%), and Quebec CF6B sand (I_D = 64%), are listed in Table 2.4. The variation of r with the applied shear strain amplitude, γ_{cyc}, for tested sands is presented in

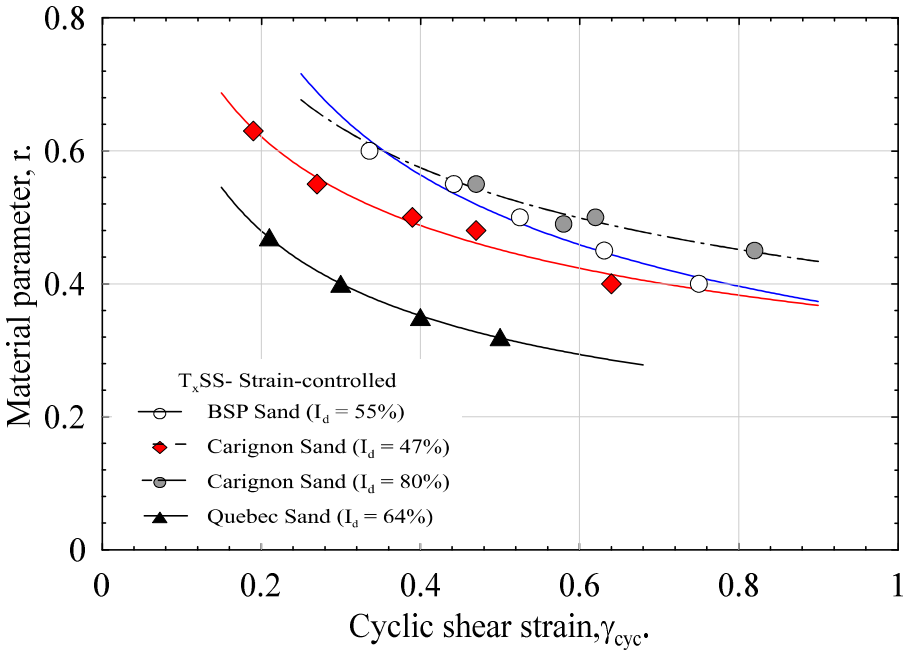

Figure 4.5. Calibration of the material parameter, *r*

Figure 4.5. It is observed in all calibrated curves that the values of *r* reduce with increasing cyclic shear strain, γ_{cyc}. Moreover, *r* changes from one soil to another wherein Quebec CF6B sand has the lowest calibration curve while Carignan sand (I_D= 80%) has the highest one. This variation may be due to the change of particle shape while the coefficient of uniformity, C_u, and coefficient of curvature, C_c, may not have a significant effect.

Liquefaction potential curves (Figure 4.3) were used in conjunction with *r* (Figure 4.5) to compute the cumulative damage by both P-M and R-N hypotheses (Eq. (4.5)) of two synthetic nonuniform strain time histories (B6 and B7) applied on BSP sand. The first strain time history (B6) (Figure 4.6a) consists of four sequences of uniform strain cycles with amplitudes of 0.3, 0.35, 0.4, and 0.45. The second strain time history (B7) (Figure 4.6b) consists of five sequences of uniform strain cycles (three sequences with amplitude 0.45 interposed with two sequences having an amplitude of 0.3). The P-M hypothesis can be yielded from Eq. (4.5) by setting r = 1 for all strain amplitudes (Green and Lee 2006). The computed cumulative damages by both P-M and R-N hypotheses are compared with the measured R_u after applying B6 and B7 in Figures 4.6(a) and 4.6(b), respectively. It is observed that the generated R_u and the computed cumulative damage by the R-N hypothesis are identical in both cases of B6 and B7. However, the corresponding cumulative damage by the P-M hypothesis is significantly less than that obtained by the R-N hypothesis and does not correctly reflect the generation of pore-water pressure during cyclic loading.

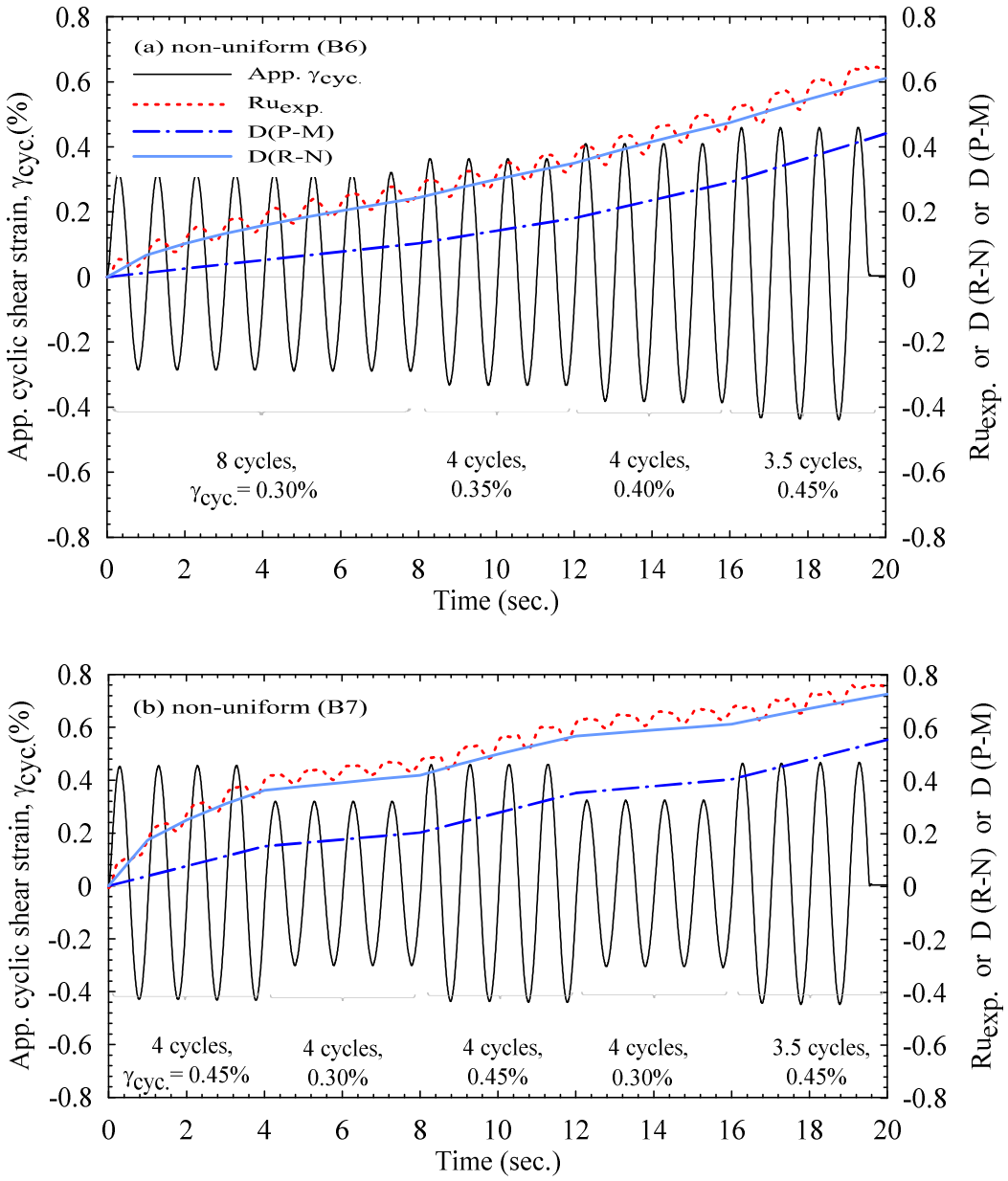

Figure 4.6. Relation between applied γ_{cyc}, measured R_{uexp}, and cumulative damage computed by P-M and R-N hypotheses for BSP sand: (a) non-uniform (B6), and (b) nonuniform (B7).

To investigate the validity of using pore-water pressure as a damage metric under earthquake time history, two synthetic earthquake ground motions introduced by Atkinson (2009) in addition to an incompatible earthquake (from USA) were used in the current study. The synthetic earthquake ground motions were first matched to the spectral accelerations reference of class A (NRC 2005) for BSP and Carignan regions (Figure 4.7). The compatible accelerograms are shown in Figures 4.8(a), and 4.8(c) wherein the incompatible earthquake shown in Figure 4.8(b).

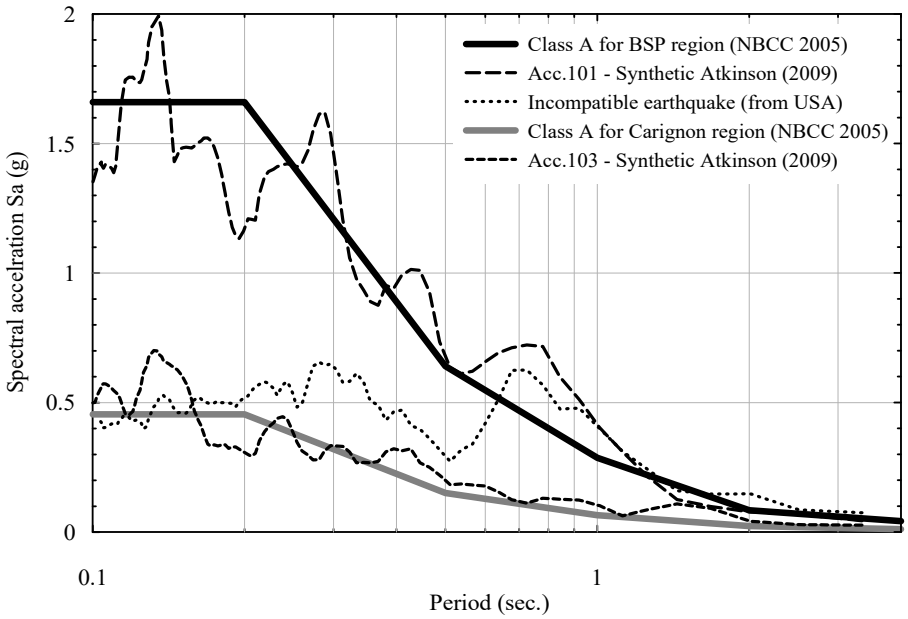

Figure 4.7. Spectra for accelerations used

The computer code FLAC 2D (Itasca 2010) was then utilized to analyze the response of the BSP and Carignan (I_D = 47%) sand deposits to the compatible and the incompatible accelerograms applied at their bases. The description of these deposits and in-situ test metrics can be found in (Karray et al. 2011). The strain time histories response, synthetic 1 and synthetic 2, of BSP deposit to acceleration (acc. 101) (Figure 4.8a) and the incompatible earthquake (Figure 4.8b) at certain depths (depending on the confining pressure applied in the test) are shown in Figures 4.9(a) and 4.9(b), respectively. Meanwhile, the strain time histories response, synthetic 3, of Carignan (I_D = 47%) deposit to acc. 103 (Figure 4.8c) are shown in Figure 4.9(c).

The strain time history responses were then applied to the BSP, B8 and B9, and Carignan (I_D = 47%), C1-6, sand samples in the T_xSS apparatus. The recorded R_u values are compared with the cumulative damage computed using the P-M and the R-N hypotheses in Figures 4.9(a), 4.9(b), and 4.9(c). It is noteworthy that the peak counting method was used to determine the number of peaks and valleys in the earthquake time history. By applying this method, all peaks above the reference level (x-axis) and valleys below the reference level (x-axis) in the earthquake time history are counted (Green and Terri 2005; Hancock and Bommer 2005; ASTM 2011). All counted peaks and valleys in computing the cumulative damage are marked as "x" in Figure 4.9. Each peak or valley value represents a half loading cycle (Seed at al. 1975a, ASTM 2011). In contrast to the previous work by Seed et al. (1975a) wherein neglecting small amplitude cycles does not influence results, all amplitudes are counted in the current study in calculation of pore-water pressure build-up "cumulative

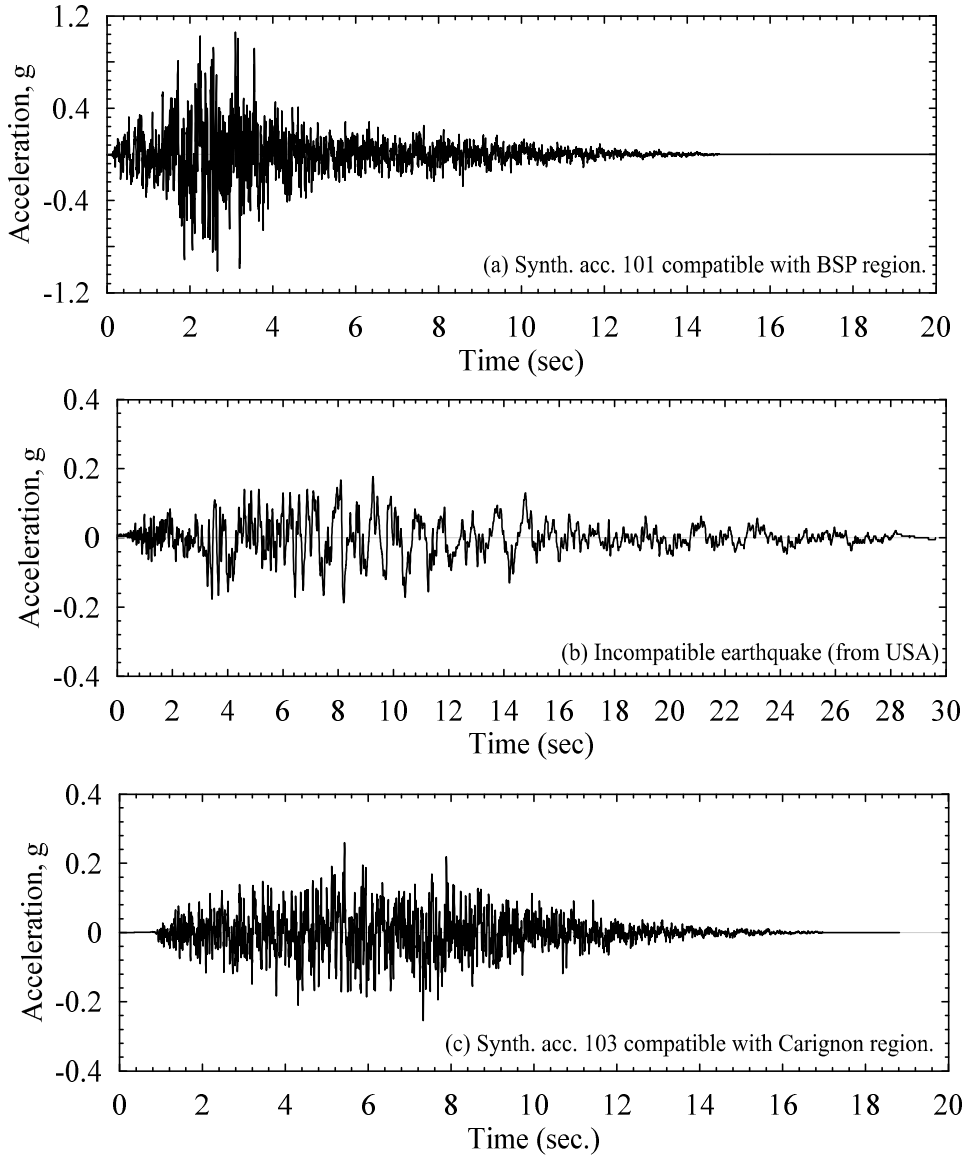

Figure 4.8. Acceleration time history used in current study for: (a, b) BSP sand, and (c) Carignan sand.

damage" and are inherent in computing the equivalent number. Figures 4.9a, 4.9b, and 4.9c show that the computed cumulative damage using the R-N hypothesis is in good agreement with the measured pore-water pressure for both BSP and Carignan sands. However, the cumulative damage computed by the P-M hypothesis doesn't correctly reflect the cumulative damage (i.e., the generated pore water pressure) during cyclic loading. This can be attributed to the deficiency of the P-M hypothesis to account for the sequence of loading peaks. As the R-N hypothesis considers the load sequence, it can be used with an acceptable degree of accuracy to compute cumulative damage, which represents pore-water pressure build-up,

during uniform, nonuniform, and irregular earthquake shear strain time histories (Figures 4.4, 4.6, and 4.9), which was theoretically concluded earlier by Green and Lee (2006).

4.3 Converting earthquake strain time history to equivalent uniform strain cycles, $N_{eq\gamma}$

As shown in the previous section, there is good agreement between the computed cumulative damage using the R-N hypothesis and the measured pore water pressure. Therefore, a new alternative formula to Eq. (4.7) can be used to predict $N_{eq\gamma}$ up to liquefaction occurrence, i.e., R_u = 0.9, using the measured pore-water pressure in the T_xSS apparatus as a damage metric

$$N_{eq\gamma} = N_{Liq.ref}\left[R_u\right]^{1/r_{ref}} \tag{4.11}$$

in which, R_u is the measured pore water pressure ratio after applying cyclic strain time history $N_{liq.ref}$ is the number of uniform strain cycles having amplitude γ_{ref} required to achieve the liquefaction occurrence (Figure 4.3) and r_{ref} is the calibrated material parameter corresponding to γ_{ref} (Figure 4.5).

Figures 4.10(a), 4.10(b) and 4.10(c) compare the generated pore-water pressure ratio, R_u, in BSP sand samples after applying uniform strain cycles, γ_{cyc}, of 0.75, 0.525, and 0.33, with that generated after applying B6 (Figure 4.6a), B8 (Figure 4.9a), and B9 (Figure 4.9b), respectively. Figure 4.10(d) compares the generated R_u in Carignan sand (I_D= 47%) after applying uniform strain cycles γ_{cyc}, of 0.27 and 0.20 with that generated after applying C1-6 (Figure 4.9c). The number of uniform strain cycles, $N_{eq\gamma}$, required to generate R_u of 0.6, 0.42, and 0.9 (corresponding to test, B6, B8 and B9, respectively) in BSP sand samples are listed in Tables 4.3a, 4.3b, and 4.3c, respectively. The number of uniform strain cycles, $N_{eq\gamma}$, required to generate R_u of 0.205 (corresponding to C1-6) in Carignan sand samples is listed in Tables 4.3d. The corresponding values of $N_{eq\gamma}$ computed using the P-M and R-N hypotheses (Eqs. (4.3) and (4.7), respectively) in conjunction with liquefaction potential curves (γ_{cyc}-N_{liq}) in Figure 4.3 of BSP sand (B6, B8, and B9) and Carignan sand (C1-6), are also listed in Table 4.3. In fact, the liquefaction potential curves (γ_{cyc}-N_{liq}) are used as weighting curves wherein N_{liq} for each peak in earthquake strain time history can be determined. It can be seen from the values presented in Table 4.3 for both BSP and Carignan sands that there is good agreement between the computed $N_{eq\gamma}$ values using the R-N hypothesis (Eq.(4.7)), and the experimentally determined values (Figure 4.10) adopting pore-water pressure as a damage metric, which strongly confirms the use of Eq. (4.11) in computation of $N_{eq\gamma}$. In contrast, the values of $N_{eq\gamma}$ computed using the P-M hypothesis (Eq. (4.3)), especially for Carignan sand,

are overestimated, which is consistent with the results reported earlier by Green and Lee (2006) based on their theoretical approach. However, in the case of liquefaction occurrence (test B9), both cumulative damage hypotheses (R-N and P-M) yielded $N_{eq\gamma}$ values equal to that obtained by using pore-water pressure build-up as a damage metric. These results provide experimental credence for the use of the R-N hypothesis in computing the cumulative damage and the equivalent number of strain cycles $N_{eq\gamma}$.

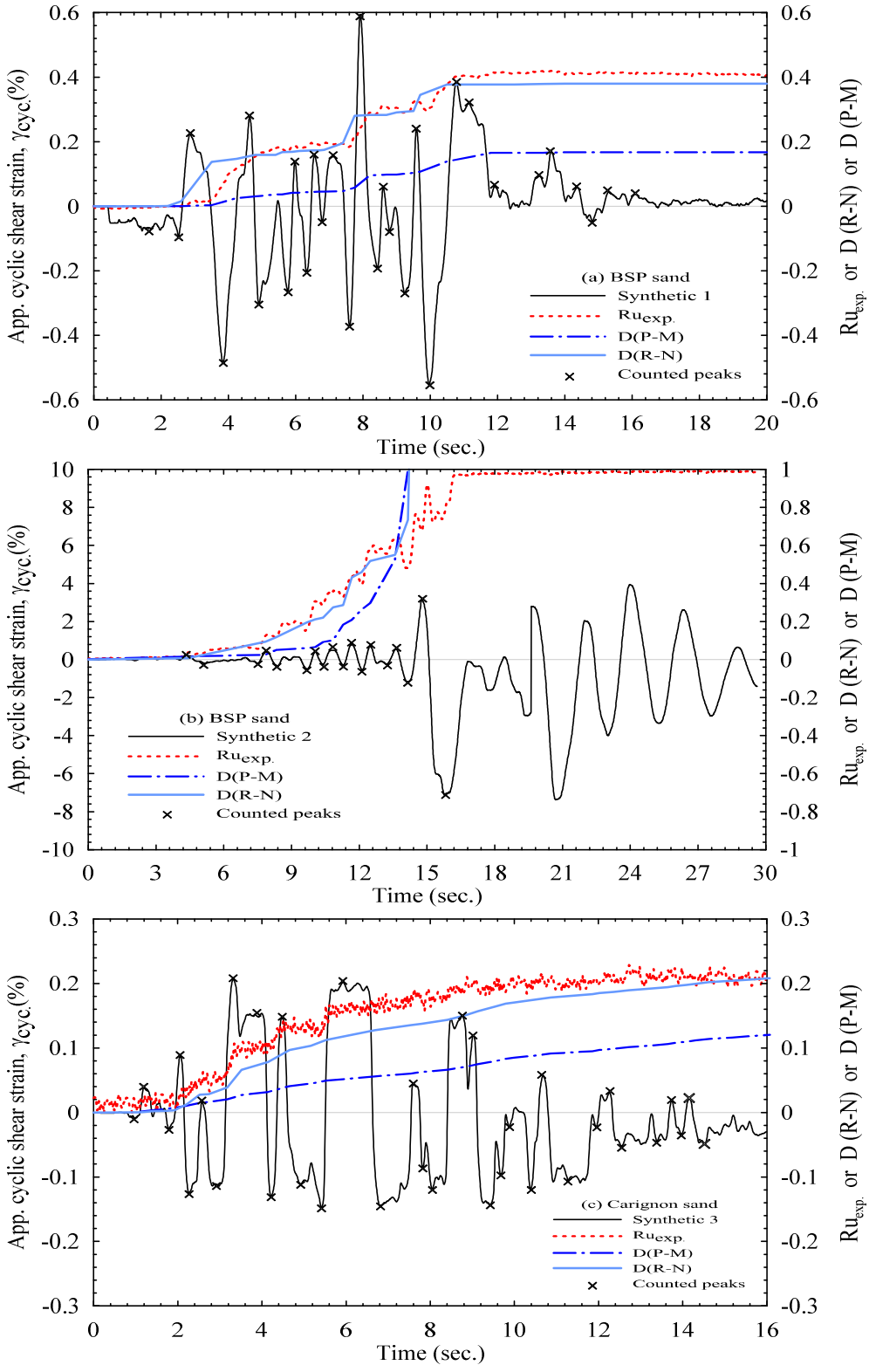

Figure 4.9. Relation between applied γ_{cyc}, measured R_u, and cumulative damage by P-M and R-N hypotheses for (a) BSP sand (B8), (b) BSP sand (B9), and (c) Carignan sand (C1-6).

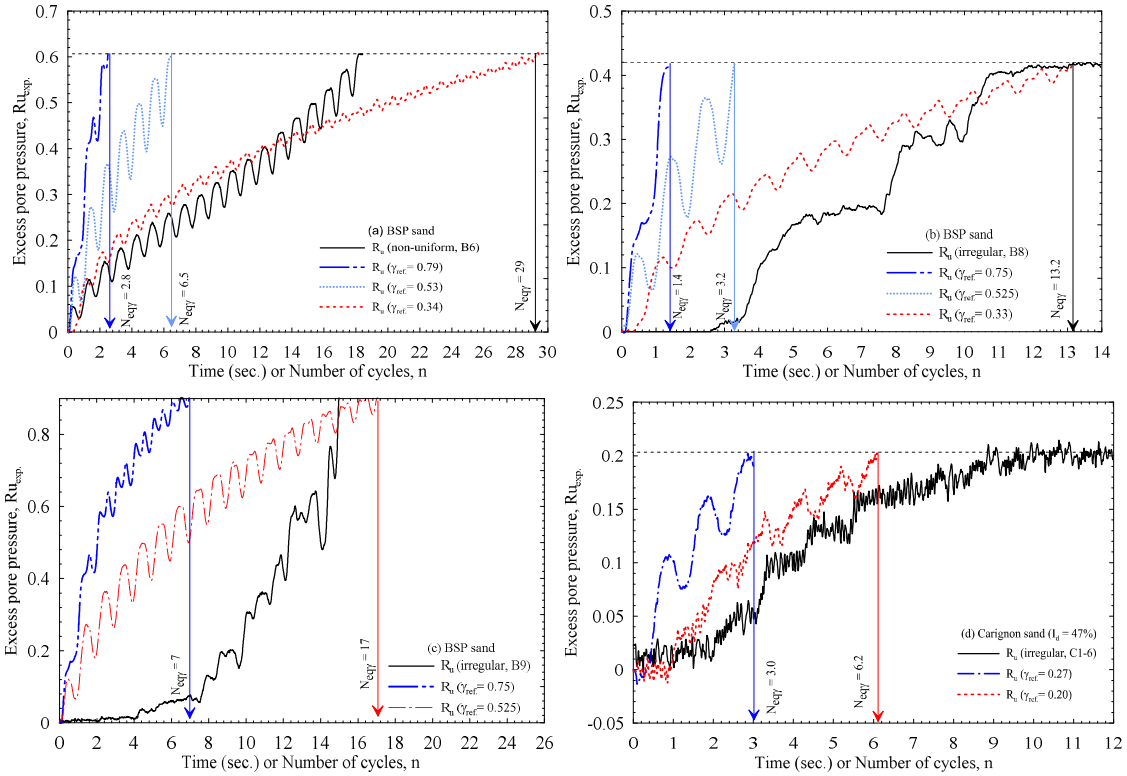

Figure 4.10. Excess pore-water pressure ratio versus time required to cause: (a) R_u = 0.6 for BSP, (b) R_u = 0.42 for BSP, (c) R_u = 0.9 for BSP, and (d) R_u = 0.205 for Carignan sands.

Table 4.3. Summary of computing procedure of $N_{eq\gamma}$.

(a) B6

γ_{ref}	$N_{liq\text{-}ref}$	r_{ref}	$N_{eq\gamma}$ (R-N)	$N_{eq\gamma}$ (P-M)	$N_{eq\gamma}$ (Fig. 4.10a)
0.330	65	0.601	28.5	28.6	29
0.525	17	0.505	6.8	8	6.5
0.750	7	0.442	2.3	3	2.8

(b) Synthetic 1 (B8)

γ_{ref}	$N_{liq\text{-}ref}$	r_{ref}	$N_{eq\gamma}$ (R-N)	$N_{eq\gamma}$ (P-M)	$N_{eq\gamma}$ (Fig. 4.10b)
0.330	65	0.601	14.15	10.9	13.2
0.525	17	0.505	2.77	3.0	3.2
0.750	7	0.442	0.88	1.17	1.

(c) Synthetic 2 (B9).

γ_{ref}	$N_{liq\text{-}ref}$	r_{ref}	$N_{eq\gamma}$ (R-N)	$N_{eq\gamma}$ (P-M)	$N_{eq\gamma}$ (Fig. 4.10c)
0.525	17	0.505	17	17	17
0.750	7	0.442	7	7	7

(d) Synthetic 3 (C1-6).

γ_{ref}	$N_{liq\text{-}ref}$	r_{ref}	$N_{eq\gamma}$ (R-N)	$N_{eq\gamma}$ (P-M)	$N_{eq\gamma}$ (Fig. 4.10d)
0.20	79	0.63	6.13	10.00	6.20
0.27	58	0.55	3.10	7.34	3.00

CHAPTER 5

LIQUEFACTION RESISTANCE FROM CYCLIC SIMPLE AND TRIAXIAL SHEARING, A COMPARATIVE STUDY

Authors and Affiliation:

Marwan Khashila: PhD Candidate, Sherbrooke University, Faculty of Engineering, Sherbrooke, QC.

Mahmoud N. Hussien: Associated Professor, Assiut University, Assiut, Egypt.

Researcher, Sherbrooke University, Faculty of Engineering, Sherbrooke, QC.

Mourad Karray: Professor, Sherbrooke University, Faculty of Engineering, Sherbrooke, QC.

Mohamed Chekired: Researcher, Institut de Recherche d'Hydro-Québec, Varennes, Quebec, Canada.

Date of submission: August 2019

State of submission: under review

Journal: Canadian Geotechnical Journal

French title: LA RÉSISTANCE À LA LIQUÉFACTION PAR CISAILLEMENT SIMPLE ET TRIAXIAL DIRECT DANS DES CONDITIONS DE CHARGE CONTRÔLÉES PAR CONTRAINTE ET DÉFORMATION, UNE ÉTUDE COMPARATIVE.

Contribution in the thesis:

This chapter introduces a coupled energy-based pore water pressure model based on a series of cyclic strain-controlled tests performed on the combined triaxial simple shear (T_xSS) apparatus. This chapter provides a link to immigrate from cyclic strain to stress-controlled loading using the energy concept. The ability of using this model to simulate element level cyclic stress-controlled T_xSS tests is presented. To further validate the accuracy of the proposed energy model, comparisons between numerically captured liquefaction potential curves with (i) alternative stress-controlled T_xSS, (ii) available liquefaction potential curves (CSR-N_{liq}) in literature, and (iii) from stress-controlled DSS testing results are illustrated. Further, correlations between stress and strain-controlled liquefaction potential curves are proposed.

Abstract: While cyclic triaxial (CTX) tests are widely used in liquefaction studies due to their simplicity, direct simple shear (DSS) tests and their ilk (e.g., the combined triaxial simple shear, T_xSS) are more representative of stress conditions produced during an earthquake. Therefore, the CTX results should be properly correlated to simulate field conditions. In the current study, a series of CTX testing results performed on reconstituted specimens of Baie-Saint-Paul, Ottawa C-109, and Quebec CF6B sands are compared to the corresponding T_xSS and DSS results under both stress and strain-controlled conditions. The T_xSS stress-controlled tests are numerically simulated by adopting a coupled energy-based pore water pressure model using the computer code, FLAC. The T_xSS numerical results are successfully compared with those obtained experimentally from (i) alternative stress-controlled T_xSS, (ii) available liquefaction potential curves (CSR-N_{liq}) in literature, and (iii) from stress-controlled DSS testing results. As anticipated, the outcomes of the stress-controlled CTX testing results in the form of liquefaction potential curves are usually higher than that of the T_xSS testing results. In contrast, due to the difference in the applied (strain-controlled tests) and the induced (stress-controlled tests) strains, the liquefaction resistance curves of T_xSS are higher than those of CTX under strain-controlled conditions.

Keywords: Liquefaction; Pore water pressure ratio; Cyclic triaxial; Triaxial simple shear apparatus; DSS; stress- controlled test; strain-controlled test.

Résumé : Bien que les essais triaxiaux cycliques (CTX) soient largement utilisés dans les études de liquéfaction en raison de leur simplicité, les essais de cisaillement simple direct (DSS) et leurs semblables (p. ex. le cisaillement simple triaxial combiné, TxSS) sont plus représentatifs des contraintes survenues pendant un séisme. Par conséquent, les résultats du CTX doivent être correctement corrélés pour simuler les conditions sur le terrain. Dans la présente étude, les résultats d'une série de tests CTX effectués sur des échantillons reconstitués de sables de Baie-Saint-Paul, d'Ottawa C-109 et du Québec sont comparés aux résultats correspondants de TxSS et de DSS dans des conditions à contrainte et déformation contrôlées. Les essais en contrainte-controlé TxSS sont simulés numériquement en adoptant un modèle de pression d'eau interstitielle à couplage basé sur l'énergie et utilisant le code informatique FLAC. Les résultats numériques du TxSS sont comparés avec succès à ceux obtenus expérimentalement à partir (i) d'autres TxSS à contrainte-contrôlée, (ii) des courbes de potentiel de liquéfaction disponibles (CSR-Nliq) dans la

littérature, et (iii) des résultats des essais DSS à contrainte contrôlée. Comme prévu, les résultats des tests CTX en contrainte-contrôlé sous forme de courbe de potentiel de liquéfaction sont habituellement plus élevés que ceux des tests TxSS. En revanche, en raison de la différence entre les déformations appliquées (essais à déformation contrôlée) et les déformations induites (essais sous contrainte contrôlée), les courbes de résistance à la liquéfaction de TxSS sont supérieures à celles de CTX en condition de déformation contrôlée.

Mots-clés : liquéfaction; taux de pression de l'eau des pores; Triaxial cyclique; appareil de cisaillement simple triaxial; DSS; essai contrainte contrôlé; essai de déformation contrôlée.

5.1 Introduction

Liquefaction of soil is one of the most damaging and important phenomena in soil dynamics. It occurs due to the degradation of saturated soil strength and stiffness when subjected to monotonic or cyclic loading in undrained conditions (Castro and Poulos 1977). Liquefaction resistance of saturated sand can be determined by field or laboratory tests, and the latter should emulate as close as possible the field conditions. The test equipment and procedure have, however, a significant effect on the liquefaction resistance of the tested soil. Among the variety of testing devices available, the cyclic triaxial (CTX) and the direct simple shear (DSS) tests are the most frequently used devices in the liquefaction studies. The DSS test is preferred as it provides the closest representation of particle rotation and particle-particle relative slips during the vertical propagation of shear waves (Zhang and Evans 2018). In addition, the cyclic shear stress is applied on the horizontal plane and the principal stresses rotate smoothly during loading whilst the specimen is kept under a plane strain condition (Woods 1978).

The earlier version of DSS was developed in Swedish Geotechnical Institute (SGI) by Kjellman (1951) and in the UK by Roscoe (1953) where the soil specimen was confined by a series of annular rings or by rigid boundary walls, respectively. Bjerrum and Landva (1966) confined the cylindrical soil specimen by a wire-reinforced membrane in the Norwegian Geotechnical Institute (NGI). Peacock and Seed (1968) adopted the DSS apparatus to conduct constant volume cyclic simple shear tests. The constant volume tests are performed under drained conditions by changing the applied vertical stress to preserve the height of the specimen constant (ASTM D6528—17). The changing in the vertical stress has been proposed to be

equivalent to the excess pore water pressure that would generate in an undrained test (Dyvik et al. 1987).

It has been recognized that the lack of complementary shear stress in the DSS test results in non-uniformities of stress distribution, which significantly affects the monotonic and cyclic strength of the soil. Another deficiency of DSS is the surrounding stresses cannot be controlled during cyclic loading in DSS and the average shear and vertical stresses on the top boundary are recorded (Budhu 1985). Simply stated, the stress state in soil specimens is unknown. Therefore, DSS cannot be used to investigate the initial K_0 effect on liquefaction resistance (Ishihara and Li 1972). Additionally, in the conventional DSS, applying back-pressure during saturation and consolidation is not possible. Because of bulging the reinforced rubber membrane due to the generation of pore water pressure and applied back-pressure (Franke et al. 1979). To alleviate this problem, Casagrande (1976) introduced an updated configuration of simple shear apparatus which was termed "gyratory apparatus", where the rubber membrane was supported by a number of flat springs in the triaxial cell. Franke et al. (1979) developed a DSS version, in which radial and vertical strains were restrained by an automatic adjustment of the cell pressure. Similarly, Mao and Fahey (2003) developed an updated DSS version at the University of Western Australia (UWA). Kang et al. (2015) developed a circumferential deformation device to monitor the radial deformation of a modified DSS that accommodate cylindrical specimen encased in a latex membrane. In the same context, Chekired et al. (2015) developed the combined Triaxial Simple Shear, T_xSS, apparatus which is employed throughout the current study. Recently, Zekkos et al. (2018) developed a large diameter DSS incorporating bender elements and accelerometers to measure the shear wave velocity of the tested specimens.

The conventional triaxial is the most common laboratory tools used in liquefaction investigation, particularly, due to its simplicity and capability of defining the principle stresses during cyclic loading. Nevertheless, it does not accurately replicate the in-situ stress condition during dynamic loading (Silver et al. 1980). Peacock and Seed (1968) and Bhatia et al. (1985) attributed the deficiency of the CTX to: (i) the abrupt rotation of principal stress directions by 90^o at the instant of stress reversal, (ii) the difference in soil behavior under axial compression and extension strains, and (iii) the lack of plane strain conditions that occur during vertical wave propagation. In particular, Seed and Peacock (1971) reported that the shear stress determined in the CTX is the maximum shear stress can be tolerated by soil [$\tau_{max}= (\sigma_1-\sigma_3)/2$]. However, the

shear stress imposed in the field or in simple shear conditions is less than the maximum value. In addition, Seed and Peacock (1971) attributed the difference of cyclic soil behavior in CTX and DSS to the difference of initial stress conditions and particularly to the difference in K_0 value. Another limitation of the CTX device is the tendency of soil grains to displace during cyclic loading resulting in non-uniformity of density and straining of the soil specimen in the form of bulging and necking (e.g. Castro 1975; Kramer 1996). The induced axisymmetric lateral deformation that occurs in triaxial tests does not mimic in-situ boundary conditions (Vipulanantham 2011). Micromechanically, Zhang and Evans (2018) owing this difference to the variation of rotation level of soil particles, which is the key parameter of pore pressure buildup. In DSS, under shear waves, the particles' rotation is much higher than that in CTX, under compression waves.

It is well recognized that, under stress-controlled conditions (uniform stress cycles), the liquefaction potential obtained from the CTX tests is higher than that obtained from the DSS tests. Accordingly, it must be correlated by applying a correction factor (C_r) that could be formed as (Seed and Peacock 1971):

$$\left(\tau_h / \sigma'_{v0}\right)_{DSS} = C_r \left(\sigma_{dc} / 2\sigma'_c\right)_{CTX} \quad (5.1)$$

where τ_h is the applied shear stress on soil specimen confined under vertical pressure (σ_{v0}') in DSS and (σ_{dc}) is the applied deviator stress on soil specimen consolidated isotropically under effective confining pressure (σ_c'). Some of the previously suggested correction factors are listed in Table 5.1. However, Vaid and Sivathayalan (1996) inferred that the correlation between CTX and DSS is not as simple as those presented in Table 5.1. They demonstrated that the correction factor depends on the relative density of soil sample and the applied confining pressure. Meanwhile, Silver et al. (1980) observed the dependence of the correction factor on the preparation method. In general, the correction factor depends on the duration of the earthquake (Seed and Peacock 1971), soil behavior (dilative or contractive under static loading) (Berghe et al. 2001), and the geometry of the soil specimen (cuboidal in Roscoe DSS or cylindrical in NGI-DSS).

Table 5.1. Correction Factor, C_r suggested in previous studies

Correction factor, C_r	Reference	Apparatus
0.55 – 0.72	Seed and Peacock (1971)	Roscoe DSS (Cubical specimen, K_0 = 0.4-1)
$\frac{1+K_0}{2}$	Finn et al. (1971) Seed and Peacock (1971)	Roscoe DSS (Cubical specimen, K_0 = 0.39 and 0.47)
$\frac{2(1+2K_0)}{3\sqrt{3}}$	Castro (1975)	Triaxial (K_0= 0.67 and 1) and SPT data
$1-0.71(1-K_0)$	Ishihara and Li (1972)	Triaxial torsional shear. (K_0 = 0.33, 0.5 and 0.75)
$\frac{1+2K_0}{3}$ (wet tamped) 1 (air pluviated)	Silver et al. (1980)	DSS under conf. pressure (cylindrical specimen, K_0 = 0.4)

Most of the previous studies aimed at comparing the liquefaction resistance based on the DSS and the CTX results under stress-controlled conditions. However, up to the present, this comparison has not been studied under strain-controlled condition (uniform strain cycles). Such an investigation is required as strain-controlled tests have been observed to generate more realistic pore water pressure regardless of specimen preparation techniques and soil fabric (e.g., Dobry 1982; Ishibashi et al. 1985; Dobry and Vucetic 1987; Ladd et al. 1989). Moreover, cyclic shear strain, rather than cyclic shear stress, is a more fundamental parameter governing the seismic response of sand (e.g., NRC 1985; Vucetic and Dobry 1988).

This paper compares the cyclic behavior and liquefaction potential of cohesionless soil in the triaxial (CTX) to that in the new combined triaxial simple shear test (T_xSS) and the conventional direct simple shear test (DSS). At first, a series of undrained cyclic tests were performed on reconstituted specimens of Baie-Saint-Paul (BSP), Ottawa C-109 and Quebec CF6B sands. This is followed by a preliminary study of the effect of the specimen size on the liquefaction potential under strain-controlled loading. An energy-based pore pressure model is proposed and its numerical implementation in a numerical FLAC code (Itasca 2010) is discussed. The validation of the numerical model to represent cyclic T_xSS tests is demonstrated. This is accompanied by a comparison of liquefaction potential curves of the aforementioned sands with emphasis on the effect of shear loading control (i.e. strain or stress-control).

5.2 Experimental work

5.2.1 Testing Apparatus

Laboratory element testing devices should accurately replicate the induced stresses and deformations under field conditions. As discussed earlier, the DSS simulates rather well the produced simple shear strain during shear wave propagation in contrast to the CTX. However, the CTX is widely used in the geotechnical engineering practice to assess the liquefaction resistance. The correlation between DSS and CTX is uncertain. In the present study, a new configuration of DSS termed the combined triaxial simple shear, T_xSS, was used as well as the conventional triaxial (CTX) apparatus, manufactured by Global Digital Systems Company (GDS), to investigate the liquefaction potential of sand under cyclic stress and strain-controlled conditions. Moreover, the conventional direct simple shear GDS-DSS (EMDCSS) was incorporated in this study to validate the T_xSS testing results.

The T_xSS was developed to investigate the cyclic behavior of saturated soil specimens in simple shear conditions (Chekired et al. 2015). The T_xSS was developed at the Institut de Recherche d'Hydro-Québec (IREQ) in collaboration with the Geotechnical group at the Université de Sherbrooke. Figure 5.1 shows the assembly of the T_xSS apparatus. The T_xSS provides the capability of saturation and consolidation (isotropically and anisotropically). The hydrostatically confined soil specimens can be subjected to monotonic or cyclic (uniform or irregular) shear strains. The generated pore water pressure, vertical and shear stresses can be directly measured during the undrained test. Furthermore, the T_xSS is capable of hosting cylindrical soil specimens enclosed in latex membranes and confined in a pressurized triaxial chamber, as shown in Figure 5.2(a). Using the pressurized cell in conjunction with latex membranes allows maintaining true K_0 conditions during the shearing phase. It can be also converted to the conventional DSS type by using annular metal rings as illustrated in Figure 5.2(b). Further, a fiberglass tape can be used to confine the radial strain during cyclic loading in the triaxial chamber, Figure 5.2(c). Using the T_xSS allows defining the state of vertical and horizontal stresses in addition to monitoring the effective stress path during cyclic loading. Further features of the T_xSS have been reported in Khashila et al. (2018) and Karray and Chekired (2019).

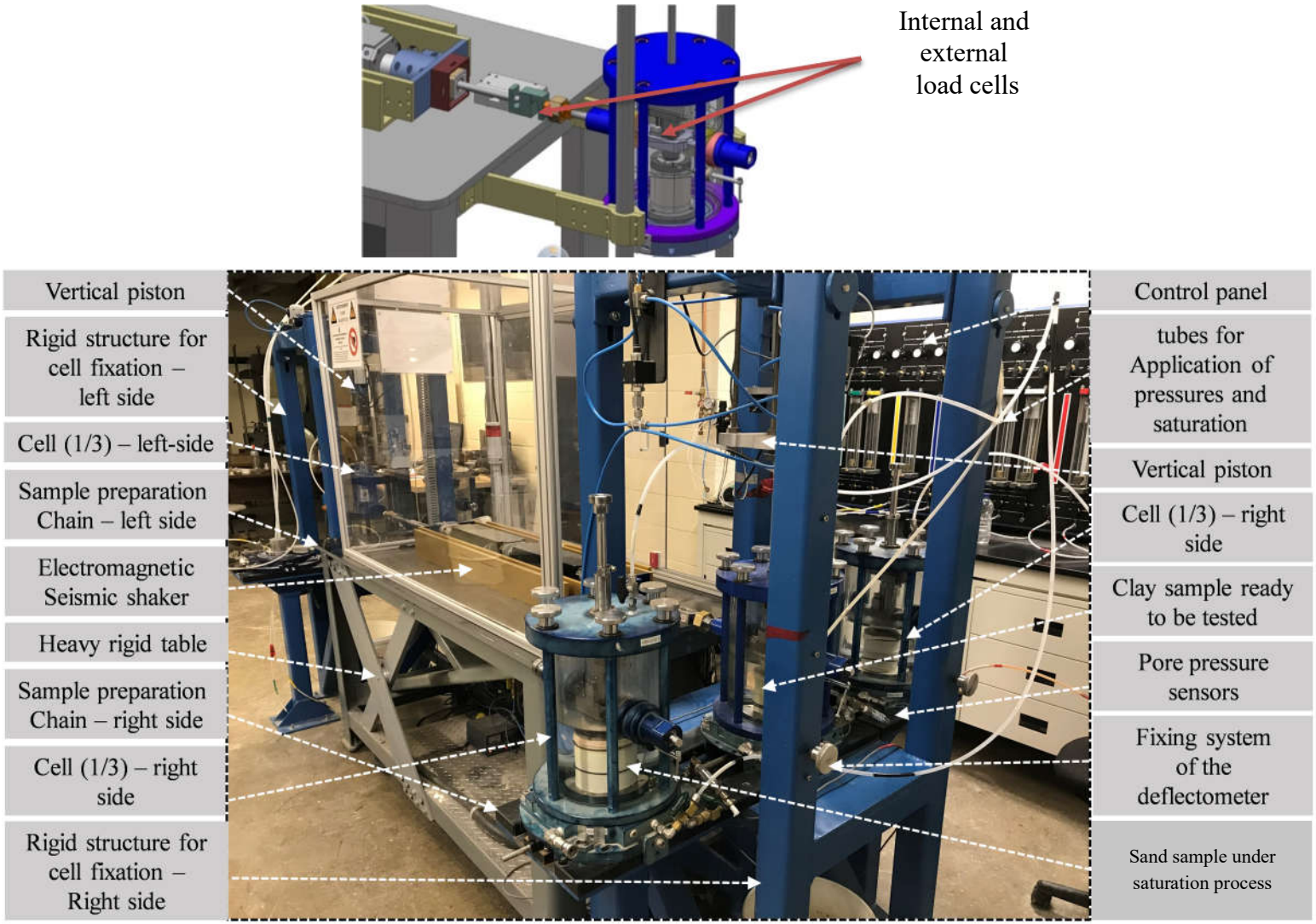

Figure 5.1. The new combined triaxial simple shear (T_xSS) apparatus

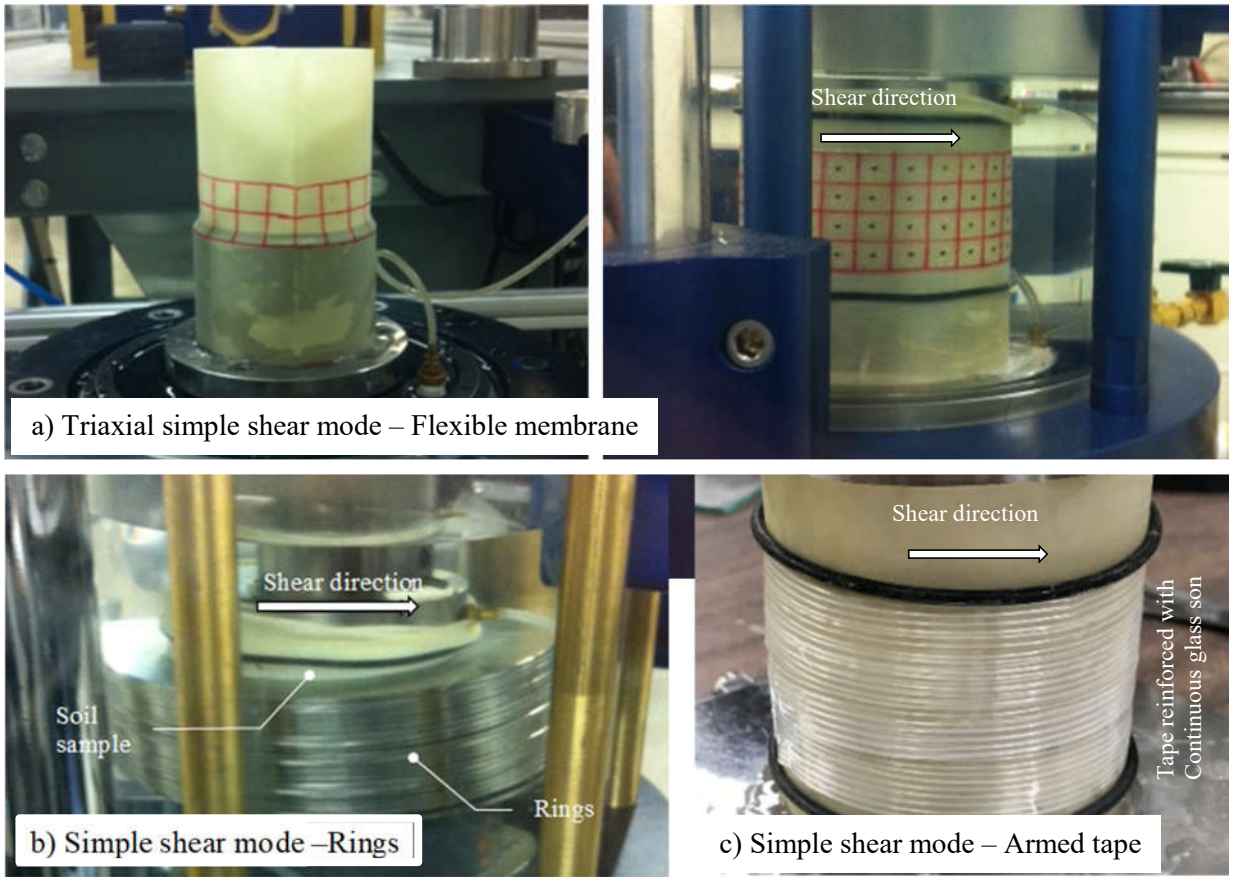

Figure 5.2. Soil specimen prepared in (a) latex membrane, (b) latex membrane and annular rings (c) constrained latex membrane by fiberglass tape

Conventional triaxial and DSS devices are capable of testing soils in both cyclic strain and stress-controlled conditions. However, the T_xSS apparatus permits conducting strain-controlled testing only. As will be discussed later, the cyclic strain-controlled T_xSS results had been used to develop a pore water pressure model that was adopted to simulate the soil behavior under T_xSS conditions using the computer code, FLAC 2D (Itasca 2010). Subsequently, the FLAC code was employed to simulate stress-controlled tests under T_xSS conditions. The numerically obtained shear strain response, from FLAC simulation, was then applied in the T_xSS device to perform uniform cyclic shear stress, which is called alternative stress-controlled testing in the following sections.

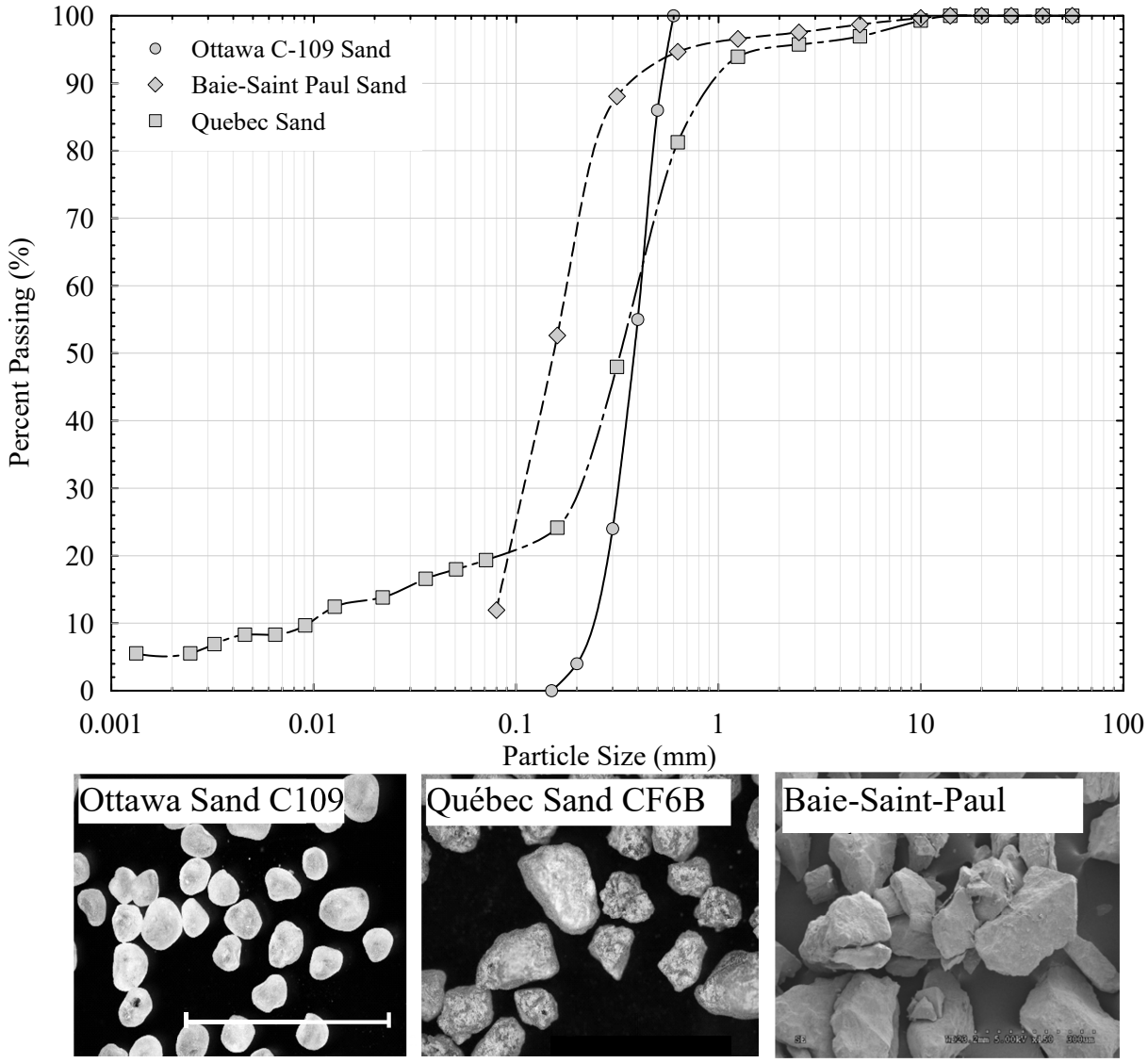

Figure 5.3. Grain size distribution and grain shape of the used sands

Table 5.2. Physical properties of the sands used

Soil properties	Baie-Saint-Paul sand	Ottawa sand C-109	Quebec sand CF6B
G_s	2.78	2.67	2.71
e_{max}	0.91	0.82	0.82
e_{min}	0.598	0.5	0.45
C_u	2.25	1.75	44.44
C_c	1	1.016	12.25
D_{50}	0.15	0.4	0.33
ϕ	28	31.8	28

5.2.2 Test program in T_xSS, DSS and CTX

Reconstituted specimens of Baie-Saint-Paul (BSP), Ottawa C-109, and Quebec CF6B sands were prepared for cyclic strain and stress-controlled testing. Sand properties are summarized in Table 5.2. The grain-size distribution curves and digital images for tested sands are shown in Figure 5.3. It is well known that the specimen preparation method has a significant influence on the liquefaction potential of soil (Mulilis et al. 1977; Ladd 1978; Tatsuoka et al. 1986; Bradshaw and Baxter 2007). The wet tamped preparation method was adopted to prepare reconstituted soil specimens in DSS, CTX, and T_xSS (Ladd 1978). In T_xSS tests, moist soil specimens of 80 mm diameters and varying heights were prepared preliminarily to investigate the specimen size effect. The DSS specimens were prepared at 20 mm height and 79 mm in diameter. The corresponding D/H ratio is 4 and meets the ASTM D6528-17 specifications (minimum D/H = 2.5). In DSS and T_xSS, the moist sands were placed into the rubber membrane in three layers and every layer was gently tamped until the pre-estimated height was reached. In triaxial tests, the soil specimen is 76 mm height and 38 mm diameter compacted in the rubber membrane in six layers. Each layer was gently tamped with a hand tamper to avoid applying pre-stress (Frost and Park 2003). After replacing the last layer and sealing the upper cap, the split mold was removed from the specimen. Subsequently, to accelerate the saturation process, carbon dioxide gas (CO_2) was flushed then de-aired water under back-pressure was applied to the specimen for 15 hours under pressure of 10 kPa. Full saturation was defined when the Skempton's pore pressure parameter ($B = \Delta u/\Delta\sigma_3$) value at least 0.96. Once an acceptable *B* value had been obtained, all BSP, Ottawa C-109, and Quebec CF6B sand specimens were isotropically consolidated under an effective confining pressure of 75, 100 and 78 kPa, respectively. After the consolidation stage, sinusoidal waveforms of cyclic stress (stress-controlled) or strain (strain-controlled) were applied in the CTX while only strain-controlled tests were performed in the T_xSS. A total of 59 tests were accomplished in the current study as summarized in Table 5.3. The cyclic stress- and strain-controlled tests were applied on BSP and Ottawa C-109 sands at a frequency of 1.0 Hz, while Quebec sand CF6B was tested at 1.8 Hz. As will be shown later, pore water pressure ratio, R_u, curves under strain-controlled condition flatten out and cannot reach the plateau of $R_u = 1$, which may be attributed to the intense increase in radial strains beyond $R_u = 0.9$; where $R_u = \underline{\Delta u/\sigma'_{co,}\,\Delta u}$ is the measured excess pore water pressure, and σ'_{co} is the initial effective confining stress.

Table 5.3. Summary of experimental work

Sand	Test No.	*Apparatus*	γ_{cyc} *or CSR*	e_{ini}	e_{cons}	I_D	σ'_{co}	B	N_{liq}	α
Baie-Saint-Paul sand (Freq. =1.0Hz)	B-S1	T_xSS (Strain)	0.780	0.771	0.738	55	75	0.95	7	1.25
	B-S2		0.440	0.768	0.735	56	75	0.97	25	1.6
	B-S3		0.632	0.767	0.732	57	75	0.97	10	1.25
	B-S4		0.525	0.773	0.732	57	75	0.97	17	1.55
	B-S5		0.326	0.771	0.743	53.5	75	0.97	65	2.25
	B-T1	CTX (Strain)	0.500	0.771	0.738	55	75	0.97	3	-
	B-T2		0.350	0.768	0.737	55	75	0.97	4	0.73
	B-T3		0.220	0.771	0.740	54.5	75	0.97	7	0.63
	B-T4		0.133	0.770	0.739	55	75	0.97	16	0.60
	B-T5		0.100	0.768	0.740	54.5	75	0.97	29	0.65
	B-TX1	CTX (Stress)	0.180	0.759	0.735	56	75	0.97	72	
	B-TX2		0.209	0.759	0.736	55.7	75	0.97	28	
	B-TX3		0.228	0.770	0.741	54	75	0.97	14	
	B-TX4		0.241	0.770	0.740	54.5	75	0.97	10	
	B-TX5		0.270	0.771	0.737	55.5	75	0.97	4	
Ottawa C-109 sand (Freq. =1.0Hz)	O-S1	TxSS (Strain)	0.450	0.725	0.688	41	100	0.96	7	-
	O-S2		0.370	0.722	0.687	41	100	0.97	9.5	-
	O-S3-A		0.350	0.722	0.688	41	96	0.97	15	0.88
	O-S4		0.340	0.723	0.688	41	100	0.97	19	1.30
	O-S5-A		0.270	0.726	0.680	43	97	0.97	23.5	0.93
	O-S6		0.255	0.725	0.688	43	101	0.96	24	1.08
	O-S7-F[1]		0.250	0.723	0.680	40	98	0.95	23	-
	O-S9-F[2]		0.250	0.722	0.688	41	103	0.97	24	1.06
	O-S10		0.230	0.725	0.689	41	102	0.96	37	-
	O-S11		0.210	0.723	0.685	42	100	0.97	39	1.05
	O-S12		0.150	0.720	0.690	40	103	0.93	60	1.8
	O-S13		Monotonic	0.722	0.682	43	100	0.96	-	-
	O-SX1	T_xSS (alt.Stress)	0.135	0.722	0.690	40	100	0.97	11.5	
	O-SX2		0.112	0.722	0.691	40	100	0.97	19	
	O-SX3		0.095	0.723	0.690	40	100	0.96	28	
	O-T1	CTX (Strain)	0.200	0.770	0.690	40	100	0.97	7	0.83
	O-T2		0.175	0.766	0.688	40	100	0.97	6	0.72
	O-T3		0.150	0.768	0.689	41	100	0.97	7	0.69
	O-T4		0.126	0.770	0.690	41	100	0.97	12	0.70
	O-T5		0.116	0.769	0.689	40	100	0.97	16	0.70
	O-T6		0.100	0.770	0.690	41	100	0.97	44	-
	O-TX1	CTX (Stress)	0.200	0.768	0.689	40	100	0.97	3	
	O-TX2		0.175	0.768	0.687	41	100	0.97	5	
	O-TX3		0.147	0.768	0.688	41.5	100	1.00	26	
	O-TX4		0.127	0.768	0.688	41	100	0.97	37	
	O-DS1	DSS (Stress)	0.22	0.750	0.698	38	106	-	1	
	O-DS2		0.145	0.739	0.696	39	106	-	6	
	O-DS3		0.121	0.761	0.712	34	102	-	16	
	O-DS4		0.255	0.761	0.717	32	81	-	<1	
	O-DS5		0.107	0.747	0.699	38	107	-	26	
	O-DS6		0.080	0.761	0.687	41.5	106	-	155	
	O-DS7		0.095	0.741	0.689	41	107	-	53	
	O-DS8		0.146	0.751	0.699	38	104	-	5	
	O-DS9		0.09	0.751	0.689	41	105	-	150	
	Q-TX1	CTX (Stress)	0.100	0.692	0.635	50	78	0.96	250	
	Q-TX2		0.14	0.692	0.638	49	78	0.96	45	
	Q-TX3		0.150	0.691	0.636	50	78	0.97	26	

Quebec sand CF6B (Freq. =1.8Hz)	Q-TX4	T_xSS (Strain)	0.175	0.693	0.633	51	78	0.97	16.5	
	Q-TX5		0.205	0.692	0.632	51	78	0.97	8	
	Q- S1		0.680	0.687	0.626	52	78	0.97	6.30	0.85
	Q- S2		0.500	0.690	0.622	53	78	0.97	15.3	-
	Q- S3		0.410	0.689	0.621	53	78	1.00	23.0	1.02
	Q- S4		0.320	0.689	0.618	54	78	1.00	27.0	0.95
	Q- S5		0.210	0.686	0.639	49	78	0.97	66.6	1.05
	Q-SX1	T_xSS (alt.Stress)	0.175	0.685	0.620	54	78	0.96	6.0	
	Q-SX2		0.125	0.689	0.622	53	78	0.96	15.0	

O-S3-A and O-S5-A: prepared specimens in armed membranes.
O-S7-F[1], O-S8-F[2], and O-S9-F[3]: prepared specimens at different D/H ratios, 5.45, 4.2, and 2.16.

Therefore, the initial liquefaction criterion was defined as the excess pore water pressure ratio, R_u reaches 0.9, the same criterion has been adopted by Chang and Hong (2008) and Khashila et al. (2018).

5.2.3 Experimental results

Parallel series of cyclic strain and stress-controlled tests performed in CTX while strain-controlled tests were performed in T_xSS in addition to a suite of cyclic stress-controlled DSS tests. Six special cyclic alternative stress-controlled tests and another monotonic one were performed in T_xSS, as listed in Table 5.3. A typical cyclic response of Ottawa sand C-109 under strain-controlled test is presented in Figure 5.4. Figure 5.4(a) shows the hysteresis loops (CSR-γ) of cyclic response of BSP sand under strain-controlled condition, where CSR is cyclic stress ratio= τ/σ_c' and τ is the maximum cyclic shear stress value induced in the T_xSS specimen. It is observed that the hysteresis loop becomes flattened out and its bounded area, which represents the dissipated energy, decreases with further cycles. Eventually, the hysteresis loop becomes horizontal at the trigger of liquefaction. Figure 5.4(b) shows the progression of pore water pressure and the decay of CSR by the sequence of loading cycles.

5.3 Influence of specimen size in T_xSS

There is abundant evidence in the literature supporting the fact that one of the shortcomings of the DSS is the non-uniformity of stress distribution due to the lack of complementary shear stress on the vertical boundaries (e.g. Boylan and Long 2009). The induced stress non-uniformity affects negatively on the soil strength under monotonic or cyclic loading (Casagrande 1976). However, according to numerical simulation studies the majority of soil specimens, approximately 70% of cross-area, had uniform stress while stress non-uniformity occurs just at

the perimeter (e.g. DeGroot 1994). To overcome the non-uniformity of shear stress in DSS, it has been suggested to use a large diameter to height ratio (D/H) (Shen et al. 1978, Budhu 1984, Amer et al. 1987, Chang et al. 2016). However, one of the main points of contention is the determination of the adequate D/H ratio at which the shear stress distribution would be almost uniform. Numerical elastic simulation of DSS by Amer et al. (1987) and Shen et al. (1978) limited the minimum D/H ratio to 8, while the ASTM D6528-17 specified the minimum D/H ratio of 2.5. Vucetic and Lacasse (1982), based on their experimental work on Haga clay, observed that the D/H ratio does not have a significant effect on the stress non-uniformity under monotonic loading. In his cyclic investigation of plastic Drammen clay specimens, having cross-section areas of 20 and 50 cm^2, Anderson (1975) indicated that the number of cyclic loading to failure is independent of D/H. Franke et al. (1979) using the BAW DSS (Bundesantalt fűr Wasserbau) found a good agreement between undrained cyclic testing results in the case of D/H ratio = 7.5 and 3.75.

Before investigating the liquefaction potential of T_xSS and CTX tests, the influence of the D/H ratio on cyclic behavior in the T_xSS apparatus is preliminarily investigated. Figures 5.5(a) and 5.5(b) show the cyclic response of Ottawa sand C-109 specimens prepared at different D/H ratios (D/H= 2.16, 3.2, 4.4 and 5.7) under cyclic strain-controlled loading having an amplitude of γ = 0.25-0.27 %. It may be indicated that the D/H ratio under T_xSS condition, where soil specimen is confined hydrostatically in the triaxial chamber, has no significant effect on liquefaction potential, as represented in Figure 5.5(c). In other words, failure (i.e., R_u = 0.9) occurs approximately at the same number of cycles under T_xSS conditions. The results of the specimen prepared in armed membranes are superimposed in Figure 5.5. It seems that the D/H ratios and the rigidity of reinforced membrane have a relatively small influence on the generation of pore pressure in the T_xSS (where the surrounding stress is maintained constant during shearing). Similar observations were reported by Franke et al. (1979) based on the BAW-DSS testing results. Presumably, it can be attributed to utilizing a hydrostatical confining pressure in BAW-DSS and T_xSS rather than a wire-reinforced membrane or annular ring. It may be owned to using a comparatively high D/H ratio wherein the minimum D/H ratio specified by ASTM D6528-17 is 2.5. It is of interest to note that H/d_{max} ratio is greater than 10 in all tests as recommended by ASTM D6528-17 to diminish the effect of the shear bandwidth, where d_{max} is the maximum particle size. Thus, in the current study, the authors selected the D/H ratio of 3.2 (i.e., D = 80

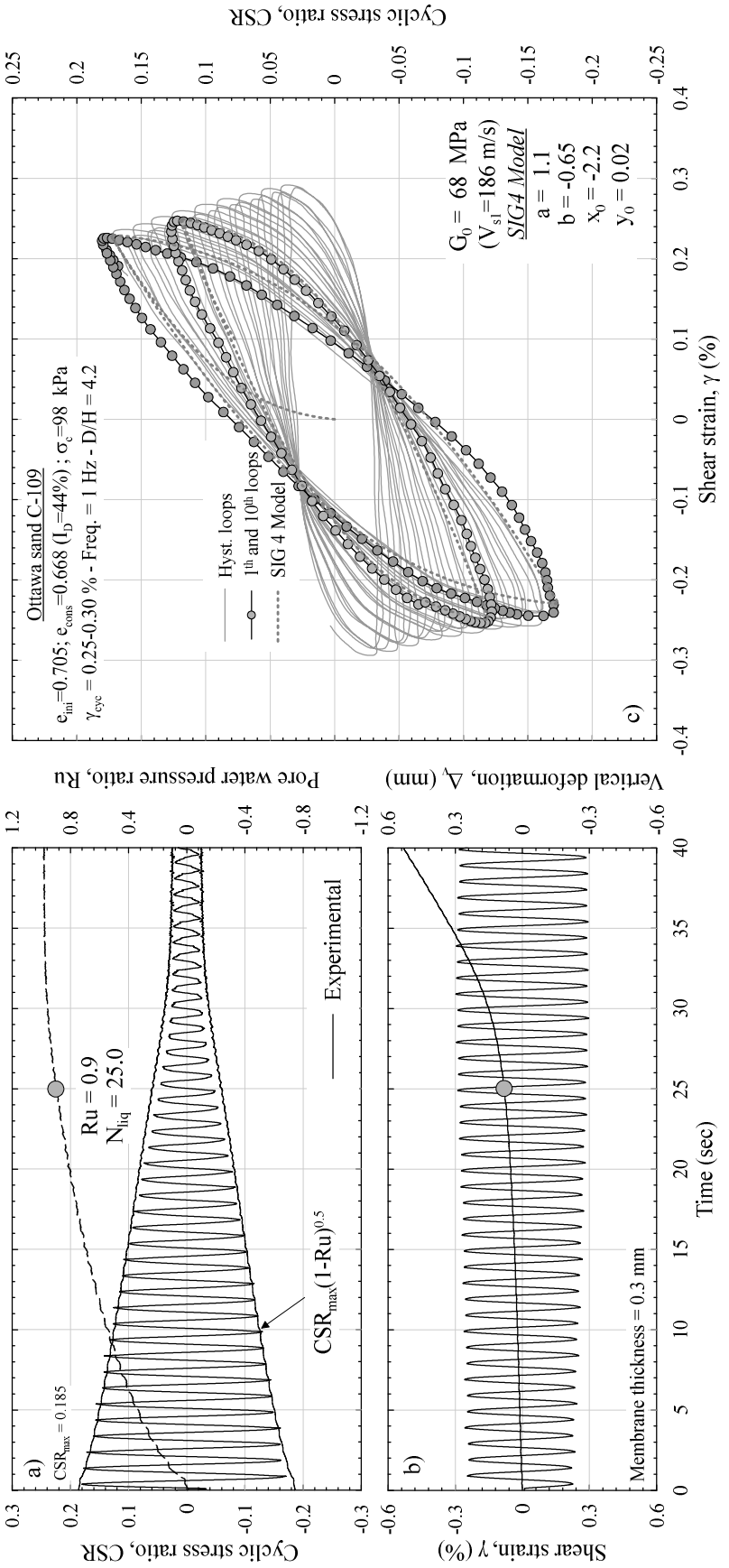

Figure 5.4. Typical records of T_xSS strain-controlled test on Ottawa sand C-109

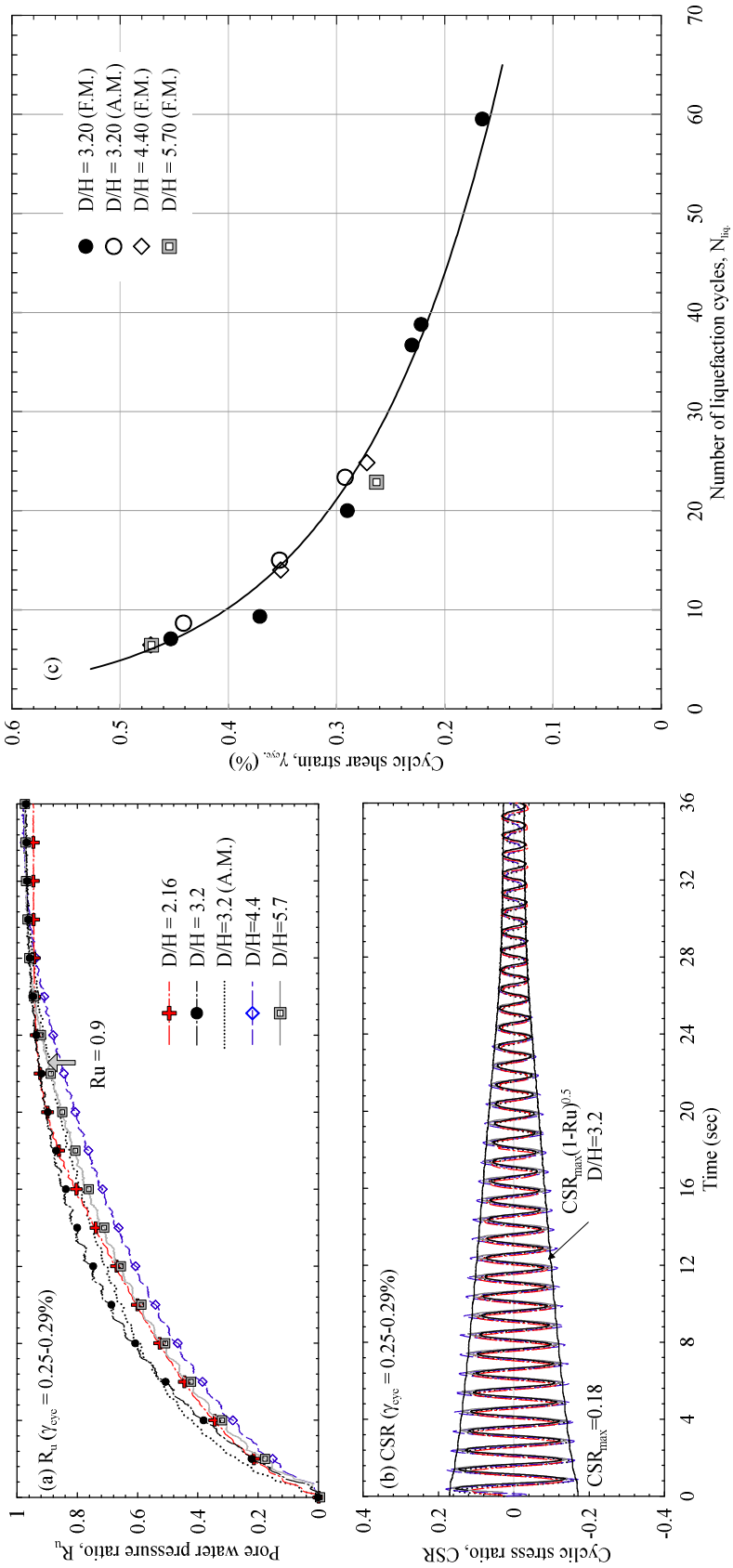

Figure 5.5. Variation of (a) the generated pore water pressure, (b) the induced CSR and (c) the liquefaction potential of Ottawa sand C-109 prepared at different D/H ratio

mm, and H ≅ 25 mm) to prepare sand specimens. It is noteworthy that the D/H ratios ranged from 3 to 3.5 have been widely used in DSS testing (e.g. Roscoe 1953; Peacock and Seed 1968; Carroll 1979; Silver et al. 1980; DeGroot 1994; Mao and Fahey 2003; Song et al. 2004; Wijewickreme et al. 2005; Chang and Hong 2008; Boylan and Long 2009; Doherty and Fahey 2011).

The decay of CSR by the load sequence is demonstrated in Figures 5.4(b) and 5.5(b). It results from soil softening and degradation of the shear modulus which is synchronous with R_u generation, Eq. (5.2), (Matasovic and Vucetic 1993; Chang et al. 2007; Moreno-Torres et al. 2010).

$$G = G_{\max}\left(1 - R_u\right)^{0.5} \tag{5.2}$$

where G_{max} is the maximum shear modulus. The degradation in the shear modulus was used in conjunction with the energy concept to develop a coupled energy-based model. This model aims at correlating the pore pressure buildup, iteratively each time step during cyclic loading, to soil properties and seismic loading (Ardoino et al. 2015). The proposed model was used to simulate T_xSS testing conditions using the FLAC platform as will be discussed in the following section.

5.4 Energy-based pore water pressure model

A variety of models have been developed to predict the residual pore water pressure generation in saturated soils subjected to earthquake loading. Most of these models are currently used in computer codes to capture the dynamic response of the soil. Early developed models were based on two main approaches: cyclic stress (Seed et al. 1975) and cyclic strain (Martin et al. 1975) approaches. Another model termed strain energy-based model was developed by Nemat-Nasser and Shokooh (1979). This model linked mathematically the dissipated energy per unit volume (W_s), the required energy to collapse soil skeleton, in the densification of dry sands and pore pressure generation of fully saturated sands under cyclic loading. The dissipated energy, W_s, can be obtained by integrating the area bounded by stress-strain hysteresis loops which can be determined by (Green et al. 2000 and Yang and Pan 2018):

$$W_s = \frac{1}{2\sigma'_{mo}} \sum_{i=1}^{n-1} (\tau_{i+1} + \tau_i)(\gamma_{i+1} - \gamma_i) \tag{5.3}$$

where W_s is the dissipated energy per unit volume of soil; τ_i is the applied shear stress at load increment i; γ_i is the shear strain at load increment i; σ'_{m0} is the initial mean effective stress; n is the total number of cycles.

The results of cyclic strain-controlled tests were adapted to delineate a unique relation between pore pressure and the normalized dissipated energy $(W_s/\alpha)^{0.5}$ for each tested sand. Figure 5.6 shows these relations which could be written in a general polynomial function as:

$$R_u = C_1\left(\frac{W_s^{0.5}}{\alpha}\right) + C_2\left(\frac{W_s^{0.5}}{\alpha}\right)^2 + C_3\left(\frac{W_s^{0.5}}{\alpha}\right)^3 \quad (5.4)$$

where C_1, C_2, and C_3 are fitting parameters enumerated in Table 5.4, α is a calibration parameter that depends on strain amplitude, density, and soil type, as shown in Figure 5.6(d) and listed in Table 5.3 (Berrill and Davis 1985; Konstadinou and Georgiannou 2013; Karray et al. 2019).

The energy-based pore water pressure model, Eq. (5.4), was used to represent the residual pore water pressure generation in the numerical simulation of the T_xSS testing. The well-established sigmoidal equation (termed the SIG4 model) with four parameters (a, b, x_0 and y_0) was employed to represent the hysteresis damping during cyclic loading in conjunction with the degradation of maximum shear modulus G_{max}, Eq. (5.2). The SIG4 model is embodied in FLAC. The calibrated SIG4 model parameters from the induced cyclic strain-controlled T_xSS hysteresis loops of the used sands are listed in Table 5.5. More details of the proposed numerical model are discussed in a companion paper (Khashila et al. 2019).

The numerical model was used to simulate cyclic stress-controlled tests under T_xSS conditions in FLAC. The numerical shear strain responses were applied, experimentally, in the T_xSS to perform cyclic tests termed "alternative stress-controlled" tests. Figure 5.7 compares the results of an alternative stress-controlled test and the results of numerical simulation of a stress-controlled test on Ottawa C-109 sand. The comparison between the numerical and experimental T_xSS testing results demonstrates a good agreement in terms of pore pressure and CSR upon triggering of liquefaction (i.e. R_u=0.9). Thereafter, a deviation in CSR time history is observed (Figure 5.7b). This may be postulated as, after triggering the liquefaction, the soil loses its stiffness and no stress can be produced on the soil specimen whatever the applied shear strain value. In contrast, it may not be observed under cyclic stress-controlled loading where the applied stress is imposed.

Table 5.4. Pore pressure model parameters

Model parameters	Baie-Saint-Paul sand	Ottawa sand C-109	Quebec sand CF6B
C_1	0.383	0.294	0.330
C_2	1.470	1.550	1.510
C_3	-0.570	-0.945	-0.927

Table 5.5. SIG4 model parameters

Model parameters	Baie-Saint-Paul sand	Ottawa sand C-109	Quebec sand CF6B
a	0.97	1.1	1.0
b	-0.55	-0.65	-0.7
x_0	-1.4	-2.2	-1.7
y_0	0.01	0.02	0.04

Figure 5.7(d) illustrates the effective stress path of undrained cyclic and monotonic responses of Ottawa sand specimen where τ is the applied shear stress and σ' is the effective confining stress. The instability line (IL) represents the initiation of the instability zone (Vaid et al. 2001, Konstadinou and Georgiannou 2014). The soil specimen exhibits an unstable response when the cyclic stress path crosses the instability line and enters the instability zone (point 1 Figure 5.7d). This unstable behavior is represented in the increase of the pore pressure generation rate, Figure 5.7(b), synchronous with the development of shear and vertical strain, Figure 5.7(c) (Konstadinoun and Georgiannou 2014). It is important to note that the volumetric vertical deformation, ε_v is marginal prior to the crossing of cyclic stress path the instability zone (point 1 Figure 5.7d). Then, ε_v increases gradually till R_u reaches 0.9 (point 2 Figure 5.7d). Then, a rigorous increase in ε_v occurs when the cyclic stress path crosses the phase transformation line.

5.4.1 Validation of liquefaction potential curves obtained from T_xSS tests

The T_xSS is capable of applying regular or irregular shear strain loading to soil specimens confined in a triaxial chamber. Based on the energy-based pore water pressure model obtained from strain-controlled tests in T_xSS (Eq. 5.4) and $G_{max.}$-R_u relation (Eq. 5.2), a loosely coupled energy-based code was used to simulate stress-controlled tests under T_xSS condition in FLAC. To validate the accuracy of the proposed numerical model and its coherence with TxSS results,

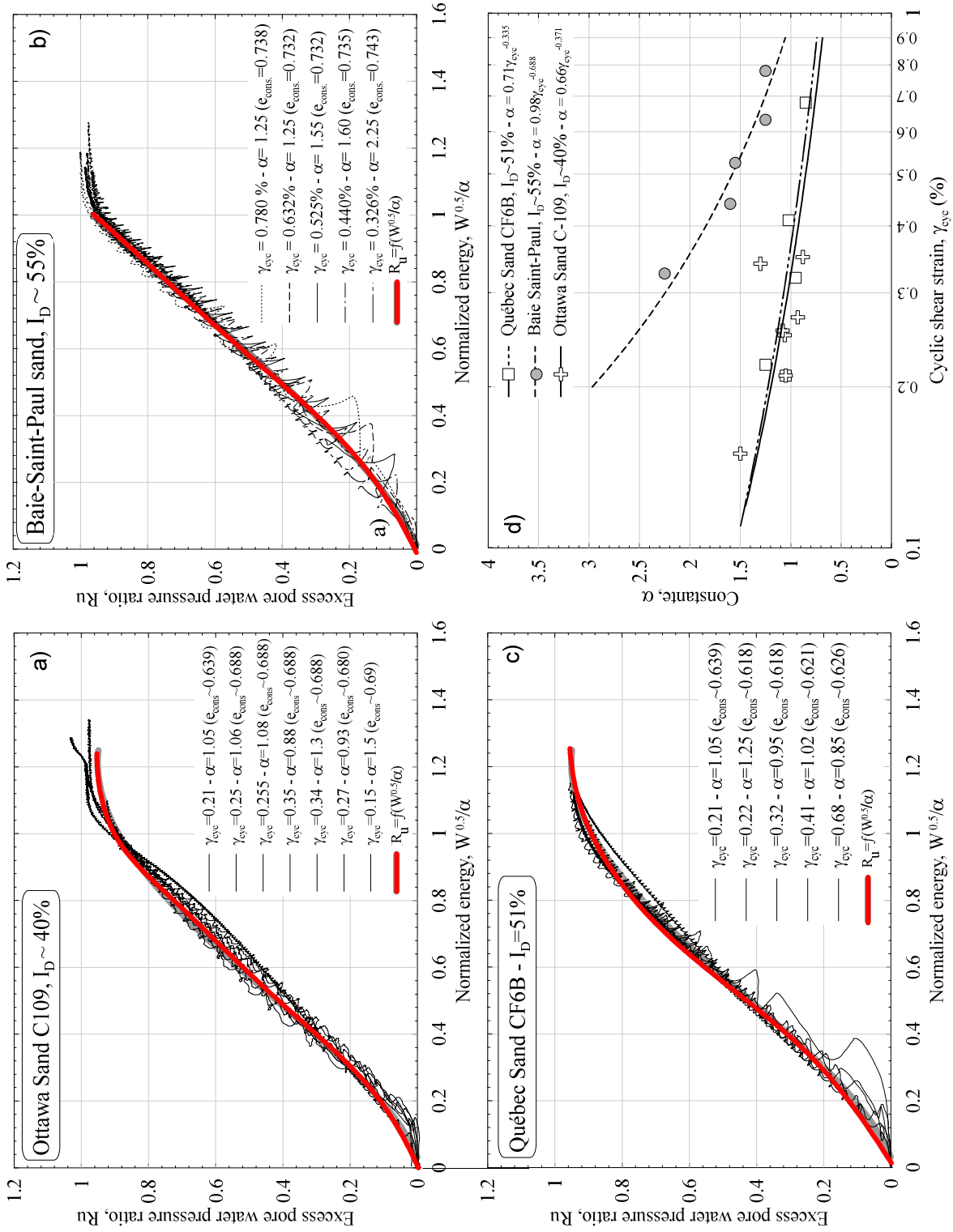

Figure 5.6. Correlations between the genera pore pressure and the normalized dissipated energy for (a) Ottawa sand, (b) BSP sand, (c) Quebec CF6B sand, (c) α as functions of shear strain γ

a comparison between the liquefaction potential (CSR-N_{liq}) curves obtained from the numerical simulation versus (i) a set of alternative stress-controlled tests (Figure 5.8a), (ii) the abundance liquefaction potential curves in the literature (Figure 5.8b), and (iii) a suit of cyclic stress-controlled DSS tests performed on reconstituted specimens (current study) (Figure 5.8c) was made.

Figure 5.8(a) demonstrates the liquefaction potential range of numerical simulation comparing to four alternative stress-controlled tests of Ottawa sand besides other special two cyclic tests performed on Quebec CF6B sand. As previously discussed in Figure 5.7, there is an excellent agreement between the numerical simulation and the alternative stress-controlled tests upon triggering the liquefaction (R_u= 0.9). Therefore, there is a good correspondence between the liquefaction potential curves obtained from numerical and experimental T_xSS results of Ottawa C-109 and Quebec CF6B sands. It may be observed that the cyclic resistance of Ottawa sand specimens prepared in a reinforced membrane (AM) is in agreement with that obtained from numerical simulation and from the latex membrane (as previously discussed in Figure 5.5).

Ottawa sand C-109 was chosen for the phase of validation because of an abundance of liquefaction resistance readily available in the literature. The liquefaction potential curves reported in the literature from the conventional DSS tests are compiled in Figure 5.8(b) (e.g. Finn et al. 1971, Vaid and Finn 1979, Bhatia 1985). Because of the scatter of complied data, the results are interpreted in a scatter band. All these data were correlated due to the variation of confining pressure by a confining pressure correction factor (K_σ) (Youd et al. 2001). [Note, K_σ was first introduced by Seed (1983) to correlate the effect of overburden pressure higher than 100 kPa].

The general correspondence between numerical and experimental liquefaction potential emphasizes the validity of using the proposed coupled energy-based model with confidence to capture the cyclic behavior under stress-controlled T_xSS conditions. Moreover, this validation reveals equivalent liquefaction resistance obtained from cyclic undrained T_xSS and previous constant volume DSS tests in the range between 6-26 cycles. This is the band of practical geotechnical engineering interest as it represents the equivalent number spectrum of earthquake magnitudes, M, ranged from 6 to 8-1/2 (Seed and Idriss 1982).

Further validation was performed by comparing the numerical model results with the liquefaction potential curve obtained from DSS tests performed on reconstituted Ottawa sand

specimens (current study) (Figure 5.8c). It may be seen that the results of the T_xSS simulation are in very good agreement with the current DSS testing results irrespective of the radial strain confining method. However, a considerable discrepancy between the liquefaction potential curves can be seen at lower number of cycles. The lower the number of cycles is the larger cyclic resistance in T_xSS than in DSS. Further, the results show that the obtained resistance under isotropic monotonic T_xSS test is larger than that obtained from DSS.

The correspondence between liquefaction resistances in the range between 6-26 cycles and the deviation at a lower number of cycles can be interpreted using observations by Ishihara and Li (1972). In the DSS apparatus, wherein the radial strain is confined, the soil specimen is initially subjected to K_0 conditions. By the consequence of cyclic loading in the DSS, the K_0 value gradually increases up to the unity while it maintains constant in the T_xSS (e.g. Ishihara and Li 1972; Dyvik and Zimmie 1982). The most pronounced increase in K_0 value occurs at the first few cycles then increases smoothly till it reaches a plateau around $k_0 \approx 1.0$ (i.e., approaching the status of isotropic state) (Youd and Craven 1975; Franke et al. 1979; Budhu 1985). Ishihara and Li (1972) noted that the induced pore pressure under isotropic (free radial strain) and anisotropically confined radial strains are almost equal and very little deviation occurred in the first few cycles. However, initial liquefaction occurs almost at the same time. That explains the resistance difference between the T_xSS and DSS at the low number of cycles and monotonic loading in contradictory to that at the higher number.

The consistency between the DSS and T_xSS results can be postulated with respect to the induced vertical strains. According to ASTM D6528-17, the DSS threshold vertical shear strain is 0.05%. The results of T_xSS reveal that the vertical strain reaches this threshold value upon R_u about 0.6 synchronous with entering the cyclic stress path the instability zone, as shown in Figure 5.7(d), (Silver and Park 1976; Konstadinoun and Georgiannou 2014). This reveals that the soil specimens could remain a relative circular cross-section like DSS with relative small compensated radial strains upon $R_u = 0.6$ when confined in a pressurized cell. This result has been described under monotonic loading by Kang et al. (2015) using a circumferential radial strain device. A similar observation has been demonstrated by Ishihara and Li (1972) in a torsional shear test where isotropic and anisotropic confined radial strain specimen imposed the same vertical strain until the triggering of liquefaction.

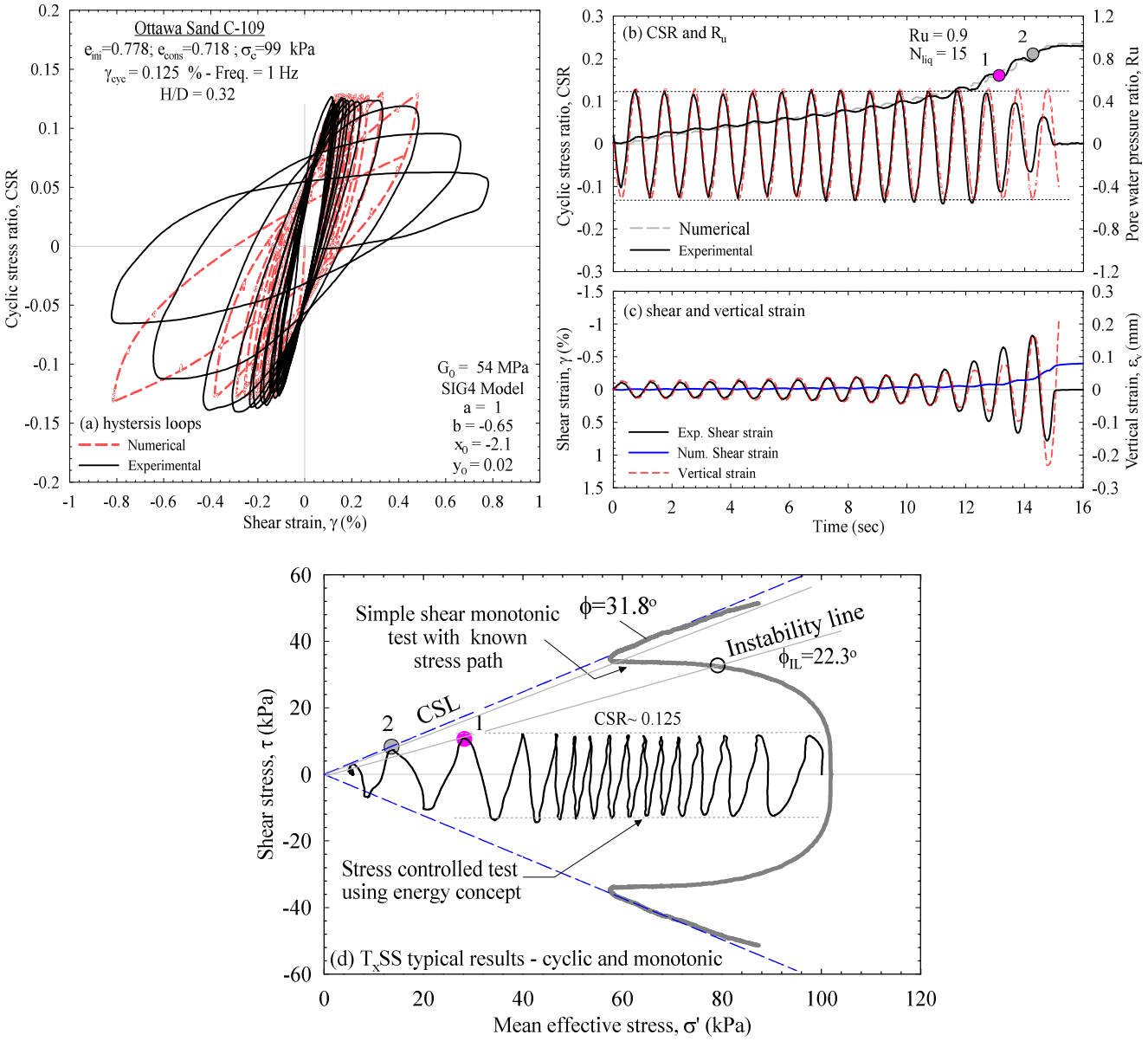

Figure 5.7. Typical records of T_xSS alternative stress-controlled test (O-SX1) on Ottawa sand C-109

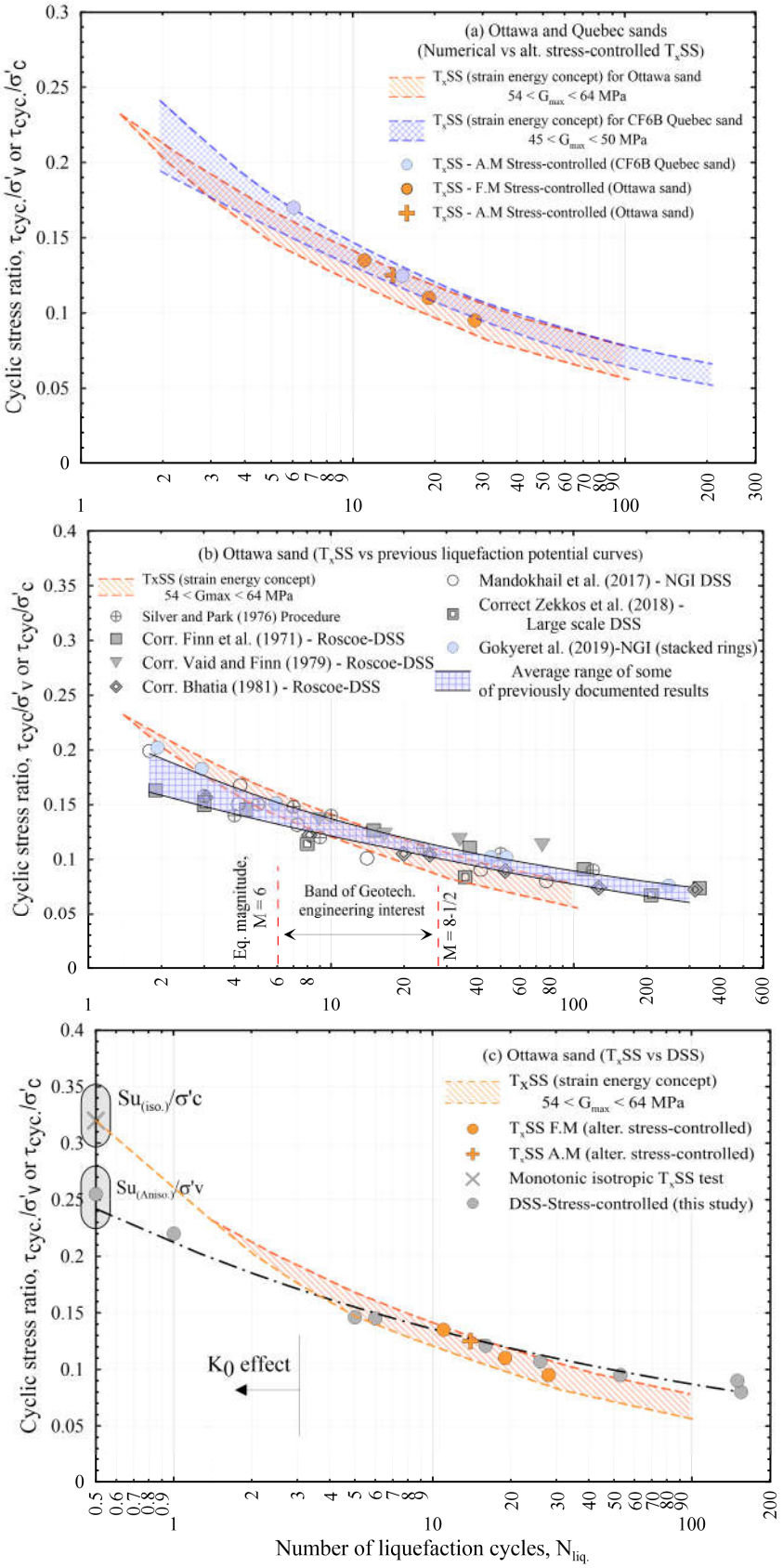

Figure 5.8. Comparison between liquefaction potential curves of Ottawa sand C-109

5.5 Analysis and Discussion

Liquefaction potential curves (CSR–N_{liq}) obtained from stress-controlled CTX tests performed on BSP, Ottawa C-109, and Quebec CF6B sands are compared to those from the simulation of T_xSS tests in Figure 5.9, where $CSR_{CTX} = \sigma_d/2\sigma'_c$, $CSR_{TxSS} = \tau/\sigma'_c$, σ_d is the applied cyclic deviator stress in CTX and τ is the maximum cyclic shear stress value induced in the T_xSS specimen. Whereas, shear strain, γ– N_{liq} and axial strain, ε– N_{liq} curves obtained from strain-controlled CTX and T_xSS tests are depicted in Figure 5.10. As anticipated, the number of liquefaction cycles (N_{liq}) is inversely proportional to either load amplitude in stress-controlled or shear strain amplitude in strain-controlled tests.

As anticipated, Figure 5.9 shows that the liquefaction potential resistance of CTX, under stress-controlled loading, is higher than that of T_xSS. It is consistent with the previous comparisons conducted between CTX and earlier DSS configurations (e.g. Seed and Peacock 1971; Finn et al.1971; Silver et al. 1980). Thus, CTX results must be correlated to match the T_xSS results, as enlisted in Table 5.1.

The performed cyclic stress-controlled tests on BSP, Ottawa and Quebec CF6B sands demonstrate that the correlated CSRs of CTX tests are in good agreement with those of T_xSS. The correlation factors of CSRs are 0.72, 0.68, and 0.7 for BSP, Ottawa and Quebec CF6B sands as shown in Figures 5.9(a), 5.9(b), and 5.9(c), respectively. These correlation factors are not at all new as it has been found to be approximately equal to $[(1+2.K_0)/3]$, where K_0 is the lateral earth pressure coefficient at rest and can be estimated by Jaky's equation, $K_0 = 1–\sin \Phi'$(Budhu 1985). This correction factor was previously drawn by Silver et al. (1980) and Tatsuoka et al. (1986) for specimens anisotropically consolidated in DSS and torsion shear tests, respectively, wherein radial strains were restrained. The key observation of this study is that the correction factor of $[(1+2.K_0)/3]$ is applicable either in the case of restrained (DSS) or unrestrained (T_xSS) radial strains. On the other hand, Figure 5.10 shows an inverse relation under strain-controlled conditions. In which, the T_xSS liquefaction potential curves are higher than that of the CTX even after correlating the axial strain value (in CTX) to shear strain according to the elastic theory (i.e. $\gamma_{CTX} = (1+\mu).\varepsilon = 1.5\varepsilon$), where, μ is the Poisson's ratio, 0.5 for saturated sands (Rollins et al. 1998; RaviShankar et. al. 2005). The discrepancy in the relation between the CTX and the T_xSS liquefaction potential curves under

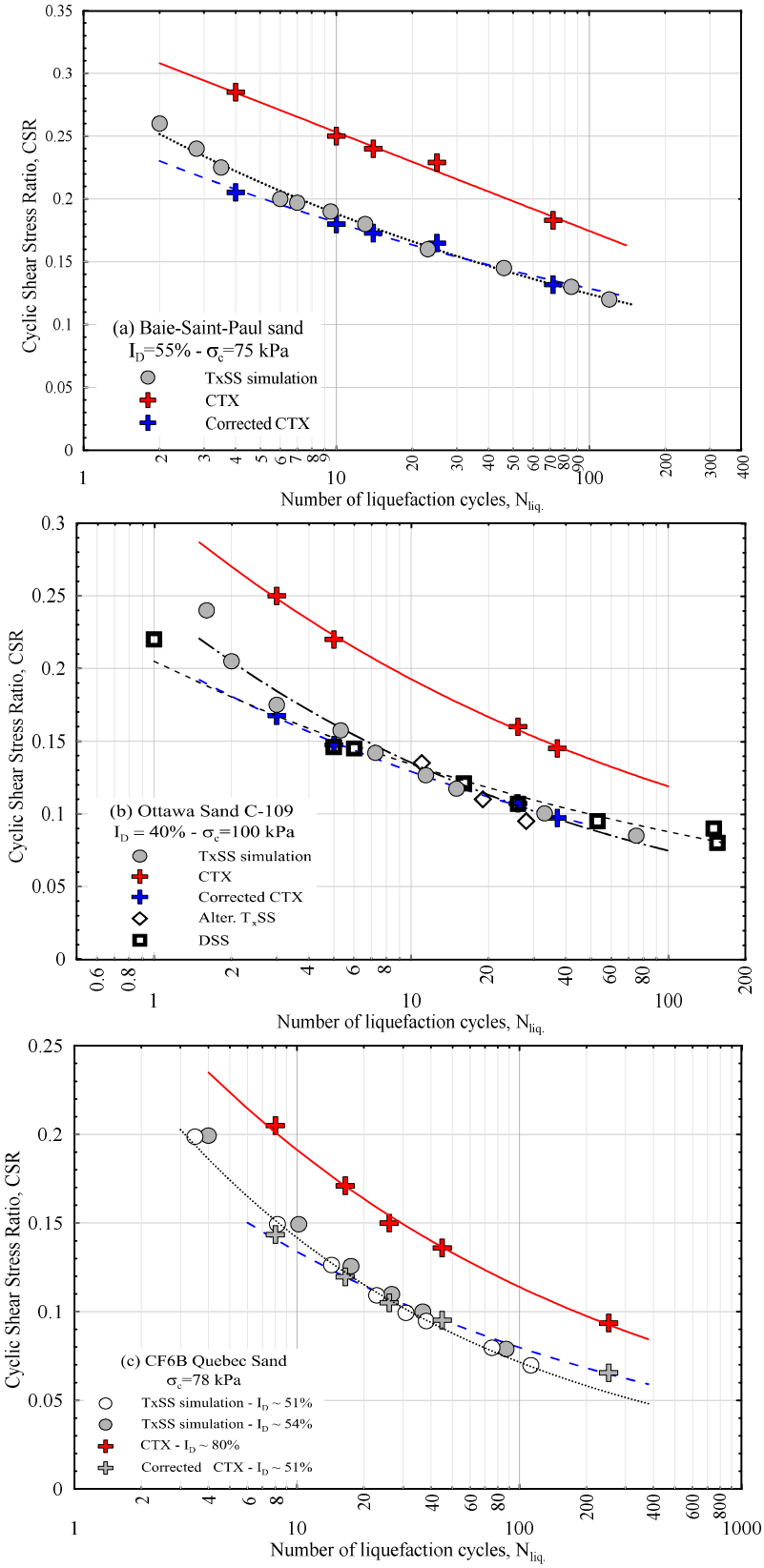

Figure 5.9. CSR – N_{liq} curve from stress-controlled T_xSS and CTX performed on: (a) Baie-Saint-Paul, (b) Ottawa C-109 and (c) Quebec CF6B sands

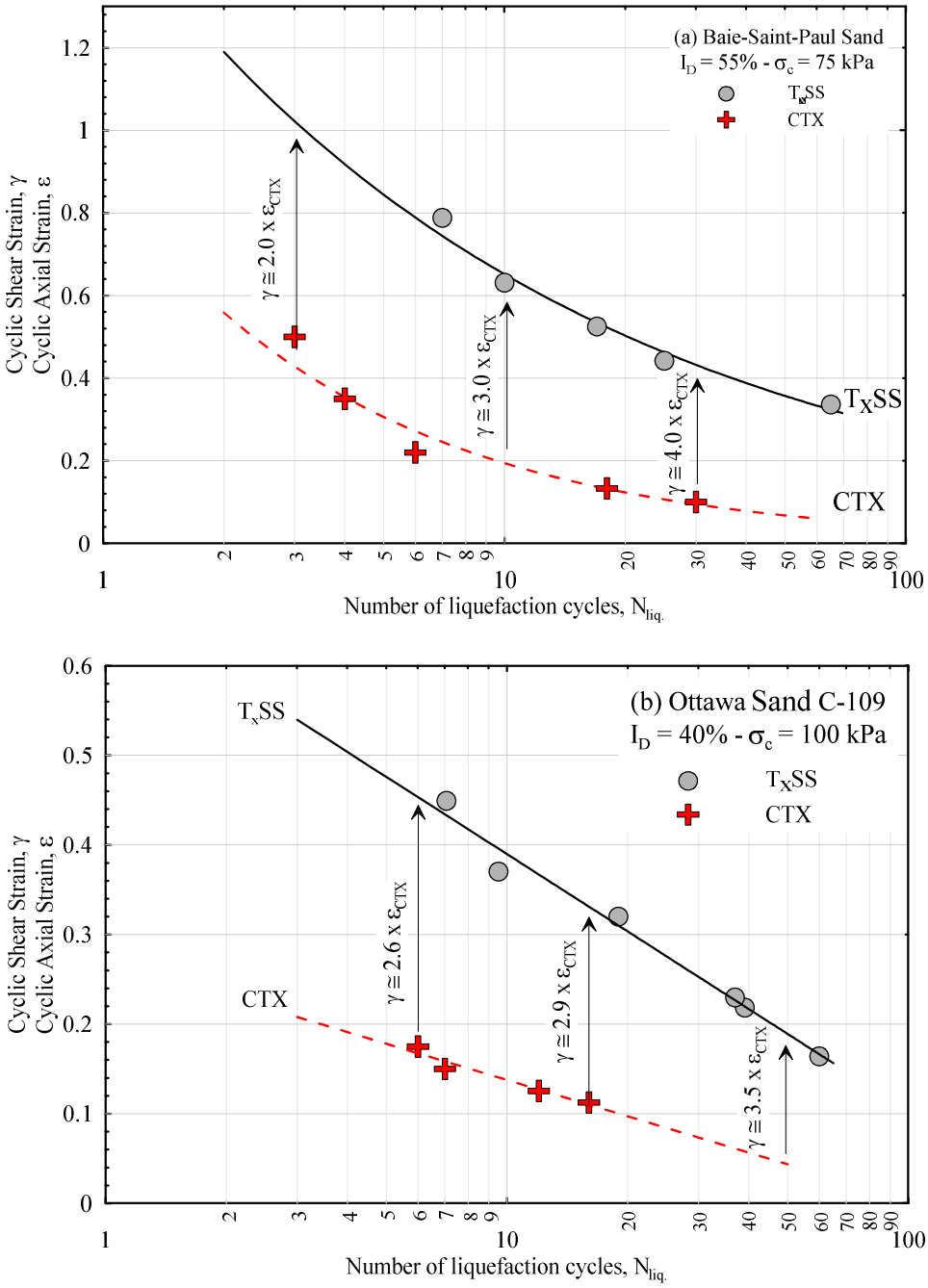

Figure 5.10. $\gamma - N_{liq}$ and $\varepsilon - N_{liq}$ curve from strain-controlled T_xSS and CTX performed on (a) Baie-Saint-Paul and (b) Ottawa Sand C-109

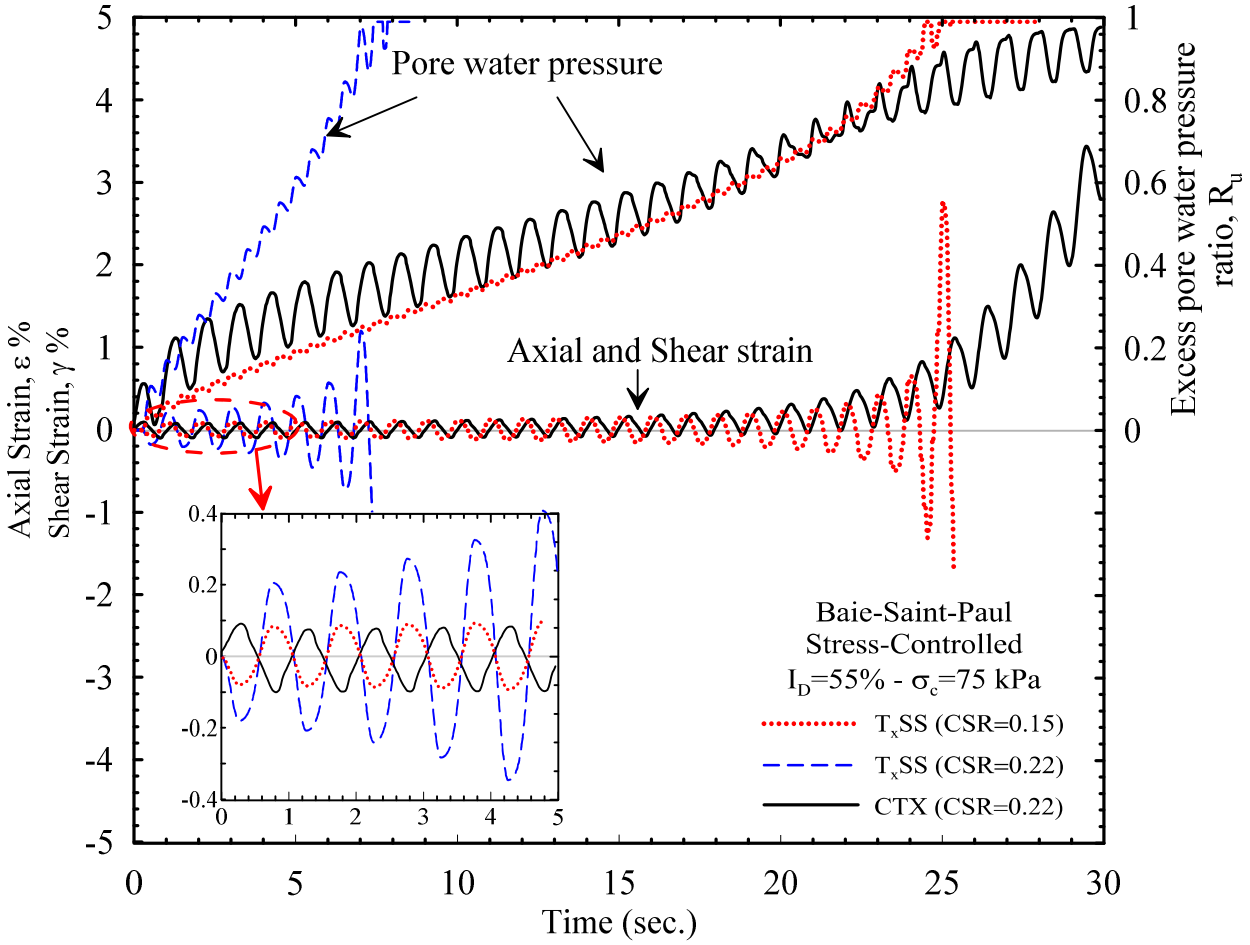

Figure 5.11. Variation of the induced strains and pore water pressure under stress-controlled tests

stress and strain-controlled conditions may be related to the difference in the induced (stress-controlled) and the applied (strain-controlled) shear strain value. There is abundant evidence supporting the fact that the shear strain is the key factor of the pore water pressure buildup (Lo 1961; Dobry and Abdoun 2017) and the associated degradation of shear modulus (Dobry 1982). It could be observed from Figure 5.10 that to correlate the CTX results, a correction factor must be applied on axial strain values, ε. In their numerical study, Zhang and Evans (2018) used the deviatoric strain to compare between CTX and DSS results (i.e., $\gamma = 2.12\ \varepsilon$). This correlation between γ and ε is consistent with the current results at the lower number of cycles (i.e. at higher strain amplitude). However, it increases by increasing the number of cycles until reaches about 4 as a function of shear strain and soil type. This correction factor is still ambiguous; therefore more experimental testing is required to investigate and correlate it with soil properties.

Figure 5.11 presents the difference between the induced strains and the generated pore pressure of BSP sand under a stress-controlled condition ($CSR_{CTX} = CSR_{TxSS} = 0.22$). The results of T_xSS simulation under a stress-controlled state of $CSR_{TxSS} = 0.15$ (which equal to C_r*0.22) is superimposed in Figure 5.11. It is observed that, at a given CSR, the induced peak strain values in the T_xSS are higher than those in the CTX. This can be ascribed to the effect of the hydrostatical back-pressure in CTX which in turn results in the confinement of the vertical deformation (Xia and Hu 1991). Xia and Hu (1991) justified that as the back-pressure changes the transfer and interact of microforces between the sand particles, and consequently influence on the deformation of soil skeleton and the generation of pore pressure in CTX. On the other hand, the mechanism of pore water generation and development of shear strain under cyclic simple shear tests is different. The pore pressure generation and shear strain are not affected by the applied back-pressure value (as in T_xSS; Archambault-Alwin et al. 2017) even in the case of DSS wherein no back-pressure is applied. Therefore, the induced shear strain and the generated pore water pressure in the T_xSS are higher than those in the CTX when subjected to the same CSR value. Consequently, the number of cycles required to triggering of liquefaction in the T_xSS is lower than that in the CTX under stress-controlled condition. On the other hand, when a correction factor of [$C_r = (1+2.K_0)/3$] is applied to the CSR_{CTX} results, a good agreement between the induced axial strain (in CTX) and shear strain (in T_xSS) as well as the generated pore water pressure is observed, Figure 5.11.

Figure 5.12 shows the variation of CSR as a function of the generated pore water pressure under strain-controlled loading in the CTX and the T_xSS simulation ($\gamma = \varepsilon = 0.33$, and $\varepsilon = 0.22$). It can be clearly seen that the CSR required to induce the same shear strain value ($\gamma = 1.5\varepsilon = 0.33$) in the CTX is usually higher comparing to its counterpart in T_xSS. Figure 5.12 shows that, under strain-controlled CTX test, higher pore pressure ratio was generated ($R_u \approx 0.4$ - 0.5) at the first cycle which in accordance with the previous results obtained by Silver and Park (1976); Sitharam et al. (2012); and Okada and Nemat-Nasser (1994). On the other hand, the generated R_u in the T_xSS increased gradually until the liquefaction occurrence (i.e., $R_u = 0.9$). The dramatically increase in R_u under strain-controlled conditions in CTX can be ascribed as follows: despite the existing of back-pressure, the soil specimen is compelled to deform to accommodate the applied axial strain which influences on the interparticle forces and leads to the generation of pore pressure (Xia and Hu 1991). In addition, in CTX, the applied axial strain is

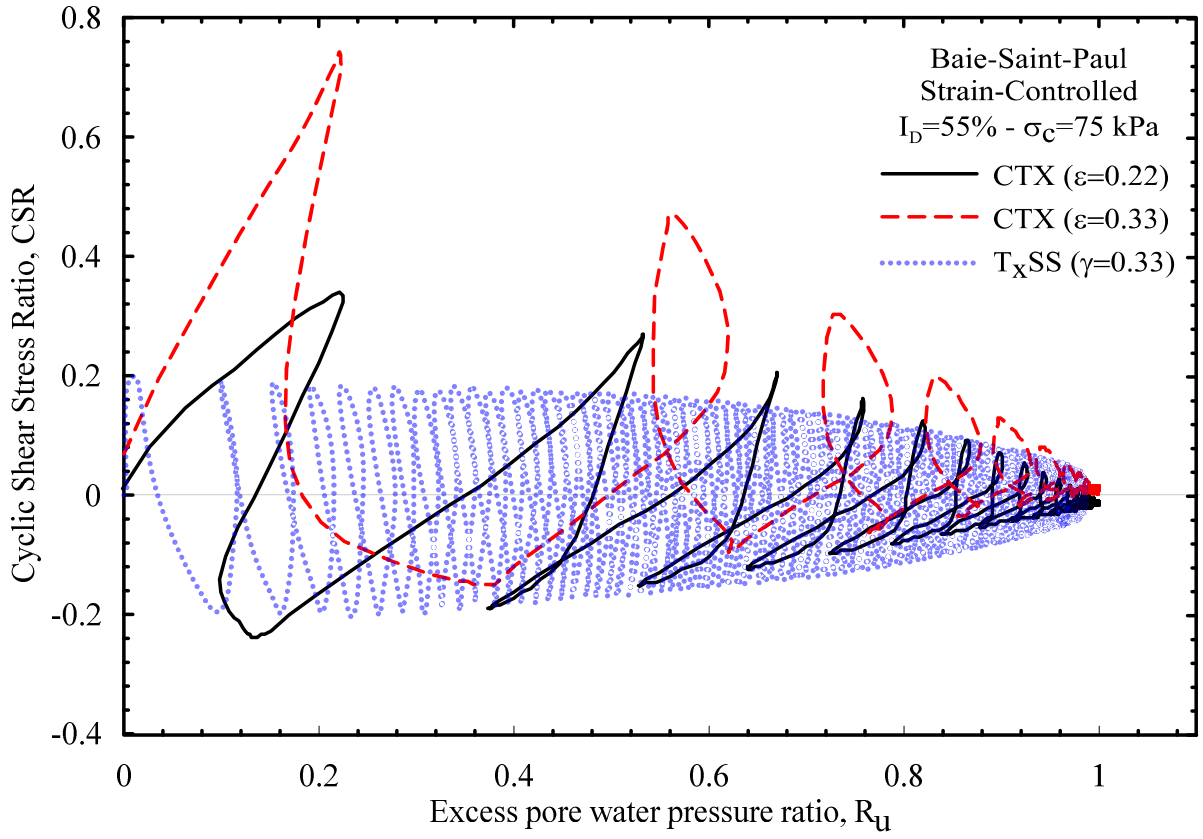

Figure 5.12. Variation of the induced strains and pore water pressure under stress-controlled tests

resisted by soil particles and pore water (back-pressure), wherein their axial compression/extension properties are totally different. It is well known that the bulk modulus of pore water is much higher than that of soil skeleton (Scott 1963; Doherty and Fahey 2011; Chen et al. 2019). Thus, a higher load/energy is required to reach the desired strain value (break the soil skeleton) which in turn causes a higher pore water pressure value (Scott 1963; Lenart 2008). This is in contrary to the mechanism of R_u generation in the T_xSS, or generally in DSS, where the applied strain (in strain-controlled) or stress (in stress-controlled) is transmitted directly to the soil particles as pore water cannot sustain any shear stress (Lenart 2008). Consequently, at the same shear strain value (γ = 1.5 ε), the generated R_u in CTX is higher than that in T_xSS under strain-controlled test. Therefore, the liquefaction resistance obtained from T_xSS results is higher than that obtained from CTX under strain-controlled conditions and must be correlated by the correlation factor proposed in this work.

CHAPTER 6

DYNAMIC SOIL BEHAVIOR UNDER SIMPLE AND TRIAXIAL SHEAR MODES

Authors and Affiliation:

Marwan Khashila: PhD Candidate, Sherbrooke University, Faculty of Engineering, Sherbrooke, QC.

Mahmoud N. Hussien: Associate Professor, Assiut University, Faculty of Engineering, Assiut, Egypt
Researcher, Sherbrooke University, Faculty of Engineering, Sherbrooke, QC

Mourad Karray: Professor, Sherbrooke University, Faculty of Engineering, Sherbrooke, QC.

Mohamed Chekired: Researcher, Institut de Recherche d'Hydro-Québec, Varennes, Quebec, Canada.

Date of submission: August 2019

State of submission: under review

Journal: Computer and Geotechnics Journal

French title: Comportement dynamique du sol en cisaillement simple et triaxial

Contribution in the thesis:

To further evaluate the capability and the accuracy of the proposed energy-based model introduced in the previous chapter, the cyclic behavior under triaxial (CTX) and combined triaxial simple shear (T_xSS) conditions are simulated using the well-known Fast Lagrangian Analysis of Continua (*FLAC*^{3D}) software comparatively with an experimental program. A brief review of the proposed model is presented followed by the proposed 3-dimensional model. The ability of the proposed model to capture the global cyclic responses of CTX and T_xSS are discussed and the local responses of each sub-zone are also demonstrated. The superiority of the T_xSS over the CTX is presented in terms of the dissipated energy and the distribution of the generated pore water.

Abstract: Although much has been discussed on liquefaction phenomenon and cyclic behavior of saturated sands, relatively little has been clarified on the difference between their cyclic behavior under simple and triaxial shear modes, particularly under strain-controlled conditions.

Thus, a comparative cyclic strain-controlled simple (DSS and T_xSS) and triaxial (CTX) shear tests were performed on reconstituted sand specimens. Firstly, the experimental results had been used to develop a simplified energy-based pore water pressure model that was employed later to simulate the cyclic behavior of sands in CTX and T_xSS testing modes through the computer code $FLAC^{3D}$. Unlike T_xSS soil models that experience relatively uniform stress state, the numerical simulation reveals the non-uniformity of the produced stress-strain and pore water pressure within the triaxial specimen. Because of the difference in the induced and the applied shear strain in cyclic stress and strain-controlled tests, respectively, the comparative cyclic strain-controlled tests reveal that the DSS and T_xSS specimens liquefied slower than triaxial specimens in contrast to cyclic stress-controlled results. A correlation between cyclic axial and shear-strains is then established and successfully verified based on the damage concept that can be used in comparing the cyclic behavior in CTX and T_xSS.

Keywords: Liquefaction; Strain-controlled; Pore water pressure ratio; $FLAC^{3D}$, Triaxial, T_xSS.

Résumé: Bien que l'on ait beaucoup étudié le phénomène de liquéfaction et le comportement cyclique du sable saturé, relativement peu de choses ont été clarifiées sur la différence entre le comportement cyclique en mode triaxial et en mode de cisaillement simple, en particulier en mode à contrainte-contrôlée. Ainsi, des essais de cisaillement simples et triaxiaux comparatifs en deformation-controlé cyclique ont été effectués sur des échantillons de sol reconstitué des sables de Baie-Saint-Paul et d'Ottawa C-109. Lors de la première phase, les résultats expérimentaux avaient été adoptés pour développer un modèle numerique simplifié de pression interstitielle basé sur l'énergie. Ensuite, le modèle proposé a été utilisé pour simuler le comportement cyclique des sables lors d'essais triaxiaux et triaxiaux combinés de cisaillement simple "TxSS" utilisant le logiciel FLAC-3D. La simulation numérique révèle la non-uniformité de la réponse en contrainte, déformation, énergie dissipée concomitante et la pression de l'eau interstitielle le long de l'échantillon de sol triaxial. Cependant, les échantillons de sol TxSS présentent un état de stress plus uniforme. Les résultats du DSS conventionnel et du TxSS sont comparés et l'effet de la méthode de confinement latéral sur la résistance à la liquéfaction est ensuite discuté. Les essais comparatifs cycliques contrôlés par déformation révèlent que la résistance à la liquéfaction du CTX est inférieure à celle du TxSS, contrairement aux résultats cycliques contrôlés par contrainte. Une corrélation entre les traînées axiales cycliques et les traînées de cisaillement est

ensuite établie et vérifiée avec succès sur la base du concept d'endommagement qui peut être utilisé pour comparer le comportement cyclique en CTX et en T_xSS.

Mots-clés : Liquéfaction; Contrôle de la déformation; taux de pression de l'eau des pores; FLAC^{3D}, Triaxial, T_xSS.

6.1 Introduction

When saturated loose soil is subjected to cyclic loading, it tends to contract due to the rearrangement of soil particles. The contractive behavior of soil results in a generation of excess pore water pressure accompanied by a deterioration of its stiffness and eventually triggering of liquefaction. During the last decades, extensive liquefaction studies have been devoted to investigate this phenomenon as it causes destruction of infra and superstructures. Experimentally, different laboratory element configurations have been developed to study this phenomenon including triaxial (CTX), direct simple (DSS) and torsional shear devices. The first two are used in the assessment of liquefaction throughout the current study.

In cyclic triaxial testing (CTX), a soil specimen is confined under a minor principal stress and a deviatoric stress is applied to the upper platen where the stress condition throughout the specimen is well known. However, in DSS, the applied shear stress and the induced shear strain could be measured on the horizontal plane wherein the surrounding stress is assumed to be equal $K_0.\sigma'_v$ (where K_0 is the coefficient of lateral earth pressure at rest, and σ'_v is the vertical confining stress). Thus, considerable studies have been devoted to simulate the DSS analytically to capture the stress conditions during static (Budhu and Britto 1987) or cyclic loading (Amer et al. 1987). Saada and Townsend (1981) introduced a critical review discussing the advantages and limitations of each device. In CTX, the principal stress directions rotate instantaneously by 90^o. However, in DSS, principal stresses rotate smoothly until failure mimicking the stress condition during earthquake wave propagation. Peacock and Seed (1968) attributed the difference between the liquefaction potential curves of CTX and DSS to the difference in the rotation of principal stress under cyclic stress-controlled tests (i.e., applying uniform cyclic stress of constant amplitude on soil specimen). In addition, they found that the different of cyclic behavior in triaxial (i.e. compression and extension) and in simple shear loading has a significant effect on the liquefaction resistance.

The widely used stress-based method has been used since the beginning of liquefaction assessment by converting the irregular ground motion to an equivalent number of cycles having

an equivalent damage effect (Seed and Idriss 1971; Lee and Chan 1972). Dobry and his colleagues proposed an alternative strain-based method (Dobry et al. 1982; Wer and Dobry 1982). Dobry et al. endorsed the strain-controlled method (i.e., applying uniform cyclic strain of constant amplitude on soil specimen) as the volumetric changes in drained cyclic loading and pore pressure generation in undrained cyclic loading have been reported to be more dependent on shear strain rather than shear stress (Silver and Seed 1971). Also, a unique relationship between the generated pore water pressure ratio (R_u) and the applied shear strain amplitude could be obtained at a given number of cycles regardless of sand type, relative density, confining pressure or deposition method (Vucetic and Dobry 1988; Dobry and Abdoun 2015). In contrast, the generation of pore pressure has been observed to be affected more fundamentally by the preparation method in stress-controlled tests. On the other hand, Arriaga and Green (2018) in their comparative assessment of strain-controlled approach deduced the inaccuracy of Dobry's procedure in liquefaction assessment. They criticized the Dobry's procedure as the soil softening is not considered when adopting strain-controlled approach in the liquefaction assessment. This crucial flaw is re-evaluated in the current numerical simulation. One of the main deficiencies of stress or strain-controlled methods is the necessity of converting earthquake motion to equivalent damage uniform stress or strain cycles (Seed et al. 1975; Khashila et al. 2018). Nemat-Nasser and Shokooh (1979) mathematically introduced the strain-energy concept to link the densification, rearrangement, of cohesionless soil and pore pressure buildup in saturated sand to the dissipated energy. Use of the energy approach in liquefaction investigation over the last few decades has attracted the attention of many researchers compared with the cyclic stress-based and cyclic strain-based approaches. The potential advantage of the energy method is circumventing the need of converting earthquake motion to a uniform wave as it is load waveform independent. It is well-recognized that the pore water pressure–dissipated energy relation is independent of loading pattern (i.e. uniform or random loading) (Liang 1995). In addition, the dissipated energy encompasses both induced shear stress and strain during cyclic loading (Lenart 2008). In fact, extensive research works have been done to correlate a relationship between pore water pressure buildup and dissipated energy per unit volume under different loading condition as well as applying the strain energy concept in liquefaction potential assessment of soil based on cyclic testing results (e.g. Liang 1995; Berrill and Davis 1985; Figueroa et al. 1994; Azeiteiro et al. 2017; among many others). An extensive review of the

previously published energy–pore pressure relations has been reported in (Green 2001; Jafarian et al. 2012). In the field realm; Davis and Berrill (1982) and Berrill and Davis (1985) applied the energy concept in the field analysis by relating the pore pressure during earthquake loading to its magnitude, epicentral distance and initial effective overburden pressure. Later, the energy concept was adopted to model the cyclic mobility of saturated silt and silty sand soils (Lenart 1995) and in one-dimensional effective stress analysis (Yamazaki et al. 1985).

In the current work, an energy-based pore pressure model is developed based on comparative cyclic stress and strain-controlled tests conducted in the triaxial and the combined triaxial simple shear "T_xSS" devices (Chekired et al. 2015; Karray et al. 2019). The proposed energy-based pore pressure model is incorporated in the finite-difference computer program FLAC^{3D} to simulate cyclic behavior in triaxial and T_xSS conditions. The numerical model allows investigating and analyzing the dynamic behavior of soil specimens which is the main objective of this study. In addition, a comparison between the liquefaction potential of strain-controlled CTX and its counterparts from T_xSS and DSS is discussed. After that, a correlation between strain-controlled liquefaction potential curves is proposed and validated successfully using the generated pore pressure as damage metric (Khashila et al. 2018).

6.2 Experimental program

6.2.1 Testing Device and soil sampling

Cyclic triaxial tests were performed by using a servo-controlled pneumatic triaxial apparatus. The used triaxial apparatus is capable of carrying out stress and strain-controlled monotonic or cyclic loading tests. The apparatus is also equipped with highly sensitive displacement sensors. The back, cell and excess pore water pressure are controlled and measured by back-pressure and cell pressure-volume controllers. The T_xSS was used in the current study to investigate the cyclic behavior under simple shear loading when soil specimens confined in a triaxial chamber. The T_xSS has been developed at Université de Sherbrooke (Chekired et al. 2015; Karray et al. 2019). The shear loading is applied with an electromagnetic shaker mounted over a highly rigid table. The T_xSS can be used to apply regular or irregular cyclic shear strain on isotropic or anisotropic consolidated saturated soil under simple shear conditions. The main advantage of the electrically operated T_xSS over the conventional DSS is to facilitate performing a simple shear test on saturated soil when confined in a triaxial cell pressure or simply when confined in a reinforced

wire membrane or stacked annular plates. Moreover, it can be used to apply regular and irregular shear waves. Using this apparatus allows measuring the generated pore pressure directly during a cyclic or monotonic shear test. It is noteworthy that the top cap was designed to allow the horizontal (shearing-direction) and vertical displacement without rotation. More advantages and illustration of the T_xSS apparatus can be found in (Khashila et al. 2018; Chekired et al. 2015; Karray et al. 2019; Abdellaziz et al. 2020). The conventional DSS apparatus was adopted to perform a comparative series of cyclic strain-controlled tests on Ottawa sand. It was supplied by GDS Company (EMDCSS) and has the ability to perform stress and strain-controlled monotonic or cyclic tests.

Reconstituted specimens of Baie-Saint-Paul (BSP) and Ottawa C-109 sands were prepared in triaxial cells with height and diameter of 76 and 38 mm, respectively (H/D=2). While T_xSS specimens were 80 mm diameter (D) to 26 mm height (H) (D/H= 3.2 (ASTM D6528-17)). (Note: the specimen size effect was investigated in a complementary paper). The grain size distribution and grain shape are shown in Figure 6.1 and Table 6.1 summarizes their physical properties. The wet tamping method (Ladd 1978) was used to prepare soil specimens in an appropriate mold. Triaxial specimens were prepared in six layers while in T_xSS and DSS soil specimens were placed in three layers. Each layer was gently tamped until the desired height and the top surface of each layer was scarified before replacing the following layer. Thereafter, CTX and T_xSS specimens were saturated by percolating carbon dioxide (CO_2) through it under a low cell pressure to displace air bubbles. After that, de-aired water was injected through the soil specimen under a differential pressure of 10 kPa. Then, the back-pressure was increased gradually to 190 kPa and the cell pressure to 200 kPa for 15 hours. Full saturation of the soil specimen was achieved when the Skempton's pore pressure parameter B ($\Delta u/\Delta\sigma_3$) became higher than 0.96 (ASTM-D5311M). Then, the soil specimen was isotropically consolidated in a triaxial chamber under an effective confining pressure of 75 and 100 kPa for BSP and Ottawa sands, respectively. However, DSS specimens were prepared in reinforced membranes and consolidated anisotropically under K_0 condition.

Cyclic stress and strain-controlled tests were conducted in the triaxial apparatus, while cyclic strain-controlled tests were performed in the T_xSS apparatus under a frequency of 1 Hz (ASTM-D5311M). The pore water pressure, axial /or shear strain, cyclic stress ratio (CSR) were

monitored during cyclic loading until the onset of liquefaction. Liquefaction occurrence was considered through this investigation as the pore pressure ratio (R_u) reaches 0.9.

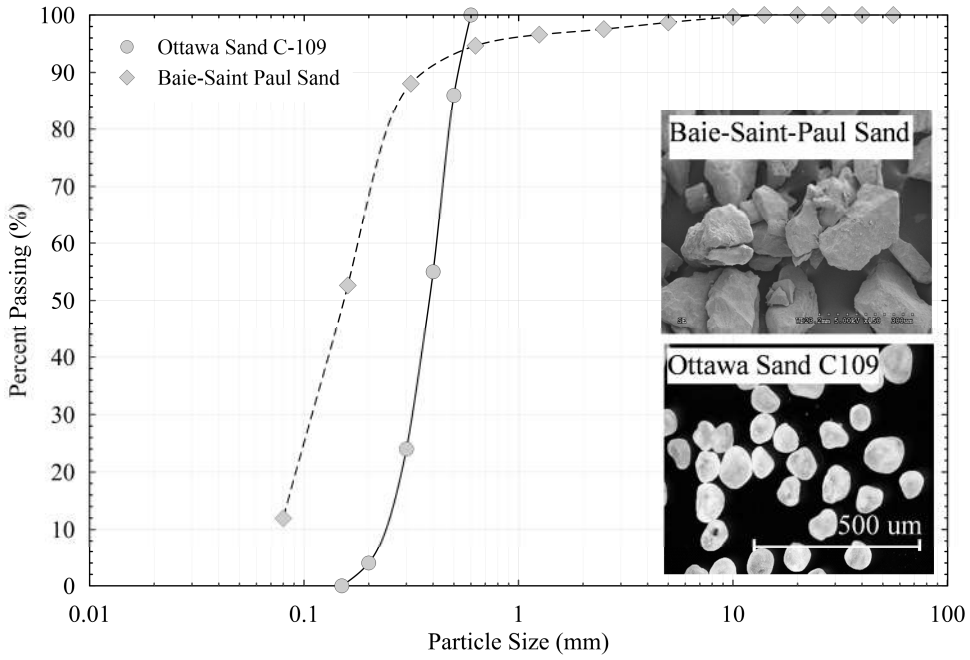

Figure 6.1. Grain size distribution of the used sands

Table 6.1: Physical properties of the used sands

Soil properties	Baie-Saint-Paul sand	Ottawa sand C-109
G_s	2.78	2.67
e_{max}	0.91	0.82
e_{min}	0.598	0.5
C_u	2.25	1.75
C_c	1	1.016
D_{50}	0.15	0.4

6.2.2 Experimental results

Figure 6.2 shows the response of BSP sand subjected to cyclic strain-controlled loading in T_xSS and CTX. By load sequence, the pore pressure increases until the trigger of liquefaction. It can be seen that the rate of pore pressure generation is higher in cyclic triaxial (Figure 6.2(e)) comparing to its rate in the T_xSS (Figure 6.2(b)). The induced cyclic stress ratio "CSR" is observed to deteriorate corresponding to the degradation of shear modulus, G (Figures 6.2(a) and

6.2(d)). It might be observed that the decay of shear modulus and CSR is a function of the generated pore pressure ratio (R_u) and can be estimated by:

$$G=G_{\max}\left(1-R_u\right)^{\nu} \tag{6.1}$$

where G_{max} is the maximum shear modulus, ν is a fitting parameter which observed to be stress path dependent (ν = 0.5 and 0.7 for T_xSS and DSS (Matasovic and Vucetic 1993; Chang et al. 2007) and CTX test results (this work), respectively).

Figures 6.2(c), 6.2(f) show the effective cyclic stress path in T_xSS and CTX. In CTX, cyclic stress path is depicted in terms of p′ (p′ = (σ'_1+2 σ'_3)/3) and q (q = σ'_1-σ'_3). However, in T_xSS cyclic test, similar to other simple shear configurations, the stress path is plotted as the applied shear stress (τ) versus the decrease of effective confining stress (σ′).

The area of hysteresis loop, the variation of cyclic stress ratio (CSR) as a function of shear strain or axial strain, response of soil specimen can be integrated using the trapezoidal rule to predict the dissipated energy per unit volume during cyclic loading that can be determined from DSS or T_xSS test results by (Green et al. 2000; Yang et al. 2018):

$$W_s=\frac{1}{2\sigma'_{mo}}\sum_{i=1}^{n-1}(\tau_{i+1}+\tau_i)(\gamma_{i+1}-\gamma_i) \tag{6.2.a}$$

and from CTX test results by:

$$W_s=\frac{1}{2\sigma'_{co}}\sum_{i=1}^{n-1}(\sigma_{d,i+1}+\sigma_{d,i})(\varepsilon_{a,i+1}-\varepsilon_{a,i}) \tag{6.2.b}$$

where i and n are the incremental and total number of increments, τ and σ_d are shear and deviator stresses; γ, ε are shear and axial strains. In Eq. (6.2), the influence of initial mean effective stress is alleviated by normalizing the energy by effevtice mean stress (σ'_{m0}) or effective confining pressure (σ'_{c0}) in T_xSS or CTX, respectively.

Based on the measured pore pressure in T_xSS and CTX apparatuses, Figure 6.3 plots the accumulated pore pressure as a function of the normalized dissipated energy during cyclic loading. From this figure, it can be indicated that the energy-pore pressure relation falls within a converge band, and can be obtained by a polynomial relationship as:

$$R_u=\mathrm{C}_1\left(\frac{W_s^{0.5}}{\alpha}\right)+\mathrm{C}_2\left(\frac{W_s^{0.5}}{\alpha}\right)^2+\mathrm{C}_3\left(\frac{W_s^{0.5}}{\alpha}\right)^3 \tag{6.3}$$

where α is a calibration parameter that depends on soil type, relative density, stress path, and stress condition. The calibrated α of each test are listed in Table 6.2 and plotted as a function of shear strain in Figure 6.3. C_1, C_2, C_3 are model fitting parameters as listed in Table 6.3.

Table 6.2: Summary of the experimental work

Sand	Test No.	*Apparatus (test type)*	γ_{cyc} *or CSR*	e_{ini}	e_{cons}	I_D	σ'_{co}	B	N_{liq}	α
Baie-Saint-Paul sand (Freq. =1.0Hz)	B-S1	T_xSS (Strain)	0.780	0.771	0.738	55	75	0.95	7	1.25
	B-S2		0.440	0.768	0.735	56	75	0.97	25	1.6
	B-S3		0.632	0.767	0.732	57	75	0.97	10	1.25
	B-S4		0.525	0.773	0.732	57	75	0.97	17	1.55
	B-S5		0.326	0.771	0.743	53.5	75	0.97	65	2.25
	B-T1	CTX (Strain)	0.500	0.771	0.738	55	75	0.97	3	-
	B-T2		0.350	0.768	0.737	55	75	0.97	4	0.73
	B-T3		0.220	0.771	0.740	54.5	75	0.97	7	0.63
	B-T4		0.133	0.770	0.739	55	75	0.97	16	0.60
	B-T5		0.100	0.768	0.740	54.5	75	0.97	29	0.65
	B-TX1	CTX (Stress)	0.180	0.759	0.735	56	75	0.97	72	
	B-TX2		0.209	0.759	0.736	55.7	75	0.97	28	
	B-TX3		0.228	0.770	0.741	54	75	0.97	14	
	B-TX4		0.241	0.770	0.740	54.5	75	0.97	10	
	B-TX5		0.270	0.771	0.737	55.5	75	0.97	4	
Ottawa C-109 sand (Freq. =1.0Hz)	O-S1	TxSS (Strain)	0.450	0.725	0.688	41	100	0.96	7	-
	O-S2		0.370	0.722	0.687	41	100	0.97	9.5	-
	O-S3-A		0.350	0.722	0.688	41	96	0.97	15	0.88
	O-S4		0.340	0.723	0.688	41	100	0.97	19	1.30
	O-S5-A		0.270	0.726	0.680	43	97	0.97	23.5	0.93
	O-S6		0.255	0.725	0.688	43	101	0.96	24	1.08
	O-S7-F[1]		0.250	0.723	0.680	40	98	0.95	23	-
	O-S8-F[2]		0.250	0.722	0.688	41	103	0.97	24	1.06
	O-S10		0.230	0.725	0.689	41	102	0.96	37	-
	O-S11		0.210	0.723	0.685	42	100	0.97	39	1.05
	O-S12		0.150	0.720	0.690	40	103	0.93	60	1.8
	O-S13		Monotonic	0.722	0.682	43	100	0.96	-	-
	O-T1	CTX (Strain)	0.200	0.770	0.690	40	100	0.97	7	0.83
	O-T2		0.175	0.766	0.688	40	100	0.97	6	0.72
	O-T3		0.150	0.768	0.689	40	100	0.97	7	0.69
	O-T4		0.126	0.770	0.690	40	100	0.97	12	0.70
	O-T5		0.116	0.769	0.689	40	100	0.97	16	0.70
	O-T6		0.100	0.770	0.690	41	100	0.97	44	-
	O-TX1	CTX (Stress)	0.200	0.768	0.689	41	100	0.97	3	
	O-TX2		0.175	0.768	0.687	40	100	0.97	5	
	O-TX3		0.147	0.768	0.688	41	100	1.00	26	
	O-TX4		0.127	0.768	0.688	40	100	0.97	37	
	O-D1	DSS (Strain)	0.400	0.722	0.698	38	100	-	8	
	O-D2		0.340	0.730	0.700	37.5	100	-	11	
	O-D3		0.240	0.720	0.690	40.6	100	-	30	
	O-D4		0.140	0.725	0.690	40.6	100	-	180	

α: pore water pressure model's parameter.

O-S3-A and O-S5-A: prepared specimens in armed membranes.

O-S7-F[1] and O-S8-F[2]: prepared specimens at different D/H ratio5.45, and 2.16.

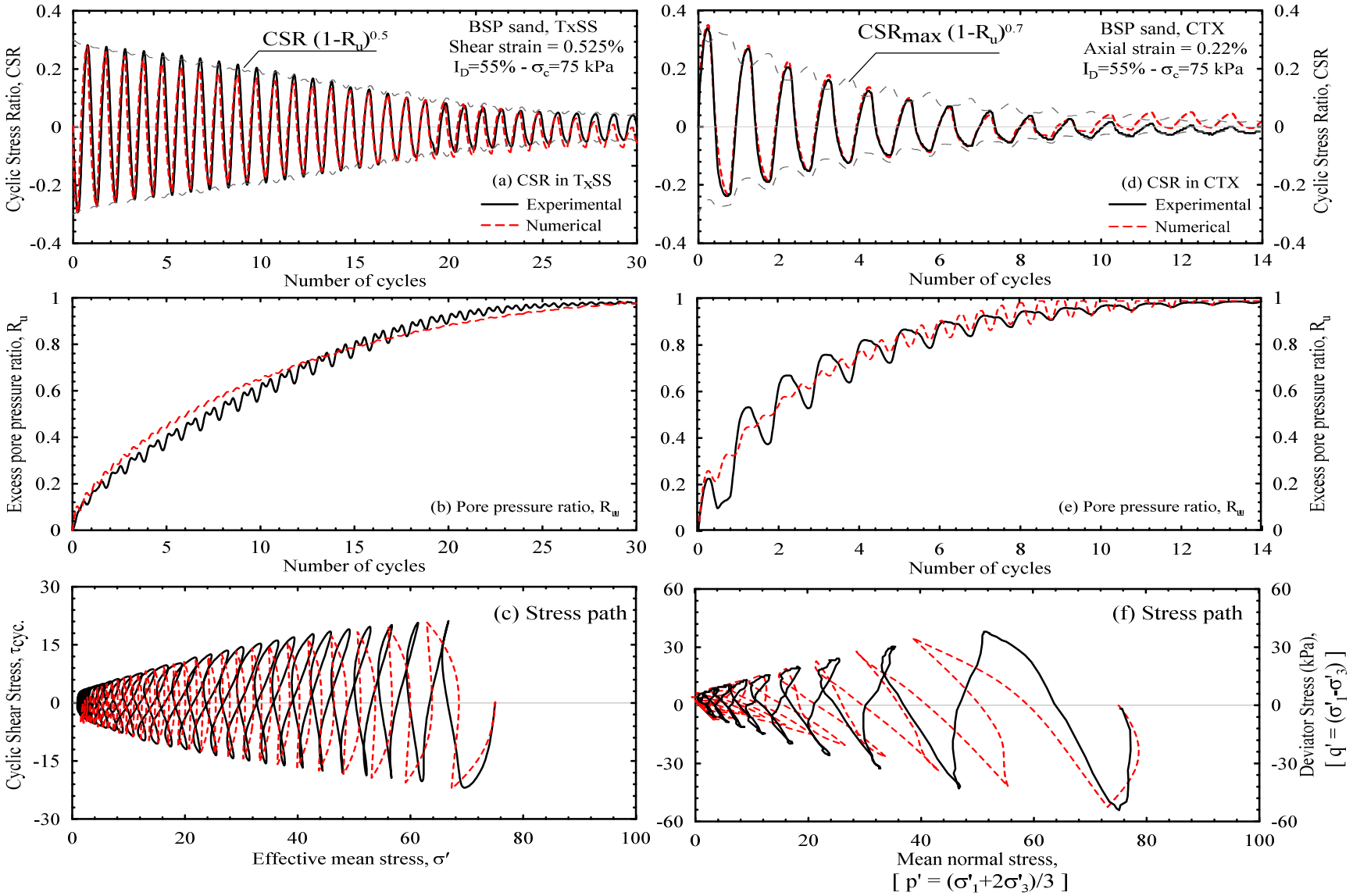

Figure 6.2. Comparison between measured and computed BSP sand response in terms of CSR, pore water pressure buildup and stress path in cyclic strain-controlled T_xSS and CTX tests

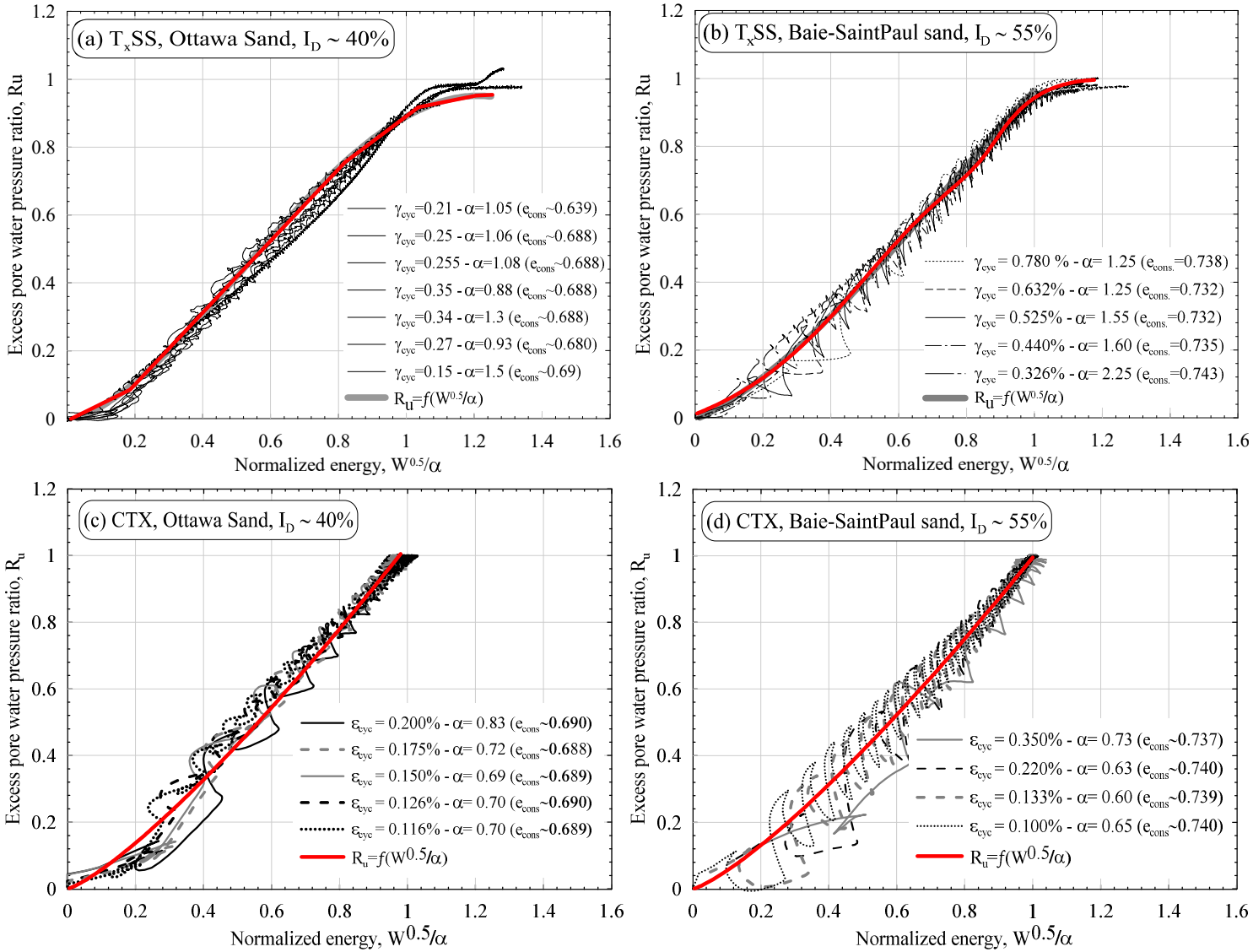

Figure 6.3. Variation of the accumulated pore pressure ratio with the normalized dissipated energy per unit volume for BSP and Ottawa sands in T_xSS and CTX

Table 6.3: Pore pressure model fitting parameters

Fitting parameters	BSP sand		Ottawa sand	
	TxSS	CTX	TxSS	CTX
C_1	0.383	1.235	0.294	0.616
C_2	1.470	-0.378	1.550	1.147
C_3	-0.570	0.145	-0.945	-0.710

Konstadinou and Georgiannou (2014), on the basis of a series of stress-controlled torsion shear tests, proposed a correlation between α and the mean grain size (d_{50}) and the grain shape. Use of Konstadinou and Georgiannou's relation overestimates α values compared to the current results under triaxial and simple shear test which infers that α-value is a load path dependent. The current results show that α is not unique for the same soil; however, it is a function of strain value, as shown in Figure 6.3 and Table 6.2.

6.3 Numerical simulation

6.3.1 Numerical model

In this study, to capture a deep understanding of the dynamic behavior under CTX and T_xSS, the well-known Fast Lagrangian Analysis of Continua (*FLAC*^{3D}) software, an explicit finite difference method program (FDM), was used compared with the experimental program to investigate the cyclic behavior in CTX and T_xSS. A prescribed linear or nonlinear constitutive model could be adopted in FLAC to model the behavior of each element or the boundary conditions. In fact, the FLAC library contains several constitutive models to simulate the behavior of soil under static or dynamic loading. The most frequently used model in the dynamic analysis is Finn model, which adopts the incremental of volumetric strain-pore pressure relations proposed by Martin et al. (1975) and Byrne (1991) into the well-established Mohr-Coulomb plasticity model. Following the pioneer work dedicated to using the energy concept, as described above, for estimating the increment pore water pressure buildup and liquefaction analysis, this study aims at simulating the cyclic behavior of soil in T_xSS and CTX tests numerically by adopting the energy concept in FLAC software.

In the analysis, soil mass was laterally divided into 84 and 100 sub-zones while its height was divided into 16 and 6 sub-zones in CTX and T_xSS models, respectively, as shown in Figure 6.4. The minimum element height was selected to be smaller than one-tenth (1/10) of the wavelength of the applied wave to ensure accurate wave transmission between elements as recommended by

(a) CTX model

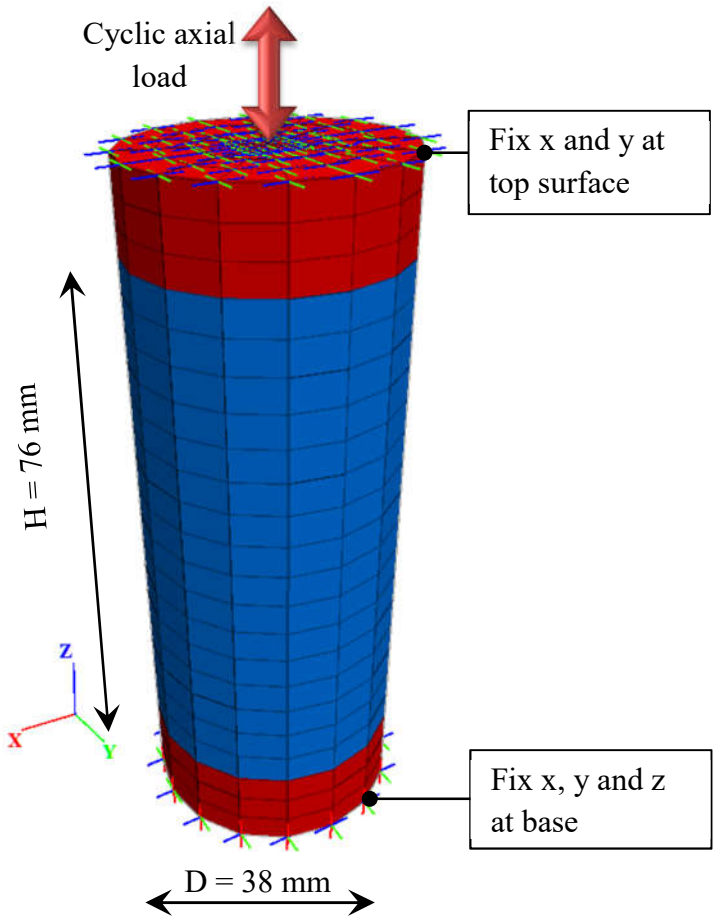

(b) T_xSS model

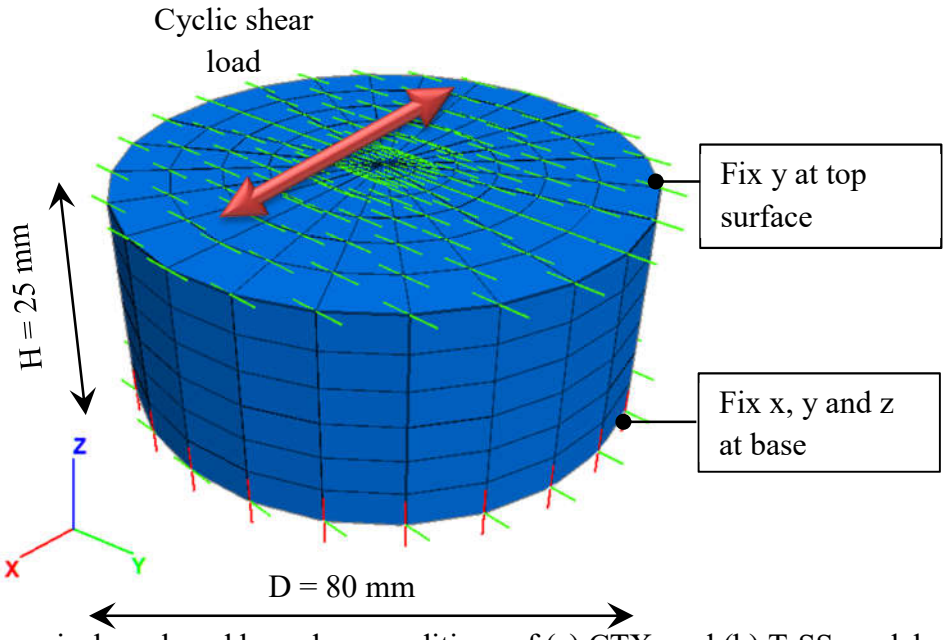

Figure 6.4. Numerical mesh and boundary conditions of (a) CTX, and (b) T_xSS models

Kuhlemeyer et al. (1973). The bottom nodes are fixed in the X-, Y- and Z-directions in both models. However, the movement in Z-direction is allowed at the top nodes to represent the applied axial strain in CTX and in the X-direction to apply shear strain at the top nodes of the T_xSS soil model, as indicated in Figure 6.4. Uniform distributed pressures were used to represent the radial boundary condition in CTX and T_xSS.At first, the consolidation stage was performed by applying isotropic stress on soil elements prior to applying a cyclic loading. Then, uniform cyclic stress or strain time histories, in stress or strain-controlled tests, respectively, were applied at the upper nodes. In order to calibrate the numerical model, the produced hysteresis loops from experimental work were compared with that obtained from the global behavior of the model (i.e., the obtained shear or axial strain from the upper nodes of the model relative to the base nodes). The cyclic behavior (hysteresis loops of shear stress-shear strain) of each zone is monitored separately (which will be referred as local behavior) by calculating the differential shear/axial strain between upper and lower nodes of each zone. Applying this procedure allows acquiring the cyclic behavior of each zone (hysteresis loop) and the correlative dissipated energy per unit volume by applying the trapezoidal equation, Eq. (6.2). Subsequently, the estimated pore pressure would be calculated according to the prior calibrated relations shown in Figure 6.3 and Eq. (6.3). In order to represent the hysteretic damping, the sigmoidal-model with four parameters (SIG4 model) was calibrated first from the experimental results. The experimental results show that, due to the pore pressure buildup, the effective stress decrease and consequently shear modulus degrades according to Eq. (6.1). Thus, the estimated pore pressure, Eq. (6.2), in conjunction with shear modulus degradation, Eq. (6.1), compiled with the SIG4 model were used to propose a coupled energy-based model to numerically simulate the degradation of soil stiffness during cyclic loading.

6.3.2 Applicability of the proposed energy-based model

Figure 6.2 presents a comparison between the measured and computed cyclic behavior of BSP and Ottawa sands in terms of cyclic stress ratio (Figures 6.2(a), 2(d)), pore pressure buildup (Figures 6.2(b), 2(e)) and effective stress path (Figures 6.2(c) and 6.2(f)). It can be seen from Figure 6.2 that there is a reasonable coherence between the results of the experimental and numerical models. This coherence implies the applicability of adopting the energy concept to capture the cyclic behavior of BSP and Ottawa sand tested in the T_xSS and CTX. This allows an

inclusive comparison between CTX and T_xSS under cyclic stress-controlled loading; however, it is beyond the scope of the current study.

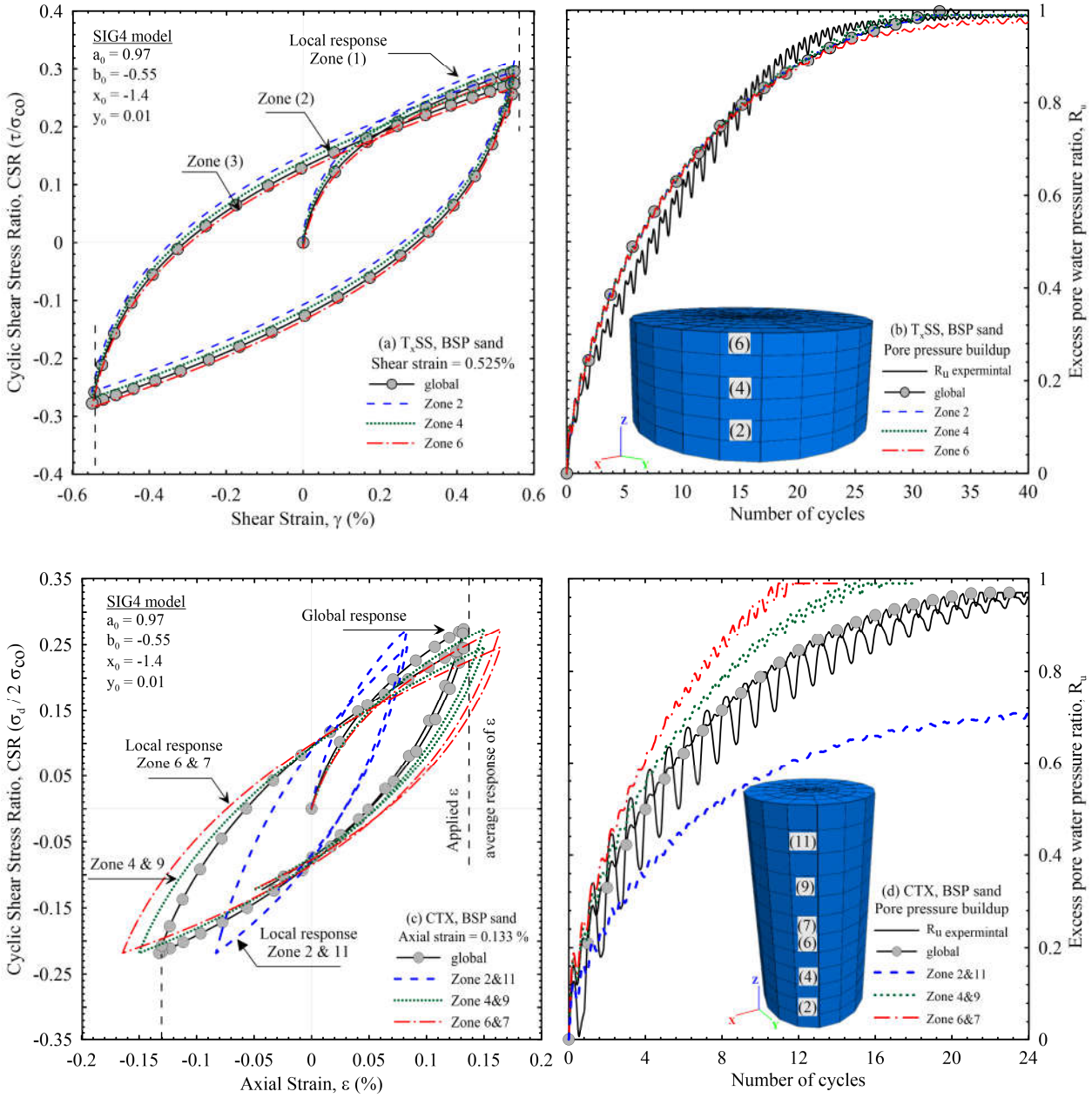

Figure 6.5. Simulation results of BSP under: (a) (b) T_xSS, (c) (d) CTX conditions

As mentioned above, adopting the energy concept allows predicting the induced pore pressure in each sub-zone of the numerical model as well as the hysteresis loop as depicted in Figure 6.5. These figures demonstrate the non-uniformity of pore water pressure throughout the CTX soil

specimen. However, the estimated pore pressure within the T_xSS specimen is almost uniform which will be discussed in the succeeding section.

6.4 Discussion

From the numerical results of the T_xSS, it can be observed that the induced shear strain and the hysteresis loops of all zones are almost identical (Figure 6.5(a)). This implies that the produced shear stress and strain in the T_xSS specimens are almost uniform. Consequently, the dissipated energy of unit volume and the induced pore water pressure are almost equal throughout the T_xSS specimen (Figure 6.5(b)). Conversely, the cyclic response of CTX reveals the non-uniformity of axial strains and normal stresses on the soil zones (Figure 6.5(c)). The induced non-uniformities of stresses in triaxial have been well-reviewed by (Saada and Townsend 1981; Tatsuoka et al. 1986). It is fundamentally occurred due to the effect of boundary condition (i.e., the effect of the top and bottom caps) which results in redistribution of specimen void ratio during cyclic loading (ASTM-D5311M). Medzvieckas et al. (2017) simulated a triaxial compression test using PLAXIS^{3D} platform and confirmed the effect of end caps on the non-uniformities of stress distribution in triaxial specimens. Moreover, they observed a generation of shear stresses at the top and bottom specimens even when using height to diameter ratio greater than the order of two. Despite using soil specimens with height to diameter ratio greater than the order of two, as recommended by (ASTM-D5311M), the current numerical simulation reveals the non-uniformities of stresses within CTX specimens.

The non-uniformities of stresses along CTX specimens result in divergence of the hysteresis loops and consequently the dissipated energy and the concomitant pore pressure in each zone (Figure 6.5(d)). This observation is in agreement with the previous observation of Castro (1975) and Whitman and Healy (1962). Consequently, the degradation of shear modulus, which is correlated to the bulk modulus, does not equalize within the soil specimens. However, during cyclic loading and pore pressure buildup, a diffusion and redistribution of the generated pore pressure occurs (Wang et al. 2004). The experimentally measured pore pressure is in accordance with the average computed pore pressure in each zone, as shown in Figure 6.5(d).

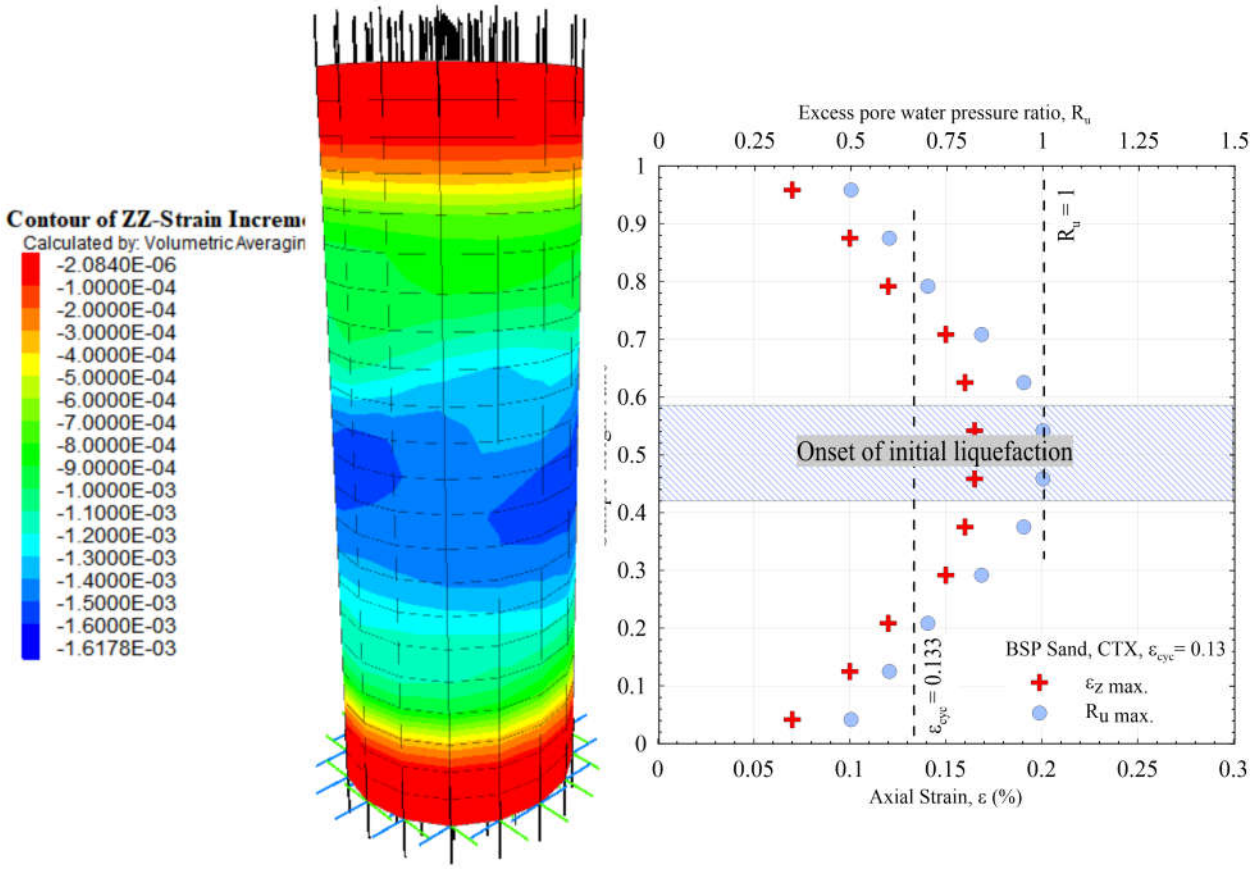

Figure 6.6. Axial strain distribution (ε_z) within CTX specimen

Calculating the generated pore water pressure in each sub-zone demonstrates premature liquefaction of soil specimens at the middle third of CTX specimens where higher induced strains occur, as depicted in Figure 6.6. Thereafter, the liquefaction triggering propagates vertically to vicinity zones. Figures 6.5(c) and 6.6 indicate that the maximum strain and specimen bulge in the triaxial specimen occurred in the middle third of the soil specimen and decrease toward the soil ends. This observation has been comprehensively reported in the literature (Lee 1978; Fu et al. 2007). In their numerical study, Zhang et al. (2011) concluded that the liquefaction initiates in the middle specimen then cascades throughout the soil specimens. It was justified to the faster decrease of the contacts number between soil particles at the middle third comparing to those near boundaries, as previously deduced from (Balla 1960).

Due to the difference in the cyclic behavior and non-uniformity of the induced strains within the CTX specimens comparing to T_xSS specimens, it was observed that the liquefaction potential is

different either under stress- or strain-controlled conditions. Figures 6.7(a) and 6.7(b) demonstrate the liquefaction potential curves (ε/or γ - $N_{liq.}$) of Ottawa and BSP sands, respectively, obtained from CTX and T_xSS cyclic strain-controlled tests. It is noteworthy that the ε/or γ -N_{liq} curves are analogous to the well-known CSR-N_{liq} curves. Indeed, the liquefaction potential obtained from strain-controlled T_xSS tests is higher than that obtained from CTX, Figure 6.7. In other words, simple shear soil specimens liquefied slower than triaxial soil specimens. This is in contrast to cyclic stress-controlled tests (Seed and Idriss 1971; Castro 1975; Ishihara and Li 1972). Under cyclic strain-controlled loading, the soil specimen is subjected to N cycles with constant strain amplitude (shear or axial), which is the key parameter of pore water pressure buildup. In a CTX test, the soil specimen loses most of its stiffness in the first few cycles due to the high generated pore pressure ratio (Dobry and Abdoun 2015), as shown in typical records in Figure 6.2. However, in the T_xSS, the generated pore pressure increases gradually as a function of the applied shear strain. Under stress-controlled tests, the induced strain time history is nonuniform. It consists of N cycles having small amplitudes at earlier cycles and increase gradually by loading sequence. Thus, the generated pore water pressure in the cyclic stress-controlled test is very small at the earlier cycles upon R_u approaches around 0.6 then a dramatic increase occurs. It may be attributed to the loss of particle-particle contacts, the collapse of the honeycomb structure of soil particles, and deterioration of soil stiffness at this stage. This deterioration of soil stiffness and abrupt increase of pore pressure coincide with intersecting the cyclic stress path with the critical stress line. In other words, by achieving the cyclic stress path the instability zone in the modified Mohr-coulomb diagram (p′-q space), an abrupt increase in pore pressure occurs and liquefaction triggers in the following few cycles, as demonstrated in detail by Konstadinou and Georgiannou (2014). However, the comparison between stress and strain-controlled tests is beyond this study and has been discussed elsewhere.

There is a difference in the radial strain confining method in DSS and T_xSS. In DSS, the radial strains are constrained by a reinforced rubber membrane. However, T_xSS soil specimens are enclosed in an unreinforced membrane and hydrostatically confined in a triaxial chamber (constant total stress lateral boundary). A set of cyclic strain-controlled tests was performed in DSS as a geotechnical laboratory element (EMDCSS), to investigate the effect of boundary constrains on the liquefaction potential. For comparison sake, the liquefaction potential curves of Ottawa sand obtained from DSS and that previously obtained from an experimental program in

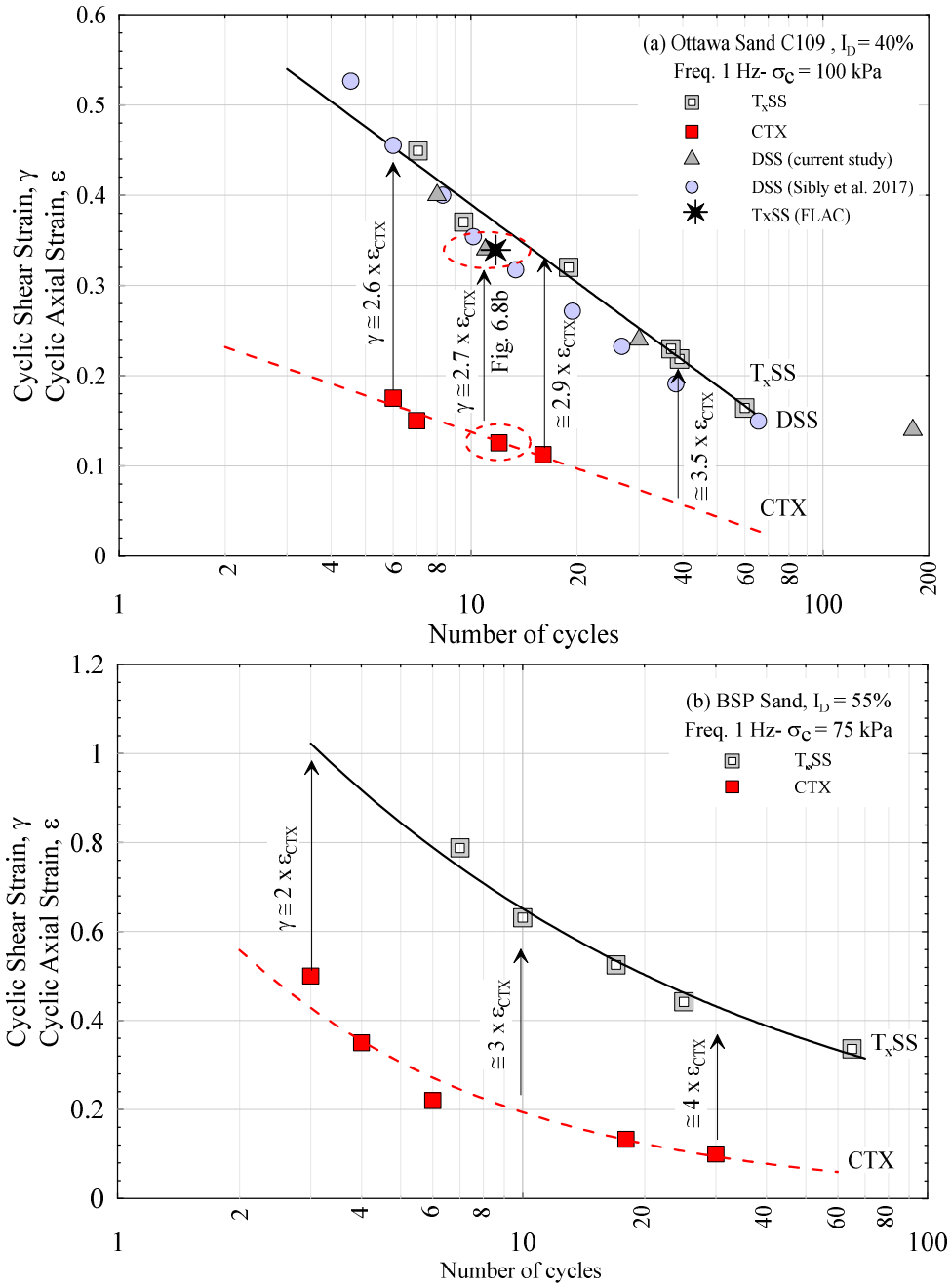

Figure 6.7. Variation of cyclic axial, ε, and shear strain, γ, with number of liquefaction cycles, N_{liq}, of (a) BSP sand (b) Ottawa sand

DSS by Sibley et al. (2017) are superimposed on T_xSS and CTX results in Figure 6.7(a). An excellent agreement between T_xSS and DSS results could be observed despite the difference of the confining element model and deduced that the effective stress-path is identical and independent of the boundary conditions. Zhang and Evans (2018) also investigated the effect of

boundary conditions in cyclic triaxial and simple shear tests using the discrete element model. They deduced that the difference in the lateral boundary confining method has a relatively little effect on the number of liquefaction cycles. In a similar manner, Verma and Wijewickreme (2020) compared the monotonic and cyclic behavior of silty soil under three modes of radial strain confinement configurations (reinforced rubber membrane, reinforced membrane surrounding by very low-friction stacked rings, and unreinforced rubber membrane confined by very low-friction stacked rings). The results were found to be similar under the three modes of radial strain boundary constraints.

The identical resistance of DSS and T_xSS tests could be discussed in the perspective of K_0 evolution during cyclic loading. According to Ishihara and Li (1972), based on a special experimental work conducted in the torsional shear apparatus, an abrupt increase of K_0 value occurs in the case of anisotropically consolidated specimens with constrained radial strains, similar to DSS conditions. The evolution of K_0 coincides with the rapid increase in pore pressure ratio at the first few cycles, then the K_0 value and pore pressure increase smoothly upon liquefaction triggering. This observation has been confirmed by Dabeet et al. (2012) based on the numerical simulation of DSS in PFC^{3D} software. Similarly, Figure 6.8(a) shows a comparison between pore pressure generation curves of DSS and T_xSS tests. As previously discussed, an abrupt increase of pore pressure ratio occurred at the first 2 cycles then increase smoothly until the liquefaction occurrence (i.e., R_u=0.9). The number of liquefaction cycles in DSS and T_xSS is approximately equal. However, the only difference is in the incremental pore pressure buildup at the first 2 cycles; as previously observed by (Zhang and Evans 2018).

It is well established that the equivalent, transformation, factor to correlate between axial and shear strains in cyclic stress-controlled studies at failure (i.e., ε=2.5 %) is 1.5 or 1.73 (Vucetic and Dobry 1988). This transformation factor deduced from the elastic theory wherein $\gamma = (1+\nu)\varepsilon$, where ν is Poisson's ratio and has been chosen as 0.5 for undrained tests. However, it would be seen in Figure 6.7 that the proposed equivalent factors for BSP and Ottawa sands are higher than 1.5 under cyclic strain-controlled tests. For example, Figure 6.8 shows a comparison between the generated pore pressure ratio of Ottawa sand subjected to axial strain, ε=0.125% in CTX and shear strain γ=0.34% in T_xSS and DSS. A similar comparison was performed for BSP sand subjected to ε=0.133% and γ=0.52%. It can be observed that the generated pore pressure curves from CTX and T_xSS (under isotropic state) are identical in contrast to that generated in DSS

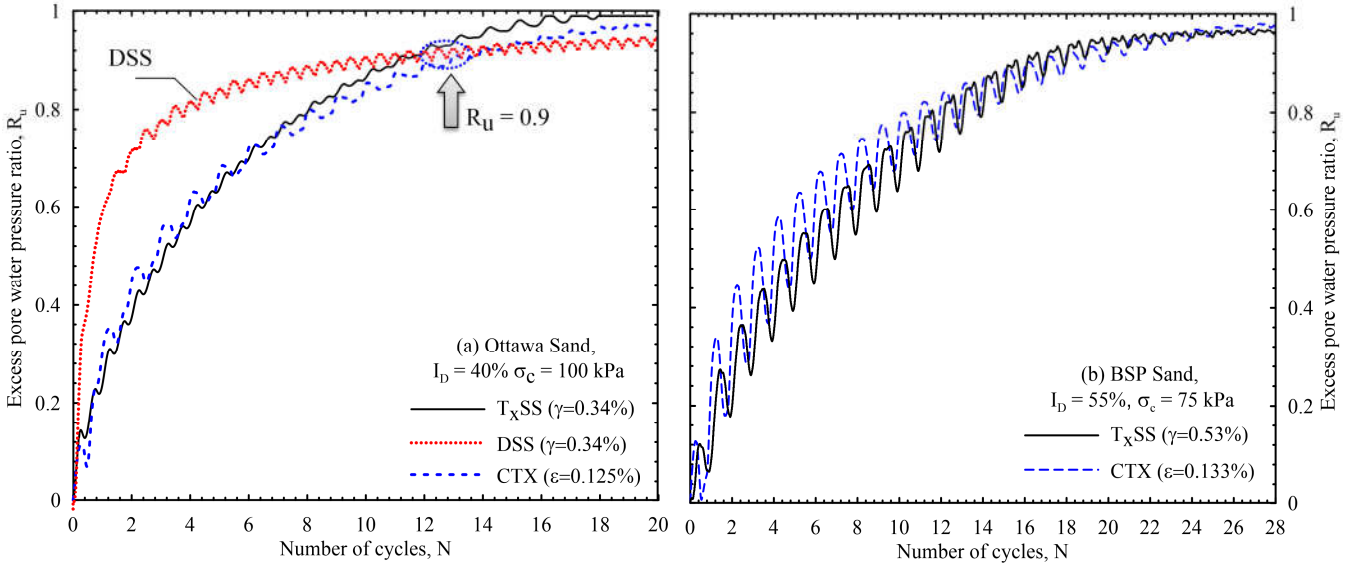

Figure 6.8. Comparison between generated pore pressure in T_xSS, DSS and CTX under strain-controlled loading (a) Ottawa sand and (b) BSP sand

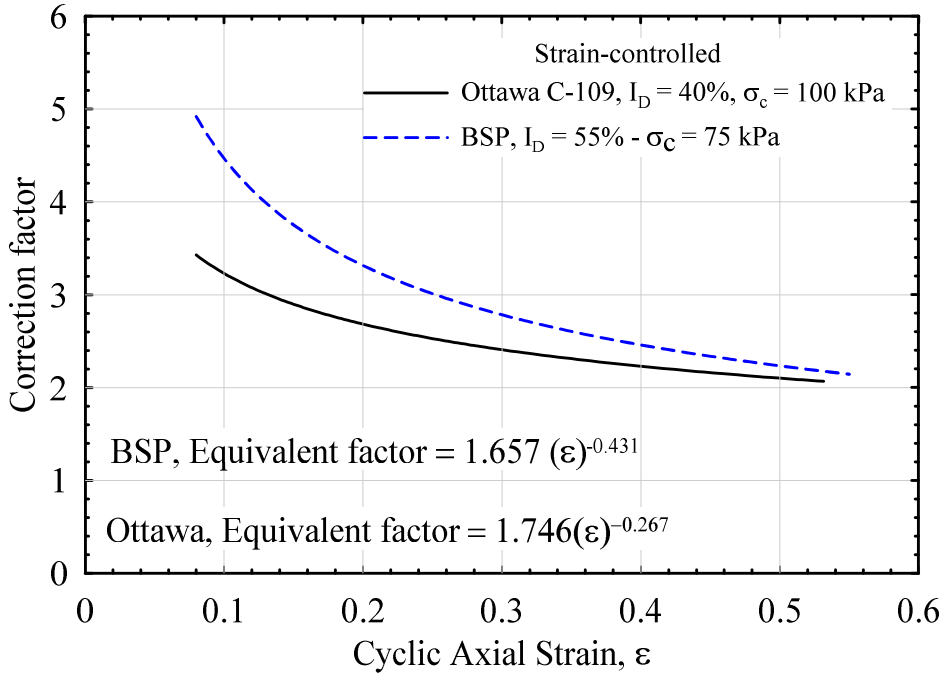

Figure 6.9. The proposed correction factor of cyclic strain-controlled tests

(anisotropic consolidated state). This implies that the trend of pore pressure increase is affected by the initial stress condition. Figures 6.8(a), 6.8(b) infer that the equivalent factor is not a constant value of 1.5, in contrast to that extrapolates from elastic theory ($\gamma=1.5\varepsilon$), and depends on the axial strain and soil type. Zhang and Evans (2018) endorsed the use of deviatoric strain to compare between CTX and DSS results (i.e., $\gamma = (3/\sqrt{2}).\varepsilon$). However, previous correlations between γ and ε are inconsistent with the current results at large shear strain amplitude. However, it increases by increasing the number of cycles (low shear strain) as a function of the applied shear strain amplitude and soil type. It has been reported that the elastic theory is valid for a linear elastic behavior (Rossato and Simonini 1991) or up to shear strain 0.5% (Park and Silver 1975). In contrast, the current results of cyclic strain-controlled tests do not favor the elastic theory inference (i.e. $\gamma= (1+\nu)\varepsilon$). Generally, the equivalent factor decreases with increasing axial strain and may be reached the plateau of 1.5 at relatively large axial strain ($\varepsilon\cong$ 2.5%) which represents the failure (NRC 1985). If the equivalent factors are read out and plotted versus cyclic axial strain in Figure 6.9, power relations could be fitted to correct the induced axial strain in CTX to shear strain for BSP and Ottawa sands, Eq. (6.4):

For BSP:

$$Equivalent\ factor = 1.657(\varepsilon)^{-0.431} \quad (6.4a)$$

For Ottawa sand:

$$Equivalent\ factor = 1.746(\varepsilon)^{-0.267} \quad (6.4b)$$

It is noteworthy that these equations have been deduced from the performed axial strain range.

As a practical application of the proposed correlation, Eq. (6.4) was used to correlate the induced axial strain time histories from cyclic stress-controlled triaxial tests to equivalent shear strain cycles, as shown in Figure 6.10. Then, the estimated equivalent shear strain was incorporated to compute the accumulated damage, or notional $R_{u\text{-}est}$, by adopting the Richart and Newmark (1948) damage hypothesis.

The damage concept was initially introduced by Palmgren (1924) and further developed by Miner (1945) to estimate the fatigue damage of metal subjected to cyclic loading. Later, Richart and Newmark (1948) considered the limitation of Palmgren and Miner damage hypothesis (P-M) by considering the loading sequence in irregular cyclic loading in their hypothesis (R-N). The

authors validated the use of the R-N hypothesis for estimating the generated pore water pressure under uniform, non-uniform and irregular cyclic strain-controlled tests (Khashila et al. 2018). According to the R-N hypothesis, the cumulative damage, D, of an irregular time history consists of m cycles with different stress or strain amplitude S_1, S_2, S_m, can be estimated after each sequent half-cycle by:

$$D_1 = \left(\frac{n_1}{N_1} \right)^{r_1} \tag{6.5a}$$

$$D_2 = \left[\left(D_1 \right)^{\frac{1}{r_2}} + \left(\frac{n_2}{N_2} \right) \right]^{r_2} \tag{6.5b}$$

$$D_m = \left[\left(D_{m-1} \right)^{\frac{1}{r_m}} + \left(\frac{n_m}{N_m} \right) \right]^{r_m} \tag{6.5c}$$

where, D_1, D_2, D_m are the cumulative damages induced after n_1, n_2, n_m cycles having amplitudes of S_1, S_2, S_m, respectively; N_1, N_2, N_m are number of liquefaction uniform cycles having amplitude S_1, S_2, S_m; r_1, r_2, r_m are the material parameters corresponding to amplitude S_1, S_2, S_m, respectively.

The measured, $R_{u\text{-}exp.}$ and the accumulated damage (notional $R_{u\text{-}est}$) of cyclic stress-controlled triaxial tests performed on Ottawa sand and BSP are compared and plotted in Figures 10(a) and 10(b), respectively. Figure 6.10 shows the measured pore pressure is in accordance with the notional $R_{u\text{-}est}$ over the performed shear strain range in T_xSS tests. This agreement infers the accuracy of the proposed equivalent factor relations that obtained from the comparison between CTX and T_xSS strain-controlled tests. Thus, this correlation can be used to predict the generated pore pressure in triaxial tests using simple shear-pore pressure models.

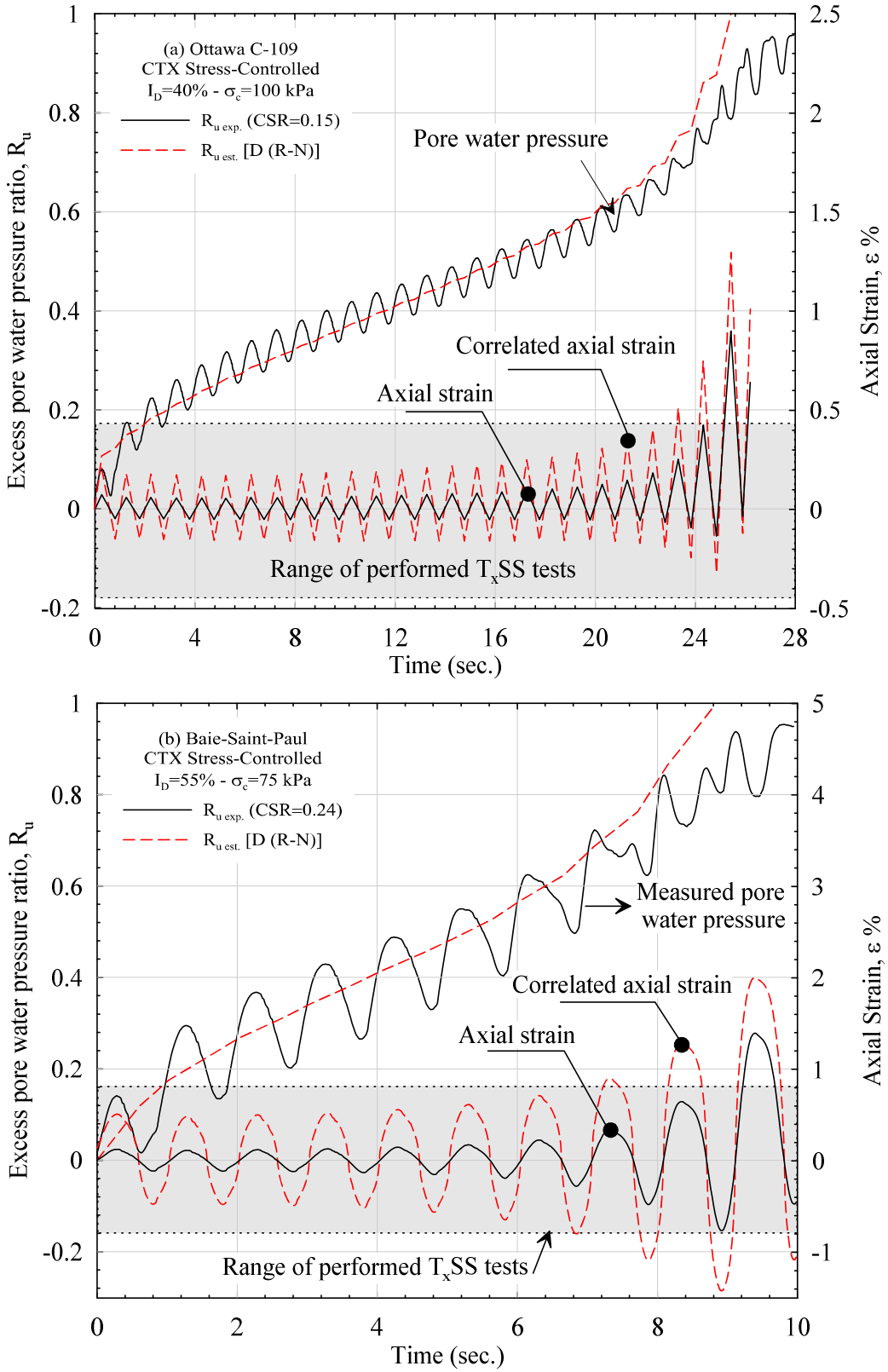

Figure 6.10. Comparison between the generated and estimated pore water pressure as well as the induced and corrected axial strain in (a) BSP and (b) Ottawa sand specimen

CHAPTER 7

ASSESSMENT OF COMPATIBILITY OF LIQUEFACTION CHARTS FOR EASTERN REGIONS OF CANADA ACCORDING TO NATIONAL BUILDING CODE (NBCC) PROVISION

Authors and Affiliation:

Marwan Khashila: PhD Candidate, Sherbrooke University, Faculty of Engineering, Sherbrooke, QC.

Mourad Karray: Professor, Sherbrooke University, Faculty of Engineering, Sherbrooke, QC.

Mahmoud N. Hussien: Associated Professor, Assiut University, Assiut, Egypt.

Researcher, Sherbrooke University, Faculty of Engineering, Sherbrooke, QC.

Mohamed Chekired: Researcher, Institut de Recherche d'Hydro-Québec, Varennes, Québec, Canada.

Date of submission: August 2019

State of submission: under review

Journal: Canadian Geotechnical Journal

French title: ÉVALUATION DE LA COMPATIBILITÉ DES CHARTES DE LIQUÉFACTION POUR LES RÉGIONS DE L'EST DU CANADA SELON LES DISPOSITIONS DU CODE NATIONAL DU BÂTIMENT (CCNB)

Contribution in the thesis:

The proposed energy-based model is incorporated in one-dimensional (1-D) soil deposit analysis to investigate the compatibility of the current design liquefaction charts for eastern regions. In order to evaluate the applicability of the proposed model in 1-D analysis, a previous dynamic centrifuge test by others is simulated using the proposed model and the well-established Finn model. Further, earthquake ground motions compatible and incompatible with eastern North America seismicity are applied on the base of hypothetical deposits having different fundamental periods to investigate the difference in the seismic response of eastern and western North America. The difference is discussed in terms of generated pore pressure, R_u, and the equivalent number of uniform stress cycles, N_{eq}.

Abstract: Due to the lack of the documented historical seismic records in eastern North America (ENA), the established liquefaction charts from western North America (WNA) and other shallow crustal active tectonic regimes (e.g. Japan and China) are employed in the liquefaction assessment in ENA neglecting the disparity in geological and earthquake characteristics. Therefore, the efficacy of applying these liquefaction charts in ENA is discussed based on numerical and experimental results. A suite of cyclic stress and strain-controlled tests were performed using the direct simple shear and the combined triaxial simple shear apparatuses to acquire the liquefaction potential and propose an energy-based pore pressure model. The proposed model was validated in element-level to simulate cyclic T_xSS tests using $FLAC^{2D}$ software. The Finn model and a dynamic centrifuge model were used to further validate the proposed model based on one-dimensional ground response analysis. Afterward, one-dimensional ground response analyses were conducted on hypothetical soil deposits using compatible and incompatible earthquake motions with the eastern seismicity. The seismic responses of a real incompatible earthquake in terms of R_u and N_{eq} are in complete accordance with the liquefaction charts. However, the current comparison highlights the uncertainty of applying the available liquefaction charts in Eastern regions.

Keywords**:** Liquefaction; *Pore water pressure*; *Energy concept; Equivalent Number concept*; *T_xSS; DSS.*

Résumé: En raison du manque de cas historiques dans la region l'Est de l'Amérique du Nord (EAN), les chartes de liquéfaction établies dans l'ouest de l'Amérique du Nord (OAN) et d'autres régions tectoniques actifs peu profonds (p. ex. Japon et Chine) sont utilisées dans l'évaluation de la liquéfaction de l'EAN, négligeant ainsi les différences des caractéristiques géologiques souterraines et sismiques. Par conséquent, l'efficacité de l'application de ces chartes de liquéfaction dans l'EAN est examinée en fonction des résultats numériques et expérimentaux. Une série d'essais cycliques à contrainte et déformation contrôlées ont été effectués à l'aide du l'appareil de cisaillement simple direct et de l'appareil combiné de cisaillement simple triaxial pour obtenir le potentiel de liquéfaction et proposer un modèle de pression interstitielle basé sur l'énergie. Le modèle proposé a été validé au niveau des éléments pour simuler des essais cycliques de TxSS à l'aide du logiciel FLAC-2D. Le modèle Finn et un modèle dynamique de centrifugeuse ont été utilisés pour valider davantage le modèle proposé afin de représenter une

analyse unidimensionnelle de la réponse au sol. Par la suite, des analyses unidimensionnelles de réponse au sol ont été effectuées sur des dépôts hypothétiques de sol à l'aide de mouvements sismiques compatibles et réellement incompatibles avec la sismicité de l'Est. Les réponses sismiques des séismes réels incompatibles en termes de R_u et de N_{eq} sont tout à fait en accord avec les chartes de liquéfaction. Toutefois, la comparaison actuelle met en lumière l'incertitude entourant l'application des chartes de liquéfaction disponibles dans les régions de l'Est.

Mots-clés : liquéfaction; taux de pression de l'eau des pores; Triaxial cyclique; appareil de cisaillement simple triaxial; DSS; essai contrainte contrôlé; essai de déformation contrôlée.

7.1 Introduction

Seismically induced pore water pressure in saturated cohesionless soil results from the tendency of the loose soil to contract under seismic loading. The increase of pore pressure is associated with a decrease in effective stress and decaying of soil stiffness and, eventually, liquefaction occurs. This phenomenon can be devastating to civil infrastructures. Over more than 50 years, numerous researchers have worked to understand more deeply the liquefaction phenomenon and how to evaluate liquefaction potential. To date, after intensive field, experimental and theoretical investigations, a variety of methods have been developed for evaluating the liquefaction potential under earthquake excitation.

The most widely used procedure among geotechnical engineers was initially developed in the 1960s by H.B. Seed and his colleague in California termed "the simplified stress-based method" based on a compilation of earthquake data from California, Japan, and New Zealand (Seed and Idriss 1971). This method has undergone updates based on evolution in understanding of liquefaction phenomenon and of the seismic behavior of soil based on previous earthquakes as well as experimentally and/or field data (e.g., standard penetration tests (SPT), cone penetration test (CPT), and shear wave velocity (Vs)) (e.g. Seed and Idriss 1982; Youd et al. 2001; Cetin et al. 2004; and Idriss and Boulanger 2008).

The simplified method aims at computing the factor of safety by comparing the induced cyclic stress ratio (CSR) during seismic loading (demand) and the cyclic resistance ratio (CRR) (capacity) of soil, where CRR could be defined experimentally (e.g. cyclic triaxial, direct simple

shear and torsion shear tests) or in situ by quantitative assessment by SPT (Idriss and Boulanger 2008), CPT (Boulanger and Idriss 2014) or V_s (Andrus and Stokoe 2000; Shelley et al. 2015).

Based on Newton's Second Law, Seed and Idriss (1971) proposed the following formula to compute the CSR at a respective depth in the soil deposit:

$$CSR = \left(\tau_{av} / \sigma'_{v0}\right) = 0.65\left(a_{\max} / g\right)\left(\sigma_{v0} / \sigma'_{v0}\right) r_d \quad (7.1)$$

where τ_{av} is the average cyclic shear stress; a_{max} is the peak horizontal acceleration at the ground surface; g is the acceleration of gravity; σ_{v0} and σ'_{v0} are the initial total and effective vertical stress; r_d is the stress reduction factor. The two questionable parameters in Eq. (7.1) are the value of r_d and defining of a_{max} for ground motion.

The profiles of depth reduction factor, r_d, could be established based on statistical analyses of one-dimensional dynamic response analysis that accounts for the non-rigid response of the soil profile. The r_d value is a function of ground motion characteristics (magnitude and the frequency content) and dynamic characteristics of the soil profile. Many investigators suggested formulation to calculate r_d values (e.g. Liao and Whitman 1986; Robertson and Wride 1998; Idriss 1999; Cetin et al. 2004; Idriss and Boulanger 2008). Most recently, driven from Cetin (2000) work, Lasley et al. (2016) performed a large number of equivalent linear site response analyses subjected to different ground motions. Using robustness statistical and regression analysis of response' results, Lasley et al. (2016) introduced a modified r_d relationship (Eq. 7.2) having the least bias comparing to other preceding models.

$$r_d = (1 - \alpha)\exp(-z / \beta) + \alpha \quad (7.2.a)$$

$$\alpha = \exp(-4.373 + 0.4491.Mw) \quad (7.2.b)$$

$$\beta = -20.11 + 6.247.Mw \quad (7.2.c)$$

where α is limiting value of r_d and can be ranged from 0 to 1; β is a curvature coefficient at shallow depths; z is depth in meters.

Another key parameter related to the application of the simplified method is the definition of a_{max} value. For practical use, Youd et al. (2001) recommended using the geometric mean of the two maximum horizontal accelerations (when there is available data). Boulanger and Idriss (2014) reported the difference between geometric mean and a_{max} of horizontal motions is often about 10% for a level ground surface that may have a relatively small effect on liquefaction analysis.

Also, using the geometric mean alleviates the uncertainty of estimating a_{max} particularly for geotechnical structures that have weak/strong directions. In the liquefaction studies, the a_{max} of a vertical component is usually neglected because its value is small relative to gravity.

The simplified method was followed by an equivalent number of uniform cycles concept in the early of the 1970s by H.B. Seed and his colleagues to facilitate the liquefaction potential calculations. This concept aimed at converting an irregular ground motion to equivalent damage uniform cycles having amplitude equals 0.65 times of the maximum experienced ground motion amplitude (Seed et al. 1975; Annaki and Lee 1977).

Although the simplified method is the most used liquefaction assessment method, it has some questionable issues that must be specified first before using it in the current study. Green et al. (2019) highlighted some of its shortcomings, particularly for computing the number of equivalent cycles (N_{eq}), and MSF as; the assumption of constant N_{eq} and MSF with depth is not reliable, the uncertainty in neglecting of pulses have an amplitude less than $0.3.a_{max}$, the doubt of separate treatment of each of the two horizontal earthquake motion, and neglect the effect of duration of ground motions on MSF. Filali and Sbartai (2017) observed uncertainty in the simplified method as compared with nonlinear response analysis for four different sites (three in the USA and one in Algeria). It was observed that at a_{max} of 0.3, the simplified method gives adequate results like the dynamic analysis. However, beyond this value, it should be correlated.

In addition to the uncertainty in the specification of its components, another issue is highlighted when applying this procedure in eastern North America (ENA). It is well known that there is a difference in the earthquake characteristics (frequency content and duration of motion) and the geological crust between east and western North America. It is well known that the crust in ENA is more intact. Thus, the attenuation of earthquake energy in the ENA crust is very low with the distance from the source as compared to WNA (Adams and Halchuck 2004; Atkinson 1989; Campbell 2013; Humar 2015; Graizer 2016). For a given earthquake magnitude, the ENA ground motion can affect distance 3 to 6 times further than in the WNA (Jacob 1991). Kramer (1996) reported due to the harder bedrock in ENA than WNA, a higher amplification could occur in the east, i.e. peak ground acceleration (PGA) is higher in ENA than in the WNA, and the applicability of western design criteria in eastern regions is questionable. In the term of motion characteristics, the ENA ground motions are featured by high-frequency content (rich in short-

period motions) wherein Western (WNA) motions characterize with low-frequency content at a given magnitude and source to site distance (i.e., Rathje et al. 1998; Rathje et al. 2004).

In contrary, Youd et al. (2001) indicated the difference between ENA and WNA is relatively small postulating that to the quick attenuation of high-frequency motions throughout soft and loose soil deposit because of filtering of high-frequency energy during the vertical propagation of shear waves. Moreover, Youd et al. 2001 reported that the difference between a_{max} in ENA and WNA could be alleviated by computing PGA using the recommended procedure in the 1996 National Center for Earthquake Engineering Research (NCEER) workshop (Youd et al. 2001). This procedure considered the type of faulting, site condition, and location.

Therefore, this study aims at analysis and demonstrates the difference of dynamic site response between two earthquake motions; one synthetic earthquake compatible with eastern Canada spectra (NBCC 2005/2015) (Atkinson 2009); and another incompatible real earthquake from western North America (Northridge earthquake). The former one is referred here as synthetic. This is accomplished by analysis the dynamic response of 1-D base shaking obtained from a $FLAC^{2D}$ coupled energy-based pore water pressure model. The used energy-based model was calibrated based on T_xSS results. It should be noted that the energy-based model was adopted by the authors to simulate the dynamic response under cyclic triaxial and new combined triaxial simple shear tests "T_xSS" (Khashila et al. 2020). Moreover, through the current study, the proposed model will be compared first with the dynamic response of a 2-D laminar container centrifuge model to study the liquefaction potential of a level site (Ramirez et al. 2017).

This paper consists of a brief review of the used devices and the experimental work that was done to introduce a coupled energy-based pore pressure model, followed by a description of the adopted numerical model. The predictive capability of the proposed model to acquire the liquefaction resistance comparing to DSS is discussed in the term of liquefaction potential curve. Subsequently, the validation of the proposed model in the element-level and comparing it with a previous centrifuge model is represented. After that, a comparison between the cyclic response of sand deposit having different natural periods (different thickness and different relative densities) are discussed.

7.2 Experimental work

7.2.1 Testing equipment

It has long been recognized that the direct simple shear apparatus is the most practical element used to mimic the cyclic condition during earthquake excitation better than the triaxial test. During the past seven decades, variant versions have been triggered aiming at better replicating field conditions (Kjellman 1951, Bjerrum and Landva 1966). Subsequently, other forms have been developed with other features to overcome the shortcoming of earlier versions. Recently, the combined triaxial simple shear "T_xSS" device was evolved to compile triaxial and simple shear features in the same apparatus (Karray et al. 2015; Karray and Chekired 2019). In the current study, the commercial direct simple shear apparatus (DSS) is used in conjunction with the new combined triaxial simple shear apparatus (T_xSS).

7.2.2 The conventional direct simple shear Apparatus (DSS)

The conventional direct simple shear apparatus, commercially provided by GDS Company, was used in the current study to perform drained constant-volume cyclic tests. In DSS, typically, the soil specimen is laterally confined by a wire-reinforced membrane. During cyclic loading, the vertical load is changed to maintain the height constant. Alternative to a truly undrained condition, the changing of the vertical stress is equivalent to the generated pore water pressure in an equivalent undrained condition (Dyvik et al. 1987). A series of cyclic stress-controlled tests were performed to acquire the cyclic resistance ratio (CRR) of reconstituted soil specimens.

7.2.3 The combined Triaxial Simple Shear Apparatus (T_xSS)

A series of undrained cyclic shear tests were performed using the T_xSS device. T_xSS is a modified version of direct simple shear apparatus, as shown in Figure 7.1. It combines the features of triaxial and DSS devices. Using T_xSS, the soil specimen can be saturated and isotropically or anisotropically consolidated in a triaxial chamber. Drained and undrained monotonic or cyclic load can be applied on soil specimen hydrostatically confined in the triaxial chamber or confined by using annular metal rings, to allow K_0 condition, like the conventional DSS. The T_xSS apparatus allows measurement of the excess pore water pressure during an undrained test using an electric piezometer. Two porous stones are embedded in the upper and

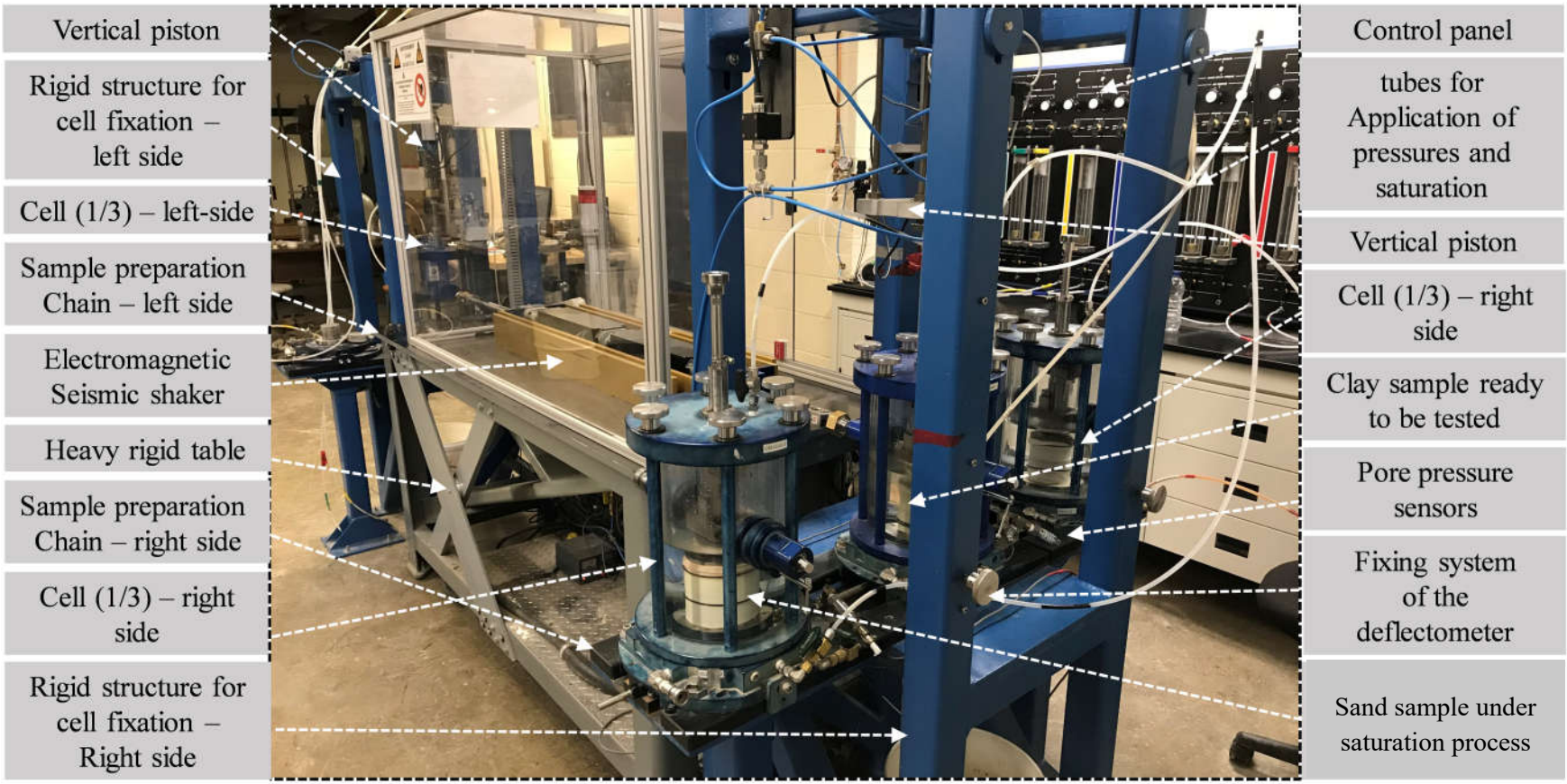

Figure 7.1. The combined triaxial simple shear (T_xSS) apparataus

lower platens to allow applying back pressure during the saturation phase as well as drainage during consolidation.

7.2.4 Specimen preparation and testing conditions

To study the cyclic behavior, reconstituted soil specimens of Ottawa sand F65 were prepared in 80-mm diameters (d) and 25~26 mm height (h) (d/h = 3.2 (ASTM D6528-17)). The Ottawa sand has a specific gravity of 2.67 and the mean diameter, D_{50} of 0.217. The maximum and minimum void ratios are 0.82 and 0.53, respectively. The grain-size distribution curve of the used sand is shown in Figure 7.2.

The moist tamping procedure was used to prepare reconstituted soil specimens in T_xSS cell as it provides an isotropic soil structure (Yang et al. 2008). The pre-weighted moist sand was placed on three layers and tamped gently to achieve the targeted relative density (I_D = 40 and 90%). Each layer's surface was scarified before placing the next layer. The saturation process was accelerated by percolated CO_2 gas followed by circulating de-aired water at a low back pressure. The saturation process was achieved when Skempton's pore pressure parameter B ($\Delta u/\Delta\sigma_3$) had been greater than 0.96. After the saturation phase, the cell pressure was increased to 300 kPa and back pressure was maintained at 200 kPa (to apply 100 kPa effective stress) to consolidate the sand specimen isotropically. After completing the consolidated process, soil specimens were sheared under undrained cyclic strain-controlled loading until initial liquefaction occurred. The triggering of initial liquefaction is defined as the excess pore pressure ratio ($R_u = \Delta u/\Delta\sigma_c$, Δu = excess pore water pressure) attained 0.9 (Khashila et al. 2018).

A series of cyclic drained constant volume stress-controlled tests (DSS) and undrained strain-controlled tests (T_xSS) were performed by applying a sweep sine wave with a frequency of 1 Hz to soil specimen. The induced shear load/strain, pore/equivalent pore water pressure, and vertical displacement were recorded using a high accuracy pressure gauge and displacement transducers. The typical records of a cyclic T_xSS test are shown in Figure 7.3. It may be seen from this figure that, by loading sequence, the magnitude of the generated pore pressure increases were accompanied by vertical displacement as well as decaying of cyclic stress ratio (CSR= τ/σ'_c). It may be seen that the area bounded by the hysteresis loop decreases by loading sequence, which represents the dissipated energy per unit volume of soil. This is due to the decrease of soil

resistance because of collapsing of the intergranular contacts by loading cycles and pore pressure generation.

7.3 Liquefaction potential and energy-based pore water pressure model

The most important parameter in the liquefaction study is the generated pore pressure. Significant efforts have been devoted to simulate the pore pressure generation during earthquake excitation based on cyclic stress or strain-controlled tests as a function of number of loading cycles (e.g. Seed et al. 1975; Khashila et al. 2018) or damage parameter (e.g. Porcino et al. 2018; Park et al. 2015). In this respect, Chiaradonna et al. (2016) adapted a damage-based pore pressure model in one-dimensional soil response analysis. Following to the pioneering work introduced by Nemat-Nasser and Shokooh (1979) to mathematically link between the densification of soil in a drained test (infer to the excess pore pressure under undrained condition) to the dissipated energy during cyclic loading, different energy-based pore pressure models have been integrated into dynamic analysis (e.g. Green et al. 2000; Polito et al. 2008; Karray et al. 2015; Abdellaziz et al. 2020).

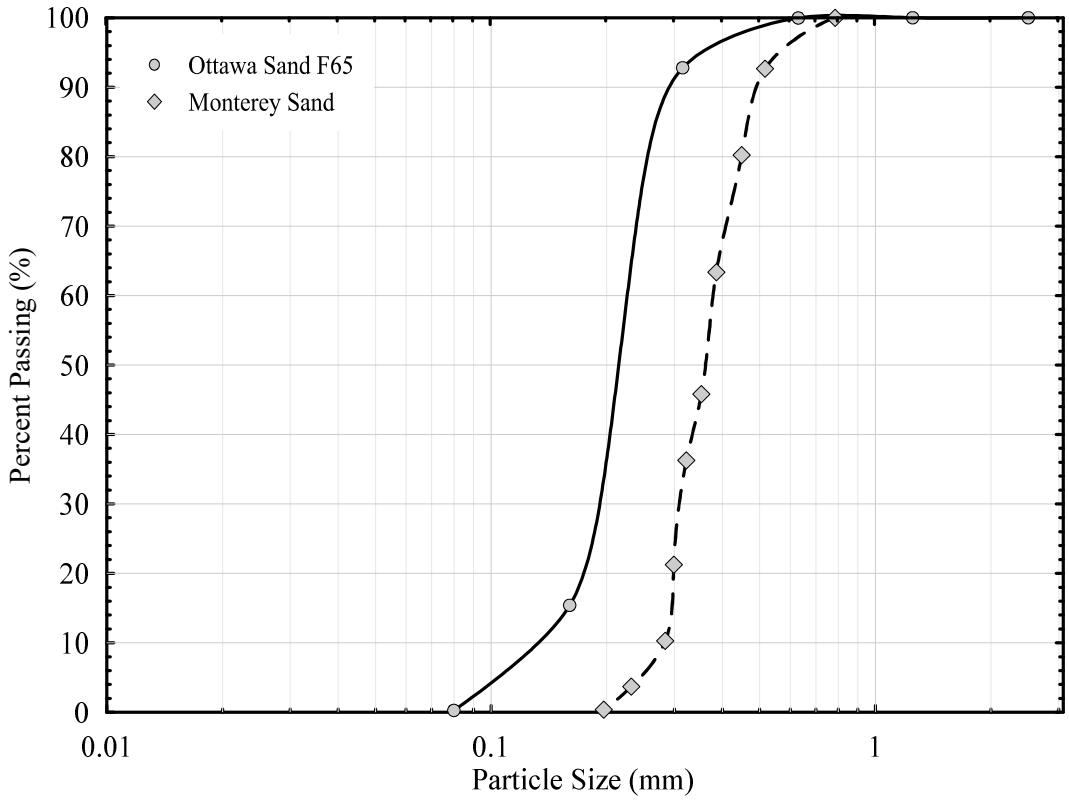

Figure 7.2. Grain size distribution of the used sands

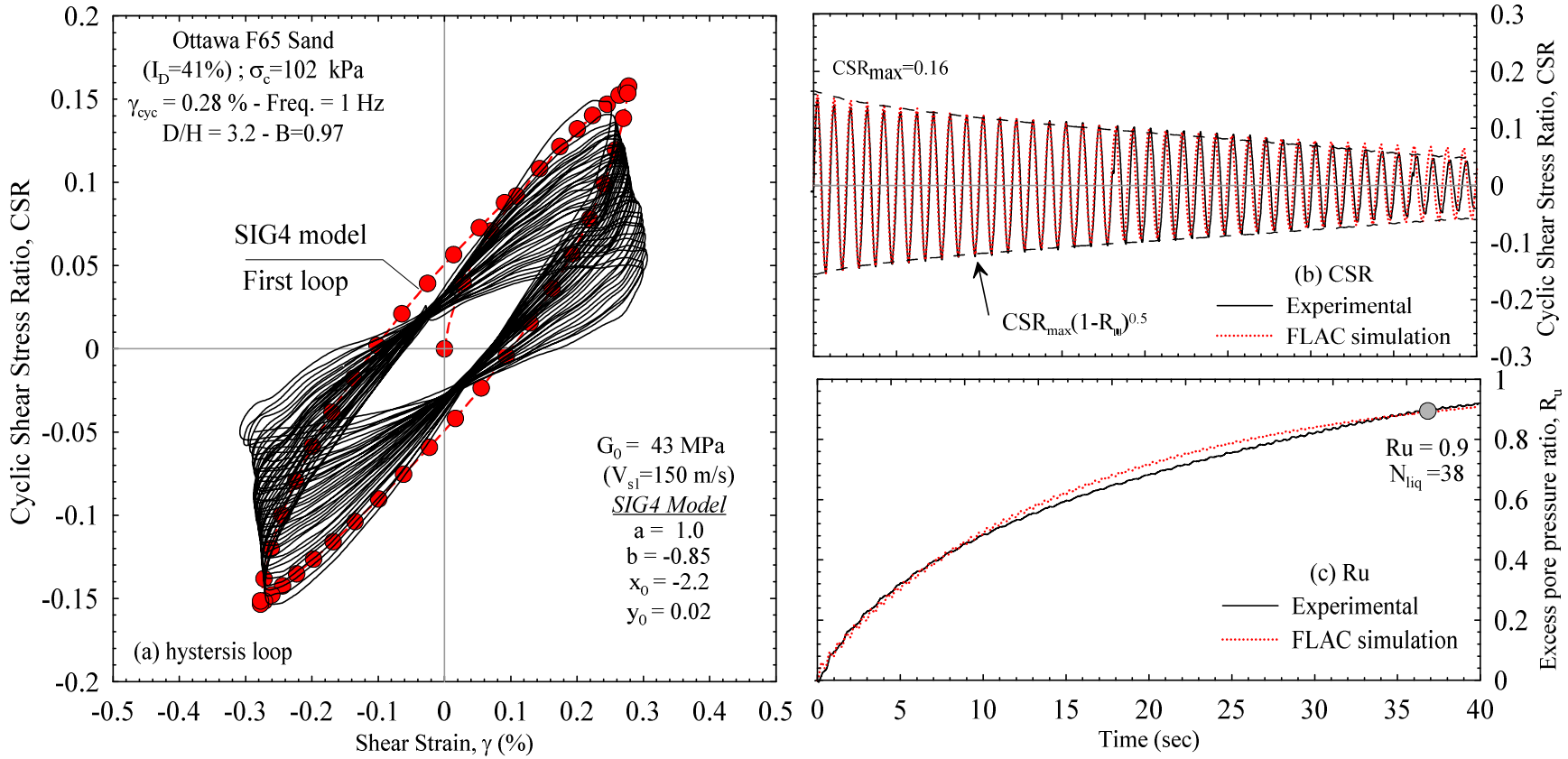

Figure 7.3. Typical results of TxSS test and numerical model in terms of (a) Hysteresis loops (CSR-γ_{cyc}), (b) decaying of CSR time history, (c) R_u time history

Energy-based pore pressure models are characterized by calibration parameters (it is often two parameters). Because of its implicit capability to consider earthquake characteristics and circumventing the need for converting a ground motion to an equivalent number of uniform cycles, the energy concept has become the most appropriate and used concept for seismic and liquefaction investigation (e.g. Davis and Berrill 1982). As much more, the energy concept was implemented in computing equivalent uniform stress cycles of irregular ground motion (Greenand and Terri 2005) as well as in computing magnitude scaling factor (e.g. Arango 1994; Arango 1996; Green 2001).

Based on a series of cyclic strain-controlled tests performed on Ottawa sand F-65, a unique polynomial relationship between the generated pore pressure, R_u, and normalized dissipated energy per unit volume of soil, W_s, was introduced as shown in Figure 7.4, with a relation given as:

For loose Sand

$$R_u = 0.11453\left(\frac{W_s}{a}\right) + 1.6739\left(\frac{W_s}{a}\right)^2 - 0.867\left(\frac{W_s}{a}\right)^3 - 0.0367\left(\frac{W_s}{a}\right)^4 \quad (7.3.a)$$

For dense Sand

$$R_u = 1.1605\left(\frac{W_s}{b}\right) - 0.0257\left(\frac{W_s}{b}\right)^2 - 0.3918\left(\frac{W_s}{b}\right)^3 + 0.1319\left(\frac{W_s}{b}\right)^4 \quad (7.3.b)$$

where a and b are curve-fitting parameters for loose and dense sand, respectively, that depend on soil type and relative density. Figure 7.4(c) emphasizes a negative correlation between fitting parameters, a and b, as a function of shear strain amplitude and can be formed as:

$$a = 0.72\,\gamma^{-0.312} \qquad 0.6 \le a \le 1.6 \quad (7.3.c)$$

$$b = 1.485\gamma^{-0.592} \qquad 1.4 \le b \le 6 \quad (7.3.d)$$

The normalized dissipated energy, W_s, is indicated by integrating the area bounded by hysteresis loops (CSR-shear strain relation). Under direct simple shear test, W_s can be indicated by the trapezoidal rule as follows:

$$W_s = \frac{1}{2\sigma'_{mo}} \sum_{i=1}^{n-1} (\tau_{i+1} + \tau_i)(\gamma_{i+1} - \gamma_i) \quad (7.4)$$

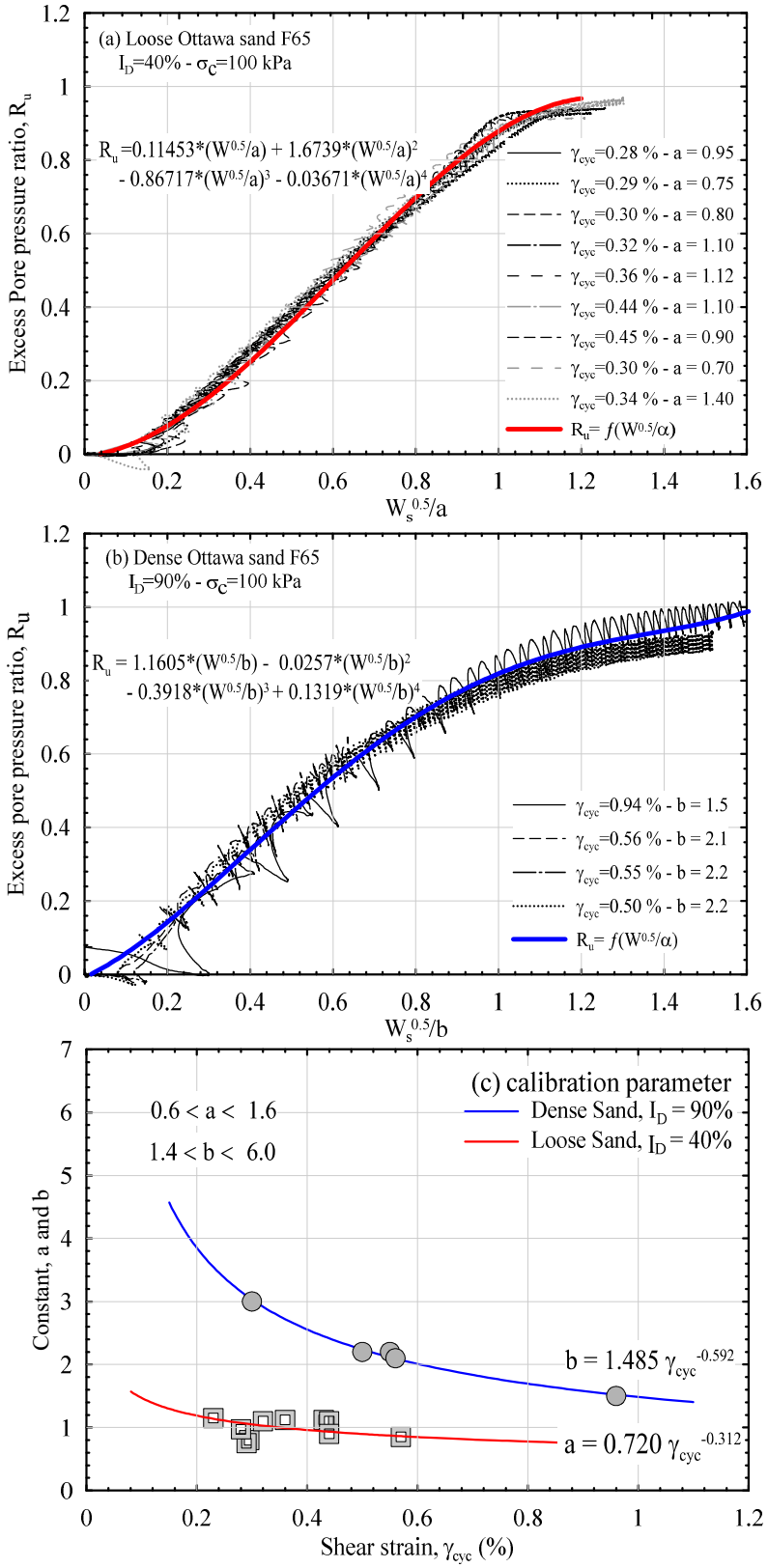

Figure 7.4. Dissipated energy-pore pressure relations (a) for loose sand; (b) for dense sand; (c) the variation of the fitting parameters

7.3.1 Numerical model in comparing with the experimental element-level results

In seismic engineering, it has been used to adopt the equivalent-linear approach developed by Seed and Idriss (1969) to investigate the one-dimensional (1-D) response of a sand deposit. In this approach, soil behavior is modeled by adjusting soil properties, G/G_{max} and damping ratio, iteratively based on the computed strain value in the previous iteration. This procedure was numerically adopted in a software program SHAKE (Schnabel 1972). In this paper, the fast Lagrangian analysis of continua (FLAC) numerical platform was employed to investigate the seismic response of soil deposit by adopting the equivalent-linear procedure and by taking into account the effect of generated pore pressure during earthquake excitation. FLAC is an explicit finite difference program that contains built-in constitutive models in addition to allowing user-defined constitutive models using the FISH language to capture soil behavior in response to different load conditions and boundary restraints.

The first phase of validation of the proposed model was performed in the element-level (T_xSS) and further on a large scale by simulating the seismic response of a level layered soil in a centrifuge model. To simulate the cyclic response under the T_xSS condition, an assembly of sub-grid zones was compiled to form the cylindrical shape of the soil specimen in T_xSS. In terms of soil properties, initial shear and bulk modulus were computed based on shear wave velocity and defined at the first phase of the numerical code. It is noteworthy that the shear wave velocities incorporated in the current model were determined precisely by the P-rate technique developed at the Université de Sherbrooke laboratory (Gamal El-Dean 2007; Éthier et al. 2011; Karray and Wali 2013; Karray et al. 2015). Unlike Dobry et al. (1982) procedure, during cyclic load consequence, stress-strain softening is typically counted by adjusting the low-strain shear modulus of each subzone each time step, in conjunction with the evolution of R_u according to Eq. (7.5) (Matasovic and Vucetic 1993; Dobry et al. 2018).

$$G = G_{\max .} \left(1 - R_u\right)^{0.5} \tag{7.5}$$

The incorporated SIG4 model in FLAC was adopted to represent the change of secant shear modulus and damping ratio during the evolution of shear strain. The SIG4 parameters were calibrated from the T_xSS results and summarized in Table 7.1. Figure 7.3 shows a comparison between cyclic responses numerically computed and experimentally measured. A reasonably good agreement between computed and measured T_xSS cyclic response is observed which

Table 7.1. SIG4 model parameters of Ottawa sand F65

Ottawa F65	a	b	x_0	y_0
I_D 40%	1.0	-0.8	-2.25	0.02
I_D 90%	1.05	-0.75	-2.6	0.15

reflects the predictive capability of the energy concept to capture the nonlinear behavior of soil under cyclic loading.

7.3.2 Comparing the liquefaction potential curves from DSS and TxSS

The ability of the proposed model in conjunction with the T_xSS device to capture the cyclic stress-based resistance of sand specimens is discussed in this section. Alternative stress-controlled tests were performed in the T_xSS device. At first, a cyclic stress-controlled test was simulated numerically and the nonuniform shear strain response was recorded. Thereafter, the numerically computed shear strain was, experimentally, applied in T_xSS to perform uniform shear stress cycles. For example, the results of this test are shown in Figure 7.5. As anticipated, Figure 7.5 shows the rate of pore pressure generation is higher at the beginning of cyclic loading then slows down till the stress path crosses the phase transformation line (Ishibashi et al. 1985). Finally, an abrupt increase occurred.

A comparison between the liquefaction potential curves for loose and dense sand obtained from DSS and T_xSS is shown in Figure 7.6. The liquefaction potential curves of the same sand deduced from the DSS device performed by Bastidas (2016) are superposed in Figure 7.6. There is a fairly good agreement between numerically computed and experimentally (T_xSS and DSS) as well as alternative stress-controlled resistance in the range from moderate to high cycles (approximately higher than 4 cycles). It is widely acknowledged that the spatial interesting range for geotechnical engineers is from 6 to 26 cycles (Seed and Idriss 1982). This is the range of the equivalent number of uniform stress cycles for the destructive earthquakes having magnitudes ranging from M 6 to M 8.5 (Seed and Idriss 1982). [Note: The cyclic resistance ratio has been determined at N=15 cycles which represent a reference magnitude of 7.5]. It is quite persuasive to attribute the variation of liquefaction resistance at the lower number of cycles to the alteration of the initial stress condition in T_xSS and DSS. It is well known that in DSS soil specimen is consolidated anisotropically under K_0 conditions where radial strains are constrained by reinforced rubber membrane or annular ring. However, after initial loading cycles, K_0 value

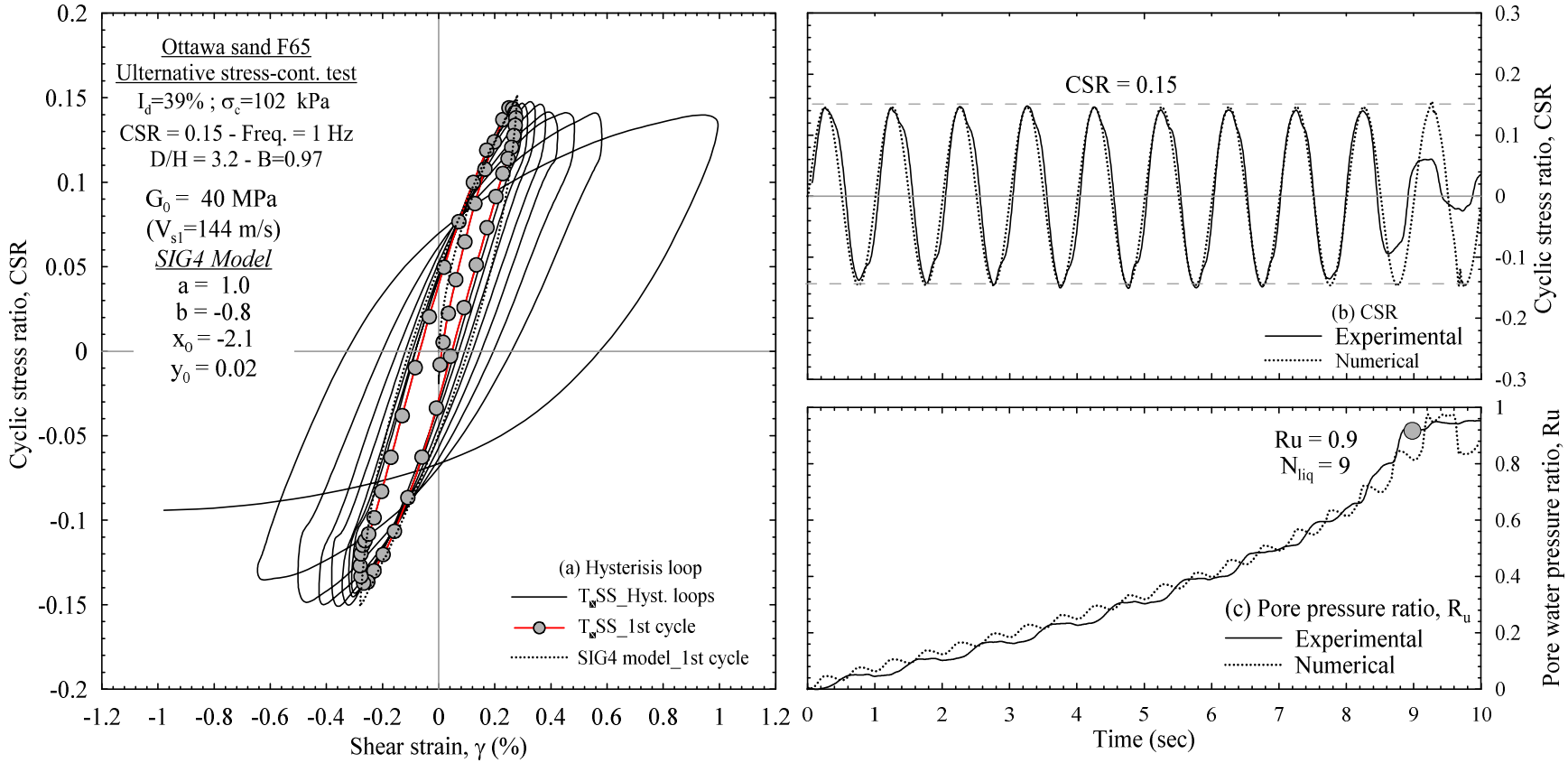

Figure 7.5. Typical records of an alternative stress-controlled test

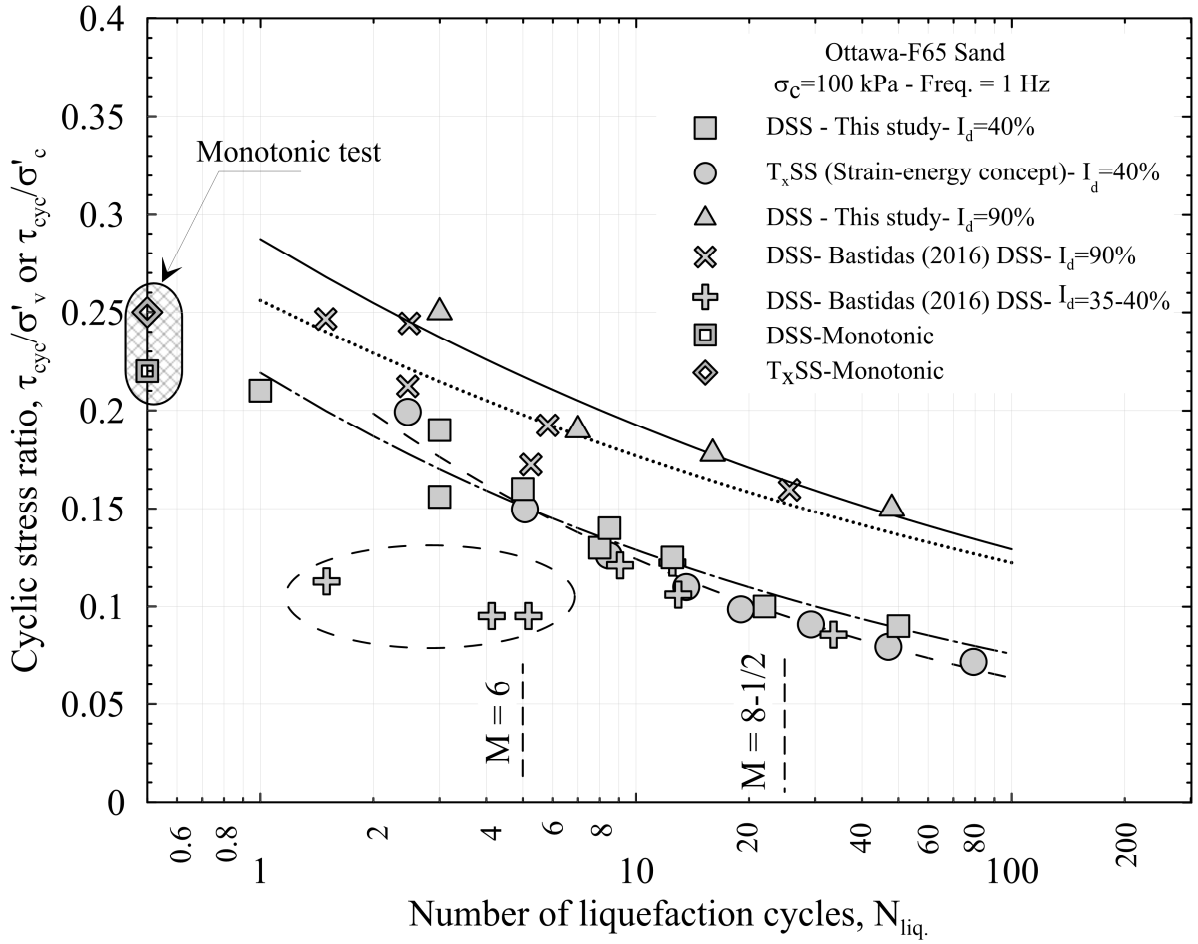

Figure 7.6. Liquefaction potential curves for dense and loose reconstituted specimens.

increases and seems to plateau around unity as a consequence of cyclic loading (i.e. reaches to isotropic states by the time). However, at higher stress amplitude, and a low number of liquefaction cycles, there is no enough time for K_0 evolution as liquefaction occurs instantly. Conversely, under the T_xSS conditions, the initial stress state is maintained constant throughout the cyclic loading. Generally, the proposed coupled energy model has a predictive capability to capture the cyclic response and estimation of the liquefaction potential under the element-level.

7.3.3 Validation of the proposed model with Finn and Centrifuge model results

Before the investigation of the seismic response of sand deposits, further validation of the proposed model to capture the induced pore pressure and seismic response of potentially liquefiable soil was done by simulating the centrifuge experimental model performed at the University of Colorado Boulder (CU Boulder) by Ramirez et al. (2017) using FLAC^{2D}. A

flexible aluminum shear beam was used in the CU Boulder centrifuge container to reduce the effect of boundary conditions and the reflection of waves during earthquake excitation. The centrifuge model consists of 12 m dense Ottawa sand F65 (I_D = 90%) overlain by a 4m loose layer of the same sand (I_D = 40%). Subsequently, a 2 m thickness of dense Monterey sand was placed at the top. The water table was set 1 m below the ground surface. The grain size distribution of Ottawa and Monterey sands are shown in Figure 7.2. More details of the centrifuge model are available in Ramirez et al. (2017) and Ramirez et al. (2018).

The seismic response was simulated in FLAC^{2D} by adopting the well-known Finn model (Finn et al. 1977; Byrne 1991) and the previously calibrated energy-based model. The soil profile was modeled as axisymmetric quadrilateral 2D zones wherein the strength properties of each soil layer were defined based on their correlation with the normalized shear wave velocity by depth ($V_s = V_{s1}\ (100/\sigma'_v)^{0.25}$ (Sykora 1987, Robertson et al. 1992). The element size was selected as 1.0x0.5 which matches with Ramirez et al. (2018) criteria (i.e. $h_{max} = V_s/4.C.f_{max}$, C=4), where f_{max} is the maximum excitation frequency. As well, the maximum element size should be smaller than one-tenth (1/10) of the wavelength of the applied wave to ensure accurate wave transmission between model elements and avoid numerical distortion. Thus, 36 elements were stacked up to represent the 18 m soil deposit in the centrifuge model. In the first phase of modeling, in-situ stresses were modeled by static equilibrium under the gravity effect before exciting the seismic loading wherein both the horizontal and vertical displacement is restricted at the model base. Plain strain configuration was assigned by attaching nodes at the same level. The scaled-up horizontal component of the 1995 Kobe, Japan earthquake registered at the Takatori station (referred herein as Kobe-L) was imposed in the base of the centrifuge model and the numerical model. The peak ground acceleration (PGA) after scaling is 0.3g.

Figure 7.7 represents a comparison between the numerical model and the centrifuge responses in terms of generated pore water pressure at the middle of dense sand (I_D=90%) as well as at the top, middle and bottom of the liquefiable loose sand layer (I_D=40%) in 1-D horizontal earthquake shaking. It is apparent from this figure that there is a good agreement between the numerically computed pore water pressure ratios and that was measured in the centrifuge model in the dense and loose layer. At the top of the loose layer, the computed energy-based pore pressure is observed to increase abruptly after reaching R_u = 0.5. This considerable discrepancy

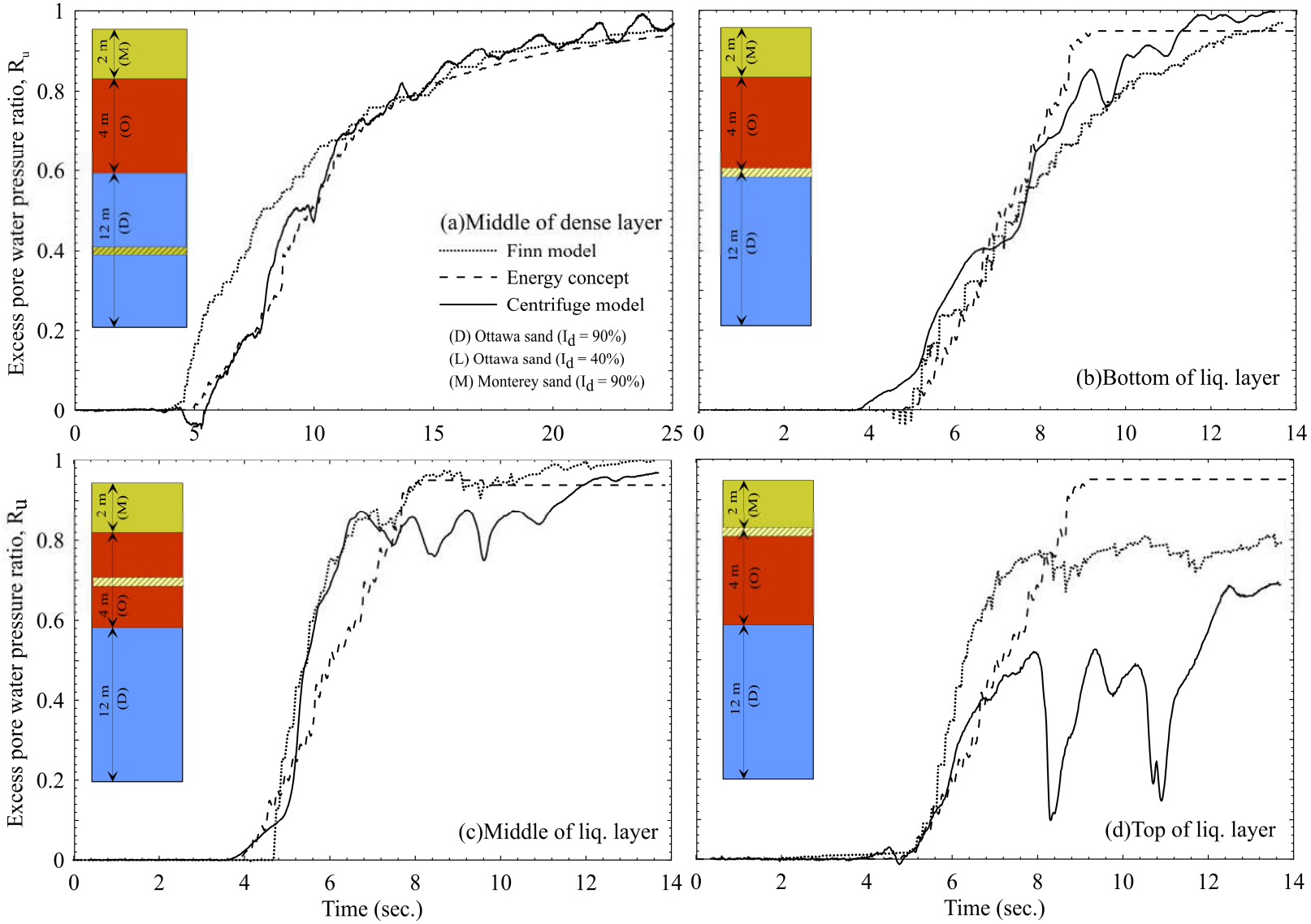

Figure 7.7. Comparison between numerically computed and experimentally measure pore pressure

may be attributed to the change of soil characterizes at this zone where a no pore pressure model was used for the Monterey sand.

The behavior of Monterey sand is beyond the scope of this study partly because of its thickness is small. As may be observed from these figures, no R_u generation observed experimentally or numerically at the first 4 seconds of earthquake excitation. This may be justified as the induced cyclic shear strain, before 4 seconds, seems to be lower than the threshold strain value (0.01 %). It is well established that the pore pressure generates only when cyclic shear strain higher than the threshold strain value (e.g. Dobry et al. 1982; Dobry et al. 2018). The comparison reveals that the proposed energy-pore pressure model is valid and sufficiently accurate to capture the excess pore pressure in dense and loose layers and to capture the seismic response in 1-D liquefaction analysis.

7.4 The response of hypothetical uniform level Ottawa sand deposits

To investigate the difference between the seismic responses of ENA and WNA, a synthetic earthquake with a magnitude of 7 (Atkinson 2009) compatible with Eastern Canada seismicity and another real earthquake registered after Northridge earthquake were used in this study. The 1994 Northridge earthquake occurred in the Los Angeles area with a magnitude of 6.7.

The accelerations were scaled-up to match class A design spectrum for the eastern Quebec City region (NRC 2005), as shown in Figure 7.8. These motions were applied to the base of hypothetical uniform loose and dense sand deposits with different heights as listed in Table 7.2. Different thickness deposits were numerically implemented herein to study the difference between ENA and WNA dynamic responses on different fundamental frequency deposits. Numerically in FLAC soil deposits were discretized into axisymmetric quadrilateral 2D zones of 0.5 m thickness. As previously mentioned, the initial shear modulus of each sub-zone was assigned based on the elastic correlation to the shear wave velocity, $G=\rho.V_s^2$. The 1D ground response of different deposit thickness in terms of average cyclic stress ratio, $CSR_{average}=0.65*\tau_{max}/\sigma'_v$, and maximum generated pore pressure, $R_{u\ max}$, are assembled in Figure 7.9. As can be seen from Figure 7.9, at different soil deposits, the greater the depth of the soil layer, the lower is the $CSR_{average}$ and the $R_{u\ max}$ as previously reported by Ni et al. (1997).

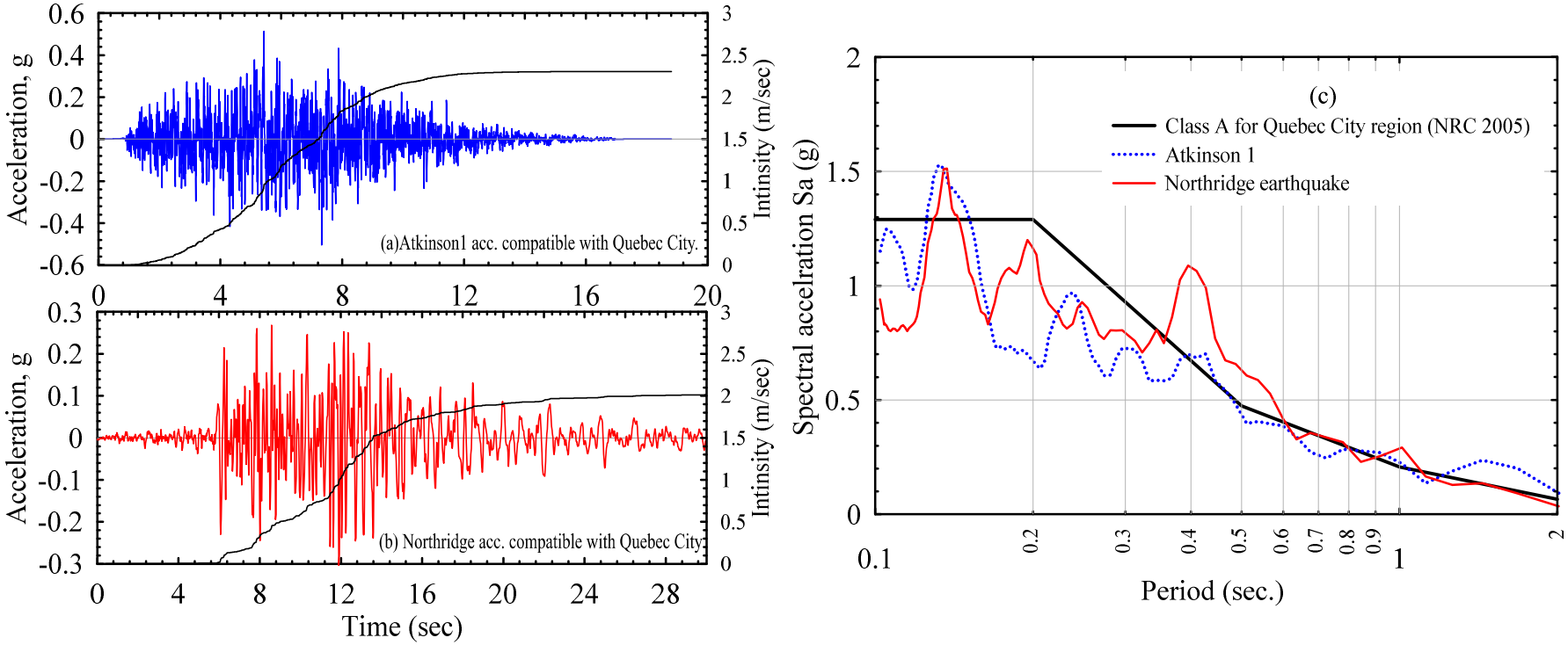

Figure 7.8. Acceleration time history of (a) synthetic earthquake; (b) Northridge earthquake; (c) spectra acceleration scaled to design spectrum of eastern Quebec City

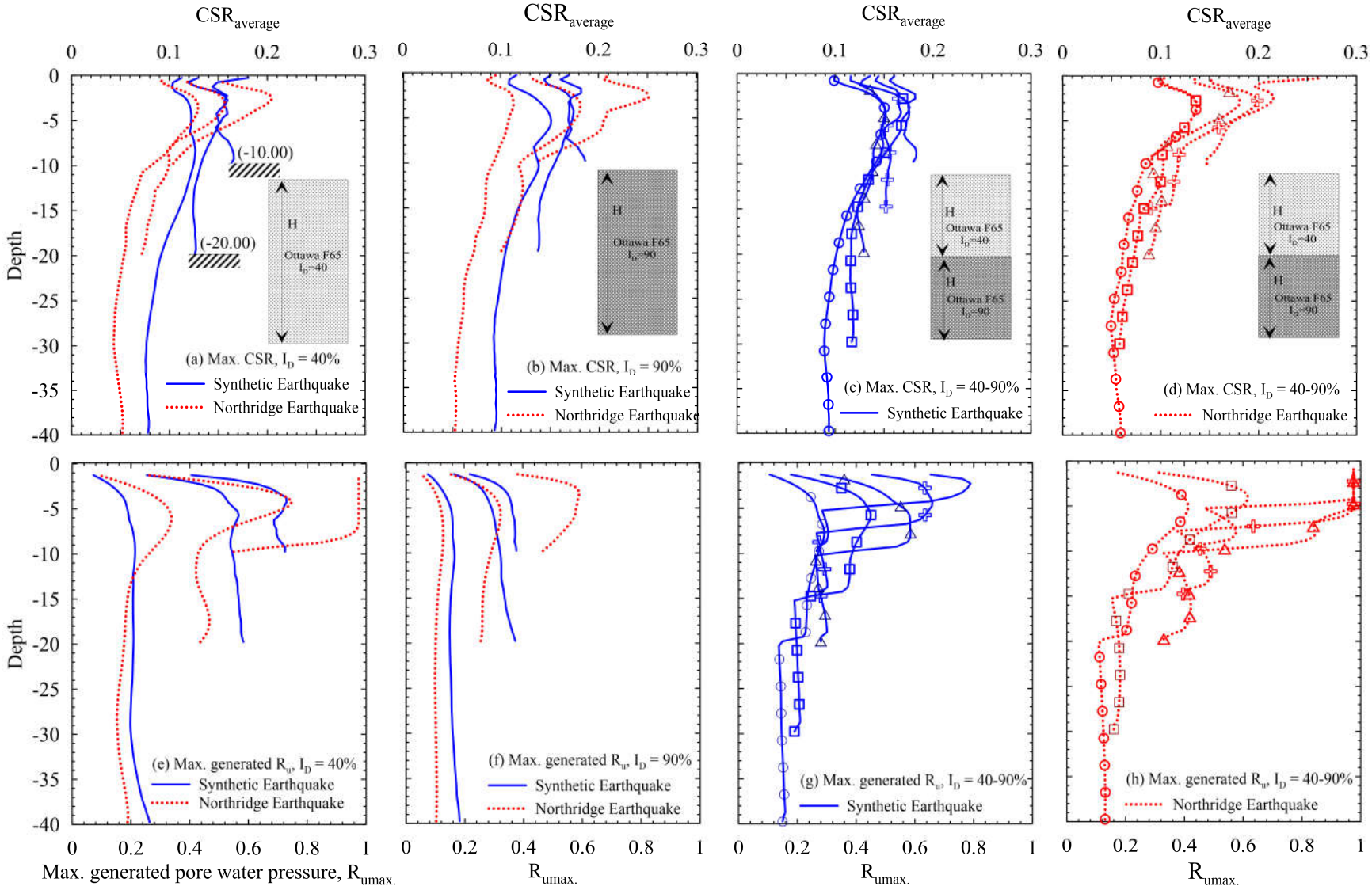

Figure 7.9. Variation of maximum computed pore pressure and average CSR along with depth

Table 7.2. Summary of cases under study

	Deposit characteristics			Atkinson (applied $a_{max} \cong 0.5g$)					Northridge (applied $a_{max} \cong 0.3g$)				
Case	I_D	Thickness	T_0	$R_{u\,max}$	CSR	CSR 7.5	a_{max}	Chart	$R_{u\,max}$	CSR	CSR 7.5	a_{max}	Chart
H10-40/90	40-90	10	0.343	0.97	0.205	0.173	0.247	Liquified	1	0.25	0.187	0.311	Liquified
H15-40/90	40-90	15	0.494	0.77	0.167	0.140	0.214	Liquified	1	0.2	0.150	0.224	Liquified
H20-40/90	40-90	20	0.5734	0.65	0.15	0.126	0.186	marginal liq.	1	0.173	0.129	0.206	Liquified
H30-40/90	40-90	30	0.7	0.47	0.18	0.151	0.173	Liquified	0.65	0.134	0.100	0.158	marginal liq.
H40-40/90	40-90	40	0.88	0.3	0.151	0.127	0.139	marginal liq.	0.45	0.14	0.105	0.151	Liquified
H10-40	40	10	0.638	0.7	0.16	0.134	0.210	Liquified	1	0.2	0.150	0.229	Liquified
H20-40	40	20	0.725	0.58	0.157	0.132	0.180	Liquified	0.75	0.157	0.117	0.161	Liquified
H40-40	40	40	1	0.21	0.125	0.105	0.173	not liq.	0.33	0.125	0.094	0.151	marginal liq.
H10-90	90	10	0.336	0.37	0.18	0.151	0.214	not liquified	0.6	0.25	0.187	0.316	not liquified
H20-90	90	20	0.46	0.23	0.17	0.143	0.209	not liquified	0.32	0.18	0.135	0.183	not liquified
H40-90	90	40	0.67	0.16	0.15	0.126	0.181	not liquified	0.12	0.115	0.086	0.140	not liquified

Note
T_0, fundament period of soil deposit;
$R_{u\,max}$, maximum computed pore pressure along soil profile;
CSR_{max}, maximum induced cyclic stress ratio;
$CSR_{7.5}$, normalized CSR_{max} to M7.5, $CSR_{7.5} = CSR_{max}/MSF.K_\sigma$;
a_{max}, maximum induced acceleration at deposit surface (g).
I_D 40-90, soil deposit consists of loose layer (I_D=40%) followed by dense layer (I_D=90%)

It is observed that the liquefaction occurs (i.e. $R_u \geq 0.90$) when the thickness of loose soil deposits less than 20m under the Northridge earthquake as indicated in Table 7.2. The thickness of the liquefied layer depends on the total deposit thickness and the underlying layers. However, under the synthetic earthquake, the liquefaction observed just in case H10-40/90 (a 5m dense layer overlain by 5m of loose sand, Table 7.2). At larger deposit thickness, liquefaction was not observed. Generally, the maximum computed pore pressure is observed to be a function of earthquake characteristics and the fundaments period of soil deposit (thickness and stiffness).

The spectral accelerations of the two used earthquakes are depicted in Figure 7.10. It is evident that, at a given period lower than 0.65 sec, the Northridge spectral acceleration is higher than the synthetic earthquake with higher energy content. In the same context, marked observations could be obtained based on the dynamic responses in terms of maximum computed pore pressure as a function of the fundamental period of deposit (thickness and stiffness) and earthquake characteristics (predominated period) as depicted in Figure 7.10. The lower the period (or low deposit thickness), the larger is the maximum computed R_u. Under the Northridge earthquake, beyond T_0=0.65 sec (H in the range from 20 to 30 m) the $R_{u\text{-}max}$ deems to not reach the unity (no liquefaction triggering) and continuing to decrease as T_0 value increases. This is because, as discussed above, prior to T_0=0.65 spectral acceleration of the Northridge earthquake is higher than the synthetic earthquake. This can elucidate the reason of deviation the simplified method, sometimes, at scenarios of very shallow and very deep layered deposits (Green et al. 2018).

Regard to the synthetic earthquake, it is observed that the $R_{u\text{-}max}$ reaches the liquefaction state just in the case of shallow loose sand deposit (Case H10-40/90, Table 7.2) with T_0 = 0.343 sec. This reveals that the seismic response of level layered soil depends on the relative correlation between the fundamental period of soil deposits and the predominated period of the used acceleration. A similar conclusion was previously reported by Lee and Chan (1972) and Kokusho and Mimori (2015).

It may be seen from Table 7.2 that there is an attenuation of maximum acceleration, a_{max}, as it travels upward toward the deposit surface for all cases under study. The higher the fundamental period, the higher is the attenuation as migrating from the driving frequency (predominated frequency) of earthquake motion. Correspondingly, the maximum induced CSR is observed to decrease as the natural period of soil deposit increases, Table 7.2. This is compliant with the

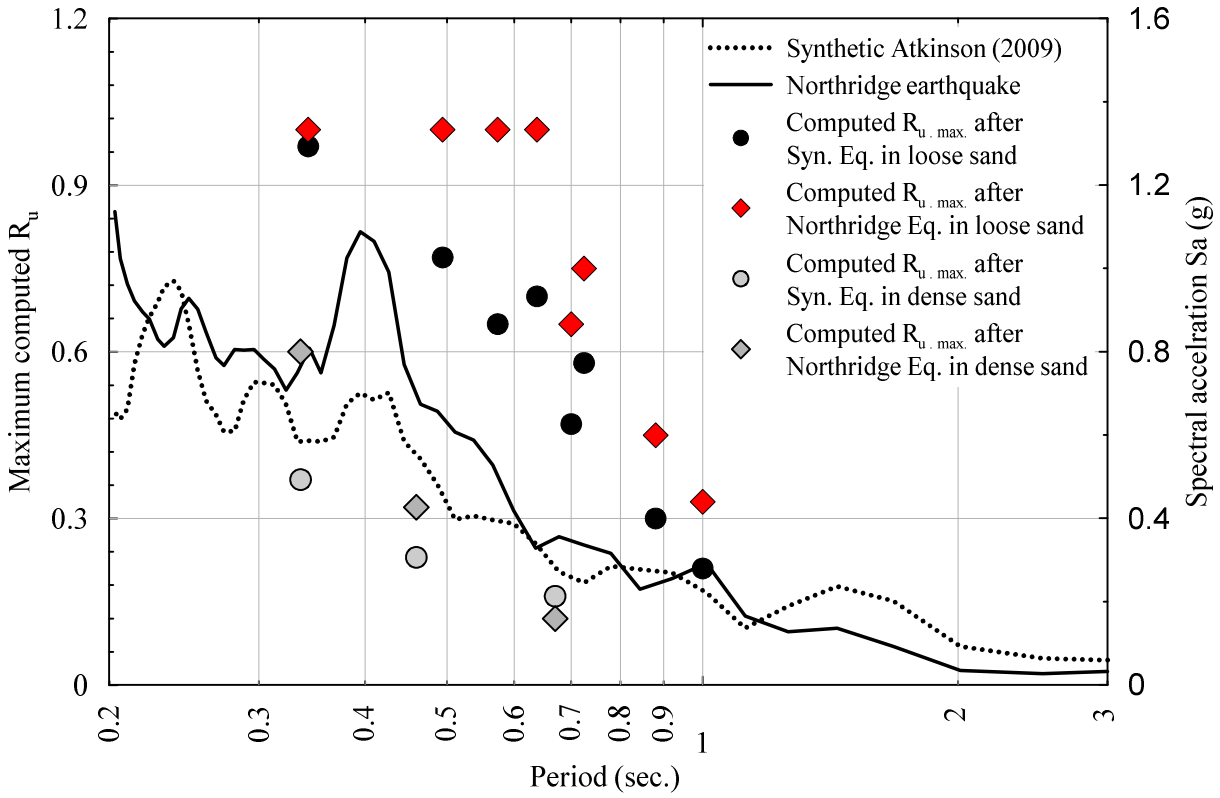

Figure 7.10. The spectrum of maximum computed pore pressure

previous results from centrifuge models performed at the Cambridge Geotechnical Centrifuge Centre by Madabhushi (1994).

Figure 7.11 shows the response of H20-40/90 and H10-40 in terms of CSR, R_u, and N_{eq} along with deposit depth computed from the numerical response. Herein, a comparison between the response of ENA and WNA is achieved in the aspects of N_{eq} (computed either by Seed or energy concept) and the computed pore pressure in addition to comparing with the available liquefaction resistance charts in the literature (CRR-$(N_1)_{60}$ curves).

With regard to the difference between ENA and WNA earthquake responses in view of the equivalent number concept, marked observations could be obtained. The variation of the number of equivalent uniform stress cycles N_{eq}, achieved by adopting Seed et al. (1975) procedure ($N_{eq\text{-}Seed}$) as well as by adopting Green and Terri (2005) procedure ($N_{eq\text{-}energy}$) at an amplitude of 0.65 times of maximum shear stress (as a normal default value), along with soil profile is superposed in Figure 7.11. [Note: In computing $N_{eq\text{-}Seed}$, each time history was normalized by its respective a_{max}]. Green and Terri (2005) procedure was based on the estimation of the cumulative dissipated

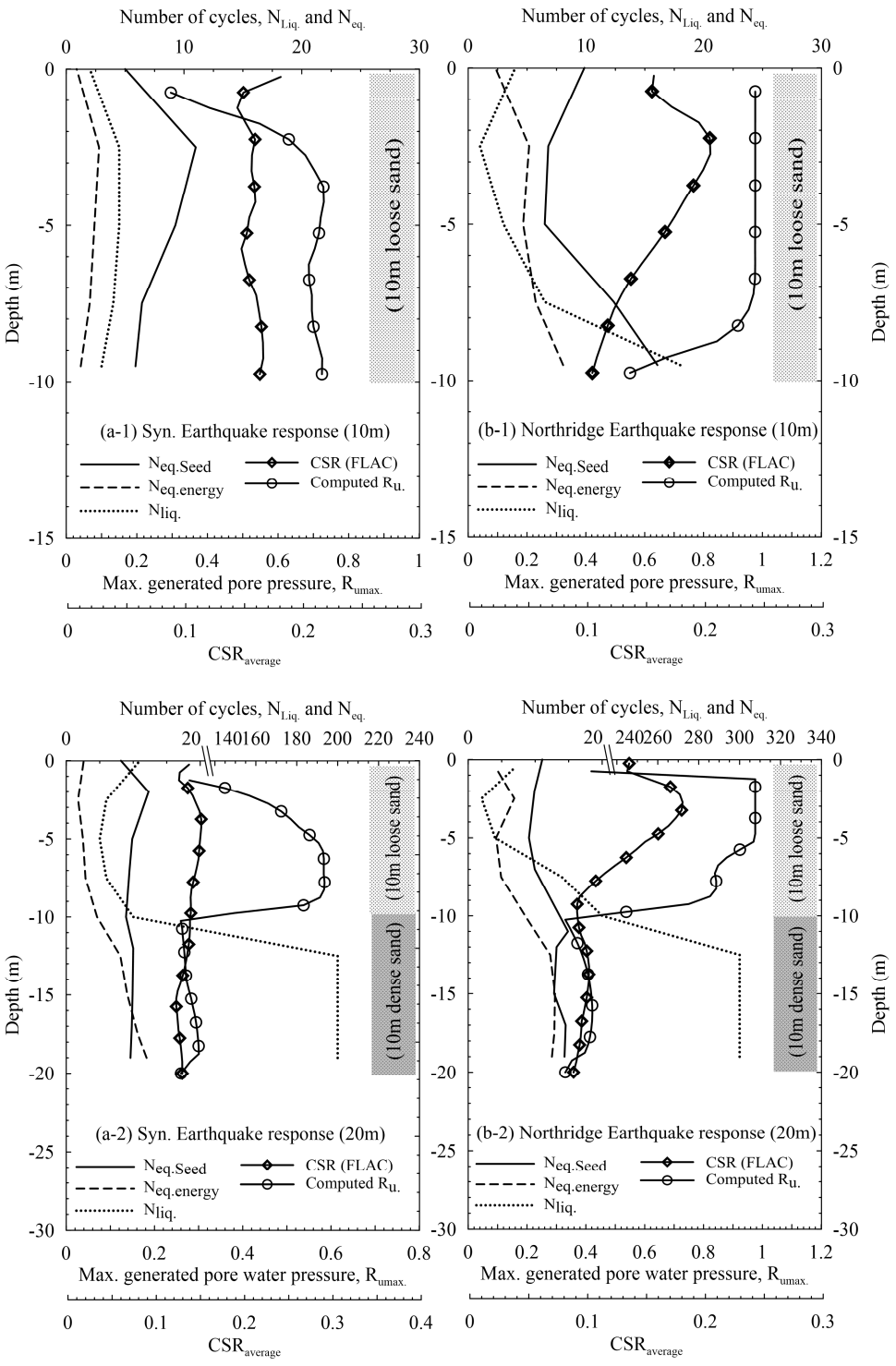

Figure 7.11. Variation of CSR_{max}, $R_{u\,max}$, and N_{eq} after (a) Synthetic earthquake; (b) Northridge earthquake

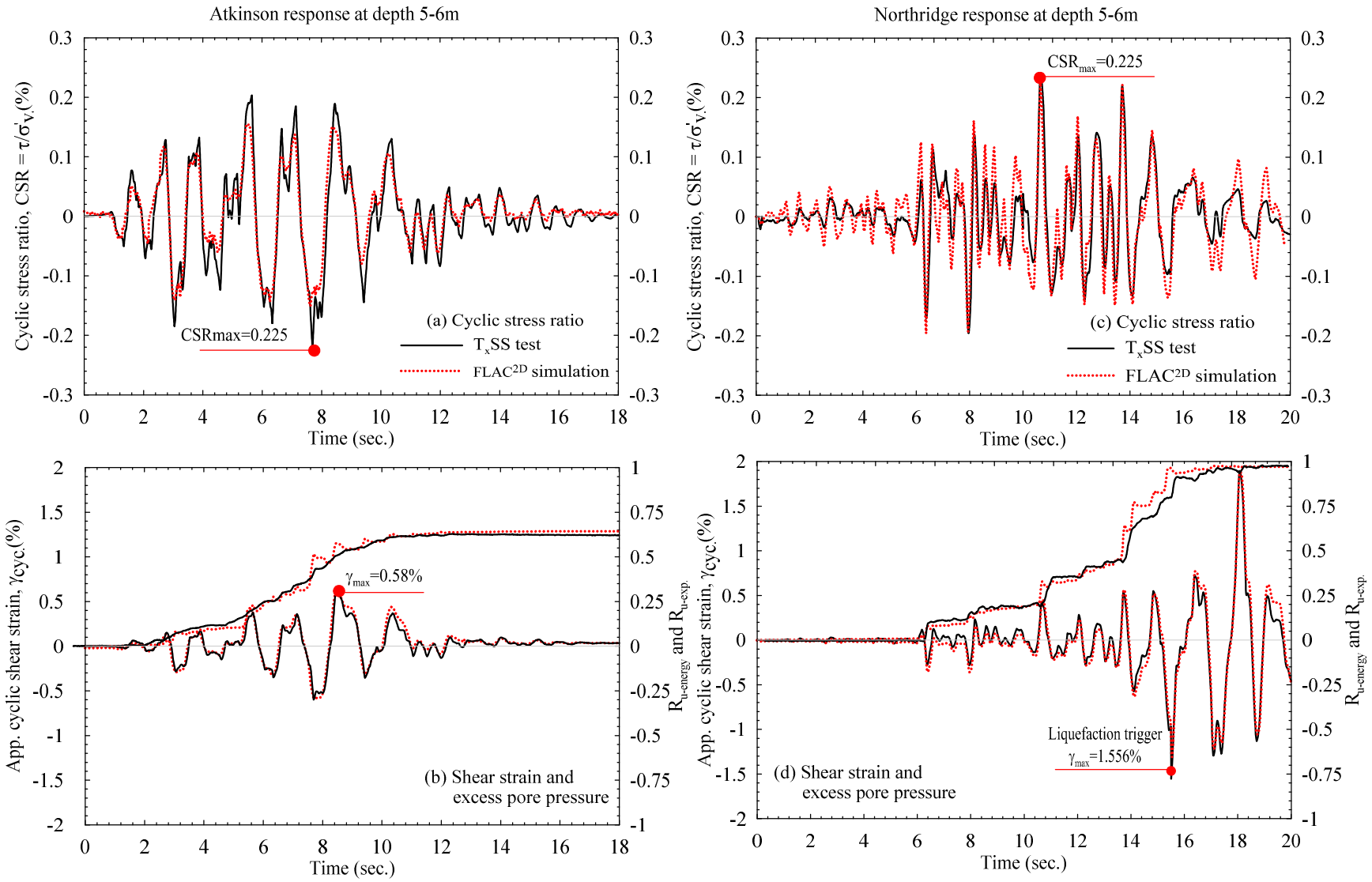

Figure 7.12. Comparison between experimentally measured and numerically computed seismic response to synthetic and Northridge earthquakes at depth 5-6 m

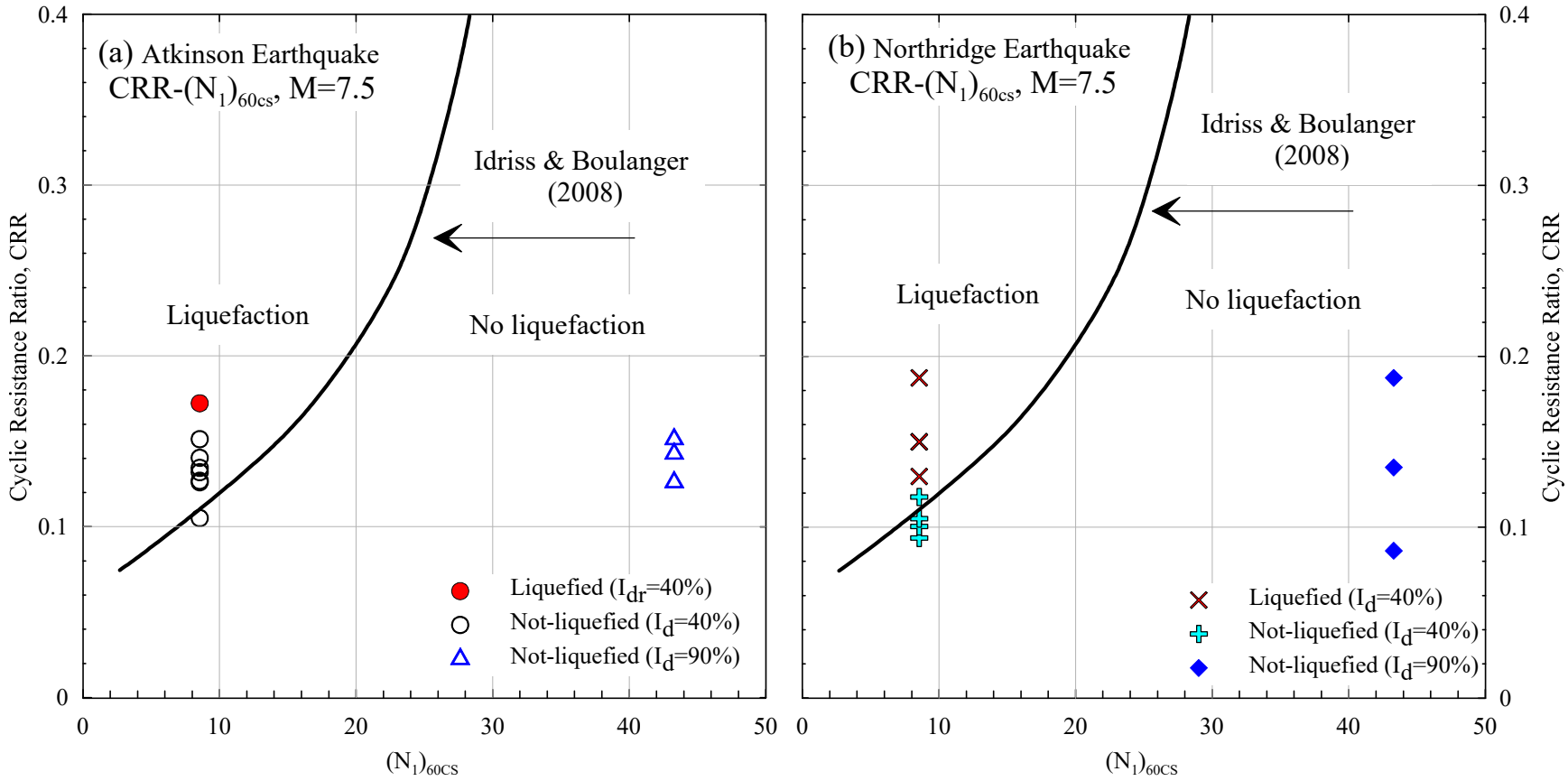

Figure 7.13. Liquefaction resistance curve after Idriss and Boulanger (2008)

energy during earthquake loading, W_s (Eq. 7.4), compared to the dissipated energy occurred at one reference uniform loading cycle of amplitude equal 0.65 times of the maximum amplitude occurred during earthquake loading, Δw_{1cycle}. [Note: Herein Δw is calculated directly from DSS results]. $N_{eq\text{-}energy}$ can be driven from:

$$N_{eq.energy} = \frac{W_s}{\Delta w_{1cycle}} \tag{7.6}$$

It can be seen that the N_{eq} varies with depth and not constant. Green and Terri (2005) observed this variation depends on earthquake magnitude and site to source distance. The numbers of liquefaction cycles read from the liquefaction potential curve (Figure 7.6) is depicted also in Figure 7.11. In general, it can be observed that $N_{eq\text{-}Seed}$ values are higher than $N_{eq\text{-}energy}$ as previously noted by Green and Lee (2006). From comparing $N_{eq\text{-}Seed}$ and N_{liq}, at cases H10-40 and H20-40/90, triggering of liquefaction is expected under both excited accelerations. However, $N_{eq\text{-}energy}$ shows triggering of liquefaction under the Northridge earthquake while under synthetic earthquake no liquefaction occurs (i.e. $N_{eq\text{-}energy} < N_{liq}$). With regard to the computed R_u, it may be assured the occurrence of liquefaction under the Northridge earthquake, however, no liquefaction triggers ($R_{u\ max} = 0.6$) after the synthetic earthquake. This observation reveals the coincidence between liquefaction estimation based on $N_{eq\text{-}energy}$ and computed R_u as opposed to Seed et al. procedure. The accuracy of the energy concept in computing N_{eq} comparing to Seed et al. procedure may be postulated as the latter was based on the P-M hypothesis which constrained for high cycle fatigue conditions (i.e., strain response constrain in elastic range compiled with a high number of cycles). Moreover, the inherent linear accumulative damage assumption of the P-M hypothesis cannot capture the softening effect during undrained cyclic loading.

The cyclic response at depth of 5-6 m from the ground surface under Northridge and synthetic earthquakes are shown in Figure 7.12. To acquire more confidence in the proposed coupled energy-based model, the computed shear strain responses of the synthetic and Northridge earthquake at depth 5-6 m from deposit surface are applied, experimentally, on reconstituted soil specimens in T_xSS apparatus. The computed responses are compared to the measured response in terms of R_u and CSR as shown in Figure 7.12. The good agreement between computed and measured responses emphasizes the predictive capability of the proposed energy-based model to capture the dynamic response and confirms its applicability in 1D soil response analysis. It can be observed that although the maximum induced CSR values are equal ($CSR_{max} = 0.225$),

liquefaction is triggered ($R_u > 0.9$) under the Northridge earthquake, conversely to the synthetic earthquake. As much more, the response of the Northridge earthquake is rich in stress cycles having amplitudes close to CSR_{max} value which is implicitly accounted in computing $N_{eq\text{-}Seed}$ in contrary to synthetic earthquake response. Thus, the computed $N_{eq\text{-}Seed}$ after Northridge earthquake is observed to be larger than in the synthetic earthquake. In all the cases under study, although loose sand layer deduced $N_{eq\text{-}Seed}$ higher than N_{liq}, as shown for example in Figure 7.11, not all cases experienced liquefaction in terms of pore pressure.

In the practical viewpoint, most of the liquefaction studies have been performed in terms of standard penetration resistance $(N_1)_{60}$. The $(N_1)_{60}$ is preferred as it correlates to I_D which reflects the inherent contractive tendency of soil under shearing load. Herein, the CRR-$(N_1)_{60CS}$ liquefaction curve obtained after Idriss and Boulanger (2008) is incorporated, Figure 7.13. The normalized CSR corresponding to earthquake magnitude 7.5, for each case study is superposed on the liquefaction resistance curves. The magnitude scaling factor (MSF) proposed by Boulanger and Idriss (2014) was used in this work as the liquefaction resistance curves proposed by the same authors (Idriss and Boulanger 2008) was used. The $(N_1)_{60CS}$ values were computed from its correlation to relative density (I_D), coefficient of uniformity (C_u), mean grain size (D_{50}) and two-dimensional angularity of particles (A_{2D}) (Ghali et al. 2019) as follows:

$$\frac{N_1}{D_r^2} = 140 \times D_{50}^{0.22} \times \exp^{-0.002\,A_{2D}} \times C_u^{0.5} \tag{7.7}$$

It is vividly seen that the CSR values computed after the Northridge earthquake are matched very well with the liquefaction resistance curve. It is observed that the cases obtained from the synthetic earthquake are plotted in the liquefaction zone although no liquefaction is experienced, which arise a doubt about using these charts in Eastern North America.

The preceding discussion in terms of pore pressure, fundamental period and liquefaction charts reveals that the simplified method and incorporated liquefaction charts give reliable results under WNA at the case of shallow deposit over a thickness range from 20 to 30 m (as a function of the fundamental period). However, in the case of deeper deposits in WNA, with a higher fundament period, as well as under the cases of ENA, the simplified procedure has conservative applicability, as shown in Figure 7.11. This can be postulated to the difference in the duration and frequency content of the used earthquakes. It has been recognized that WNA features with higher duration and low frequency than in ENA, as shown in Figure 7.8 where low-frequency

motions result in higher pore pressure generation, and soil softening, than for high-frequency ground motions (Popescu 2002; Ghosh and Madabhushi 2003). In the term of shear strain, which is the key parameter of pore pressure buildup, it is seen in Figures 12(b) and 12(d) that the induced shear strain time history is totally different under WNA than ENA as will be discussed in the subsequent section.

7.4.1 Pore pressure as damage metric in soil deposits.

It has been established that the shear strain is the key parameter of pore pressure generation comparing to CSR value. The shear strain responses after Northridge and synthetic earthquakes are strikingly varied, Figures 12(b) and 12(d). Careful observation of these figures indicates that the shear strain response of a synthetic earthquake consists of a low number of cycles with a maximum amplitude of 0.58%. However, under the Northridge earthquake, the number of strain cycles is higher wherein the amplitude increases until the liquefaction trigger. In Figure 7.14, it is observed that the pore pressure increases by a sequence of shear strain cycles. To elucidate the influence of shear strain amplitude on the pore pressure buildup, the procedure of predicting the pore pressure buildup as a damage metric using the Richart and Newmark (R-N) hypothesis (Richart and Newmark 1948) is implemented herein (Khashila et al. 2018). The R-N hypothesis is an expanded form of the well-known Palmgren–Miner hypothesis (P-M; Palmgren 1924; Miner 1945) wherein both hypotheses were devoted first to compute the damage of the metal under cyclic loading. Afterward, Seed and his colleague adapted the P-M hypothesis to compute N_{eq} of earthquake ground motion and recently Green and Lee (2006) implemented the R-N hypothesis in computing the cumulative damage after irregular time history. Opposed to the P-M hypothesis, the R-N hypothesis has a feature of counting the sequence of load amplitude in the irregular motion (Green and Lee 2006). The cumulative of the generated pore pressure, till liquefaction trigger, after applying an irregular shear strain time history could be estimated as damage metric according to Khashila et al. (2018) by:

$$R_{u\,m} = \left[\left(R_{u\,m-1} \right)^{\frac{1}{r_m}} + \left(\frac{n_m}{N_{liq.m}} \right) \right]^{r_m} \tag{7.8}$$

where $R_{u.m}$ is the cumulative pore pressure after m cycles in the irregular shear strain time history and r_m is a calibrated material parameter corresponding to amplitude γ_m. n_m and $N_{liq.m}$ are the numbers of cycles and liquefaction cycles that have an amplitude γ_m that can be obtained

from Figure 7.4, respectively. More details about this relation and calibration procedure of material parameter, r_m, are discussed in Khashila et al. (2018).

Applying the P-M and R-N hypotheses on the synthetic and Northridge earthquake responses reveals a reasonable consistency between the experimentally (T_xSS) and numerically computed R_u using either the energy concept or R-N damage hypothesis, Figure 7.14. However, the estimated cumulative damage by adopting the P-M hypothesis, by setting $r_m = 1$ in Eq. (7.6), underestimates the cumulative damage before failure occurrence (i.e. liquefaction).

It can be seen that by the load sequence, the pore pressure increases cumulatively based on the amplitude of shear strain. In the synthetic earthquake response, the maximum increase occurred at shear strain amplitude of 0.58% and then a marginal increase occurred. In the Northridge response, which is rich in high shear strain cycles, the pore pressure increased gradually as a function of shear strain amplitude till reaches around 0.8 (at 15 sec.) followed by an abrupt increase due to a high shear strain amplitude of 1.55%. In the same context, based on the statistical analysis of previously compiled earthquake data, Rodriguez-Arriaga and Green (2018) reported that the liquefaction triggering distinctly possible when induced shear strain is higher than 0.5%.

Particularly noticeable is, although the CSR_{max} values are equal, the shear strain and stress time histories are different which causes a variation of the cumulative damage represented in pore pressure generation. This confirms that the liquefaction assessment in ENA based on CSR_{max} and current liquefaction resistance charts is questionable and gives more conservative estimation.

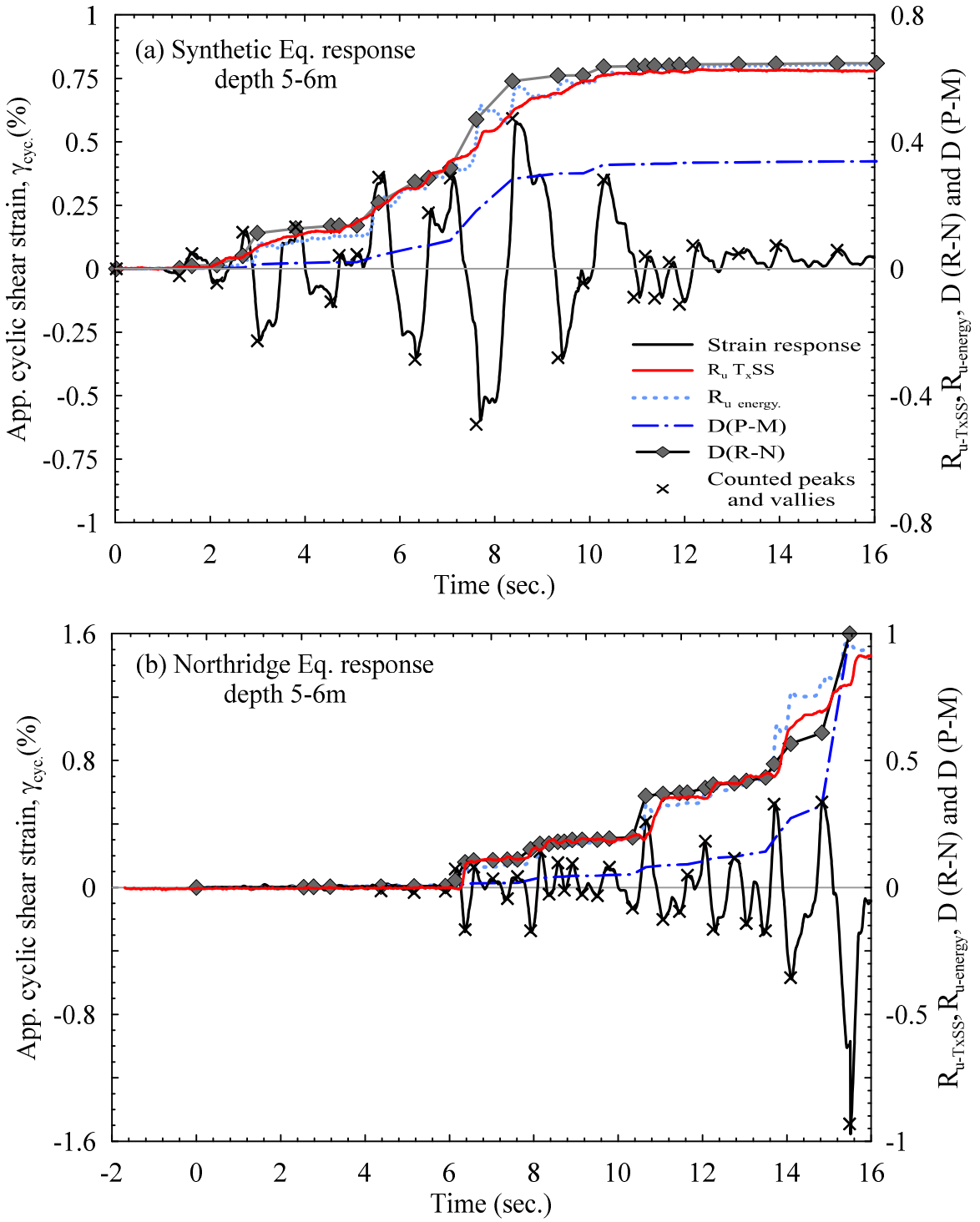

Figure 7.14. Induced shear strain and computed pore pressure at depth 5-6 m after (a) Synthetic earthquake; (b) Northridge earthquake

CHAPTER 8

CONCLUSIONS ET RECOMMANDATIONS

8.1 Conclusions (en français)

L'objectif principal de la présente étude est d'examiner la différence de réponse sismique entre les régions de l'Est et de l'Ouest de l'Amérique du Nord en adoptant un modèle de taux de pression de l'eau des pores dans une analyse dynamique unidimensionnelle des dépôts hypothétiques. Pour ce faire, un modèle de taux de pression de l'eau des pores basé sur l'énergie a été proposé à partir d'une série d'essais TxSS cycliques contrôlés par déformation sur des échantillons de sol reconstitué de différents sols sans cohésion. Ce modèle a été validé au niveau des échantillons pour simuler le comportement cyclique lors d'essais CTX et TxSS contrôlés par contraintes et déformations cycliques et pour effectuer une analyse unidimensionnelle de la réponse du site pour un essai dynamique de centrifugation de sable propre.

Premièrement, à la suite des travaux théoriques de Green et Lee (2006), une série d'études expérimentales a été menée à l'aide de l'appareil T_xSS pour étudier le concept du nombre équivalent. Des essais à déformation uniforme contrôlée ont été effectués dans des conditions sur des échantillons non drainées reconstitués de sables de Baie-Saint-Paul (BSP), Carignon et Québec afin de développer des courbes (γ_{cyc}-$N_{liq.}$) analogues aux courbes types (CSR-$N_{liq.}$) qui peuvent être utilisées pour évaluer la liquéfaction et estimer le $N_{eq\gamma}$. La pression de l'eau de porosité générée lors d'essais uniformes à déformation contrôlée a été utilisée comme mesure des dommages avec un degré de précision adéquat pour étalonner le paramètre du matériau, r. On observe que le paramètre du matériau est fonction du type de sol, de l'amplitude de déformation par cisaillement cyclique, $\gamma_{cyc,}$ et de la densité du sol.

L'utilisation du paramètre de matériau étalonné pour appliquer l'hypothèse R-N à l'évolution temporelle des tremblements de terre et des phénomènes non uniformes permet d'obtenir une bonne concordance entre la pression mesurée dans l'eau des pores et les dommages

cumulatifs calculés. Toutefois, la présente étude montre que l'hypothèse de la P-M sous-estime les dommages cumulatifs (la pression d'eau des pores générée) pendant la charge cyclique jusqu'au début de la liquéfaction. De plus, une comparaison entre le $N_{eq\gamma}$ calculé à l'aide de R-N pour l'historique de temps de déformation irrégulier appliqué sur le BSP et les sables de Carignon montre une bonne concordance avec les estimations expérimentales qui considèrent l'accumulation de pression dans l'eau des pores comme une mesure des dommages. Au début de la liquéfaction, l'utilisation de l'hypothèse P-M donne à $N_{eq\gamma}$ des valeurs égales à celles obtenues par l'hypothèse R-N et par l'accumulation de pression dans l'eau des pores comme mesure des dommages. Cependant, avant le déclenchement de la liquéfaction, l'hypothèse P-M conduit à une prédiction trop conservatrice de $N_{eq\gamma}$, confirmant les résultats antérieurs de Green et Lee (2006). Ces résultats indiquent la possibilité d'utiliser la pression de l'eau des pores comme mesure des dommages jusqu'à la liquéfaction pour estimer le $N_{eq\gamma}$.

Dans la deuxième partie, une comparaison entre le comportement cyclique et le potentiel de liquéfaction des essais triaxiaux cycliques et des essais de cisaillement simples a été étudiée. Une série d'essais cycliques contrôlés par la déformation et la contrainte ont été effectués sur les sables de Baie-Saint-Paul, d'Ottawa C-109 et du Québec au moyen du "CTX" triaxial cyclique. Dans le même temps, des essais cycliques à déformation contrôlée ont été réalisés dans la nouvelle combinaison triaxiale "T_xSS". De plus, des essais DSS cycliques sous contrainte contrôlée ont été effectués pour valider les courbes de potentiel de liquéfaction obtenues à partir des essais T_xSS. Un modèle de pression d'eau des pores à couplage lâche basé sur l'énergie, étalonné à partir d'essais T_xSS cycliques à contrainte contrôlée, a été adopté pour simuler des essais T_xSS cycliques à contrainte contrôlée en utilisant la plate-forme FLAC^{2D}. D'autres essais alternatifs sous contrainte ont été effectués dans T_xSS pour évaluer le modèle numérique proposé au niveau des éléments. Sur la base des résultats des essais cycliques contrôlés par la déformation et le stress, les conclusions suivantes peuvent être tirées :

- Les essais cycliques DSS et T_xSS sont supérieurs aux essais CTX car ils simulent étroitement les états de contrainte pendant la propagation verticale des ondes.
- Il y a une bonne concordance entre les courbes de potentiel de liquéfaction du sable d'Ottawa C-109 obtenues numériquement et celles obtenues dans le cadre d'études antérieures, de la présente étude sous contrainte cyclique (déformation radiale limitée) et d'autres essais sous

contrainte dans du TxSS (où l'échantillon de sol est enrobé dans une membrane de latex et confiné dans une chambre triaxiale).

- L'étude du rapport diamètre/hauteur (D/H) en T_xSS a révélé que le D/H n'a pas d'effet significatif sur la résistance à la liquéfaction du sable d'Ottawa C-109 lors d'essais cycliques à contrainte contrôlée.
- La comparaison entre CTX et TxSS dans des conditions cycliques contrôlées par les contraintes a montré que la résistance à la liquéfaction obtenue par CTX est supérieure à sa contrepartie dans TxSS et doit être corrélée par un facteur de correction, $C_r= [(1+2K_0)/3]$. Ce facteur est applicable pour corréler l'échantillon CTX préparé par bourrage humide en DSS ou T_xSS.
- Contrairement aux essais cycliques sous contrainte, les échantillons de sol présentent une résistance à la liquéfaction plus élevée sous charge TxSS, en terme de (γ-$N_{liq.}$), qu'en CTX sous contrainte contrôlée.
- Un facteur de corrélation entre la déformation axiale cyclique (en CTX) et la déformation en cisaillement cyclique (en T_xSS) a été obtenu à partir d'essais contrôlés par déformation cyclique. On suggère que ce facteur de correction est fonction de la contrainte de cisaillement et du type de sol.

De plus, le modèle énergétique proposé a été incorporé à la plate-forme $FLAC^{3D}$ pour simuler numériquement le comportement cyclique des sables Ottawa C-109 et BSP dans le cadre des essais triaxiaux cycliques (CTX) et des nouveaux essais combinés triaxiaux de cisaillement simple (T_xSS). Les résultats montrent la capacité d'incorporer numériquement le concept d'énergie pour capturer le comportement cyclique dans les essais CTX et T_xSS dans des conditions de contrainte ou de déformations contrôlées. Les résultats numériques révèlent l'effet de la condition de limite finale sur le comportement cyclique du CTX, même lorsque le rapport hauteur/diamètre est de l'ordre de 2, ce qui affecte significativement la distribution de déformation axiale et donc l'énergie dissipée et la pression d'eau des pores. On observe que le renflement maximal des échantillons de sol considérés dans cette étude et les rapports de pression d'eau des pores générés se situent dans le tiers médian. Ainsi, la liquéfaction prématurée se déclenche dans le tiers médian de l'échantillon CTX et d'autres cascades vers les autres zones. Cependant, la simulation numérique de T_xSS révèle une distribution relativement uniforme de la

contrainte de cisaillement et de la déformation dans les échantillons de sol et une égalisation relative de la pression de pore théorique dans l'échantillon du sol. De plus, les résultats numériques et expérimentaux montrent que la résistance à la liquéfaction est plus élevée dans les conditions T_xSS et DSS que dans les conditions CTX. Une corrélation basée sur la déformation entre le CTX et le T_xSS a été proposée sur la base des essais de déformation cycliques contrôlés. Un facteur équivalent a été proposé pour corréler les déformations axiales induites dans les CTX à contrainte et à déformation contrôlées. La validité de cette corrélation a été vérifiée avec succès en comparant la pression des pores mesurée et estimée à partir des résultats du CTX contrôlé par contrainte sur la base de l'accumulation de pression des pores comme mesure des dommages.

De la même manière, le résultat d'essais non drainés à contrainte et déformation cycliques contrôlées effectués sur un échantillon de sol reconstitué de sable Ottawa F-65, un modèle couplé de pression de pore énergétique a été proposé. Ce modèle a été validé au niveau des éléments par comparaison avec les résultats des tests TxSS. Il existe un assez bon accord entre la résistance à la liquéfaction obtenue par DSS, T_xSS et déduite précédemment de Bastidas (2016). À grande échelle, la réponse sismique des dépôts de sol stratifiés obtenus à partir du modèle proposé a été comparée avec succès aux résultats des modèles finlandais et centrifuges. Numériquement, on a utilisé 11 dépôts hypothétiques au niveau du sol avec des épaisseurs différentes et des périodes fondamentales pour étudier la différence des réponses sismiques entre l'ENA et le WNA. Cette différence a été discutée dans de nombreux aspects importants de la pression des pores calculée, R_u, période fondamentale, T_0, cycles de contraintes uniformes équivalents, N_{eq}, et l'efficacité des graphiques actuels de liquéfaction. En comparant les réponses de l'ENA et du WNA aux tremblements de terre, les observations suivantes ont pu être tirées.

- Pour les cas étudiés, la méthode simplifiée semi-empirique et la méthode N_{eq} incorporée sont valides pour la région ouest de l'Amérique du Nord lorsque la période fondamentale de dépôt du sol est inférieure à 0,65 sec, sur la plage étudiée de T_0.
- La réponse sismique, en termes de $R_{u.max}$ et CSR_{max}, et l'efficacité de la méthode simplifiée peuvent être davantage liées au rapport relatif entre la période fondamentale de dépôt et la période prédominante du mouvement appliqué.
- Bien que la magnitude et le $N_{eq\text{-}Seed}$ des tremblements de terre utilisés soient presque égaux, la liquéfaction a été ressentie sous le tremblement de terre WNA et sous un tremblement de

terre non compatible. Cela est dû à la différence de fréquence entre les deux tremblements de terre.

- L'adoption du concept d'énergie dans le calcul de $N_{eq\text{-}energy}$ permet d'obtenir une estimation plus précise de la liquéfaction que la méthode de Seed et al.
- La comparaison entre les réponses sismiques montre que l'évaluation du déclencheur de liquéfaction sur la base du CSR maximum induit dans l'ENA est discutable.
- L'utilisation des diagrammes de résistance à la liquéfaction actuels en termes de $(N_1)_{60cs}$ dans l'évaluation de la liquéfaction de l'ENA permet d'établir des prévisions prudentes.
- Les dommages cumulatifs représentés dans l'accumulation de pression des pores sont davantage influencés par l'amplitude de la déformation par cisaillement que par l'amplitude de la contrainte.

8.2 Recommandations pour la recherche future s (en français)

Les résultats actuels présentés au chapitre 4 montrent une étape prometteuse vers la mise en œuvre de la pression d'eau de pore comme mesure des dommages. Ainsi, la formule de l'hypothèse de dommages pourrait raisonnablement saisir l'augmentation de la pression des pores due à l'excitation sismique et prédire le nombre de cycles équivalents. Le paramètre de l'hypothèse d'endommagement (paramètre matériau, r) peut être étalonné simplement à partir de tests TxSS cycliques. Des recherches supplémentaires sont donc nécessaires pour valider le concept d'endommagement et calibrer le paramètre matériel, r, pour différents types de sol, en tenant compte de l'influence des caractéristiques des particules, de la teneur en particules fines, de la densité relative et de la pression de confinement. En outre, d'enquêter sur l'hypothèse de l'égalité de $N_{eq\gamma}$ et $N_{eq\tau}$.

Sur la base des résultats expérimentaux T_xSS et CTX présentés aux chapitres 5, 6 et 7, un modèle simple de pression de pore énergétique a été proposé par calibration simple (α) et paramètres d'ajustement (C_1, C_2 et C_3). Ce modèle a assez bien prédit la pression des pores et la résistance à la liquéfaction générées au niveau de l'élément et en effectuant une analyse unidimensionnelle de la réponse du site pour un essai dynamique de centrifugation de sable propre. Toutefois, des travaux de recherche supplémentaires sont encore nécessaires pour généraliser le modèle proposé afin de couvrir les points suivants:

- Introduire une corrélation entre les paramètres d'étalonnage (α) et les propriétés physiques du sol comme le D_{50}.
- Incorporer le concept d'énergie dans les diagrammes de conception de la liquéfaction et le facteur d'échelle de magnitude.
- Établir un lien entre les courbes de potentiel de liquéfaction lors d'essais sous contrainte et sous déformation contrôlés basés sur le concept énergétique.
- Dans le cadre de la présente étude, tous les essais ont été préparés à l'aide de la méthode de bourrage humide. Cette méthode a été choisie car elle permet de contrôler le taux de vide avant consolidation. Cependant, d'autres méthodes de préparation sont suggérées pour généraliser les conclusions obtenues.
- D'autres travaux sont encore nécessaires pour étudier la corrélation proposée entre la contrainte axiale et la contrainte de cisaillement pour différents types de sol préparés à différentes densités relatives et pressions de confinement.

Dans le cadre de la mise en œuvre pratique du modèle énergétique proposé, la différence entre de nombreux aspects importants de la pression d'eau de pore, de la CSR et de la réponse N_{eq} des régions Est et Ouest de l'Amérique du Nord a été examinée au chapitre 7. L'analyse de réponse 1-D pour 11 dépôts hypothétiques soumis à un séisme compatible avec la sismicité de la région Est et un autre incompatible a été effectuée. Bien que les résultats actuels interprètent la différence de réponse sismique, un cadre de référence supplémentaire est nécessaire pour obtenir une explication directe et fondamentale de cette différence et fixer les conditions d'utilisation des graphiques de conception de la liquéfaction actuels :

- Les dépôts de sol utilisés ici sont hypothétiques. Il faudrait donc des dépôts de sol réalistes pour mieux comprendre cette différence.
- Il faudrait beaucoup plus de mouvements du sol d'amplitude différente pour étudier cette différence.
- L'incorporation de la dissipation de la pression de l'eau des pores dans l'analyse 1-D et la densification du sol pendant et après le tremblement de terre peuvent affecter l'exactitude des résultats.

8.3 Conclusions (in English)

The main objective of the current study is to examine the difference of seismic response between Eastern and Western North America regions by adopting an energy-based pore water pressure model in one-dimensional dynamic analysis of hypothetical deposits. To achieve this, an energy-based pore water pressure model was proposed based on a series of cyclic strain-controlled T_xSS tests on reconstituted soil samples of different cohesionless soils. This model was validated in element level to simulate the cyclic behavior under cyclic stress- and strain-controlled CTX and T_xSS tests and in performing one-dimensional site response analysis for dynamic centrifuge test of clean sand.

Firstly, following the theoretical work by Green and Lee (2006), a series of experimental investigations was conducted using the T_xSS apparatus to investigate the equivalent number concept. Uniform strain-controlled tests were conducted under undrained conditions on reconstituted samples of Baie-Saint-Paul (BSP), Carignon, and Quebec sands to develop (γ_{cyc}–$N_{liq.}$) curves analogous to the typical (CSR-$N_{liq.}$) curves that can be used in liquefaction assessment and $N_{eq\gamma}$ estimation. Pore-water pressure generated in uniform strain-controlled tests was used as damage metric with an adequate degree of accuracy to calibrate the material parameter, r. It is observed that material parameter is a function of soil type, cyclic shear strain amplitude, γ_{cyc}, and soil density.

Using the calibrated material parameter to apply the R-N hypothesis on nonuniform and earthquake time histories results in good agreement between the measured pore-water pressure and the computed cumulative damage. However, the current study shows that the P-M hypothesis underestimates the cumulative damage (i.e., the generated pore water pressure) during cyclic loading until the onset of liquefaction. Furthermore, a comparison between the computed $N_{eq\gamma}$ using R-N for irregular strain time history applied on BSP and Carignon sands shows a good agreement with those estimated experimentally considering pore-water pressure build-up as a damage metric. At the onset of liquefaction, using the P-M hypothesis yields $N_{eq\gamma}$ values equal to that obtained by the R-N hypothesis and by pore-water pressure build-up as a damage metric. However, prior to the trigger of liquefaction, the P-M hypothesis leads to overly conservative prediction of $N_{eq\gamma}$, confirming previous findings by Green and Lee (2006). These results indicate

the possibility of using pore-water pressure as damage metric until occurrence of liquefaction to estimate $N_{eq\gamma}$.

In the second part, a comparison between cyclic behavior and liquefaction potential of cyclic triaxial and simple shearing tests were investigated. A series of cyclic strain- and stress-controlled tests were conducted on Baie-Saint-Paul, Ottawa C-109 and Quebec sands using cyclic triaxial "CTX". Meanwhile, cyclic strain-controlled tests were conducted in the new combined triaxial "T_xSS". Moreover, cyclic stress-controlled DSS tests were performed to validate the liquefaction potential curves obtained from T_xSS tests. A loosely coupled energy-based pore water pressure model, had been calibrated from cyclic strain-controlled T_xSS tests, was adopted to simulate cyclic stress-controlled T_xSS tests using the FLAC^{2D} platform. Other alternative stress-controlled tests were conducted in TxSS to evaluate the proposed numerical model at element level. Based on the outcomes of cyclic strain- and stress-controlled tests, the following conclusions can be drawn:

- Cyclic DSS and T_xSS tests are superior to CTX tests as they closely simulate stress states during vertical wave propagation.
- There is a good agreement between the numerically obtained liquefaction potential curves of Ottawa sand C-109 and those have been obtained from previous studies, the current study under cyclic stress-controlled DSS tests (constrained radial strain), and from alternative stress-controlled tests in T_xSS (where soil sample encased in latex membrane and confined in a triaxial chamber).
- The investigation of Diameter to height ratio (D/H) in T_xSS revealed that the D/H does not have a significant effect on the liquefaction resistance of Ottawa sand C-109 under cyclic strain-controlled tests.
- The comparison between CTX and T_xSS under cyclic stress-controlled condition showed that the liquefaction resistance obtained by CTX is higher than its counterpart in T_xSS and must be correlated by a correction factor, $C_r = [(1+2K_0)/3]$. This factor is applicable to correlate CTX sample prepared by wet tamping method in DSS or T_xSS.
- In contrast to the cyclic stress-controlled tests, soil samples suffer higher liquefaction resistance under T_xSS loading, in term of (γ-$N_{liq.}$), than in CTX under strain-controlled tests.

- A correlation factor between cyclic axial strain (in CTX) and cyclic shear strain (in T_xSS) has been obtained from cyclic strain-controlled tests. This correction factor is suggested to be a function of shear strain and soil type.

Furthermore, the proposed energy-based model was incorporated in $FLAC^{3D}$ platform to numerically simulate the cyclic behavior of Ottawa C-109 and BSP sands under cyclic triaxial (CTX) and the new combined triaxial simple shear (T_xSS) tests. The results show the capability of incorporating the energy concept numerically to capture the cyclic behavior in CTX and T_xSS tests under stress- or strain-controlled conditions. The numerical results reveal the effect of the end boundary condition on the cyclic behavior in CTX even when the height to diameter ratio crosses the order of 2. The end boundary significantly affects the axial strain distribution and consequently on the dissipated energy and pore water pressure. It is observed that the maximum bulge of the soil samples considered in this study and the generated pore water pressure ratios occurs within the middle third. Thus, premature liquefaction triggers in the middle third of the CTX sample and further cascades to the other zones. However, the numerical simulation of T_xSS reveals a relatively uniform distribution of shear stress and strain throughout soil samples and a relative equalization of the notional pore pressure throughout the soil sample. Moreover, the numerical and experimental results show that the liquefaction resistance is higher under T_xSS and DSS conditions than its counterparts under CTX. A strain-based correlation between CTX and T_xSS was proposed based on the cyclic strain-controlled tests. An equivalent factor was proposed to correlate the induced axial strains in stress- and strain-controlled CTX. The validity of this correlation was successfully verified by comparing the measured and estimated pore pressure from stress-controlled CTX results on the basis of the using pore pressure buildup as damage metric.

In the same manner, the result of undrained cyclic stress- and strain-controlled tests performed on reconstituted soil sample of Ottawa F-65 sand, a coupled energy-based pore pressure model was proposed. This model was validated in element-level comparing to T_xSS test results. There is a fairly well agreement between liquefaction resistance obtained from DSS, T_xSS and previously deduced from Bastidas (2016). On a large scale, the seismic response of layered soil deposit obtained from the proposed model was compared successfully with the results of Finn and centrifuge models. Numerically, 11 hypothetical level soil deposits with variant thickness and fundamental periods were employed to investigate the difference of seismic responses

between ENA and WNA. This difference was discussed in many important aspects of computed pore pressure, R_u, fundamental period, T_0, equivalent uniform stress cycles, N_{eq}, and the efficacy of the current liquefaction charts. In comparing the ENA and WNA earthquake responses, the following observations could be drawn.

- For cases studied, the semi-empirical simplified method and the incorporated N_{eq} method are valid for Western North America region when fundamental period of soil deposit is lower than 0.65 sec, over the studied range of T_0.
- The seismic response, in terms of $R_{u.max}$ and CSR_{max}, and the efficacy of the simplified method may be more related to the relative ratio between the fundament period of deposit and predominated period of the applied motion.
- Although the magnitude and $N_{eq-Seed}$ of the used earthquakes are almost equal, liquefaction was experienced under the WNA earthquake while under compatible earthquake not. This is inherently due to the difference of frequency content between both earthquakes.
- Adopting the energy concept in computing $N_{eq-energy}$ results in more accurate liquefaction estimation than Seed et al. procedure.
- The comparison between seismic responses shows that the assessing of liquefaction trigger based on the maximum induced CSR in the ENA is questionable.
- Using the current liquefaction resistance charts in term of $(N_1)_{60cs}$ in ENA liquefaction assessment results in conservative prediction.
- The cumulative damage represented in pore pressure buildup is more influenced by the shear strain amplitude rather than the stress amplitude.

8.4 Recommendation for future research (in English)

The current results presented in chapter 4 shows a promising step toward implementing the pore water pressure as damage metric. Thus, the damage hypothesis formula could reasonably capture the pore pressure buildup due to earthquake excitation and predicting the number of equivalent cycles. The damage hypothesis parameter (material parameter, r) can be simply calibrated from cyclic T_xSS tests. So, additional researches are required to validate the damage concept and calibrate the material parameter, r, for different type of soil addressing the influence of particle characteristics, fine content, relative density, and confining pressure. Moreover, investigate the assumption of the equality of $N_{eq\gamma}$ and $N_{eq\tau}$.

Based on the experimental T_xSS and CTX results presented in chapter 5, 6 and 7, a simple energy-based pore pressure model was proposed by simple calibration (α) and fitting (C1, C2 and C3) parameters. This model has predicted quite well the generated pore pressure and liquefaction resistance in element level and in performing one-dimensional site response analysis for dynamic centrifuge test of clean sand. However, elaborating more research work is still needed to generalize the proposed model to cover the following points:

- Introduce a correlation between calibration parameters (α) and physical properties of soil such as D_{50}.
- Incorporating the energy-concept in liquefaction design charts and the magnitude scaling factor.
- Set a link between liquefaction potential curves under stress- and strain-controlled tests based on the energy concept.
- Through the current study, all tests were prepared using the wet tamping method. This method was chosen as it allows controlling the pre-consolidation void ratio. However, other preparation methods are suggested to be used to generalize the obtained conclusions.
- Further work is still required to investigate the proposed correlation between axial and shear strain for different types of soil prepared at different relative density and confining pressure.

As a practical implementation of the proposed energy-based model, the difference of many important aspect of soil deposits pore water pressure, CSR, and N_{eq} response of Eastern and Western North America regions was discussed in chapter 7. The 1-D response analysis for 11 hypothetical deposits subjected to an earthquake compatible with Eastern region seismicity and another incompatible were performed. Although the current results interpreted the difference of seismic response, further benchmark framework is necessary to obtain straight forward and fundamental explanation about this difference and set conditions to use the current liquefaction design charts:

- The used soil deposits here are hypothetical. So, realistic soil deposits would be required to get better understanding of this difference.
- Much more ground motions have different magnitude would be required to investigate this difference.

- Incorporating the dissipation of pore water pressure in 1-D analysis and the densification of soil during and after earthquake shaking may affect the accuracy of the results.

LISTE DES RÉFÉRENCES

Abdellaziz, M., Hussien, M. N., Chekired, M., & Karray, M. 2019. Does long-term storage of clay samples influence their mechanical characteristics?. *Can Geotech J.*, (ja).

Abdellaziz, M. Karray, M. Hussien, M. Delisle, M-C. Locat, P. Ledoux, C. Mompin, R. Chekired, M. 2020. Experimental and numerical investigation of the Saint-Adelphe landslide after the 1988 Saguenay earthquake. *Can Geotech J.*, (ja).

Adams, J., and Halchuck., S. 2004. A review of NBCC 2005 seismic hazard results for Canada—the interface to the ground and prognosis for urban risk mitigation. In *57th Canadian Geotechnical Conference, Quebec, Canada.*

Airey, D. W., Budhu, M. and Wood, D. M. 1984. Some aspects of the behaviour of soils in simple shear. University of Cambridge Department of Engineering.

Airey D.W., & Wood D.M. 1986. Pore pressures in simple shear. Géotechnique, 37(1):25–35.

Almani, Z., A., Ansari, K., and Memon, N.,A., Liquefaction potential of silty sand in simple shear. *J. of Engineering & Technology*, Volume 32, No. 1, 2013.

Ambraseys, N. N. 1988. Engineering seismology. Earthquake Engrg. and Struct. Dynamics, 17, 1–105.

Amer, M. I., Kovacs, W. D., and Aggour, M. S. 1987. Cyclic Simple Shear Size Effects. *J. Geotech. Eng.*, 113(7), 693–707, https://doi.org/10.1061/(ASCE)0733-9410(1987)

Andersen, K. H., 1975. Research Project, Repeated Loading on Clay; Summary and Interpretation of Test Results. *Report, 74037-9,* Norwegian Geotechnical Institute, Oslo, Norway.

Andrus, R. D., and Stokoe, K. H., II 1997. Liquefaction resistance based on shear wave velocity. Proc., NCEER Workshop on Evaluation of Liquefaction Resistance of Soils, Nat. Ctr. for Earthquake Engrg. Res., State Univ. of New York at Buffalo, 89–128.

Andrus, R. D., and Stokoe, K. H., II 2000. 'Liquefaction resistance of soils from shear-wave velocity. *J. Geotech. and Geoenvir. Engrg.*, ASCE, 126(11), 1015–1025.

Annaki, M., and Lee, K.L. 1977. Equivalent uniform cycle concept for soil dynamics. *J. Geotech. Eng, Div.*, ASCE, 103(6): 549–564.

Arango, I. 1994. Methodology for liquefaction potential of sites east of the Rockies. Bechtel Corporation, San Francisco, Calif. Technical report.

Arango, I. 1996. Magnitude Scaling Factors for Soil Liquefaction Evaluations. *J. Geotech. Eng.*, 122(11), 929–936. https://doi.org/10.1061/(ASCE)0733-9410(1996)122:11(929)

Archambault-Alwin, X., James, M. Karray, M. and Chekired, M. 2017. The influence of back pressure on the cyclic resistance of saturated tailings using the triaxial-simple shear device. *In Proceedings of the 70th Canadian Geotechnical Conference*, 1-4 October, Ottawa ON. 8 p.

Ardoino, F., D. Bertalot, C. Piatti, and O. Zanoli. 2015. Effect of Pore Pressure Build-up on the Seismic Response of Sandy Deposits. *Frontiers in Offshore Geotechnics III--Meyer (Ed.). Taylor & Francis Group, London, UK* 978–1.

Asadzadeh, M., & Soroush, A. 2017. Macro- and micromechanical evaluation of cyclic simple shear test by discrete element method. *Particuology*, 31: 129–139. Elsevier B.V. doi:10.1016/j.partic.2016.05.015.

ASTM. 2011. Practices for cycle counting in fatigue analysis. ASTM standard E1049-85(2011)e1. ASTM, West Conshohocken, Pa. doi:10.1520/E1049-85R11E01.

ASTM-D5311-2013. Standard Test Method for Load Controlled Cyclic Triaxial Strength of Soil. ASTM International, West Conshohocken, Pa.

ASTM D6528-2017. Standard test method for consolidated undrained direct simple shear testing of fine grain soils. ASTM standard D6528-17. ASTM International, West Conshohocken, Pa. doi:10.1520/D6528-17.

Atkinson, G. M. 2009. Earthquake time histories compatible with the 2005 National building code of Canada uniform hazard spectrum. *Can. J. Civil Eng.*, 36(6), 991–1000. https://doi.org/10.1139/L09-044

Atkinson, G. M. 1989. Implications of Eastern Ground-Motion Characteristics for Seismic Hazard Assessment in Eastern North America. *Annals of the New York Academy of Sciences*, 558(1), 128–135.

Azeiteiro, R.J., Coelho, P.A., Taborda, D.M. and Grazina, J.C. 2017. Energy-based evaluation of liquefaction potential under non-uniform cyclic loading. *Soil Dyn. Earthquake Eng.*, 92:650–665. doi:10.1016/J.SOILDYN.2016.11.005.

Balla A. 1960. Stress Conditions in Triaxial Compression. . *J. Soil Mech. Foun. Div.*, 86(SM86),57–84.

Bashir, K., Bhaumik, C. and Saha, R. 2017. Assessment of Liquefaction Potential Using Empirical Equations and 1D Ground Response Analysis for Agartala City. In Indian Geotechnical Conference. 14-16 December 2017, 1-5.

Bastidas, A.M.P. 2016. Ottawa F-65 Sand Characterization. Ph.D. Thesis, Department of Civil Engineers, University of California, Davis.

Basu, D., Boga, M., Bhowmik, C., Saha, R. and Dey, A. 2017. Nonlinear GRA for assessing the liquefaction susceptibility of a typical subsurface profile at Agartala city. *Proc. of the 19th Int. Conf. on Soil Mech. and Geotech. Eng.*, Seoul 2017.

Baziar MH, Jafarian Y. 2007. Assessment of liquefaction triggering using strain energy concept and ANN model: Capacity Energy. *Soil Dyn. Earthquake Eng*., 27(12):1056–1072. doi:10.1016/J.SOILDYN.2007.03.007.

Beaty, M. H., and Byrne, P. 2000. A synthesized approach for predicting liquefaction and resulting displacements. *Proc. of the 12th World Conf. on Earthquake Engineering*, Auckland, New Zealand, Paper No. 1589.

Beaty MH and Byrne, PM. 2011. UBCSAND constitutive model: version 904aR. Documentation

report: UBCSAND constitutive model on Itasca UDM Web Site, February 2011.

Berghe Vanden, J.-F., Holeyman, A.& Dyvik, R. 2001 Comparison and modeling of sand behavior under cyclic direct simple shear and cyclic triaxial testing. In Prakash S. (ed.) Proc. 4th Int. Conf. on Recent Advances in Geotechnical Earthquake Engineering and Soil Dynamics, San Diego (ed. S. Prakash).

Berrill, J.B., R. O. Davis. 1985. Energy Dissipation and Seismic Liquefaction of Sands: Revised Model. *Soils Found.,* 25(2), 106–18.

Bhatia, S., J. Schwab, and I. Ishibashi. 1985. Cyclic Simple Shear, Torsional Shear and Triaxial, A Comparative Study. *Advances in the Art of Testing Soils under Cyclic Conditions* 232–54.

Bishop, A. W. & Henkel, D. J. 1962. .The measurement of soil properties in the triaxial apparatus. London: Arnold.

Bjerrum, L. and Landva, A. 1966. Direct Simple-Shear Test on a Norwegian Quick Clay. *Géotechnique*, 16(1), 1-20.

Booker, J.R., Rahman, M. S., Seed, H.B. 1976. A Computer Program for the Analysis of Pore Pressure Generation and Dissipation During Cyclic or Earthquake Loading. Rep. No. EERC 76-24, Earthquake Engineering Research Center, Univ. of California at Berkeley, California, USA.

Boulanger, R., Chan, C., Seed, H., Seed, R., and Sousa, J. 1993. A Low-Compliance Bi-Directional Cyclic Simple Shear Apparatus. *Geotech. Test. J.*, 16(1), 36–45. https://doi.org/10.1520/GTJ10265J.

Boulanger, R. W., and Idriss. M. I. 2014. CPT and SPT based liquefaction triggering procedures. *Report No. UCD/CGM.-14*1.

Boulanger, R.W., Seed, R.B., Chan, C.K., Seed, H.B., and Sousa, J. 1991. Liquefaction behavior of saturated sands under unidirectional and bi-directional monotonic and cyclic simple shear loading. University of California, Berkeley, Calif. Report No. UCB/GT/91-08.

Boulanger RW, Wilson DW, Idriss IM. 2012. Examination and reevaluation of SPT-based liquefaction triggering case histories. *J Geotech Geoenviron Eng*. 138(8):898–909.

Boulanger, R., and Ziotopoulou, K. 2015. A sand plasticity model for earthquake engineering applications, UCD/CGM-15(May), 1–114. https://doi.org/10.1016/j.soildyn.2013.07.006.

Boyland, N. & Long. M. 2009. Development of a direct simple shear apparatus for peat soils. *Geotech. Test. J.*, 32(2),126-138.

Bradshaw, A.S., Baxter, C.D. 2007. Sample preparation of silts for liquefaction testing. *Geotech. Test. J.*, 30 (4), 324–332.

Budhu, Muniram, 1984. On comparing simple shear and triaxial test results. *J. Geotech. Eng.*, 110(12), 1809-1814

Budhu, M. 1985. Lateral Stresses Observed in Two Simple Shear Apparatus. *J. Geotech. Eng.*, 111(6), 698–711.

Budhu, M. 1988. The mechanism of failure under cyclic simple shear strain. *Soil and Foundations*, 28(4): 119-129.

Budhu M, Britto A. 1987. Numerical analysis of soils in simple shear devices. *Soils Found.*, 27(2):31–41.

Byrne. P.M. 1991. A cyclic shear volume coupling and pore-pressure model for sand. Proc. of the 2nd International Conference on Recent Advances in Geotechnical Engineering and Soil Dynamics, St Louis, Mo. Paper 1.24 47–55.

Cabalar, A.F., Dulundu, K., and Tuncay, K. 2013. Strength of various sands in triaxial and cyclic direct shear tests. *Eng. Geol.*, 156: 92–102. https://doi:10.1016/j.enggeo.2013.01.011.

Campbell KW. 2013. An evaluation of eastern North American ground-motion models developed using the hybrid empirical method. *Bull Seismol Soc Am*, 104(1), 347–359.

Carroll, M. D., and Zimmie, T. F. 1979. Sample size effects using the NGI direct simple shear

apparatus. NSF Directorate for ASRA, Rensselaer Polytechnic Institute, Troy, N.Y.

Carter, L., Green, R., Bradley, B., and Cubrinovski, M. 2013. The influence of near-fault motions on liquefaction triggering during the Canterbury earthquake sequence. In Proceedings of the New Zealand – Japan Workshop on Soil Liquefaction during Recent Large-scale Earthquakes. pp. 51–61.

Casagrande, A. 1976. Liquefaction and Cyclic Deformation of Sands: A Critical Review. *Proc. of the Panamerican Conf. Soil Mech. and Found. Eng.,* (88):79–133.

Castro, Gonzalo, Steve J. Poulos. 1977. Factors Affecting Liquefaction and Cyclic Mobility. *J. Geotech. Eng. Div., ASCE,* 103(GT6), 501–516.

Castro, Gonzalo. 1975. Liquefaction and Cyclic Mobility of Saturated Sands. *J. Geotech. Eng. Div.,* ASCE, 101(GT6):551–569.

Castro G. 1987. On the behavior of soils during earthquakes-liquefaction. In: Cakmak A.S., editor. Soil dynamics and liquefaction. Amsterdam: Elsevier Science Publication. 169–204.

Cetin, K. O., Seed, R. B., Der Kiureghian, A., Tokimatsu, K., Harder, L. F., Kayen, R. E., and Moss, R. E. S. 2004. Standard Penetration Test-Based Probabilistic and Deterministic Assessment of Seismic Soil Liquefaction Potential. *J. Geotech. Geoenviron. Eng.*, 130(12), 1314–1340. https://doi.org/10.1061/(ASCE)1090-0241(2004)130:12(1314).

Cetin, K. O. and Bilge, H. T. (2012) 'Cyclic Large Strain and Induced Pore Pressure Models for Saturated Clean Sands', *J. Geotech. and Geoenvir. Engrg.*, 138(3), 309–323. doi: 10.1061/(ASCE)GT.1943-5606.0000631.

Chang, W.J. and Hong, M.L., 2008. Effects of clay content on liquefaction characteristics of gap-graded clayey sands. *Soils Found.*, *48*(1): 101-114.

Chang, W.J., Phantachang, T., and Ieong, W.M. 2016. Evaluation of size and boundary effects in simple shear tests with distinct element modeling. *J. GeoEngng.*, 11(3): 133–142. doi:10.6310/jog.2016.11(3).3.

Chang, W.J., Rathje, E.M., Stokoe, K.H., and Hazirbaba, K. 2007. In situ pore pressure generation behavior of liquefiable sand. *J. Geotech. Geoenviron. Eng.*, 133(8): 921–931. https://doi:10.1061/(ASCE)1090- 0241(2007)133:8(921).

Chehat, A., Hussien, M.N., Abdellaziz, M., Chekired, M., Harichane, Z., and Karray, M. 2019. Stiffness– and damping–strain curves of sensitive champlain clays through experimental and analytical approaches. Can. Geotech. J., 56(3): 364–377. doi:10.1139/cgj-2017-0732.

Chekired, M., Lemire, R., Karray, M., and Hussien, M.N. 2015. Experiment setup for simple shear tests in a triaxial cell: TxSS. *Proc. 68th Conf. Can. Geotech. Society*, Quebec City. Paper No. 365.

Chen, G., Zhao, D., Chen, W., & Juang, C. H., 2019. Excess Pore-Water Pressure Generation in Cyclic Undrained Testing. *J. Geotech. Geoenviron. Eng.*, *145*(7), 04019022. https://doi.org/10.1061/(ASCE)GT.1943-5606.0002057.

Chiaradonna A, Tropeano G, d'Onofrio A, Silvestri F (2016) A simplified method for pore pressure buildup prediction: from laboratory cyclic tests to the 1D soil response analysis in effective stress conditions. Pro. Eng 158:302–307. doi:10.1016/j.proeng.2016.08.446.

Cole E.R.L. 1967. The behaviour of soils in the simple shear apparatus. PhD thesis, University of Cambridge, Cambridge, UK.

Dabeet a., Wijewickreme D, Byrne PM. 2012. Simulation of cyclic direct simple shear loading response of soils using discrete element modelling. *Proc. 15th World conference on Earthquakes Engineering*.

Darendeli M. 2001. Development of a new family of normalized modulus reduction and material damping. Doctoral thesis, University of Texas

Davis RO, Berrill JB. Energy dissipation and seismic liquefaction in sands. 1982. Earthquake Eng. and Structural Dyn., 10:59–68.

DeAlba, P., Chan, C.K., and Seed, H.B. 1975. Determination of soil liquefaction characteristics by large-scale laboratory tests. *Earthquake Engineering Research Center*. University of California, Berkeley, Calif. Report No. EERC 75-14.

DeGroot, D. J., Germaine, J. T., and Ladd, C. C. 1994. Effect of Nonuniform Stresses on Measured DSS Stress-Strain Behavior. *J. Geotech. Eng.*, 120(5), 892–912, https://doi.org/10.1061/(ASCE)0733-9410(1994)120:5(892)

Dief, H. D. and Figueroa, J. L. 2007. Liquefaction assessment by the unit energy concept through centrifuge and torsional shear tests. *Can. Geotech. J*. 44, No. 11, 1286–1297.

Dobry, R., and Abdoun, T. (2015b). "Cyclic shear strain needed for liquefaction triggering and assessment of overburden pressure factor Kσ." *J. Geotech. and Geoenvir. Engrg.*, 10.1061/(ASCE)GT.1943-5606.0001342 .

Dobry, R, and Abdoun T. 2017. Recent Findings on Liquefaction Triggering in Clean and Silty Sands during Earthquakes. *J. Geotech. Geoenviron. Eng*. 143(10):04017077. HTTPS://DOI:10.1061/(ASCE)GT.1943-5606.0001778.

Dobry, R., and Vucetic, M. 1987. Dynamic properties and seismic response of soft clay deposits. *Proc. Int. Symposium on Geotech. Eng. of Soft Soils*, Mexico City. pp. 51–87.

Dobry, R., Ladd, R.S., Yokel, F.Y., Chung, R.M., and Powell, D. 1982. Prediction of pore water pressure buildup and liquefaction of sand during earthquakes by the cyclic strain method. Building Science Series 138. National Bureau of Standards, Washington, D.C.

Dobry, R. 1985. Liquefaction of Soils during Earthquakes, National Research Council (NRC), Committee on Earthquake Engineering, Report No. CETS-EE-001, Washington DC.

Dobry, R., Pierce, W.G., Dyvik, R., Thomas, G.E., and Ladd, R.S. 1985. Pore pressure model for cyclic straining of sand. *Rensselaer Polytechnic Institute*, Troy, New York.

Doherty, J. and Fahey, M. 2011. Three-dimensional finite element analysis of the direct simple shear test. *Comp. Geot.*, 38(7), 917-924. https://doi:10.1016/j.compgeo.2011.05.005.

Dowling, N. E. 1971. Fatigue failure predictions for complicated stress-strain histories (Vol. 337). Illinois University at Urbana Dept. of Theoretical and Applied Mechanics.

Dounias, G.T. & Potts, D.M. 1993. Numerical analysis of drained direct and simple shear tests. J. Geotech. Engng 119(12): 1870–1891.

Duncan, J.M., & Dunlop, P. 1969. Behavior of soils in simple shear tests. Proc. 7th International Conference on Soil Mechanics and Foundation, 101–109.

Dyvik, R., Berre, T., Lacasse, S., and Raadim, B. 1987. Comparison of truly undrained and constant volume direct simple shear tests. *Géotechnique*, 37(1), 3–10.

Dyvik, R., Zimmie, T. F. 1982, Lateral stress measurements during static and cyclic direct simple shear testing. *Proc. 3rd Int. Conf. on the Behavior of Off-Shore Structures*, Vol. 2, Massachusetts Institute of Technology Press, Cambridge, Mass., 363–372.

Éthier, Y., Karray, M., Lefebvre, G. 2011. Simulations of elastic wave propagation using FLAC to optimize the measurement of shear wave velocity in the laboratory. *Proc. 2nd int. FLAC/DEM Symposium, Continuum and distinct element numerical modeling in geomechanics*, Merbourne, Australia: 519-527.

Figueroa JL, Saada AS, Liang L, Dahisaria NM. 1994. Evaluation of Soil Liquefaction by Energy Principles. *J. Geotech. Eng.*, 120(9),1554–1569. https://doi:10.1061/(ASCE)0733-9410(1994)120:9(1554).

Filali, K., and Sbartai, B. 2017. A comparative study between simplified and nonlinear dynamic methods for estimating liquefaction potential. *J. of Rock Mechanics and Geotech. Eng.*, 9(5), 955–966.

Finn, W. D. 1985. Aspects of Constant Volume Cyclic Simple Shear. *presented at the Advances in the Art of Testing Soils Under Cyclic Conditions, Detroit, MI, ASCE*, New York, NY, 74–98.

Finn, W. D., Bransby, P. L., and Pickering, D. J. 1970. Effect of Strain History on Liquefaction of Sand. *J. Soil Mech. Found. Div.*, 96(6), 1917–1934.

Finn, W. D., Dennison J. Pickering, and Peter L. Bransby. 1971. Sand Liquefaction in Triaxial and Simple Shear Tests. *J. Soil Mech. Found. Div.* 97(SM4), 639-659.

Finn, W. D. L., Martin, G. R., and Lee, K. W. 1977. An effective stress model for liquefaction. *J. Geotech. Engrg Div.*, ASCE, 103(6), 517—533.

Franke, Eberhard, Manfred Kiekbusch, and Bernd Schuppener. 1979. "New Direct Simple Shear Device." *Geotech. T. J.* 2(4), 190–99.

Fu Q, Hashash YMA, Jung S, Ghaboussi J. 2007. Integration of laboratory testing and constitutive modelling of soils. *Comp. Geot*., 34(5):330–345. https://doi:10.1016/J.COMPGEO.2007.05.008.

Frost, J.D., and Park, J.-Y. 2003. A critical assessment of the moist tamping technique. *Geotech. T. J.*, 26(1): 57–70. https://doi:10.1520/GTJ11108J.

Frydman, S., Zeitlen, J.G. and Alpan, I., 1973. The membrane effect in triaxial testing of granular soils. Journal of Testing and Evaluation, 1(1), 37-41

Gamal El-Dean, D. 2007. Development of a new piezo-electric pulse testing device and soil characterization using shear waves. Ph.D. thesis, Université de Sherbrooke, Sherbrooke, Canada.

Ghali, M., Chekired, M., and Karray, M. 2019. Laboratory Simulator for Geotechnical Penetration Tests. *Geotechnical Testing Journal*-ASTM, 43(1), https://doi.org/10.1520/GTJ20170413.

Gheibi, E., and Bagheripour, M. H. 2011. Alterations of equivalent number of cycles in depth of soil profile. *Proc., 6th International Conference of Seismology and Earthquake Engineering* (SEE6), doi: 10.13140/RG.2.2.16539.67360

Ghosh, B., and Madabhushi, S. P. G. 2003. A numerical investigation into effects of single and multiple frequency earthquake motions. *Soil Dyn. and Earthquake Eng.*, 23(8), 691–704. https://doi.org/10.1016/j.soildyn.2003.07.004

Graizer, V. 2016. Ground-Motion Prediction Equations for Central and Eastern North America. *Bulletin of the Seismological Society of America*, 106(4), 1600–1612. https://doi.org/10.1785/0120150374

Green, R.A. 2001. Energy-based evaluation and remediation of liquefiable soils. Ph.D. dissertation, Virginia Polytechnic Institute and State University, Blacksburgh, Va. Available from http://scholar.lib.vt.edu/theses/available/etd-08132001-170900/.

Green, R.A., and Lee, J. 2006. Computation of number of equivalent strain cycles: a theoretical framework. *Geomechanics II*: Testing, Modeling, and Simulation, 156: 471–487. https://doi:10.1061/40870(216)31.

Green, R. A., J. K. Mitchell, and C. P. Polito. 2000. An Energy-Based Excess Pore Pressure Generation Model for Cohesionless Soils. *John Booker Memorial Symposium*. Developments in Theoretical Geomechanics, Rotterdam, The Netherlands. 383–390.

Green, R.A., and Terri, G.A. 2005. Number of equivalent cycles concept for liquefaction evaluations—revisited. *J. Geotech. and Geoenvir. Engrg.*, 131(4): 477–488. https://doi:10.1061/(ASCE)1090-0241(2005)131: 4(477).

Green, R. A. et al. 2019. Addressing limitations in existing "simplified" liquefaction triggering evaluation procedures: application to induced seismicity in the Groningen gas field. Bulletin of Earthquake Engineering. Springer Netherlands, 17:4539-4557. doi: 10.1007/s10518-018-0489-3.

Groholski DR, Hashash YMA, Kim B, Musgrove M, Harmon J, Stewart JP. 2016. Simplified model for small-strain nonlinearity and strength in 1D seismic site response analysis. *J. Geotech. and Geoenvir. Engrg.*;142(9):04016042. http://dx.doi.org/10.1061/(ASCE)GT.1943-5606.0001496.

Haldar, A., and Hochaimi. N.S. 1984. Uniform cycles in earthquake motions. *Proc. 8th World Conf. on Earthquake Eng.*, San Francisco, Calif. pp. 151–157.

Hancock, J., and Bommer, J.J. 2005. The effective number of cycles of earthquake ground motion. *Earthquake Eng. Structural Dyn.*, 34(6), 637– 664. https://doi:10.1002/eqe.437.

Hashash YMA. DEEPSOIL V 2.6, tutorial and user manual. 2002–2005. In: University of Illinois at Urbana-Champaign, Urbana Illinois, 2005.

Hashash YMA, Park, D. 2001. Non-linear one-dimensional seismic ground motion propagation in the Mississippi embayment. Engineering Geology, 62 (1-2), 185-206.

Hazirbaba K. Pore pressure generation characteristics of sand and silty sands: a strain approach. 2005. Dissertation presented for Ph.D. program to the faculty of Graduate School, University of Texas.

Hazirbaba, K., and Rathje, E.M. 2009. Pore pressure generation of silty sands due to induced cyclic shear strains. *J. geotech. geoenviron. eng.*, 135(12): 1892–1905. https://doi:10.1061/(ASCE)GT.1943-5606.0000147.

Humar, J. 2015. Background to some of the seismic design provisions of the 2015 National Building Code of Canada. *Can. J. Civil Eng.*, 42(11), 940–952. https://doi.org/10.1139/cjce-2014-0385.

Hussien, M. N., Karray, M., and Chekired, M. 2015. Evaluation of DSS test results on granular soils based on T_xSS results." *Proc. 68th Conf. Canadian of Geotech.*, Quebec, paper no. 393.

Iai, Susumu, Yasuo Matsunaga, and Tomohiro Kameoka. 1992. Strain space plasticity model for cyclic mobility. *Soils Found.* 32(2): 1-15. doi:10.3208/sandf1972.32.2_1.

Idriss, I. M. 1990. Response of soft soil sites during earthquakes. Proc., H. Bolton Seed Memorial Symp., Vol. 2, BiTech Publishers, Ltd., Vancouver, 273–290.

Idriss, I.M., and Sun, J.I. 1992. User's manual for SHAKE91: a computer program for conducting equivalent linear seismic response analyses of horizontally layered soil deposits, Department of Civil & Environmental Engineering, University of California, Davis, California.

Idriss, I. M. 1999. An update to the Seed-Idriss simplified procedure for evaluating liquefaction potential. *Proc. of TRB Worshop on New Approaches to Liquefaction, Pubbl. n. FHWA-RD-99-165, Federal Highway Administation*.

Idriss, I. M. and Boulanger, R. W. 2008. Soil liquefaction during earthquakes. MNO-12. Oakland, CA, USA: Earthquake Engineering Institute.

Ishibashi, I., Makoto Kawamura, and SK Bhatia. 1985. Effect of Initial Shear on Cyclic Behavior of Sand. *Geotech. J. Eng.* 111(12):1395–1410. http://ascelibrary.org/doi/abs/10.1061/(ASCE)0733-9410(1985)111:12(1395).

Ishibashi, I., Sharif and M. A., and Cheng, W. L. 1982. The Effect of Soil Parameters on Pore Pressure Rise and Liquefaction, *Soil and Foundation*, 22(1), 39–48

Ishibashi, I., Sherif, M. A. and Tsuchiya, C. 1977. Pore-pressure rise mechanism and soil liquefaction. *Soil and Foundations*., 17(2), 17–27.

Ishihara, K. 1996. Soil behaviour in earthquake geotechnics. The Oxford engineering science series, No. 46, Oxford, U.K.

Ishihara, K., and Nagase, H. 1988. Multi-directional irregular loading tests on sand. *Soil Dyn. Earthquake Eng.*, 7(4): 201–212. doi:10.1016/ S0267-7261(88)80004-6.

Ishihara, Kenji, and Sang Li. 1972. Liquefaction of Saturated Sand in Triaxial Torsion Shear Test. *Soils Found., Japanese Society of Soil Mechanics and Foundation Engineering* 12(2):19–39.

Itasca Consulting Group, Inc. 2010. Fast Lagrangian analysis of continua in 2-dimensions. Version 6.0 [manual]. Itasca, Minneapolis, Minn.

Jacob, K. H. 1991. Seismic Hazard in New York City Area. Seminar Notes for the Practical Aspects of Earthquake Engineering, Architecture, and Construction, New York City, May 23, 1991.

Jafarian Y, Towhata I, Baziar MH, Noorzad A, Bahmanpour A. 2012. Strain energy based evaluation of liquefaction and residual pore water pressure in sands using cyclic torsional shear experiments. *Soil Dyn. Earthquake Eng.*, 35:13–28. doi:10.1016/J.SOILDYN.2011.11.006.

Juang, C.H., Yuan, H., Lee, D.H., and Lin, P.S. 2003. Simplified cone penetration test-based method for evaluating liquefaction resistance of soils. *J. Geotech. and Geoenvir. Engrg.*, 129(1): 66–80. doi:10.1061/ (ASCE)1090-0241(2003)129:1(66).

Kang, Xin, Louis Ge, Kuang-Tsung Chang, and Annie On-Lei Kwok. 2015. Strain-Controlled Cyclic Simple Shear Tests on Sand with Radial Strain Measurements. *J. Mat. Civil Eng.* 28(4):04015169.

Karray, M., Chekired, M. Triaxial Simple Shear test: TxSS. 2019. *Proc. 7th Int. Symposium on Deformation Characteristics of Geomaterials (IS-Glasgow 2019).* Paper No. 02014: 1-6.

Karray, M., Lefebvre, G. and Ethier, Y. 2011. Relevés MMASW et évaluation du potentiel de liquéfaction au site du couvent de Baie-Saint-Paul. Rapport soumis aux Les Petites Franciscaines de Marie, Géowave Inc., Sherbrooke, Québec, Canada, p. 78.

Karray, Mourad, Mahmoud N. Hussien, and Mohamed Chekired. 2015. "Evaluation of Compatibility between Existing Liquefaction Charts in Eastern Regions of North America." *Proc. 68e Conf. Can. de Géotech. et 7e Conf. Can. Sur Le Pergélisol, 20 Au 23 Septembre 2015, Québec, Québec.* (Sept. 2015).

Karray, M., Ben Romdhan, M., Hussien, M. N., and Éthier, Y. 2015. Measuring shear wave velocity of granular material using the piezoelectric ring-actuator technique (P-RAT) *Can. Geotech. J.*, 52:1302–1317.

Karray, M. and Wali, S. 2013. Mesure de la vitesse de cisaillement au laboratoire des enrochements de la romaine II - Etablissement de relations entre le module oedometrique et le module de cisaillement. Geo-13-02, Rapport soumis.

Kayen R, Moss RES, Thompson EM, Seed RB, Cetin KO, Der Kiureghian A, Tanaka Y, Tokimatsu K. 2013. Shear-wave velocity–based probabilistic and deterministic assessment of seismic soil liquefaction potential. *J. Geotech. and Geoenvir. Engrg.*139(3):407–19.

Kazama, M., Yamaguchi, A., and Yanagisawa, E. 2000. Liquefaction resistance from a ductility viewpoint. *Soils Found.*, 40(6): 47–60. doi:10.3208/ sandf.40.6_47.

Khashila MM, Hussien MN, Karray M, Chekired M. 2018. Use of pore pressure build-up as damage metric in computation of equivalent number of uniform strain cycles. *Can Geotech J.*, 55(4): 538-550. https://doi.org/10.1139/cgj-2017-0231.

Khashila MM, Hussien MN, Karray M, Chekired M. 2020. Analysis of dynamic soil behavior under triaxial and simple shear modes. *Comp. Geotech.* In Revision.

Kjellman, W., 1951, Testing the Shear Strength of Clay in Sweden. *Géotechnique*, 2 (3): 225–232, https://doi.org/10.1680/geot.1951.2.3.225.

Kokusho, T. 2013. Liquefaction Potential Evaluations: Energy-Based Method versus Stress-Based Method', *Canadian Geotech. J.*, 1099(September), p. 130912073701005. doi: 10.1139/cgj-2012-0456.

Kokusho, T. and Mimori, Y. (2015) 'Liquefaction potential evaluations by energy-based method and stress-based method for various ground motions', *Soil Dynamics and Earthquake Engineering*. Elsevier Ltd, 75, pp. 130–146. doi: 10.1016/j.soildyn.2015.04.002.

Kondner R.L., Zelasko J.S. (1963). "A hyperbolic stress-strain formulation for sands". Proc. 2nd Pan-American Conference on Soil Mechanics and Foundations Engineering, Brazil, I: 289-324.

Konstadinou M, Georgiannou VN. 2014. Prediction of pore water pressure generation leading to liquefaction under torsional cyclic loading. *Soils and Foundations*, 54(5):993–1005. doi:10.1016/j.sandf.2014.09.010.

Konstadinou, M., and V. N. Georgiannou. 2013. Cyclic behaviour of loose anisotropically consolidated Ottawa sand under undrained torsional loading. *Géotechnique*, 63.13: 1144-1158.

Kovacs, W. D,, and Leo, E. 1981. Cyclic simple shear of large scale samples: Effects of diameter to height ratio." *Int. Conf. on Recent Advances in Geotech. Earthquake Eng.*, Univ. of Missouri, Rolla, Mo., 897-904.

Konstadinou, M., and V. N. Georgiannou. 2014. Prediction of pore water pressure generation leading to liquefaction under torsional cyclic loading. *Soils Found.* 54 (5): 993-1005.

Kramer, S.L. 1996. *Geotechnical earthquake engineering*. Chapter 9: Liquefaction. Prentice Hall. pp. 348–422.

Kuhlemeyer, R. L., and Lysmer, J. 1973. Finite element method accuracy for wave propagation problems. *J. Soil Mech. Found Div.* 99.

Kuhlemeyer, R. L., and Lysmer, J., "Finite Element Method Accuracy for Wave Propagation Problems," Journal of the Soil Mechanics and Foundations Division, ASCE, Vol. 99, No. SM5, Proc. Paper 9703, May, 1973, pp. 421–427.93qJ. Soil Mech. and Found. Div.

Ladd, C. C. and Edgers, L. 1972. Consolidated-undrained direct-simple shear tests on saturated clays. MIT Research Report R72-82, Massachusetts Institute of Technology.

Ladd, R.S. 1978. Preparing test specimens using under compaction. *Geotech. T. J.*, *1*(1), 16-23.

Ladd, R.S., Dobry, R., Dutko, P., Yokel, F.Y. & Chung, R.M. 1989. Pore water pressure buildup in clean sands because of cyclic straining. *Geotech. Testing* J., GTJODJ, 12(1), 77-86.

Lasley, S.J., Green, R.A. & Rodriguez-Marek, A. 2016. New Stress Reduction Coefficient Relationship for Liquefaction Triggering Analyses', *J. Geotech. and Geoenvir. Engrg.*, 142(11), p. 06016013. doi: 10.1061/(ASCE)GT.1943-5606.0001530.

Lasley, S.J., Green, R.A., and Rodriguez-Marek, A. 2017. Number of equivalent stress cycles for liquefaction evaluations in active tectonic and stable continental regimes. *J. Geotech. and Geoenvir. Engrg.*, 143(4). doi:10.1061/(ASCE)GT.1943-5606.0001629.

Law, K. T., Y. Cao, and G. He. 1990. An Energy Approach for Assessing Seismic Liquefaction Potential. Canadian Geotechnical Journal 27 (3):320–329. doi:10.1139/t90-043.

Lee KL. 1978. End restraint effects on undrained static triaxial strength of sand. *J. Geotech. Eng. Div., ASCE.* 104 (GT6):687-704.

Lee, K.L., and Chan, K. 1972. Number of equivalent significant cycles in strong motion earthquakes. *Proc. Int. Conf. on Microzonation for Safer Construction Research and Application*, University of Washington. 2. 609–627.

Lefebvre, G. and Serge, M. 1987. Cyclic shear strength of a loose glacial till. *Canadian Geotech J.*, 25(2). 401–407

Lenart, S. 2008. The use of dissipated energy at modeling of cyclic loaded saturated soils. *Earthquake Engineering: New Research. Nova Science Publishers*. Chapter 8. doi:10.3109/10903127.2014.942478.

Li, X. S., Wang, Z. L., and Shen, C. K. (1992). "SUMDES: A nonlinear procedure for response analysis of horizontally-layered sites subjected to multi-directional earthquake loading." Dept. of Civil Engineering, Univ. of California, Davis, CA.

Liang, L., Figueroa, J. L., and Saada, A. S. 1995. Liquefaction under random loading: unit energy approach. *J. Geotech. Engrg.*, ASCE, 121(11), 776–781.

Liao, S. S. C., and Whitman, R. V. 1986. Overburden correction factors for SPT in sand. *J. Geotech. Eng.*, 112(3), 373–377.

Liu, A.H., Stewart, J.P., Abrahamson, N.A., and Moriwaki, Y. 2001. Equivalent number of uniform stress cycles for soil liquefaction analysis. *J. Geotech. and Geoenvir. Engrg.* 127(12): 1017–1026. doi:10.1061/(ASCE)1090-0241(2001)127:12(1017).

Liu, C., and Xu, J. 2015. Experimental study on the effects of initial conditions on liquefaction of saturated and unsaturated sand. Int. *J. Geomech.,* 15(6). doi:10.1061/(ASCE)GM.1943-5622.0000350.

Lucks, A., Christian, J., Brandow, E. and Höeg, K. (1972). Stress conditions in NGI simple shear test. *J. Soil Mech. Found Div.*, 98(1): 155–160.

Madabhushi, S. P. G. 1994. Natural frequency of a horizontal soil layer Part II: Saturated sand bed. Technical report TR273. Cambridge Department of Engineering, University of Cambridge.

Mandokhail, S.U.J., Park, D. and Yoo, J.K., 2017. Development of normalized liquefaction resistance curve for clean sands. *Bulletin of earthquake engineering*, *15*(3), 907-929.

Mao, X. and M. Fahey. 2003. Behaviour of Calcareous Soils in Undrained Cyclic Simple Shear. *Géotechnique* 53(8):715–27.

Martin, G.R., Finn, W.D.L., and Seed, H.B. 1975. Fundamentals of liquefaction under cyclic loading. *J. Geotech. Eng.*, 101(5): 423–438.

Masing, G. 1926. Eigenspannungen und Verfestigung Beim Messing, Proceedings of 2nd International Congress on Applied Mechanics, Zurich.

Matasovic, N., and Vucetic, M. 1993. Cyclic characterization of liquefiable sands. *J. Geotech. Eng.*, 119(11): 1805– 1822. doi:10.1061/(ASCE)0733-9410(1993)119:11(1805).

Medzvieckas J, Dirgėlienė N, Skuodis Š. Stress-strain States Differences in Specimens during Triaxial Compression and Direct Shear Tests. Procedia Engineering. Modern Building Materials, Structures and Techniques, MBMST 2017. Amsterdam: Elsevier Ltd. 2017; 172: 739–745. doi:10.1016/J.PROENG.2017.02.094.

Miner, M.A. 1945. Cumulative damage in fatigue. Transactions of the American Society of Mechanical Engineers, 67, 159–164.

Moreno-Torres, O., Hashash, Y.M.A., and Olson, S.M. 2010. A simplified coupled soil-pore water pressure generation for use in site response analysis. In Advances in Analysis, Modeling and Design. *Proc. GeoFlorida 2010 Conf*. pp. 3080–3089. doi:10.1061/41095(365)314.

National Research Council. 1985. Liquefaction of soils during earthquakes. National Academy Press, Washington, D.C., p. 240.

Nemat-Nasser, S., and Shokooh, A. 1979. A unified approach to densification and liquefaction of cohesionless sand in cyclic shearing. *Can. Geot. J.*, 16(4): 659–678. doi:10.1139/t79-076.

Newmark NM. 1959. A method of computation for structural dynamics. *J Eng. Mech. Div.*85:67–94.

Ni, S.-D., Siddharthan, R. V, and Anderson, J. G. 1997. Characteristics of Nonlinear Response of Deep Saturated Soil Deposits. *Bulletin of the Seismological Society of America*. 87(2). 342-355.

Norambuena, R, Tsaparli, V., Kontoe, S., Taborda, D. and Potts, D. 2019. The effect of irregular seismic loading on the validity of the simplified liquefaction procedures. *Obras y Proyectos*, 25,

42-50. ISSN 0718-2813.

NRC. 2005. National Building Code of Canada. National Research Council of Canada, Ottawa, Ont.

Mulilis, J.P., Seed, H.B., Chan, C.K., Mitchell, J.K., and Arulanandan, K. 1977. Effect of sample preparation on sand liquefaction. *J. Geotech. Eng. Div., ASCE*, 103(G2): 91–108.

Okada N, Nemat-Nasser S. 1994. Energy dissipation in inelastic flow of saturated cohesionless granular media. *Géotechnique*,44(1):1–19. http://dx.doi.org/10.1680/geot.1994.44.1.1.

Palmgren, A. 1924. Die lebensdauer von kugella geru. ZVDI, 68(14): 339–341.

Pan, K., Yang, Z. X. 2017. Evaluation of the Liquefaction Potential of Sand under Random Loading Conditions: Equivalent Approach Versus Energy-Based Method, *J. Earthquake Eng.*, DOI: 10.1080/13632469.2017.1398693.

Park, J.Y. 1999. A critical assessment of moist tamping and its effect on the initial and evolving structure of dilatant triaxial specimens. Ph.D. dissertation, Georgia Institute of Technology.

Park, T., Park, D., and Ahn, J.-K. 2015. Pore pressure model based on accumulated stress. *Bulletin of Earthquake Engineering*, *13*, 1913–1926. https://doi.org/10.1007/s10518-014-9702-1.

Park TK, Silver ML. 1975. Dynamic Triaxial and Simple Shear Behavior of Sand. *J. Geotech. Geoenviron. Eng.*, 101(GT6):513–29.

Peacock, W.H., and Seed, H. 1968. Sand liquefaction under cyclic loading simple shear conditions. *J. Soil Mech. Found. Div., ASCE*, 94(SM3): 689–708.

Phillips C, Hashash YMA. 2009. Damping formulation for nonlinear 1D site response analyses. *Soil Dyn Earthq Eng* 29:1143–1158. https://doi.org/10.1016/j.soildyn.2009.01.004

Polito, C.P. 1999. The effects of non-plastic and plastic fines on the liquefaction of sandy soils. Ph.D. dissertation, Virginia Polytechnic Institute and State University, Blacksburg, Va.

Polito, C.P., Green, R.A., and Lee, J. 2008. Pore pressure generation models for sands and silty soils subjected to cyclic loading. *J. Geotech. and Geoenvir. Engrg.*, 134(10): 1490–1500. doi:10.1061/(ASCE)1090- 0241(2008)134:10(1490).

Popescu, R. 2002. Finite element assessment of the effects of seismic loading rate on soil liquefaction. *Can. Geot. J.*, 39(2), 331–344. https://doi.org/10.1139/t01-098

Porcino, D. D., Tomasello, G., and Diano, V. 2018. Key factors affecting prediction of seismic pore water pressures in silty sands based on damage parameter. *Bulletin of Earthquake Engineering*, 16(12), 5801–5819. https://doi.org/10.1007/s10518-018-0411-z.

Prevost, J.-H., & Høeg, K. 1976. Reanalysis of simple shear soil testing. *Can. Geotech. J.*, 13(4): 418–429. doi:10.1139/t76-042.

Pyke, R. 1979. Nonlinear soil models for irregular cyclic loadings, Journal of Geotechnical Division ASCE, Vol. 105(GT6), pp. 715-726

Rahman, M.M., Baki, M.A.L., and Lo, S.R. 2014. Prediction of undrained monotonic and cyclic liquefaction behavior of sand with fines based on the equivalent granular state parameter. *Int. J. Geomech.*, 14(2): 254–266. doi:10.1061/(ASCE)GM.1943-5622.0000316.

Ramirez, J., Badanagki, M., Rahimi Abkenar, M., ElGhoraiby, M. A., Manzari, M. T., Dashti, S., Liel, A. 2017. Seismic performance of a layered liquefiable site: validation of numerical simulations using centrifuge modeling. *Geotechnical Frontiers*, 332–341. https://doi.org/10.1061/9780784480489.033.

Ramirez, J., Barrero, A. R., Chen, L., Dashti, S., Ghofrani, A., Taiebat, M., and Arduino, P. 2018. Seismic performance of a layered liquefiable site: validation of numerical simulations using centrifuge modeling. *J. Geotech. and Geoenvir. Engrg.*, 144(10), 04018073. https://doi.org/10.1061/(ASCE)GT.1943-5606.0001947.

Rathje, E. M., Abrahamson, N. A., and Bray, J. D. (1998). "Simplified frequency content estimates of earthquake ground motions." *J. Geotech. and Geoenvir. Engrg.*, ASCE, 124(2), 150-159.

Rathje EM, Chang WJ, Stokoe II KH (2004) Development of an in situ dynamic liquefaction test.

ASTM Geotechnical Testing Journal, 28(1).

Ravishankar, B. V., Sitharam, T. G., & Govindaraju, L. 2005. "Dynamic properties of Ahmedabad sands at large strains." *In Proceedings, Indian Geotechnical Conference, Ahmedabad, INDIA*: 369-372.

Richart, F.E., and Newmark, N. 1948. An hypothesis for determination of cumulative damage in fatigue. *ASTM Proceedings*, 48: 767–800.

Robertson, P. K., Woeller, D. J., and Finn, W. D. L. 1992. Seismic cone penetration test for evaluating liquefaction potential under cyclic loading. *Can. Geotech. J.*, 29(4), 686–695. https://doi.org/10.1139/t92-075.

Robertson, P. K., and Wride, C. 1998. Evaluating cyclic liquefaction potential using the cone penetration test. *Can. Geot. J.*, 35(3), 442–459. https://doi.org/10.1139/t98-017.

Rodriguez-Arriaga E, Green RA. 2018. Assessment of the cyclic strain approach for evaluating liquefaction triggering. *Soil Dyn. Earthquake Eng*. 113:202–214. doi:10.1016/J.SOILDYN.2018.05.033.

Rollins, K.M., Evans, M.D., Diehl, N.B. and III, W.D.D. 1998. Shear modulus and damping relationships for gravels. *J. Geotech. Geoenviron. Eng.*, *124*(5), 396-405.

Ronald D. Andrus and Kenneth H. Stokoe II. 2000. Liquefaction resistance of soils from shear-wave velocity. *J. Geotech. and Geoenvir. Engrg.*, 126(11), 1015–1025.

Roscoe KH. 1953. An apparatus for the application of simple shear to soil samples. *Proc. 3rd int. Con. on soil mechanics*, Zurich, vol 1, 186–191.

Rossato G, Simonini P. 1991. Stress–strain behaviour of sands in triaxial and direct simple shear tests. Can. Geot. J.,28:276–81. doi:10.1139/t91-033.

Roww P. W. Barden L. 1964. Importance of free ends in triaxial testing. J. Soil Mech. Found. Eng. Div. ASCE, vol. 90, 1-27

Saada F. C., AS, Townsend. State of the art: laboratory strength testing of soils. *Lab. Shear strength soil, ASTM STP 740.* 1981:7–77.

Schnabel, P.B., Lysmer, J. and Seed, H.B., 1972, SHAKE - A computer program for earthquake analysis of horizontally layered sites, Earthquake Engineering Research Center, University of California, Berkeley, *EERC Report No. EERC 72-12*.

Scott RF. 1963. Principles of soil mechanics. Addison-Wesley, Reading, Mass.

Seed, H.B. 1979. Considerations in the Earthquake-Resistant Design of Earth and Rockfill Dams. *Géotechnique* 29(3): 215-263.

Seed, H. B. 1979. Soil liquefaction and cyclic mobility evaluation for level ground during earthquakes. *J. Geotech. Engrg. Div.*, ASCE, 105(2), 201–255.

Seed, H.B. 1983. Earthquake-resistant design of earth dams. Proc. Symposium on Seismic Design of Earth Dams and Caverns, Philadelphia, Pa., 16–20 May 1983. Edited by T.R. Howard. American Society of Civil Engineers, New York. 41–64.

Seed, B., and Lee, K.L. 1966. Liquefaction of saturated sands during cyclic loading. *J. Geotech. and Geoenvir. Engrg.*, 92(6): 105–134.

Seed, H.B., and Idriss, I.M. 1971. Simplified procedure for evaluating soil liquefaction potential. *J. Soil Mech. Found. Div., ASCE,* 97(9): 1249–1273.

Seed, H.B., Idriss, I.M., Makdisi, F., and Banerjee, N. 1975a. Representation of irregular stress time histories by equivalent uniform stress series in liquefaction analysis. Earthquake Engineering Research Center, College of Engineering, University of California, Berkeley, Calif. Report No. EERC 75-29.

Seed, H. B., and Idriss, I. M. 1982. Ground motions and soil liquefaction during earthquakes. Earthquake Engineering Research Institute Monograph, Oakland, California.

Seed, H.B., Martin, P.P., and Lysmer, J. 1975b. The generation and dissipation of pore water pressures during soil liquefaction. Earthquake Engineering Research Center, College of Engineering, University of California, Berkeley, Calif. Report No. EERC 75-26.

Seed, H. B., and Idriss, I. M. (1969). "Rock motion accelerograms for high magnitude earthquakes." *EERC Report No. 69-7*, Earthquake Engineering Research Center, University of California at Berkeley

Seed, H. B., and Idriss, I. M. (1982). "Ground motions and soil liquefaction during earthquakes." Earthquake Engineering Research Institute Monograph, Oakland, Berkeley, Calif.

Seed, H.B., Idriss, I.M., and Arango, I. 1983. Evaluation of liquefaction potential using field performance data. *J. Geotech. Eng.*, 109(3): 458–482. doi:10.1061/(ASCE)0733-9410(1983)109:3(458).

Seed, H. B., Peacock, W. H. 1971. Test Procedures for Measuring Soil Liquefaction Characteristics. *J. Soil Mech. Foundations Div*. ASCE. 97(SM9), 1249-1273.

Seed, H. B., Tokimatsu, K., Harder, L. F., and Chung, R. M. 1985. The influence of SPT procedures in soil liquefaction resistance evaluations. *J. Geotech. Engrg.*, ASCE, 111(12), 1425–1445.

Shelley EO, Mussio V, Rodriguez M, Chang JGA (2015). Evaluation of soil liquefaction from surface analysis. *Geofísica Int* 54(1), 95–109

Shen C.K. Sadigh K. and Herrmann L.R. 1978. An analysis of NGI simple shear apparatus for cyclic soil testing. *ASTM Dynamic geotechnical testing*, STP 654, 148-162

Sibley ELD, Olson SM, Polito CP. 2017. A Framework for Evaluating the Effects of Drained Cyclic Preshearing on the Liquefaction Resistance of Ottawa Sand. *Geotech. Front. 2017*, Reston, VA: American Society of Civil Engineers.:131–40. doi:10.1061/9780784480489.014.

Silver, M. L., and Park, T.E.D.K. 1976. Liquefaction potential evaluated from cyclic strain-controlled properties tests on sands. *Soils Found.*, 16(3): 51– 65. doi:10.3208/sandf1972.16.3_51.

Silver, M. L., Fumio Tatsuoka, and Apichart Phukunhaphan. 1980. Cyclic Undrained Strength Of Sand By Triaxial Test And Simple Shear Test. *Proc.7th World Conf. on Earthquake Engineering* 281–88.

Silver, M.L., and Seed, H.B. 1971. Deformation characteristics of sands under cyclic loading. *J. Soil Mech. Found. Div.,* ASCE, 97(8): 1081–1098.

Sitharam, T.G., Ravishankar, B.V., and Patil, S.M. 2012. Liquefaction and pore water pressure generation in sand: cyclic strain controlled triaxial tests. *Int. J. Geotech. Earthquake Eng*., 3(1): 57–85. doi:10.4018/IJGEE.2012010104.

Stroud, M. A. 1971. The behavior of sand at low stress levels in the simple shear apparatus. Ph.D. thesis, University of Cambridge, Cambridge, United Kingdom, 296p.

Skempton, A. W. 1954. "The Pore-Pressure Coefficients A and B." *Geotechnique* 4(4):143–47.

Sykora, D. 1987. Examination of existing shear wave velocity and shear modulus correlations in soils. US Army WES. Miscellaneous Paper GL-87-22, Vicksburg, MS.

Sze, H.Y., and Yang, J. 2014. Failure modes of sand in undrained cyclic loading: impact of sample preparation. *J. Geotech. and Geoenvir. Engrg.*, 140(1): 152–169. doi:10.1061/(ASCE)GT.1943-5606.0000971.

Talaganov, K.V. 1996. Stress-strain transformations and liquefaction of sands. *Soil Dyn. Earthquake Eng.*, 15(7): 411–418. doi:10.1016/0267- 7261(96)00024-3.

Tatsuoka, F., Kenzo Ochi, Shinji Fujii, and Masahiro Okamoto. 1986. Cyclic Undrained Triaxial and Torsional Shear Strength of Sands for Different Sample Preparation Methods. *Soils Found.,* 26(3):23–41.

Tatsuoka, F., Muramatsu, M., and Sasaki, T. 1982. Cyclic undrained stress-strain behavior of dense sands by torsional simple shear test. *Soils Found.*, 22(2): 55–70. doi:10.3208/sandf1972.22.2_55.

Tokimatsu, K., and Seed, H.B. 1987. Evaluation of settlements in sands due to earthquake shaking. *J. Geotech. Eng.*, 113(8): 861–878. doi:10.1061/(ASCE)0733-9410(1987)113:8(861).

Tokimatsu, K., Uchida, A. 1990. Correlation between liquefaction resistance and shear wave velocity. *Soils Found., Japanese Society of Soil Mechanics and Foundation Engineering*, 30(2), 33–42.

Vanden Berghe, J. F., Alain Holeyman, and Rune Dyvik. 2001. Comparison and Modeling of Sand Behavior Under Cyclic Direct Simple Shear And Cyclic Triaxial Testing. *Int. Conf. on Recent* Advances in Geotechnical Earthquake Engineering and Soil Dynamics. Paper no. 34.

Vaid, Y. P., and Chern, J. C. 1985. Cyclic and monotonic undrained response of saturated sands. Advances in the art of testing soils under cyclic conditions, ASCE Annual Convention, Detroit, Mich., 120–147.

Vaid, YP and Finn, WDL. 1979. Static Shear and Liquefaction Potential. *J. Geotech. Eng. Div., ASCE*, 105(GT10), 1233–1246.

Vaid, Y. P., Negussey, D., and Zergoun, M. 1987. A Stress- and Strain-Controlled Monotonic and CycBc Loading System. *Advanced Triaxial Testing of Soil and Rock, ASTM STP 977,* Robert T. Donaghe, Ronald C. Chaney, and Marshall L. Silver, Eds., American Society for Testing and Materials, Philadelphia, 119-131.

Vaid, Y. P. and S. Sivathayalan. 1996. Static and Cyclic Liquefaction Potential of Fraser Delta Sand in Simple Shear and Triaxial Tests. *Can. Geotech. J.* 33(2):281–89.

Vaid, Y.P., Stedman, J.D., and Sivathayalan, S. 2001. Confining stress and static shear effects in cyclic liquefaction. *Can Geotech J*.: 38(3): 580–591. doi:10.1139/t00-120.

Verma, P. and D. Wijewickreme, D. 2020. Effect of Different Modes of Lateral Boundary Constraints of the Direct Simple Shear (DSS) Device under Monotonic and Cyclic Shear Loading. *Geotechnical Testing Journal.* 43 (in press). https://doi.org/10.1520/GTJ20180357.

Vipulanantham, M. 2011. Initial stress state and stress history effects on liquefaction susceptibility of sands. MSc Thesis, Carleton University, Ottawa, Canada.

Vucetic, M. 1994. Cyclic threshold shear strains in soils. J. Geotech. Eng., 120(12): 2208–2228.

Vucetic, M., and Dobry, R. 1988. Cyclic triaxial strain controlled testing of liquefiable sands. *In Advanced triaxial testing of soil and rock. ASTM STP 977*. Edited by R.T. Donaghe, R.C. Chancy, and M.L. Silver. American Society for Testing and Materials, Philadelphia, Pa. pp. 475–485.

Vucetic, M. and Lacasse, S. 1982. Specimen size effect in simple shear test. *J. Geotech. Eng. Div., 108*(12), 1567-1585.

Wang, B., Popescu, R. and Prevost, J.H. 2004. Effects of boundary conditions and partial drainage on cyclic simple shear test results—a numerical study. *Int. J. Numer. Anal. Methods Geomech.* 28(10),1057–1082

Wer, R., and Dobry, R. 1982. The equivalent number of cycles of recorded accelerograms for soil liquefaction studies. M.Sc. thesis, Rensselaer Polytechnic Institute, Troy, New York.

Whitman R V., Healy KA. 1962. The Response of Soils to Dynamic Loadings. *Report 9. Shearing Resistance of Sands During Rapid Loadings.*

Wijewickreme, D., Sriskandakumar, S. and Byrne, P., 2005. Cyclic loading response of loose air-pluviated Fraser River sand for validation of numerical models simulating centrifuge tests. *Can. Geotech. J.*, 42(2), 550–561.

Woods, Richard D. 1978. Measurement of Dynamic Soil Properties. in *From Volume I of Earthquake Engineering and Soil Dynamics-Proceedings of the ASCE Geotechnical Engineering Division Specialty Conference, Pasadena, California.*

Wu Z, Dano C, Hicher PY, Yin Z. 2018. Estimating normal effective stress degradation insand under undrained simple shear condition. *Eur. J. Environ. Civ. Eng.*,1 20. https://doi.org/10.1080/19648189.2018.1521750.

Xenaki, V.C., and Athanasopoulos, G.A. 2003. Liquefaction resistance of sand-silt mixtures: an experimental investigation of the effect of fines. *Soil Dyn. Earthquake Eng*., 23(3): 183–194. doi:10.1016/S0267-7261(02)00210-5.

Xia, H. and Hu, T. 1991. Effects of saturation and back pressure on sand liquefaction. *J. Geotech. Eng.*, *117*(9), pp.1347-1362.

Yamazaki F, Towhata I, Ishihara k. 1985. Numerical model for liquefaction problem under multi-directional shearing on horizontal plane. *Proc. 5th Int. Conf. on Numerical Methods in Geomechanics.*,1,339-406.

Yang Z, Lu J, Elgamal A. 2008. OpenSees soil models and solid-fluid fully coupled elements. San Diego: University of California.

Yang, J., Yang, Z.X., and Li, X.S. 2008. Quantifying and modelling fabric anisotropy of granular soils. *Géotechnique*, 58(4), 237–248. doi:10.1680/geot.2008. 58.4.237.

Yang, Z. X., and Pan, K. 2018. Energy-Based Approach to Quantify Cyclic Resistance and Pore Pressure Generation in Anisotropically Consolidated Sand. 30,04018203. doi:10.1061/(ASCE)MT.1943-5533.0002419.

Youd, B.T.L., Idriss, I.M., Andrus, R.D., Arango, I., Castro, G., Christian, J.T., Dobry, R., Finn, W.D.L., Harder, L.F., Jr., et al. 2001. Liquefaction resistance of soils: Summary Report from the 1996 NCEER and 1998 NCEER/NSF Workshops on Evaluation of Liquefaction Resistance of Soils. *J. Geotech. and Geoenvir. Engrg.*, 127(10): 817–833. doi:10.1061/(ASCE)1090-0241 (2001)127:10(817).

Youd, T. L. and T. N. Croven. 1975. Lateral Stress in Sands during Cyclic Loading. *J. Geotech. Eng. Div.* 101(GT2):217–21.

Zekkos, D., Athanasopoulos-Zekkos, A., Hubler, J., Fei, X., Zehtab, K., and Marr, W. 2018. Development of a LargeSize Cyclic Direct Simple Shear Device for Characterization of Ground Materials with Oversized Particles. *Geotech. T. J.* 41(2). https://doi.org/10.1520/GTJ20160271. ISSN 0149-6115.

Zhang, W., and A. T. C. Goh. 2013. Multivariate Adaptive Regression Splines for Analysis of Geotechnical Engineering Systems. Computers and Geotechnics 48:82–95. doi:10.1016/j.compgeo.2012.09.016

Zhang, L., and Evans, T. M. 2018. Boundary effects in discrete element method modeling of

undrained cyclic triaxial and simple shear element tests. *Granular Matter*, *20*(4), 60.

Zhang K, Jung J, Zhang T. 2011. True Triaxial Experimental Study of Stress-Induced Anisotropy of Sand. *Instrumentation, Testing, Model Soil Rock Behavior*.186–93. doi:10.1061/47633(412)25.

APPENDIX **A**

ONE-DIMENSIONAL RESPONSE OF UNIFORM SAND DEPOSITS

To further investigate the difference in the seismic response between ENA and WNA, additional earthquake motions having different earthquake magnitudes, intensities and predominated frequencies were utilized to perform one-dimensional response analysis. These motions were applied to the base of two hypothetical soil deposits of Ottawa sand F-65; one 20m thickness deposit of loose sand (H20-40) and another deposit (H20-40/90) of 10m dense layer overlain by 10m of loose sand. The energy-based pore pressure model was adapted in $FLAC^{2D}$ to predict the dynamic response and pore pressure generation in the soil model.

Table A-1 summarizes the data of the earthquakes. Time histories and corresponding spectral accelerations of these motions are shown in Figure A-1, and A-2 respectively. The one-dimensional responses in terms of average CSR and maximum generated pore pressure, $R_{u\text{-}max}$, are shown in Figure A-3.

The current results, shown in Figure A-3, endorse the outcomes shown and discussed previously in chapter 7. The comparison of dynamic responses reveals that the generated pore pressure is different even when CSR_{max} values are equal. Although the applied earthquake records have the same magnitude, the soil deposit is potentially liquefied under western and Kobe-L earthquakes while liquefaction was not observed due to the eastern earthquake (SAG-La Malbaie (1988). This reveals that the use of current liquefaction design charts in terms of $(N_1)_{60cs}$ in assessing the liquefaction potential in the Eastern Regions of Canada should be revisited.

Table A-1. Summary of earthquake motions

Earthquake	M	Intensity	T
SAG-La Malbaie (1988)	5.9	1.9	0.12
Livermore (1980)	5.8	1.3	0.20
Syn. West (Atkinson)	6.7	1.4	0.21
Kobe-L (1995)	6.9	1.4	1.15

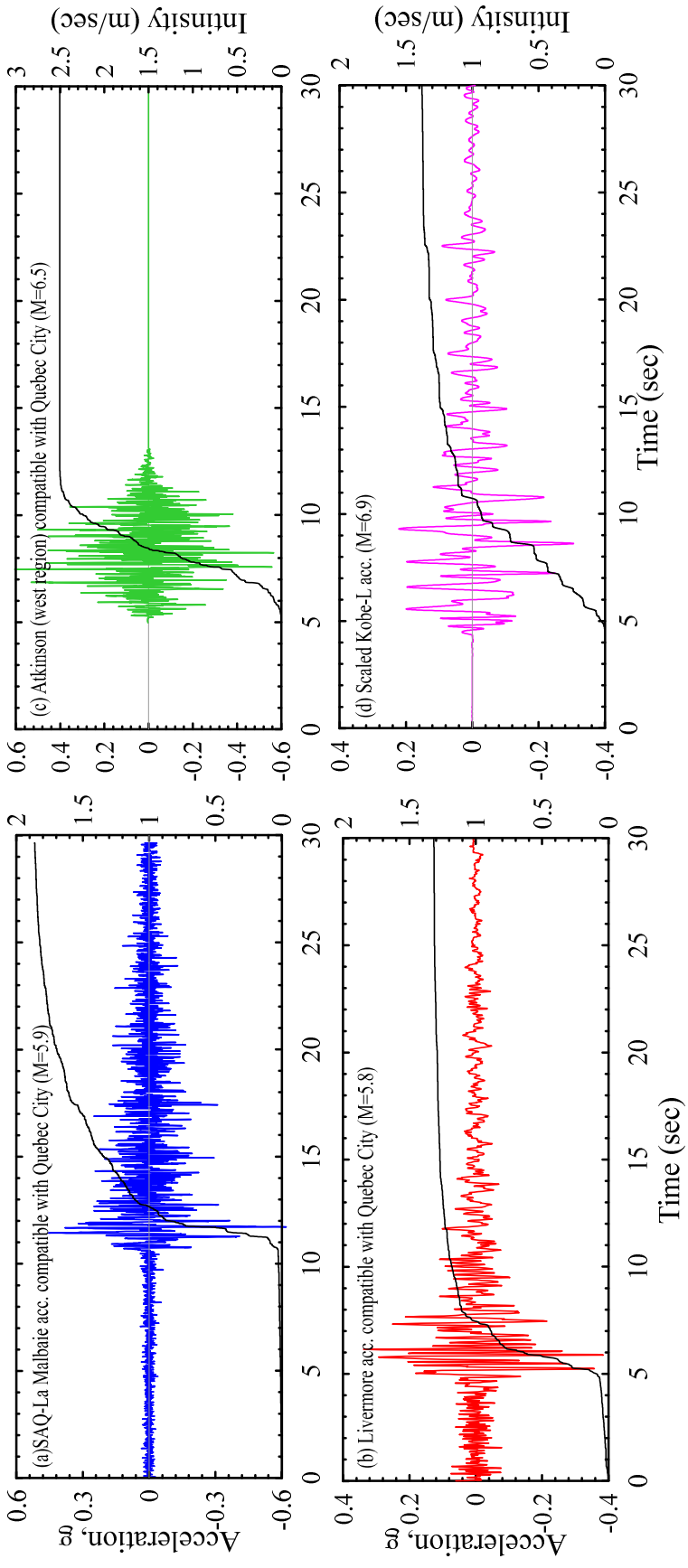

Figure A.1. Scaled time histories of the accelerations used (a) SAG-La Malbaie, (b) Livermore, (c) Syn. west (Atkinson), and (d) Kobe-L earthquakes.

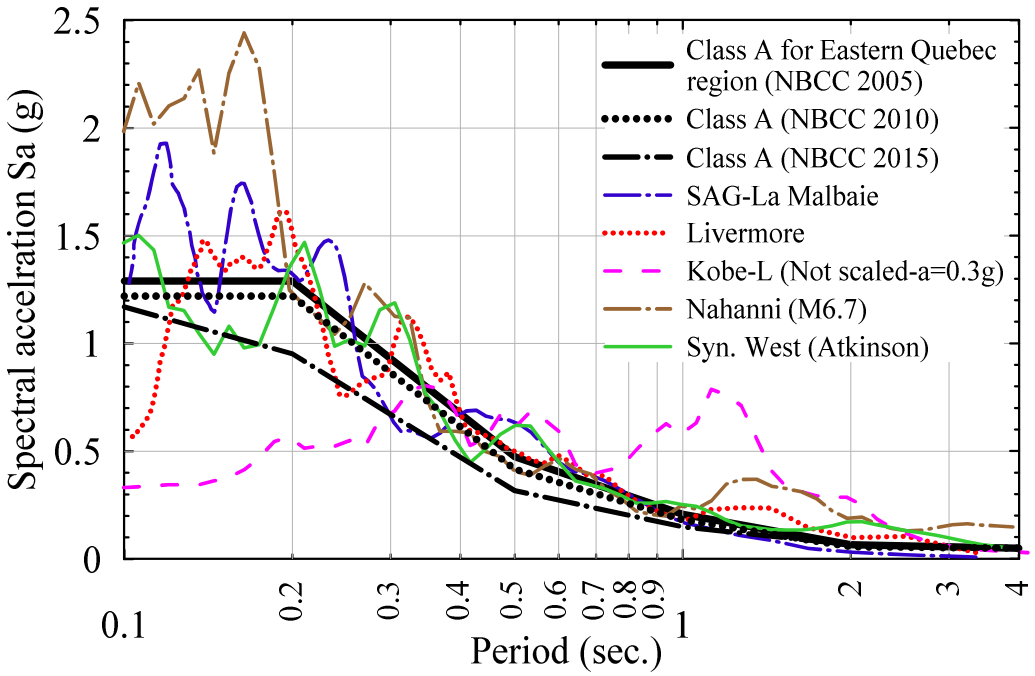

Figure A.2. Acceleration spectra for the used earthquakes

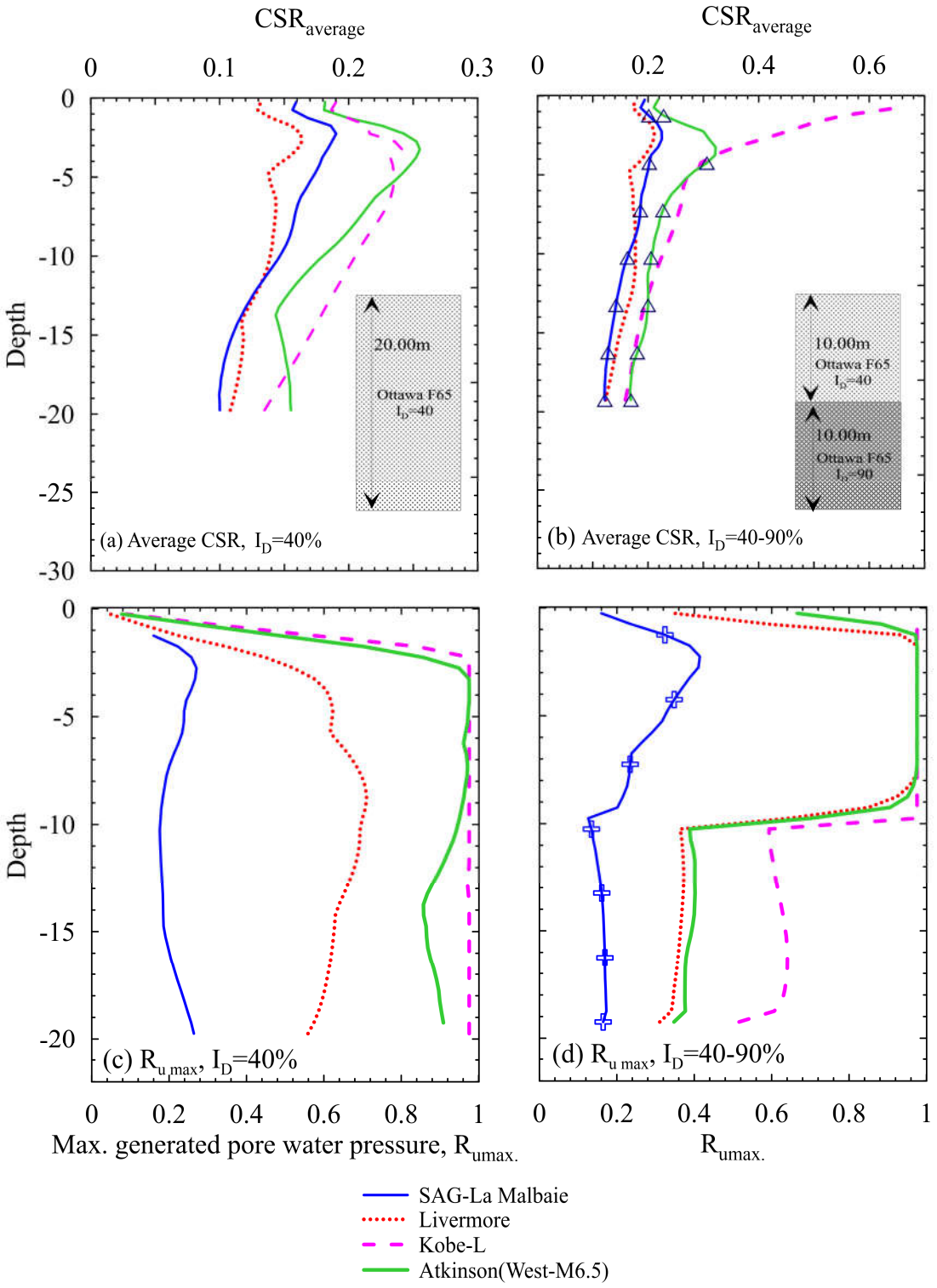

Figure A.3. Seismic responses of the applied earthquakes

APPENDIX B

SPECIMEN SIZE EFFECT ON CYCLIC BEHAVIOR AND LIQUEFACTION POTENTIAL USING THE TxSS APPARATUS

Authors and Affiliation:

Researcher, Department of Civil Engineering, Université de Sherbrooke, Sherbrooke (Québec) J1K 2R1, Canada
Marwan Khashila: Ph.D. Candidate, Sherbrooke University, Faculty of Engineering, Sherbrooke, QC.
Mourad Karray: Professor, Sherbrooke University, Faculty of Engineering, Sherbrooke, QC.
Mohamed Chekired: Researcher, Institut de Recherche d'Hydro-Québec, Varennes, Quebec, Canada.

Abstract: Owing to the lack of complementary shear stress on vertical boundaries of direct simple shear device, the stresses and strain distribution throughout soil specimens are not uniform. Considering a high diameter to height (D/H) ratio was suggested previously to produce more uniform stresses and strains distribution. In this study, the influence of the D/H ratio on the cyclic behavior and liquefaction potential is experimentally investigated using the combined triaxial simple shear (T_xSS) apparatus. Thus, reconstituted soil specimens of Ottawa C-109 sand were prepared at four different D/H ratios. The stress distribution inside the specimen was deduced and demonstrated by numerical simulation of the T_xSS test using a pre-calibrated coupled energy-based pore pressure model. The experimental results reveal the influence of the D/H ratio on the cyclic behavior in terms of pore pressure generation and decaying of cyclic stress ratio. However, soil specimens with D/H ratio higher than 2.5 induce comparable liquefaction potential irrespective of the D/H ratio.

Keywords: Direct simple shear; Triaxial simple shear apparatus; Liquefaction; Pore water pressure ratio.

A.1 Introduction

A number of different apparatus have been developed over the past few decades to apply simple shear to soil specimens. The most common types of simple shear tests on cuboidal or cylindrical specimens used in practice were developed at the University of Cambridge (Roscoe, 1953; Cole, 1967; Stroud, 1971; Airey, 1984) and Norwegian Geotechnical Institute (NGI) (Kjellman, 1951; Bjerrum and Landva, 1966), respectively. In both cases, the soil specimen has been confined laterally such that shear deformations are allowed while the horizontal specimen length is

constant. This is accomplished by hinged metallic walls in the Cambridge device and a cylindrical wire-reinforced rubber membrane in the NGI device. The NGI apparatus is an alternative set-up of the Swedish Geotechnical Institute–type device (SGI; Kjellman, 1951) where the soil specimen has been enclosed in a latex membrane while being supported laterally by a stack of smooth circular close-fitting rings. In these devices, the undrained simple shear response of soil is normally investigated by performing drained tests at constant volume. Since these devices constrain the lateral deformation of the soil specimen, only the height has to be maintained during shear to achieve constant-volume conditions. This is done by either physically fixing the specimen height with a rigid cross-member or with an automatic loading-unloading system which always maintains a constant specimen height (Franke et al., 1979; Mao and Fahey, 2003).

Many experimental (e.g. Wright et al., 1978; Airey and Wood, 1986; Kishida and Uesugi, 1987; Budhu, 1988) and analytical works (e.g. Roscoe, 1953; Lucks et al., 1972; Prevost and Høeg, 1976; Budhu and Brittio, 1987; Dounias and Potts, 1993; Doherty and Fahey, 2011; Dabeet et al., 2012) provided insight into the stress state and the strain distributions within the specimen in different configurations of the direct simple shear apparatus and drainage conditions. Other researchers compared controversial aspects of the generated stress-strain non-uniformities in apparatus with different lateral restraints and discussed the effect of specimen size (diameter to height ratio, D/H) on stress and strain distributions during simple shearing (e.g. Chang et al., 2016; Shen et al., 1978; Doherty and Fahey, 2011). Partial observations in these regards are highlighted in Table B.1.

These researchers unanimous concluded that due to the non-uniform stress-strain condition within the specimen induced by the incomplete mobilization of shear stress along its sidewalls (i.e., lack of complementary shear forces); none of the developed DSS devices can thoroughly mirror the ideal simple shear conditions. However, it has been observed that the nonuniformities occurred at the outer edge and approximately 70-80% of soil specimen cross-section area is subjected to uniform stresses and strains (Chang et al., 2016). The numerical simulation performed by Asadzadeh and Soroush (2017) revealed that the nonuniformity within DSS specimen increases rapidly beyond approaching the critical state line wherein localized zones experience contractive behavior while other zones impose dilative behavior. This contradictory

behavior within the soil sample does affect negatively on the accuracy of the liquefaction strength analysis. Similar conclusions were drawn by Budhu (1984) using a radiographic technique.

Although several studies have concluded the decrease of stress-strain non-uniformities with increasing the D/H ratio, there is no consensus of the adequate specimen size at which the static and cyclic properties are independent of specimen size. The details of these experimental (Amer, 1987; Carroll, 1979; Franke et al., 1979; Kovacs and Leo, 1981; Vucetic and Lacasse, 1982) and numerical (Shen et al., 1978, Amer et al., 1987) investigations can be found in Table B.1. Most recently, the ASTM D6528-17 specified the minimum D/H ratio as 2.5. The diversity in the suggested specimen sizes in these studies may be attributed to their differences in methods of assessment (experimental, or numerical), drainage (constant volume drained, or undrained) and loading conditions (static, or cyclic), types of materials tested (cohesive, or non-cohesive), cross-section configurations (rectangular, or cylindrical), and methods of confinement (metallic walls, wire-reinforced membrane, stacked rigid rings, or cell pressure). Vucetic and Lacasse (1982) attributed this contradiction to the inability of theoretical linear elastic analyses to capture actual nonlinear clay behavior beyond the yield. Moreover, Budhu and Britto (1987) indicated that the stress concentration produced by elastic analysis is higher than that in the modified Cam Clay analysis.

Despite many critical views put forward by the previous researchers, many advancements such as servo-controlled cyclic loading, cell pressure, and bidirectional shear loading have been made to the direct simple shear to overcome its shortcomings. One of the newly developed apparatus is the triaxial simple shear (T_xSS) apparatus. This apparatus has been designed and constructed through a collaboration between Hydro-Québec research institute and Université de Sherbrooke to permit the application of monotonic loading as well as both regular and irregular shear stresses or strains to soil materials.

In the current research, the specimen size effect on the cyclic behavior of cohesionless materials confined in a pressurized cell and the liquefaction potential was evaluated using the T_xSS apparatus. The results of the specimens with different D/H ratios and boundary conditions were compared to assess the probable impact of specimen size on the shearing behavior of tested specimens during cyclic shear testing.

A.2 TxSS apparatus, sample preparation, and testing program

The combined triaxial simple shear (T_xSS) apparatus has the ability to apply monotonic loading as well as both regular and irregular shear stresses or strains to soil materials. The T_xSS system permits testing soil samples under either drained or undrained conditions as well as direct measurement of pore water pressure generation during the undrained shear test. The T_xSS consists of a simple shear apparatus incorporated in a triaxial cell. The soil sample, which is enclosed in an unreinforced or reinforced rubber membrane, can be confined hydrostatically in a triaxial chamber, or similar to the conventional DSS apparatus supported laterally by stacks of smooth circular close-fitting rings. The general assembly of the T_xSS apparatus was comprehensively described in (Karray and Chekired, 2019; Chehat et al., 2019). The commercial direct simple shear DSS (EMDCSS) manufactured by Global Digital Systems Company (GDS) was employed in this study to compare the liquefaction potential of T_xSS tests.

To study the effect of the D/H ratio and type of confinement in T_xSS tests, two parallel sets of T_xSS tests on Ottawa-C109 were conducted. The natural silica Ottawa sand has a specific gravity of 2.67 g/cm^3 and the mean particle size of 340 μm. Its maximum and minimum void ratios are 0.82 and 0.5, respectively. Both series of samples were prepared using the moist tamping method (Ladd, 1978) and placed in the pressure cell, while the former series enclosed in an unreinforced membrane and the latter in a reinforced membrane. During sample preparation, the unreinforced or wire-reinforced membrane was placed along the interior wall of a split mold and held aligned by vacuum pressure. For the first series of tests, specimens were prepared with approximately 80 (mm) in diameter and different heights to achieve different D/H ratio of 2.16, 3.2, 4.4 and 5.7. The second series of specimens were enclosed in a reinforced rubber membrane with a diameter of 80 mm and a height of 25 mm (D/H=3.2). Two saturated porous stones were also placed at the top and bottom of the sample to provide the frictional surfaces and allow drainage in the vertical direction. After the specimen was prepared and installed in the cell, filled with de-aired water, a saturation of the specimen was performed in three stages. Carbon dioxide gas first flushed through the specimen in the upward direction for 20 min. Thereafter, de-aired water was flushed followed by back pressure application with maintained effective stress of 10 kPa. During these stages, the sample saturation was verified using the Skempton's pore-pressure parameter, $B = \Delta u/\Delta\sigma_c$, not less than 0.96. When the saturation phase of the test was completed, the maximum back pressure was held constant and the cell pressure was increased until the difference between

the cell pressure and the back pressure equaled the desired consolidation pressure. All specimens were confined hydrostatically under confining stress of approximately 100 kPa and specimen volume change during consolidation was measured to determine the final specimen density of 40-45%.

Following consolidation, the T_xSS system permits testing soil samples under either drained or undrained conditions as well as the direct measurement of the pore water pressure generation during the undrained shear test. The cyclic shearing typically involves controlling either the horizontal displacement in strain-controlled tests or the horizontal shearing load in stress-controlled tests.

In the current study, two different sinusoidal cyclic shear strain γ_{cyc} of amplitude 25-27%, and 45-47% at a frequency of 1 Hz were imposed on each specimen in undrained condition until the liquefaction triggering by displacing the specimen's top cap using a shear ram connected to an electromagnetic shaker mounted on a horizontal rigid table. A computer-automated feedback-loop-controlled system provides excellent control of stresses and strains. The initial liquefaction was presumed to occur at a stage where the gradually developed pore water pressure reaches more than 90% of the initially applied effective confining stress (i.e., $R_u=\Delta u/\sigma_c=0.9$).

The difference between the test configurations of the T_xSS test using unreinforced and reinforced membranes, together with the direct simple shear test are illustrated in detail in Figure B.1. As shown in Figure B.1(a), during direct simple shearing the volume of the samples confined in a reinforced membrane is kept constant. In this type of cyclic test, the pore water pressure buildup is not measured directly. The comparison of truly undrained and constant volume direct simple shear tests (Dyvik et al., 1987; Finn, 1985) suggested that the changes in vertical stress required to keep constant volume throughout a direct simple shear test can be considered equal to the measured pore pressures in an undrained direct simple shear test. This aspect distinguishes them from the direct simple shear devices in which the sample is enclosed in an unreinforced latex membrane and constrained in a pressurized cell (Hussien et al., 2015).

Figure B.1(b) corresponds to the sample subjected to the cyclic shearing in the T_xSS apparatus. In this case, in addition to the confining pressure surrounded the sample in the cell, the sample is also enclosed in a reinforced membrane to prevent the sample to deform in radial directions and assure respecting the plane strain condition. This apparatus has been developed so that a back pressure can be applied to the soil, thus ensuring specimen saturation, and excess pore pressures

Method		Description of the test conditions
DSS (constant volume)	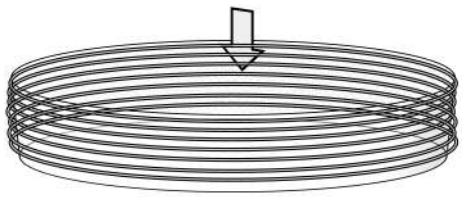	- Horizontal strain $\varepsilon_h \approx 0$ - Vertical strain $\varepsilon_v \approx 0$ - Pore pressure deduced from the variation of vertical stress (σ'_v) to maintain constant volume ($\varepsilon_v \approx 0$) - σ'_h = variable (unknown) - K_0 increase during cyclic loading.
T_xSS (constant volume) reinforced membrane	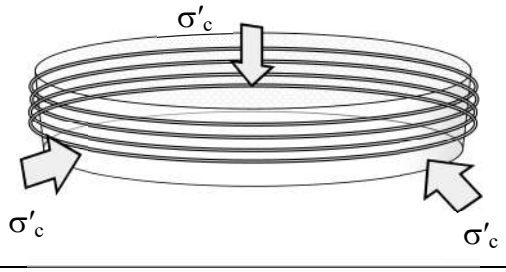	- Horizontal strain $\varepsilon_h \approx 0$ - Vertical strain $\varepsilon_v \approx 0$ - Pore pressure can be measured directly without any correction. - σ_h = unknown
T_xSS (constant stress) Flexible membrane	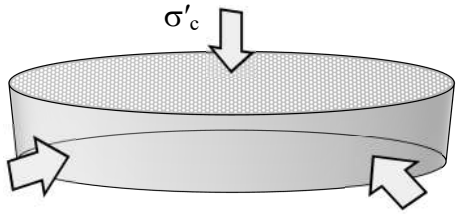	- Vertical and radial strains are negligible until the critical state line is approached by cyclic stress path (ε_{vol}=0, fully undrained condition). - Pore pressure can be measured directly without any correction even at very low strain. - σ_c = constant

Figure B.1. Different configurations of DSS tests

can be directly measured during undrained shearing. In Figure B.1(c) the sample placed in an unreinforced latex membrane, instead of the wire-reinforced membrane.

A.3 Result and analysis

Typical T_xSS strain-controlled test results of the sample reconstituted with a relative density of 44%, and D/H ratio of 4.2 under the cyclic shear strain of 0.25-0.27% is shown in Figure B.2. This figure shows the decaying of the cyclic stress ratio CSR, concurrently with the increase of pore pressure ratio, R_u, with time. The cyclic stress ratio CSR defined as the amplitude of the applied cyclic shear stress (τ_{cyc}) divided by the initial effective confining stress (σ_c). Figure B.2(a) indicates that excess pore pressure gradually accumulates within the soil sample, and the

initial liquefaction (R_u=0.9) is likely to occur after 25 cycles. After initial liquefaction was reached, the vertical strain increased more significantly as shown in Figure B.2(b).

For the first series of tests on specimens enclosed in an unreinforced membrane, four samples with D/H ratios of 2.16, 3.2, 4.4, and 5.7 were subjected to two different small and large cyclic shearing strains of γ_{cyc}= 0.25-0.27%, and γ_{cyc}= 0.45-0.47%. The development of excess pore pressure, R_u, and cyclic stress ratio, CSR, versus the number of cycles, N, of these tests (with different D/H ratios) are shown in Figure B.3. This Figure shows that the D/H ratio has a quite effect on the cyclic behavior of unreinforced specimens in terms of incremental R_u and decaying of CSR. However, all specimens liquefied approximately at the same number of cycles irrespective of the sample size. This reinforces the cyclic results performed on both sand (Franke et al., 1979) and clays (Andersen, 1975). However as shown in Figures B.3(a-1) and 3(a-2), before reaching the initial liquefaction the excess pore pressure and CSR value of the soil specimens with the smallest D/H ratio of 2.16 slightly deviated from those recorded for other D/H ratios. Wang et al. (2004) postulated that as the increasing specimen's height, the non-uniformities would become more pronounced and causes a deviation of cyclic behavior from other tested specimens, as shown in Figure B.3.Therefore, the γ_{cyc}-N_{liq} curve of soil specimens with D/H=2.16 slightly deviated from those with higher D/H ratios. In other words, for a given cyclic strain, a smaller number of cycles is required for the sample with D/H=2.16 to get liquefied and this difference became more pronounced by decreasing the cyclic strain amplitude. In addition, as can be seen in this figure the cyclic shearing behavior of the sample with D/H ratios of 3.2 confined in a reinforced membrane is completely consistent with that of the sample with the same D/H ratio but confined in an unreinforced membrane.

Modeling the dynamic behavior of a given soil requires defining of the stress-strain relationship of the soil and estimating the change in pore pressure by the variation of the effective stress during excitations. The energy concept takes account of all these elements by linking the energy dissipated per unit volume of soil, Ws, during cyclic loading to the generated pore pressure. This concept was developed to evaluate liquefaction potential and residual excess pore pressure generation in the 1970s by (Nemat-Nasser and Shokooh, 1979). as an alternative to stress-based procedures developed by prof. Seed and his colleagues at the University of California at Berkeley (Seed and Idriss, 1971). By adopting the energy concept for both series of TxSS test, unreinforced and reinforced membrane, an energy-based pore pressure model, Eq. (B.1), was

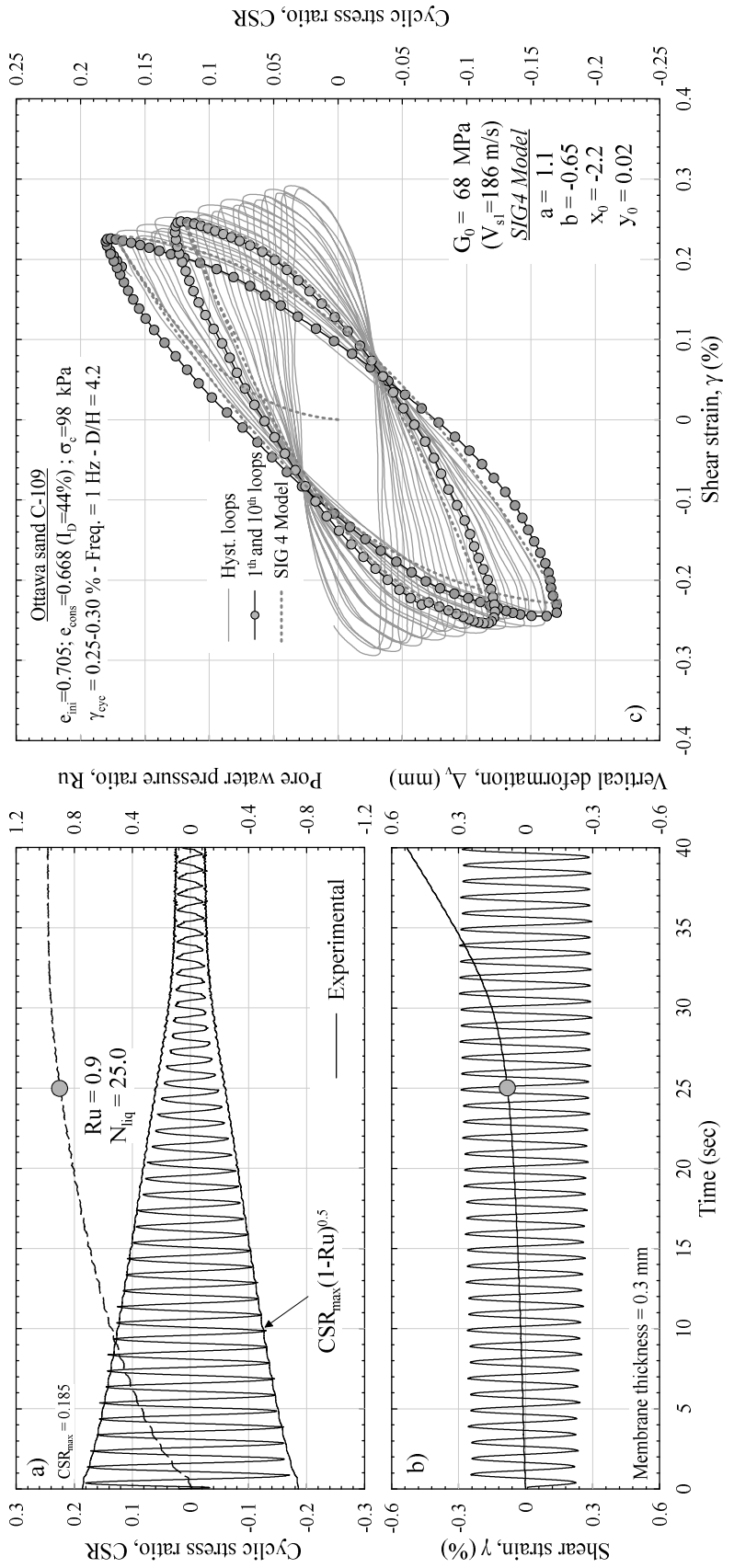

Figure B.2. Typical results of strain controlled- T_xSS test

established irrespective of D/H value, as shown in Figure B.5. The dissipated energy, Ws, can be determined by integrating the area bound by each stress-strain hysteresis loops, Eq. (B.2), as suggested by Green et al. (2000), Eq. (B.2).

$$R_u = 0.294\left(\frac{W_s^{0.5}}{\alpha}\right) + 1.55\left(\frac{W_s^{0.5}}{\alpha}\right)^2 - 0.945\left(\frac{W_s^{0.5}}{\alpha}\right)^3 \quad \text{(B.1)}$$

where α is a calibration parameter that depends on strain amplitude, as shown in Figure B.5.

$$W_s = \frac{1}{2\sigma'_{mo}} \sum_{i=1}^{n-1} (\tau_{i+1} + \tau_i)(\gamma_{i+1} - \gamma_i) \quad \text{(B.2)}$$

where τ_i is the applied shear stress at load increment i; γ_i is the shear strain at load increment i; σ'_{m0} is the initial mean effective stress; n is the total number of cycles.

In Figure B.5, the normalized unit energy, W_s, for both series of test samples, unreinforced and reinforced membrane, with different D/H ratios are plotted against the generated pore pressure ratio. As can be seen in this figure for a given γ_{cyc}, the R_u- $W_s^{0.5}$ curves of all tests are fall in a converged range, regardless of their D/H ratios or confinement methods. It is important to note that R_u- $W_s^{0.5}$ curves in Figures B.5(a) and B.5(b) have the same trend and can be yielded by Eq. (B.1). In a complementing paper, this concept had been employed to introduce a coupled energy based-pore pressure model that was adopted to numerically simulate the cyclic behavior of cohesionless soil under cyclic triaxial and T_xSS tests in FLAC^{3D} platform (Khashila et al., 2020). This model was used herein to demonstrate the stress-strain non-uniformity within T_xSS specimens having D/H ratios of 3.2 and 2, as shown in Figures B.6(a) and B.6(b), respectively.
As anticipated, the non-uniformity of shear stress increases with increasing the sample height (decrease the D/H ratio) which was observed to have a quite effect on cyclic behavior and number of liquefaction cycles (as shown in Figure B.4). Figure B.4 demonstrates that, as concluded previously by Doherty and Fahey (2011), around 70-80 % of specimen cross-section experiences uniform stress and nonuniformity occurred at the exterior perimeter. This percent increases with decreasing the height of the soil specimen and depends on the Poisson's ratio (Saada and Townsend; 1981).

To investigate the specimen size effect under stress-controlled conditions, a series of DSS tests were conducted on the same relative density with the D/H ratio of 3.9 using the conventional

DSS (EMDCSS-type). The liquefaction potential of special alternative stress-controlled tests performed in the T_xSS and that obtained from numerical simulation of T_xSS tests are depicted in Figure B.7. The cyclic stress-controlled test results of DSS and T_xSS are compared to liquefaction potential curves published in the literature for Ottawa sand C-109 specimens having different D/H ratios in Figure B.7. In the range of D/H ratio between 2.5 and 3.9, it can be observed a comparable trend between the obtained curves irrespective of D/H ratio. However, the large-diameter DSS, developed by (Zekkos et al., 2018) induces a relatively lower resistance. This reinforces the ASTM 6528-17 recommendation of the minimum D/H ratio that could be used in liquefaction investigation is 2.5.

A.4 Conclusion

The present work investigated the effect of the specimen size under cyclic stress- and strain-controlled tests. This was done by performing a series of cyclic stress- and strain-controlled tests on the reconstituted specimens of Ottawa sand C-109 using DSS and T_xSS devices. The obtained results were compared to previously published liquefaction potential curves. The results show that, under cyclic strain-controlled tests, soil specimens with D/H = 2.2 give slightly lower resistance than those with a higher D/H ratio. Employing the energy concept to develop a coupled energy-based numerical model, the non-uniformity of shear stresses distinctly appears at the outer edge of soil specimens with a higher D/H ratio. However, under cyclic stress-controlled tests, the specimen size effect was eliminated at a D/H ratio higher than 2.5.

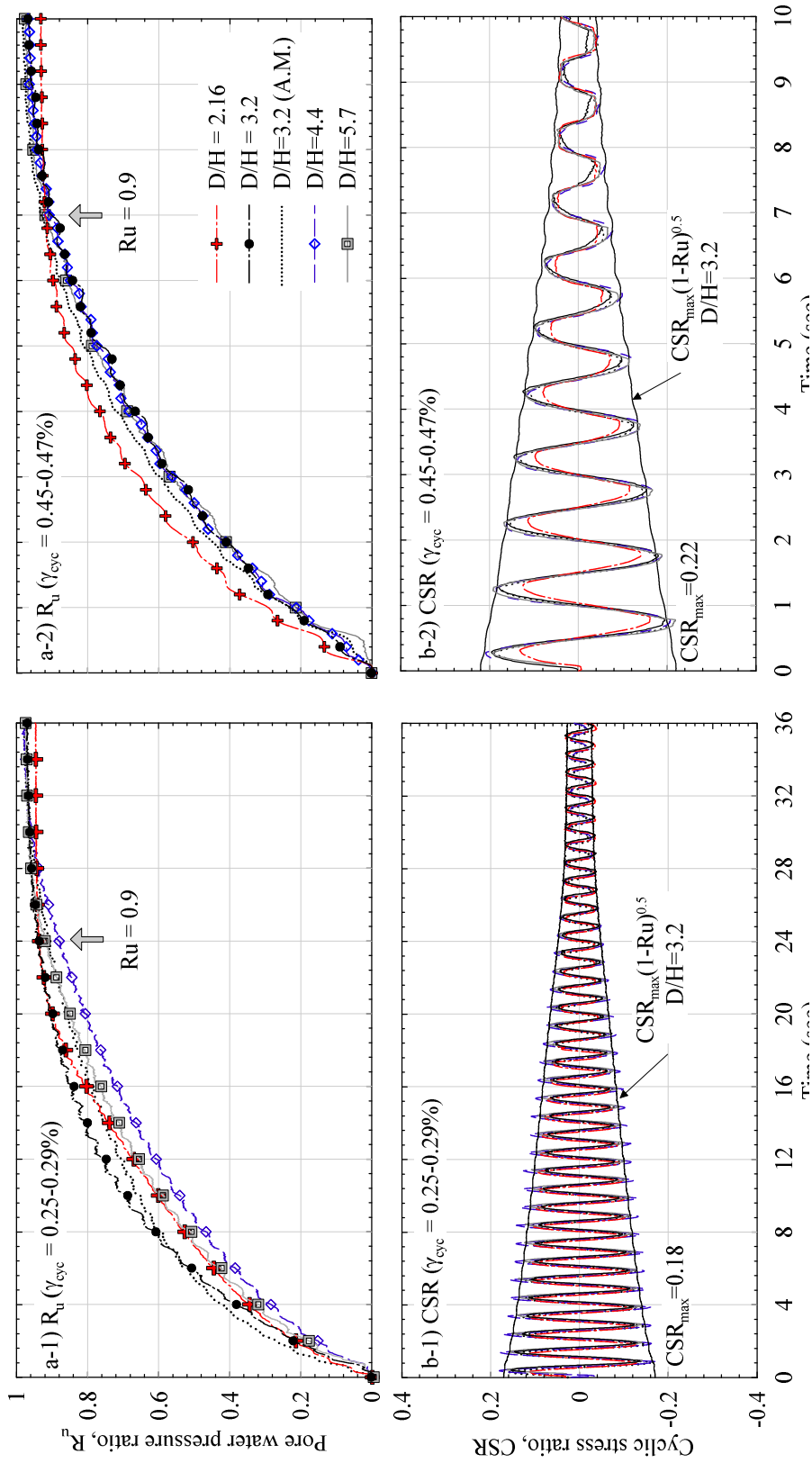

Figure B.3. Variation of pore pressure ratio and CSR as a consequence of cyclic shear strain loading

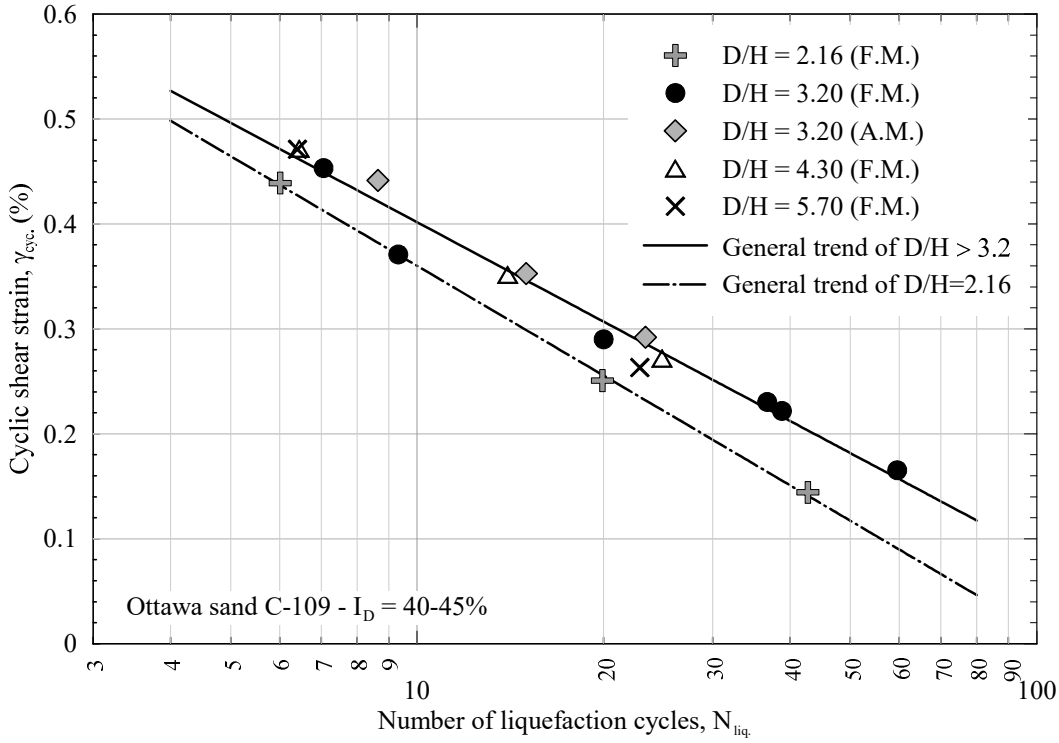

Figure B.4. Variation of the number of cycles to produce liquefaction as a function of cyclic strain

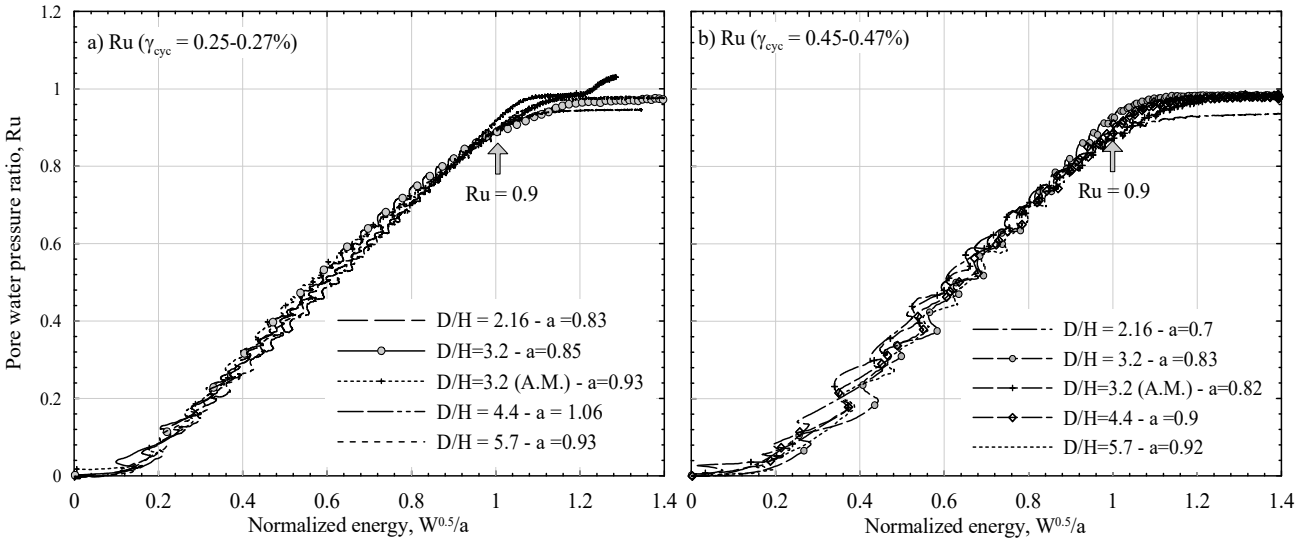

Figure B.5. Variation of normalized energy with H/D for different cyclic strain

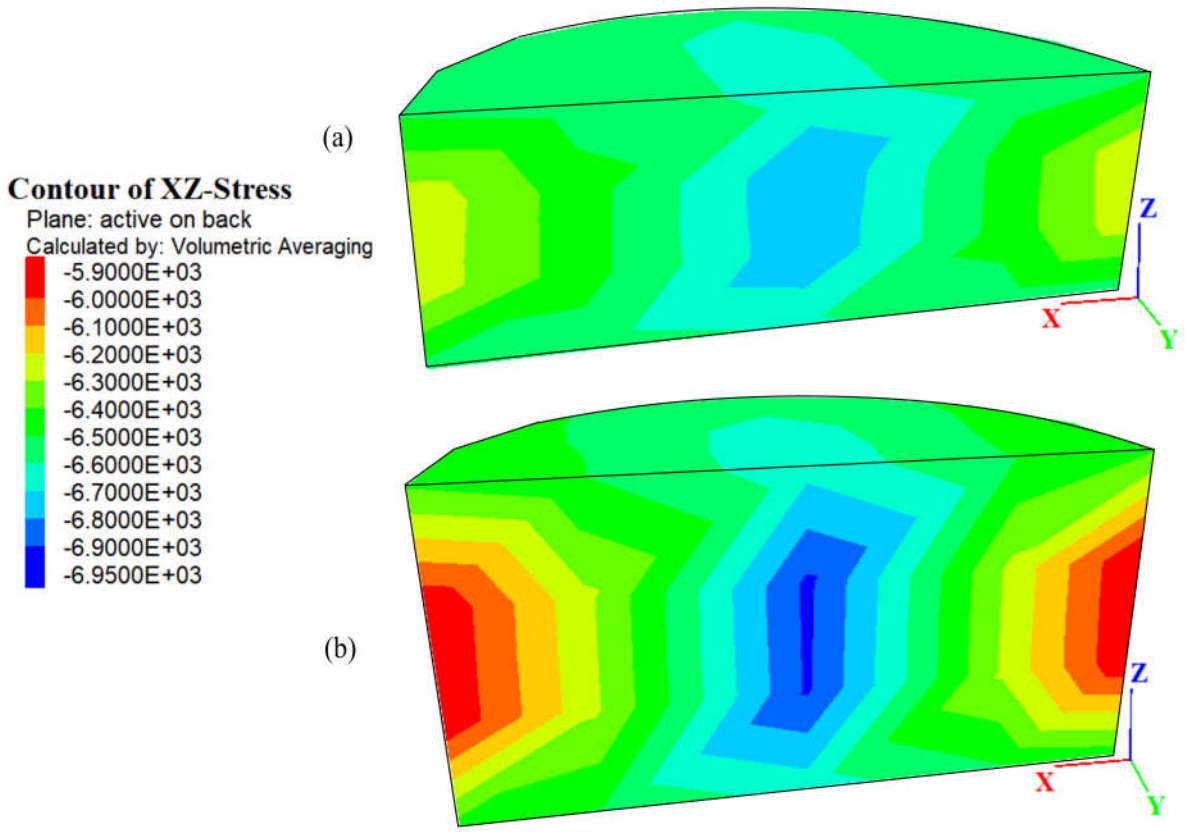

Figure B.6. Shear stress distribution in T_xSS specimen at the liquefaction triggering (a) D/H = 3.2, (b) D/H = 2

A.5 References

Airey, D. (1984). Clays in circular simple shear apparatus. PhD thesis, University of Cambridge, Cambridge, United Kingdom.

Airey D.W., & Wood D.M. (1986). Pore pressures in simple shear. *Géotechnique*, 37(1):25–35.

Amer, M. I., Kovacs, W. D., & Aggour, M. S. (1987). Cyclic Simple Shear Size Effects. *J. Geotech. Eng.,* 113(7), 693–707, https://doi.org/10.1061/(ASCE)0733-9410(1987)

Andersen, K. H., (1975). Repeated Loading on Clay. Summary and Interpretation of Test Results, (Research Project), NGI Internal Report No. 74037-9.

Asadzadeh, M., & Soroush, A. (2017). Macro- and micromechanical evaluation of cyclic simple shear test by discrete element method. *Particuology*, 31: 129–139. Elsevier B.V. doi:10.1016/j.partic.2016.05.015.

ASTM D6528-17. (2017). Standard Test Method for Consolidated Undrained Direct Simple Shear Testing of fine grain Soils. *ASTM International*, West Conshohocken, PA, www.astm.org

Bjerrum, L., & Landva, A. (1966). Direct simple-shear tests on a Norwegian quick clay. *Geotechnique*, 16(1): 1–20.

Budhu, M. (1984). Nonuniformities imposed by simple shear apparatus. *Can. Geotech. J.*, 21(1): 125–137. doi:10.1139/t84-010.

Budhu, M. (1988). The mechanism of failure under cyclic simple shear strain. *Soil and Foundations*, 28(4): 119-129.

Budhu, M., & Britto, A. (1987). Numerical analysis of soils in simple shear devices. *Soil and Founds*, 27(2): 31–41.

Carroll, M.D. (1979). Sample size effects using the NGI direct simple shear apparatus. Rensselaer Polytechnic Institute, Troy, N.Y.

Chang, W.J., Phantachang, T., & Ieong, W.M. (2016). Evaluation of size and boundary effects in simple shear tests with distinct element modeling. *J. GeoEngng.*, 11(3): 133–142. doi:10.6310/jog.2016.11(3).3.

Chehat, A., Hussien, M.N., Abdellaziz, M., Chekired, M., Harichane, Z., & Karray, M. (2019). Stiffness– and damping–strain curves of sensitive champlain clays through experimental and analytical approaches. *Can. Geotech. J.*, 56(3): 364–377. doi:10.1139/cgj-2017-0732.

Cole E.R.L. (1967). The behaviour of soils in the simple shear apparatus. PhD thesis, University of Cambridge, Cambridge, UK.

Dabeet, a., Wijewickreme, D., & Byrne, P.M. (2012). Simulation of cyclic direct simple shear loading response of soils using discrete element modeling. *Proc. 15th World conference on Earthquakes Engineering*.

DeGroot, D.J., Germaine, J.T., & Ladd, C.C. (1994). Effect of nonuniform stresses on measured DSS stress-strain behavior. *J. Geotech. Engng*, 120(5): 892–912. doi:10.1061/(ASCE)0733-9410(1994)120:5(892).

Doherty, J., & Fahey, M. (2011). Three-dimensional finite element analysis of the direct simple shear test. *Comp. Geot.*, 38(7): 917–924. doi:10.1016/j.compgeo.2011.05.005.

Dounias, G.T. & Potts, D.M. (1993). Numerical analysis of drained direct and simple shear tests. *J. Geotech. Engng* 119(12): 1870–1891.

Duncan, J.M., & Dunlop, P. (1969). Behavior of soils in simple shear tests. *Proc. 7th International Conference on Soil Mechanics and Foundation.* pp. 101–109.

Dyvik, R., Berre, T., Lacasse, S., & Raadim, B. (1987). Comparison of truly undrained and constant volume direct simple shear tests. *Geotechnique*, 37(1): 3–10.

Finn, W.D. (1985). Aspects of Constant Volume Cyclic Simple Shear. presented at the Advances in the Art of Testing Soils Under Cyclic Conditions, Detroit, MI, ASCE, New York, NY,: 74–98.

Franke, E., Kiekbusch, M., & Schuppener, B. (1979). New Direct Simple Shear Device. *Geotech. T. J.*, 2(4): 190–199. doi:10.1520/GTJ10457J.

Green, R.A., Mitchell, J.K., & Polito, C.P. (2000). An energy-based excess pore pressure generation model for cohesionless soils. John Booker memorial symposium,.

Hussien, M.N., Karray, M., & Chekired, M. (2015). Evaluation of DSS test results on granular soils based on T x SS results. *Proc. 68th Conf. Canadian of Geotech.*, Quebec, paper no. 393.

Kjellman W. (1951). Testing the shear strength of clay in Sweden. *Géotechnique*, 2(3):225–32.

Karray, M., & Chekired, M. (2019). Triaxial Simple Shear test: T_xSS. *Proc. 7th Int. Symposium on Deformation Characteristics of Geomaterials (IS-Glasgow 2019).* Paper No. 02014: 1-6.

Khashila MM., Hussien MN., Karray M., & Chekired M. (2020). Analysis of dynamic soil behavior under triaxial and simple shear modes. *Computer and Geotech*. Under review.

Kishida, H. & Uesugi, M. (1987). Tests of the interface between sand and steel in the simple shear apparatus. *Géotechnique*, 37(1): 45-52

Kovacs, W.D., & Leo, E. (1981). Cyclic simple shear of large scale sand samples: effects of diameter to height ratio. first international conference on Recent Advances in Geotechnical Earthquake Engineering and Soil Dynamics, Missouri S&T (formerly the University of Missouri-Rolla),: Paper 19.

Ladd, R.S. 1978. Preparing test specimens using under compaction. *Geotech. T. J.*, *1*(1),16-23.

Lucks, A., Christian, J., Brandow, E. and Höeg, K. (1972). Stress conditions in NGI simple shear test. *J. Soil Mech. Found Div.*, 98(1): 155–160.

Mao, X., & Fahey, M. (2003). Behaviour of calcareous soils in undrained cyclic simple shear. *Géotechnique*, 53(8): 715–727. doi:10.1680/geot.2003.53.8.715.

Prevost, J.-H., & Høeg, K. (1976). Reanalysis of simple shear soil testing. *Can. Geotech. J.*, 13(4): 418–429. doi:10.1139/t76-042.

Roscoe, K.H. (1953). An apparatus for the application of simple shear to soil samples. *Proc. of the 3rd International Conference on Soil Mechanics and Foundation Engineering.* pp. 186–191.

Saada, A.S., & Townsend, F.C. (1981). State of the art: laboratory strength testing of soils. laboratory shear strength of soil, ASTM STP 740,: 7–77.

Seed, H.B., & Idriss, I.M. (1971). Simplified procedure for evaluating soil liquefaction potential. *J. Soil Mech. Found Div., ASCE,* 97(9): 1249–1273.

Seed, H.B. (1979). Considerations in the Earthquake-Resistant Design of Earth and Rockfill Dams. *Géotechnique* 29(3): 215-263.

Shen, C. K., Sadigh, K., & Herrmann, L.R. (1978). An Analysis of NGI Simple Shear Apparatus for Cyclic Soil Testing. Dynamic Geotechnical Testing. *ASTM International*,: 148–162.

Stroud M.A. (1971). The behaviour of sand at low stress levels in the simple shear apparatus. PhD thesis. University of Cambridge. Cambridge, UK.

Vucetic, M., & Lacasse S. (1982). Specimen Size Effect in Simple Shear Test. *J. Geotech. Eng, Div.*, *ASCE,* 108(12): 1567–1585.

Wang, B., Popescu, R., & Prevost, J.H. (2004). Effects of boundary conditions and partial drainage on cyclic simple shear test results-a numerical study. *Int. J. for Numerical and Analytical Methods in Geomechanics*, 28(10): 1057–1082. doi:10.1002/nag.377.

Wright, D. K., Gilbert, P. A. & Saada, A. S. (1978). Shear devices for determining dynamic soil properties, *Proc. Spec. Conf.Earthquake Engineering and Soil Dynamics*, ASCE, Pasadena (2): 1056–1075.

Zekkos, D., Athanasopoulos-Zekkos, A., Hubler, J., Fei, X., Zehtab, K.H., & Allen Marr, W. (2018). Development of a large-size cyclic direct simple shear device for characterization of ground materials with oversized particles. *Geotech. T. J.*, 41(2): 263–279. doi:10.1520/GTJ20160271

Table B.1. Examples of experimental and analytical works on different types of simple shear apparatus

Author(s)	Type of study	Method of confinement	Loading condition	Material tested	D/H suggested	Observation
Roscoe (1953)	Exp. + 2D Math. Analysis Cambridge DSS	Rigid walls Cuboidal sample 6 cm×6 cm×2.2 cm	Monotonic	Plasticine Linear elastic material	-	The shear stress on the specimen faces is approximately uniform across the middle third of each face. However, the shear stress diminished at the corners of the sample
Duncan and Dunlop (1969)	Exp .+ 2D Num. FE analysis Cambridge DSS	Rigid walls Cuboidal sample 6 cm×2 cm	Monotonic	Clay Linear elastic material	-	Progressive failure has no effect on the ultimate simple shear resistance of clay, but pronounced effect on the behavior of brittle soils.
Lucks et al. (1972)	Num. 3D FE analysis NGI DSS	Rigid walls Cuboidal sample		Clay	-	70% of the sample exhibits fairly uniform stress conditions while stress concentrations at the edges were quite local.
Prevost and Høeg (1976)	Exp. + 2D Math. Analysis Cambridge DSS	Rigid walls Cuboidal sample 6 cm×2 cm	Monotonic Cyclic	Sand Linear elastic material	-	More potential of non-uniformity development with the increase of slippage at the top and bottom specimen boundaries.
Shen, C. K. et al. (1978)	Num. 2D FE analysis NGI DSS	Wire-reinforced Cylindrical sample D/H= 2,4, and 8 D= 8 cm	Monotonic Cyclic	Linear elastic material	8	Uniformity of shear strain distribution improves as the specimen diameter-to-height ratio is increased, the percent of wire-reinforcement is increased, the elastic modulus of the soil decreases, the Poisson's ratio of the soil decreases, and the applied horizontal displacement is increased.
Carroll (1979)	Exp. NGI DSS	Wire-reinforced Cylindrical sample D= 4.76 & 8 cm H= 1.1, 1.65, 2.1 cm (1.5 recommended)	Monotonic Cyclic	Clay		K_0 is affected by changes in height; the smaller cross-sectional sample size produces higher static and cyclic shear strain resistance, but a much greater degree of scatter; and sample height had little obvious and consistent effects on cyclic shear results.
Kovacas and Leo (1981)	Exp. DSS	Stacked rings D= 12 in	Cyclic	Sand	>4	The D/H effect on the shear modulus is significant at lower shear strain (<1%).

		H= 1, 2 and 4 in				
Vucetic and Lacasse (1982)	Exp. Geonor DSS	Wire-reinforced Cylindrical sample D/H= 3.125, 5, 7.187 H= 1.6 cm	Monotonic	Clay	No restriction	The D/H ratio has no significant influence on the measured strength of the Haga and Drammen clays.
Budhu and Britto (1987)	Exp. + Num. 3D FE analysis Modified Cam-Clay NGI DSS, Cambridge DSS	Rigid walls Cuboidal sample 10 cm×10 cm×2 cm Wire-reinforced Cylindrical sample D= 10 cm, H= 2 cm	Monotonic	Elasto-plastic or elastic material 14/25 Leighton Buzzard sand	-	The elastic analysis tended to produce larger stress concentrations at the ends of the sample in the plane of shear deformation than analysis based on the assumption that the behavior of the soil specimen can be modeled by the modified Cam-Clay.
Amer et al. (1987)	Exp. + Num. 2D FE analysis Large Scale DSS	Thin aluminum rings Cylindrical sample D/H=3, 6, 9, 12 D= 7.62 to-30.48 cm H= 0.64 to 10.16 cm	Cyclic	Ottawa 20-30 Linear elastic material	8	The specimen size has an important effect on both damping and shear modulus of dry sand at low strain amplitudes. When the specimen became larger in diameter and smaller in height the dynamic behavior appeared to be independent of the size.
DeGroot et al. (1994)	Exp., MDSS[1] Geonor DSS	Wire-reinforced Cylindrical sample	Monotonic	Rubber Boston Blue Clay	-	The non-uniformity results in measured stress-strain behavior that is not exclusively dependent on the soil type and over-consolidation ratio. It has little effect on the measured peak strength since this typically occurs at relatively low values of shear strain where the influence of the apparatus is minimal.
Doherty and Fahey (2011)	Num. 3D FE analysis Modified Cam-Clay Cambridge DSS, NGI DSS, UWA DSS	Metallic wall Stacked-ring Wire-reinforced Unreinforced + Cell pressure D=7.2 cm H=2.5 cm	Monotonic	kaolin clay	-	All boundary condition types produce identical effective stress paths, but, significant differences in total stress paths and excess pore pressures. The undrained shear strength is underestimated by around 10% and the friction angle by around 4% for the soil model used.
Chang et al.	Exp. + Num. 2D DEM	rigid wall	-	-	H/d_{max}[2]>7	The boundary effects can be reduced effectively

(2016)	PFC Modified NGI DSS (Cambridge or NGI)	Cylindrical sample Stacked-ring Boundary effect: D/H=2.85, 3.33, 5 D=10 cm D/H=2.5, 3.33, 5			Regardless of D/H ratio	by reducing the H/D value. The core zone has uniform force chains and the displacement field is about 60 to 70% of the total area of the model for H/D value ranging from 0.2 to 0.4. The difference in boundary effects is insignificant between NGI and Cambridge.

[1] multidirectional direct simple shear
[2] maximum particle size